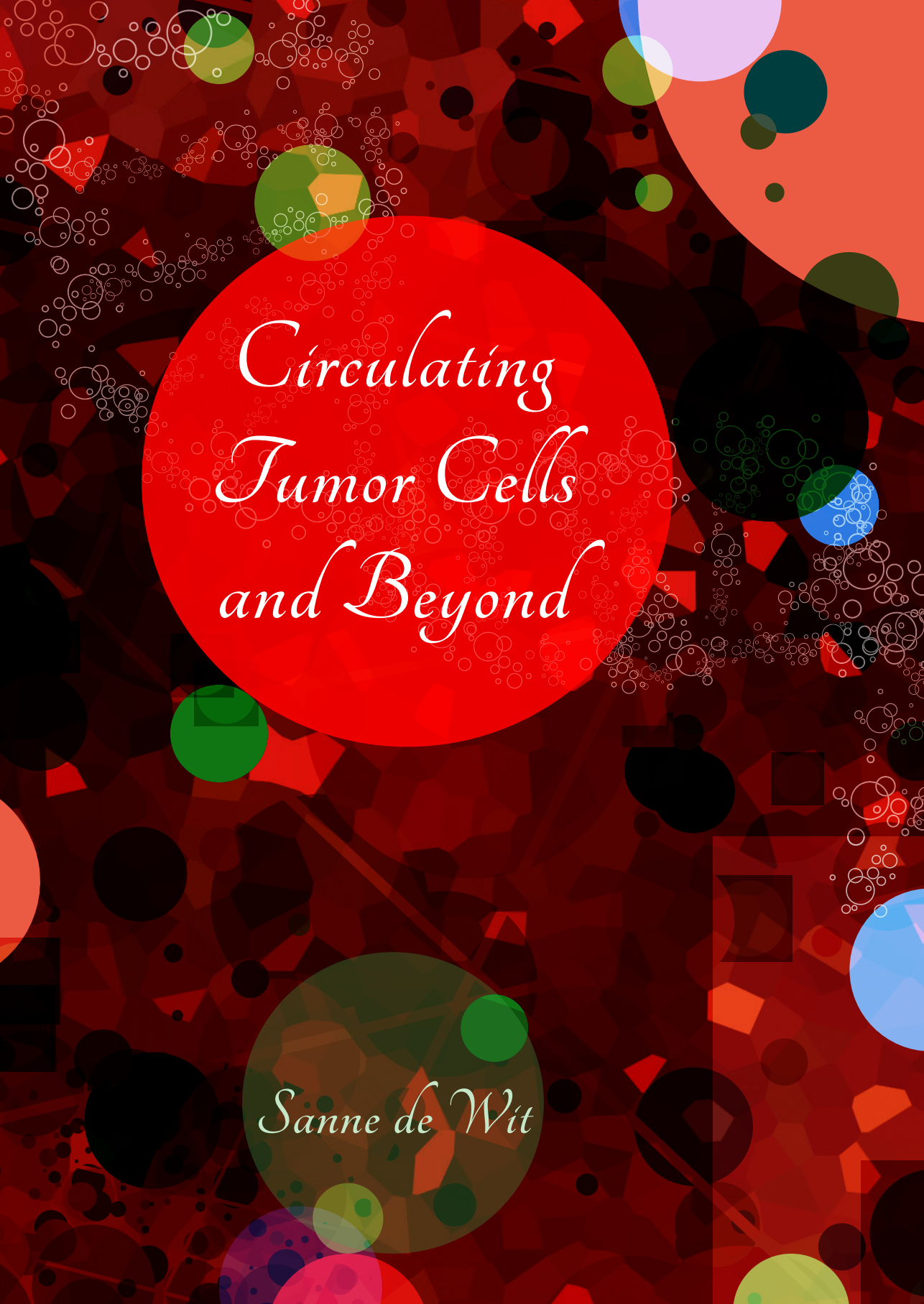
Circulating Tumor Cells and Beyond
Sanne de Wit

Circulating Tumor Cells and Beyond

Sanne de Wit

Samenstelling promotiecommissie:

Prof. dr. ir. J.W.M. Hilgenkamp	Universiteit Twente (voorzitter/secretaris)
Prof. dr. L.W.M.M. Terstappen, MD	Universiteit Twente (promotor)
Prof. dr. M.J. IJzerman	Universiteit Twente/University of Melbourne
Dr. J. Prakash	Universiteit Twente
Prof. dr. H.J.M. Groen, MD	Rijksuniversiteit Groningen
Prof. dr. J.S. de Bono	Institute of Cancer Research
M. Connelly, PhD	Silicon Biosystems, Inc. (referent)

This work has been financially supported by:
EU FP-7 "CTC-Trap"; health.2012.1.2-1 #305341

ISBN 978-90-365-4566-2
DOI 10.3990/1.9789036545662

CIRCULATING TUMOR CELLS AND BEYOND

PROEFSCHRIFT

ter verkrijging van
de graad van doctor aan de Universiteit Twente,
op gezag van de rector magnificus,
prof. dr. T.T.M. Palstra,
volgens besluit van het College voor Promoties
in het openbaar te verdedigen
op vrijdag 22 juni 2018 om 12:45 uur

door

Sanne de Wit

geboren op 7 april 1987
te Zwolle, Nederland

Dit proefschrift is goedgekeurd door:

Prof. dr. L.W.M.M. Terstappen, MD (promotor)

voor Thijs & Sofia

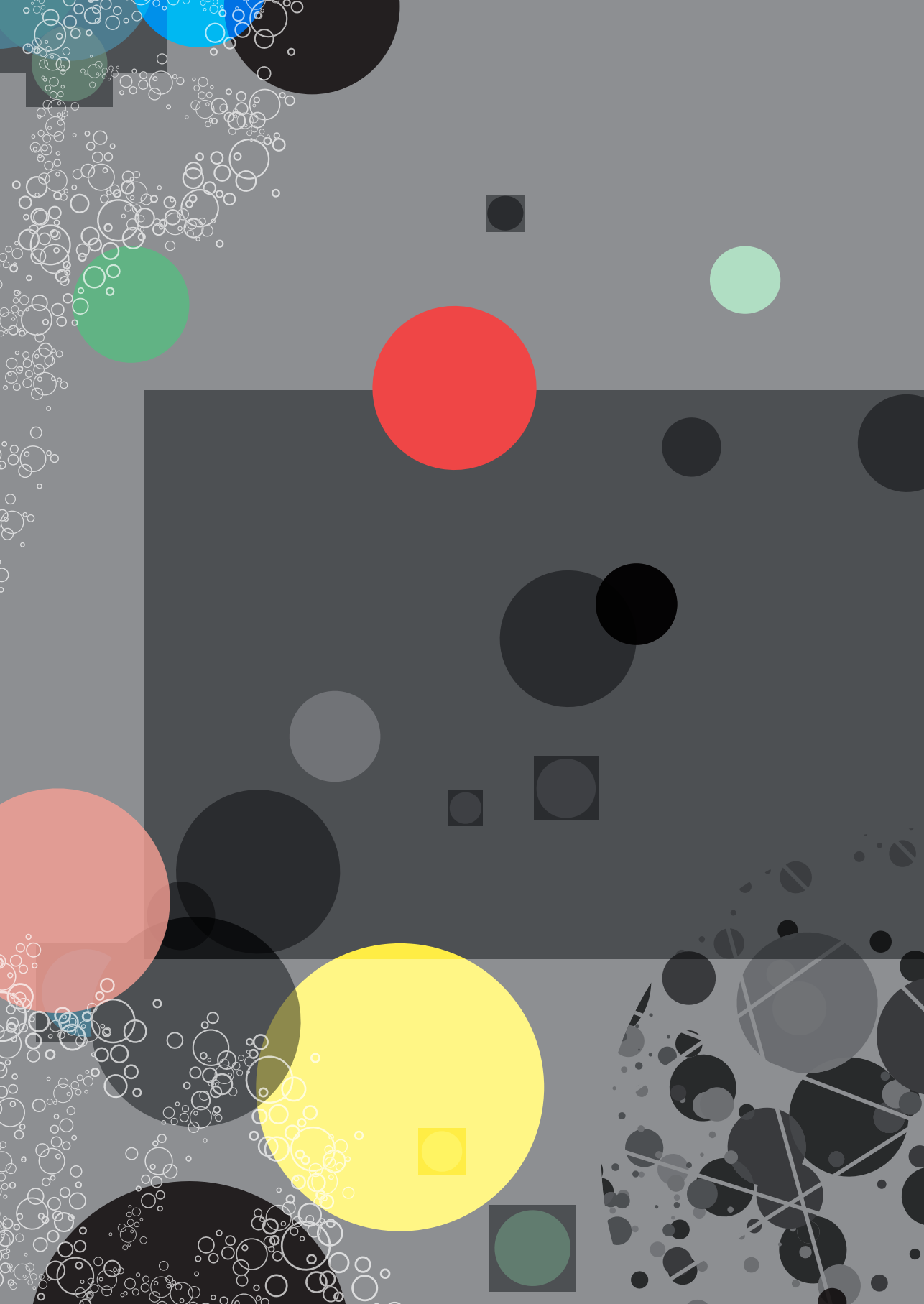


Introduction
to Circulating
Tumor Cells
and Beyond

This thesis

Globally, there were an estimated 14.1 million cancer cases in 2012. This number is expected to increase to 24 million by 2035[1]. These incredibly high numbers do not make it hard to believe that cancer is the second leading cause of death; nearly 1 in 6 deaths is due to cancer. Therefore, not surprisingly, the field of cancer research is quite extensive and subject to fast changing insights. In 2017 alone already 73 new oncology research projects were funded for €42 million by the Dutch KWF Kankerbestrijding Institute, whom are supporting currently over 400 studies in cancer diagnostics, biology, new innovations for the clinic and treatment or quality of life for patients[2].

With our growing understanding of cancer it has become clear that it is a very diverse, complex and dynamic disease. Between patients, but also within patients, tumor cells are changing fast due to genetic or micro-environmental factors. The heterogeneous nature of cancer cells is one of the reasons each patient responds differently on the applied treatment or has the ability to develop resistance. Therefore, a personalized and targeted approach of treatment for each patient is urgently needed. A treatment that is not based on the diagnosed cancer type, but one that is based on the patients' personal tumor characteristics. To make this possible, it is of vital importance to have access to these tumor characteristics prior, during and after treatment. This can be achieved via the so-called "liquid biopsy". This non-invasive method uses blood to analyze the presence and composition of cancer biomarkers, similar to a tissue biopsy from a tumor. The initial subject of liquid biopsies were cancer cells that leave the site of a tumor and enter into the blood, where some will settle at a distant location to form a new tumor, a metastasis. These circulating tumor cells (CTC) carry real-time information about the composition of the tumor and their presence can be used to evaluate and monitor the treatment effect on the patient. CTC are rare cells when compared to the abundance of leukocytes which surrounds them and therefore, to find and isolate them is a challenge in most cases. Tumors are derived from epithelial tissue and a large portion of CTC from these tumors is likely to express the epithelial cell adhesion molecule (EpCAM). This molecule can be used to capture CTC, as it is not expressed by leukocytes. But, with the presence of a heterogeneous tumor, CTC will reflect this heterogeneity and CTC populations might be present that express low or no EpCAM and thereby escape detection. Therefore, challenges have arisen to capture and identify all CTC. Besides CTC, the use of other biomarkers present in blood is rising fast. Circulating tumor

DNA and RNA, proteins and extracellular vesicles secreted from tumor cells can also carry precious information for a personalized approach in treating patients. Whereas the isolation and interpretation of circulating tumor DNA is more advanced, the isolation of vesicles and their contents is currently under development and both are making their way into clinical studies and applications.

This thesis describes the road into capturing and identifying CTC, with and without EpCAM expression, where their clinical value is examined in several patient studies. Circulating biomarkers like tumor DNA and tumor vesicles are explored for their potential as a liquid biopsy as well.

Outline

A major part of this thesis is dedicated to the capture and identification of $EpCAM^{high}$ and $EpCAM^{low}$ expressing CTC. In **Chapter 1**, the FDA-approved CellSearch® system that is clinically validated to isolate and identify $EpCAM^{high}$ CTC is reviewed, as well as the relation of these CTC with survival and challenges in CTC isolation. One of those challenges is the low frequency of CTC present in blood. To face this challenge, the EU-FP7 consortium "CTC Therapeutic Apheresis" – in short CTC-Trap – was started. This project and its execution over four years are described in **Chapter 2**. Experiments performed during the project for testing antibodies, immunostainings and microscope scanning procedures, are presented in **Chapter 8**. These results were all put together to form standard operating procedures to be used by all members in the CTC-Trap project (**Appendix**).

In **Chapter 3** we validate the tools developed in the CTC-Trap for the capture of $EpCAM^{high}$ and $EpCAM^{low}$ CTC. Cell lines were used to validate the procedures at all clinical sites and finally we applied this procedure in 108 metastatic castrate resistant prostate cancer and 22 metastatic breast cancer patients, whom we have followed for almost two years to determine the survival with relation to the CTC that were present in these patients.

In **Chapter 4** we analyze the presence of $EpCAM^{low}$ CTC in a small cohort of 28 metastatic non-small cell lung cancer patients. In this pilot study we developed the capture of $EpCAM^{low}$ CTC by means of microfiltration and subsequent immunostaining. To genetically proof we captured tumor cells on the microsieves, we developed a protocol to perform fluorescent in situ hybridization on the identified $EpCAM^{low}$ cells. One patient from this pilot study was eligible for this test and this case report is described in **Chapter 5**.

To explore the potential of multiple biomarkers as a liquid biopsy, we analyzed four cancer biomarkers. In **Chapter 6**, 97 non-small cell lung cancer patients are described in which we determine the presence of $EpCAM^{high}$ CTC, $EpCAM^{low}$ CTC, $EpCAM^{high}$ tumor derived extracellular vesicles and circulating tumor DNA in a single blood sample.

To improve detection of CTC, we classified all cells that are present after EpCAM enrichment with CellSearch in **Chapter 7.** For this, we used advanced image analysis by using the open source imaging program ACCEPT and Deep Learning. networks We determine the amount of nucleated cells present in patients and controls, include CD16 for identification of leukocytes and explore several alternatives in order to increase the identification of EpCAM-enriched cells.

1. World Health Organization, Cancer Fact Sheet, February 2017. http://www.who.int/mediacentre/factsheets/fs297/en/
2. KWF Kankerbestrijding, Onderzoek, Dit onderzoek maken we mogelijk. https://www.kwf.nl/onderzoek/welk-onderzoek-krijgt-geld/pages/default.aspx

Table of contents

Supplemental

Appendix

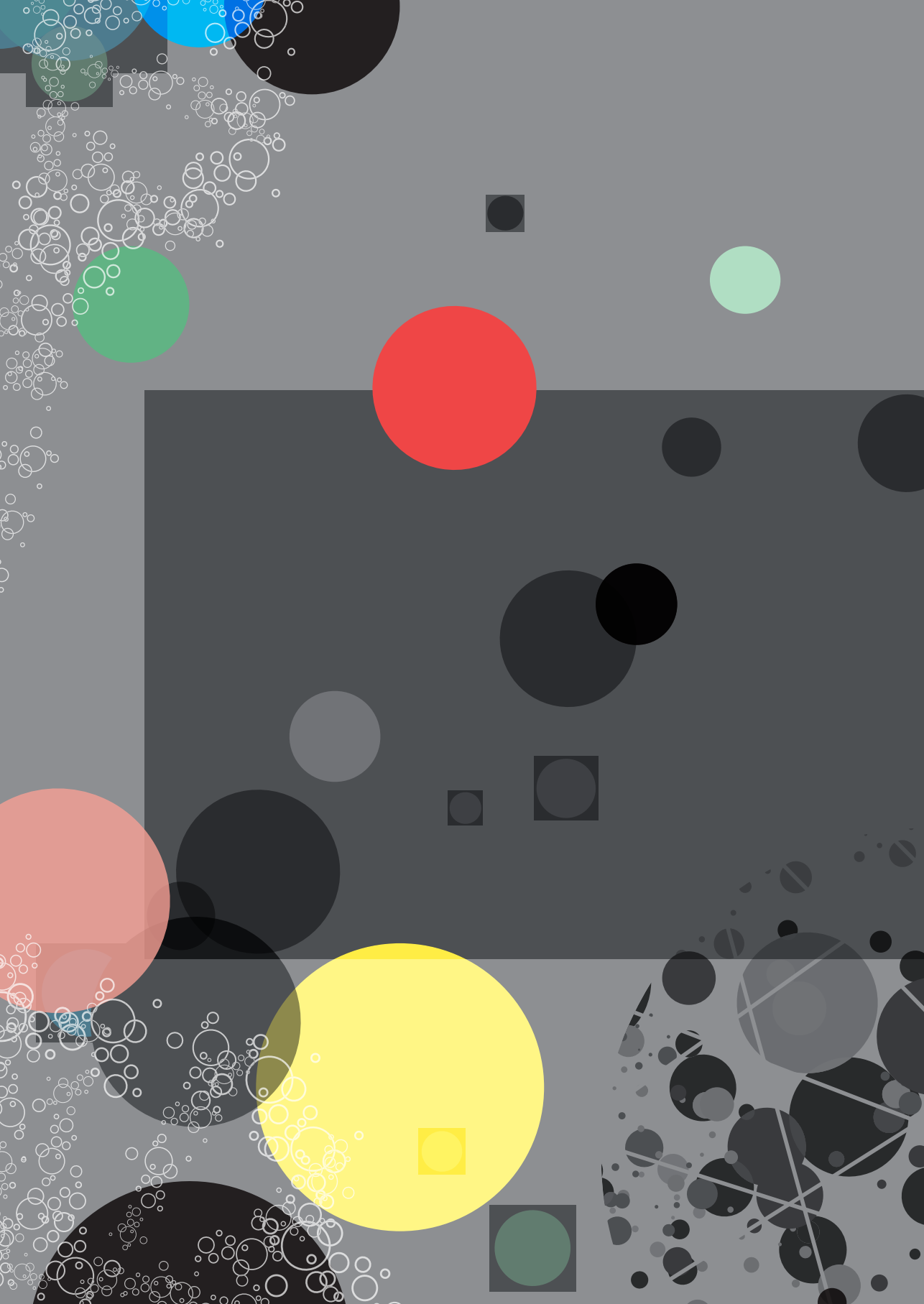

Chapter 1

Detection of Circulating Tumor Cells

Sanne de Wit, Guus van Dalum, Leon W.M.M. Terstappen

Scientifica (Cairo). 2014:819362; doi:10.1155/2014/819362

Abstract

The increasing number of treatment options for patients with metastatic carcinomas has created an accompanying need for methods to determine if the tumor will be responsive to the intended therapy and to monitor its effectiveness. Ideally, these methods would be noninvasive, and provide quantitative real-time analysis of tumor activity in a variety of carcinomas. Assessment of circulating tumor cells shed into the blood during metastasis may satisfy this need. Here, we review the CellSearch® technology used for the detection of circulating tumor cells and discuss potential future directions for improvements.

Introduction

In 1869, Thomas Ashworth described the microscopic observation of circulating tumor cells (CTC) in the blood of a man with metastatic cancer. He concluded that the CTC must have passed through the circulatory system to arrive at the vein from which the blood was collected[1]. The critical role that circulating tumor cells play in the metastatic spread of carcinomas has been demonstrated more than 100 years later[2]. Only recently technology has become available with the requisite sensitivity and reproducibility to explore the diagnostic potential of CTC[3].

Via a rigorous clinical testing program, CellSearch® is the only system validated for CTC detection to date[4–10]. The device is cleared by the FDA for the monitoring of patients with metastatic breast, colorectal and prostate cancer and clinical utility has also been demonstrated in metastatic small and non-small cell lung cancer, stomach cancer, pancreas cancer, ovarian cancer and bladder cancer[11–18].

For the enumeration of CTC, the CellSearch reagent kit uses ferrofluids labeled with the epithelial cell adhesion molecule (EpCAM), a DNA dye to stain nuclei and antibodies to target CD45 and cytokeratin 8, 18 and 19. The enrichment of endothelial and melanoma cells was enabled by replacing EpCAM ferrofluids with CD146 ferrofluids in the CellSearch system. Replacement of cytokeratin antibodies with CD105 allowed the enumeration of endothelial cells and studies showed an increase in endothelial cells in metastatic cancer and cardiovascular diseases[19–21]. Replacement of cytokeratin antibodies with antibodies to high molecular weight melanoma antigen, allowed the enumeration of melanoma cells and their presence is associated with a poor prognosis[22].

The potential to assess the presence of treatment targets in CTC such as Bcl-2, Her-2, AR, IGFR1 at both the DNA and protein level by the CellSearch system, has spurred the interest in this field as it holds the promise of a "real-time liquid biopsy"[23–27].

Cancer and the formation of metastasis

In the USA, 1.7 million people are expected to be diagnosed with cancer and 0.6 million people are expected to die from cancer[28]. At present, cancer is the second leading cause of mortality in USA and Europe[28,29]. Although the 5-year relative survival rate for all cancers is improving (49% in 1975-1977 and 68% in 2002-2008), the number of people diagnosed with cancer is expected to increase due to the increase in age of the overall population. The improvement in survival reflects both progress in diagnosing certain cancers at an earlier stage, and improvements in treatment. The costs associated with these improvements are however also increasing and will have an enormous economic impact in the time to come.

Death of cancer patients is rarely caused by the primary tumor and can be contributed in most cases to metastases at distant sites. Understanding the metastatic process is therefore of utmost importance to get more insight into the prognosis of patients and to identify potential ways to prevent tumors to form metastases. Figure 1 illustrates the evolution of cancer. At the early stages of tumor cell formation, diversity of the tumor cells already occurs and some will gain a greater ability than other cells to expand (tumor stem cells). At the time a tumor reaches around 100 μm in diameter, its need for nutrients increases. This is supplied through neo-vascularization, which permits the tumor to grow. At this time, cells from the tumor can enter the blood either directly or through the lymphatic system. Although the majority of these cells will succumb, some will survive and either passively or actively penetrate the endothelial cell layer at different sites in the body, forming distant metastasis that ultimately will kill the patient.

Cancers have preferences for certain tissues to form metastasis. The mechanisms and antigens expressed on their cell surface and the ligands on the capillaries of that specific tissue are still poorly understood. As time passes, the diversity of tumor cells increase, making the treatment more difficult. Moreover, the diversity further increases under the influence of therapy as tumor cells become resistant to therapy. Today, the potential sensitivity of a tumor is assessed on tumor cells taken at the time of surgery. In cases that the tumor has not been completely irradiated from the body

tumor cells, tumor cells will remain dormant or will expand. At the time the tumor cells have formed a detectable metastasis, the cells may no longer have the same sensitivity to therapies as at the time of surgery. This makes it again necessary to obtain a tumor biopsy and assess the best treatment options. However, biopsies are difficult, if not impossible, to take from metastatic sites. The ability to isolate tumor cells from the blood provides a unique opportunity for a "real time liquid biopsy". Of course, detection of cancer before dissemination has taken place is preferred. However, to make this possible, a leap in technology development is required. It has been modeled that tumors are very small at the moment of dissemination, and traditional imaging techniques need to be improved to detect these small tumors. Also, to detect CTC in such early disease conditions, sensitivity of these tests will need to be improved significantly[30].

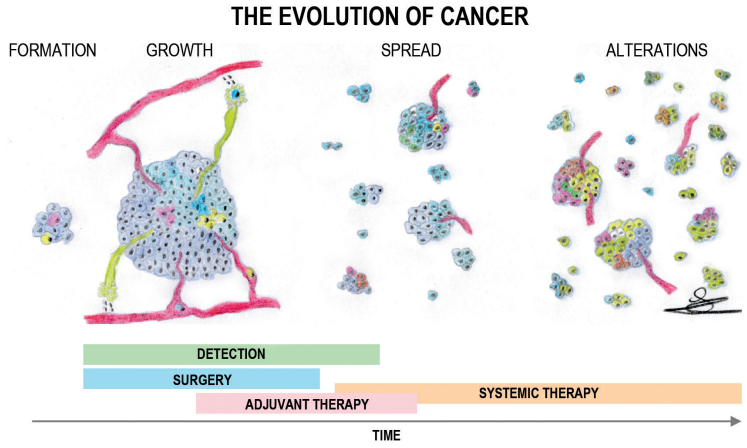

Figure 1. The evolution of cancer. After initial formation of cancer cells, growth of the tumor attracts blood vessels to supply oxygen and nutrients. Cancer cells then spread via these vessels forming metastases at distant sites. Mutations in DNA result in a heterogeneous population of cancer cells, with the potential of an increase in resistance against medicine. Patient care is depicted during the time of this evolution.

Identification of CTC by the CellSearch system

The CellSearch® System (Janssen Diagnostics, LLC; Raritan, NJ) consists of the CellTracks® Autoprep®, CellTracks Magnest®, CellSearch Epithelial Cell Kit and the CellTracks Analyzer II. The reagent kit used for the enumeration of CTC (CellSearchTM Epithelial Cell Kit) contains: ferrofluids labeled

with EpCAM to select for cells of epithelial origin, the staining reagents 4',2-diamidino-2-phenylindole, dihydrochloride (DAPI) for a nuclear stain, CD45-Allophycocyan (CD45-APC) to label leukocytes, cytokeratin 8, 18 Phycoerythrin and cytokeratin 19 Phycoerythrin (CK-PE) to label cells of epithelial origin, and buffers to enhance cell capture, permeabilize and fix the cells[31,32]. Samples that will be processed up to 96 hours after collection are drawn into 10 mL evacuated blood draw tubes (Janssen Diagnostics, LLC; Raritan, NJ) and maintained at room temperature.

To obtain viable CTC or investigate the expression of RNA in CTC, blood should be collected in EDTA and preferably processed within 24 hours. For these experiments the CellSearchTM Profile Kit (Janssen Diagnostics, LLC; Raritan, NJ) should be used. In this kit epithelial derived cells are enriched by the use of ferrofluids labeled with antibodies targeting the EpCAM antigen. After processing with the CellTracks Autoprep, a cell suspension is obtained including the CTC and 5000 residual leukocytes. This number will increase with the age of the blood samples. These samples can be used to investigate the mRNA expression of CTC or analyzed at the single cell level after staining and sorting by, for example, flow cytometry[33,34].

The CellTracks Autoprep immunomagnetically enriches cells expressing EpCAM from 7.5 mL of blood and fluorescently labels the enriched cells with DAPI, CD45-APC and CK-PE. The resuspended cells are deposited in the cartridge that is positioned in the CellTracks Magnest. This semi-automated fluorescence-based microscopy system acquires images using a 10X NA0.45 objective with filters for DAPI, PE, APC and FITC (not used) to cover the complete surface area of the analysis chamber. A computer identifies objects staining with DAPI and PE in the same location and generates images for the DAPI, PE, APC and FITC filters. Figure 2 shows a typical display of the fluorescent images that passed the threshold set by the computer program. A reviewer selects the CTC defined as nucleated DAPI+ cells, lacking CD45 and expressing CK-PE from the gallery of objects, which are tabulated by the computer. After processing 7.5 mL of blood from healthy donors, the median number of objects that need to be scored are approximately 50. In blood samples from cancer patients, the number of objects can be quite large. In general these are not all CTC, but can mostly be contributed to the presence of CTC fragments[35,36]. Presence of these CTC fragments is also related to poor outcome[36]. The heterogeneity in morphology is partly caused by the large diversity in the viability or apoptotic stage of the CTC. This makes it difficult to set criteria of what does and what does not account as a CTC. Differences in assigning objects as CTC is the largest

error currently in the system, and extensive training is required to keep the variations in assigning objects as CTC to a minimum[37,38]. Recently, we developed a CTC detection algorithm that counts CTC in images recorded by the CellSearch system[39]. This algorithm used survival data of metastatic prostate cancer patients to arrive at a definition that optimally stratified the patients into groups with favorable and unfavorable survival. It was not developed to copy human reviewers that assign events, but it eliminates reviewer variability. In addition, it is fast and decreases the cost of the CTC assay by eliminating the time a reviewer spends on reviewing the images. Also, quantitative information can be derived about the objects counted as CTC, such as morphological features or quantitative expression of antigens expressed on the CTC[24,40].

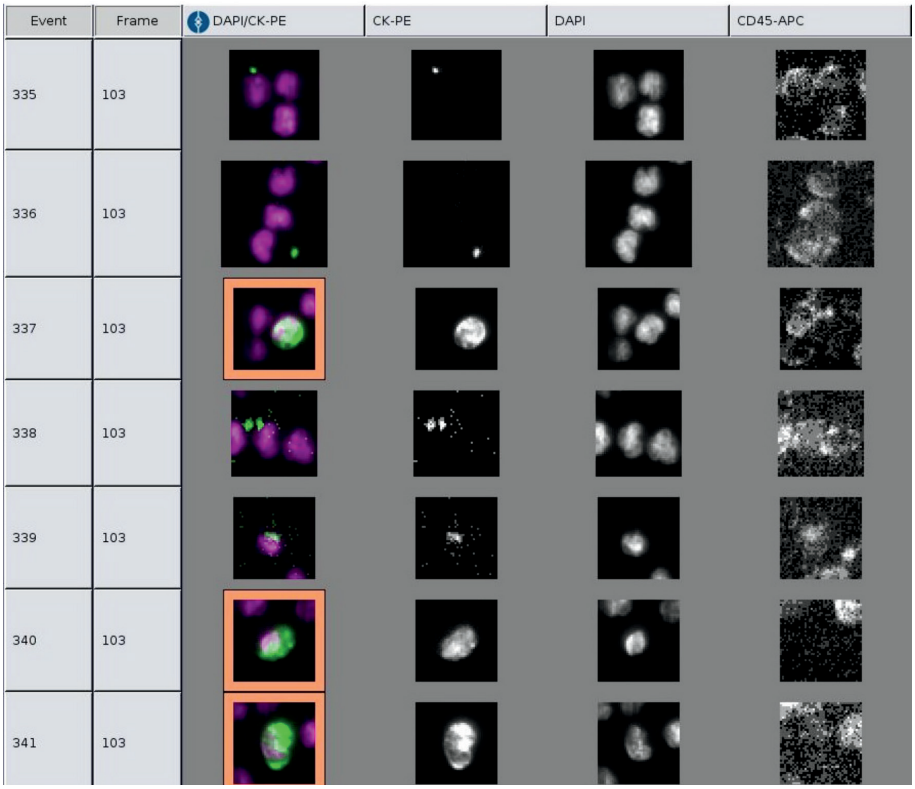

Figure 2. CellSearch thumbnail gallery. The software of the CellSearch CellTracks displays thumbnails of all objects that are positive for both DAPI and CK. Event 337, 340 and 341 shows a CTC: positive for DAPI and PE and negative for CD45. Note the weak CD45-staining of several white blood cells in event 340 and 341.

Frequency of CTC detected by the CellSearch system

The number of cells with features that are consistent with those of CTC detected with the CellSearch system in 7.5 mL of blood from healthy donors or patients with non-malignant diseases is remarkably low[3]. Lowering the stringency of the criteria to assign cells or objects increases the number of CTC detected in both controls and patients[36,39]. The limited number of controls tested and less strict criteria to assign objects as CTC is an important reason of the high number of CTC reported by new technologies for detection of CTC. In fact, our earlier work used flow cytometry as the platform to analyze the immunomagnetically enriched samples and the number of CTC detected in both controls and patients was clearly higher. This can be contributed to the less stringent criteria, such as a no cell morphology criterion[41,42].

Many new studies have reported the frequency of CTC detected by the CellSearch system, since the original report on the frequency of CTC detected with the CellSearch system in controls and patients with a variety of carcinomas[3]. Table 1 provides a summary of the frequency of CTC at various thresholds reported in these studies in several carcinomas, healthy donors and patients with non-malignant diseases. If CTC are to be used for the assessment of treatment targets to choose the most appropriate therapy, sufficient number of CTC will need to be available for detailed analysis. The heterogeneity of the tumor cells forces one to examine multiple individual cells and a minimum of 10-100 cells seems reasonable[25,26,43–45]. Table 1, however, shows that the number of patients (n) with sufficient number of CTC in 7.5 mL of blood for this purpose, is very low. Therefore, the number of CTC in larger volumes of blood was estimated by fitting the frequency distribution of CTC present in 7.5 mL of blood[46]. Figure 3 shows the frequency distribution of CTC detected in 7.5 mL of blood by the CellSearch system in patients with metastatic breast cancer (stair plot green line), metastatic colorectal cancer (stair plot blue line) and metastatic prostate cancer (stair plot red line). The solid lines show the best fit for this distribution and the dotted line is the 95% confidence level around this distribution. This figure shows that a 100-fold increase in blood volume is needed to detect CTC in all patients. All the blood will need to be analyzed to obtain sufficient number of CTC for characterization and guidance of therapy.

Table 1. Summary of CTC counts in 7.5 mL of blood from patients (n) with various types of metastatic carcinomas. It represents the percentage of patients (%) from the total group of patients (n) above a certain CTC cut-off, detected with the CellSearch System.

	% (n) ≥ 1 CTC		% (n) ≥ 2 CTC		% (n) ≥ 3 CTC		% (n) ≥ 10 CTC		% (n) ≥ 5 CTC		% (n) ≥ 50 CTC		% (n) ≥ 100 CTC		References
Subject															
Healthy	2	(330)	0.3	(330)	0	(185)	0	(330)	0	(330)	0	(330)	0	(330)	4,13,47-49
Non-malignant	5	(398)	1	(398)	0	(101)	0	(101)	0	(101)	0	(101)	0	(101)	4,47
Metastatic cancer type															
Bladder	47	(53)	35	(20)	-		25	(53)	5	(20)	0	(20)	0	(53)	50,51
Breast	55	(200)	53	(562)	33	(91)	38	(671)	32	(562)	18	(268)	12	(562)	4,47,52-55
Colorectal	48	(545)	34	(455)	32	(676)	18	(455)	12	(455)	0	(42)	0	(455)	8,56-59
Gastric	67	(27)	56	(27)	41	(27)	26	(27)	19	(27)	4	(27)	4	(27)	13
Lung, non- small cell	46	(57)	28	(117)	20	(20)	11	(57)	10	(20)	5	(20)	5	(20)	53,60,61
Lung, small cell	95	(38)	89	(62)	79	(38)	79	(38)	74	(38)	53	(38)	47	(38)	12,62
Ovarian	-		14	(216)	-		-		-		-		-		63
Pancreatic	35	(72)	19	(72)	15	(72)	8	(72)	7	(72)	3	(72)	3	(72)	64,65
Prostate	60	(149)	80	(40)	66	(95)	59	(314)	53	(40)	33	(40)	18	(40)	10,48, 49, 53, 66, 67

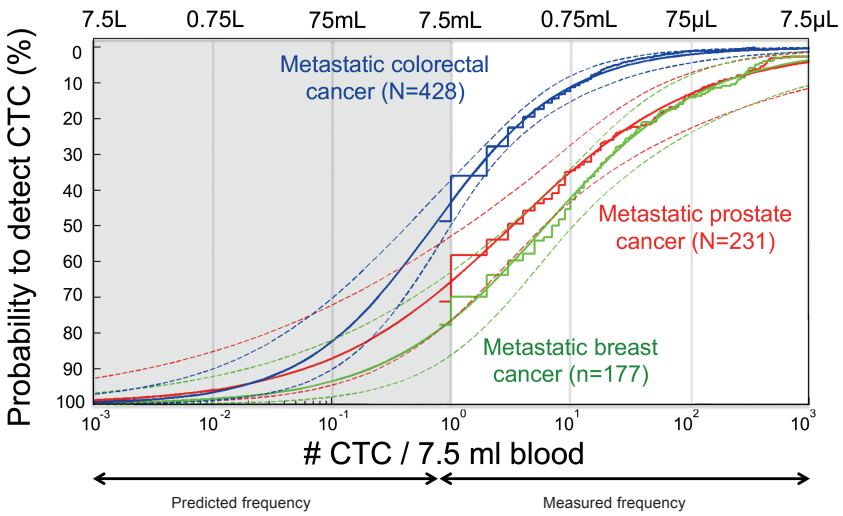

Figure 3. Frequency of CTC in metastatic colorectal prostate and breast cancer. Frequency was measured in 7.5ml of blood (right half of the figure) and predicted in larger blood volumes (left half of the figure). Extrapolation of number of CTC was performed by a log-logistic function (solid line) including 95% confidence interval (dashed lines) and fitted through the empirical cumulative distribution functions (stair plots) for metastatic breast, colon and prostate cancer. The fitted curve shows the blood volume that is needed (7.5 L) to detect the presence of CTC in all patients (100% probability) in a metastatic setting, using the CellSearch approach. Adapted figure from reference 46.

Relation between presence of CTC and survival

The presence of CTC is associated with a relative poor prognosis. This was demonstrated in prospective multicenter studies in metastatic breast camcer, colorectal cancer, prostate cancer and breast cancer[4,8,10]. A discrimination between patients with favorable CTC (<3 for colorectal cancer or <5 for breast and prostate cancer) and unfavorable CTC (>3 or >5) was made in the original papers reporting the results of these studies. In practice, a further discimination in patients with unfavorable CTC can be made when the actual peripheral blood tumor load is considered. This is illustrated by the Kaplan Meier plots in Figure 4. Blood is drawn before starting a new line of therapy and patients are devided in categories with 0 CTC, 1-4 CTC, 5-24 CTC and >25 CTC. The difference in survival curves become larger after the first cycles of therapy, as the CTC in those patients benefitting from therapy, are eliminated. A guide for the interpretation of changes in CTC is described in detail elsewhere[68]. Altogether, it is clear that all CTC will need to be eliminated for a treatment to be truly effective and prolong survival of the patient.

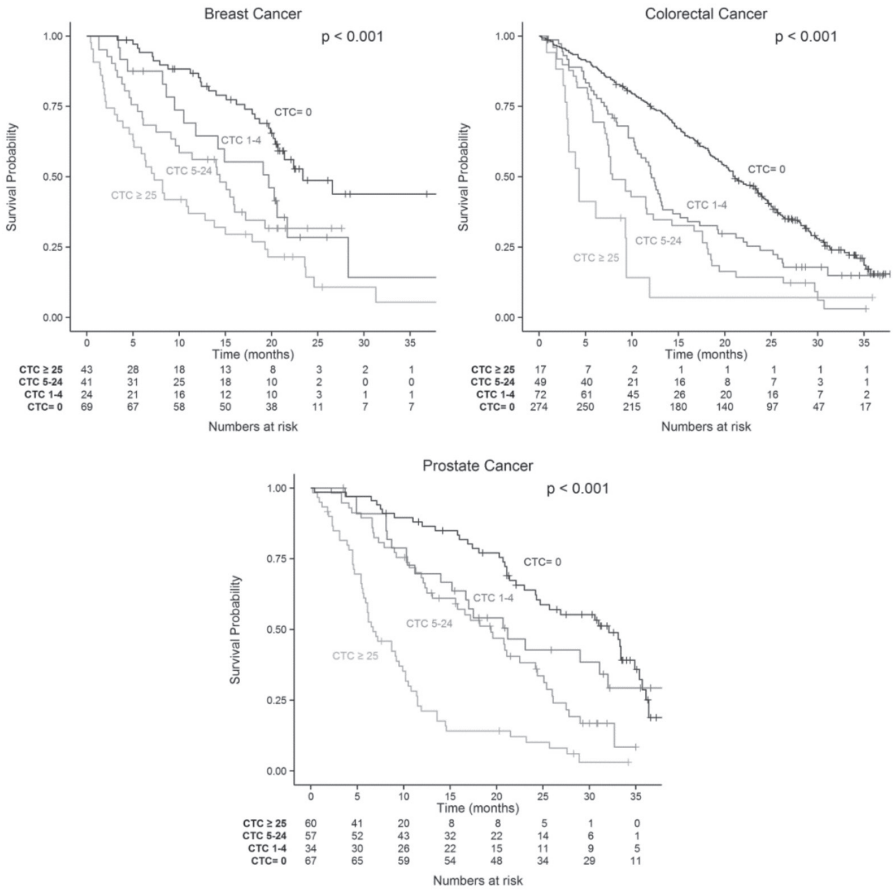

Figure 4. Kaplan-Meier plots of samples from metastatic breast (left), colon (right) and prostate (bottom) cancer patients with 0, 1-4, 5-24 and >25 CTC at the start of therapy. The number of patients at risk is listed at every time point of measurement.

Challenges in CTC identification

The potential of CTC detection and characterization has stimulated the interest of many investigators to develop new CTC platforms[69–82]. The challenge in identifying CTC lies in the detection of these rare cells in blood. In metastatic cancer patients, approximately 1 CTC per mL blood will be surrounded by approximately 5×10^6 white blood cells and 5×10^9 red blood cells[3,46]. Differences in the approaches taken to enrich and detect CTC have been reviewed extensively elsewhere[83–86].

One of the approaches we are currently evaluating, is filtration of blood to enrich for CTC that have a relatively large size and stiffness compared to blood cells[87,88]. In the optimization of this approach, we envisioned the ideal filter for CTC enrichment to be constructed of a stiff, flat material that is impervious to blood cells. To effectively pass blood collected in CellSave tubes, at least 100,000 regularly spaced 5 µm pores with a low porosity are needed[72,89]. To determine whether CTC have escaped the EpCAM immunomagnetic detection in CellSearch, we constructed a device that collects the blood discarded by the system after immunomagnetic selection of EpCAMhigh cells[88,90]. This blood, lacking EpCAMhigh cells, is then passed through a 64 mm^2 microsieve with 111,800 pores of 5 µm in diameter.

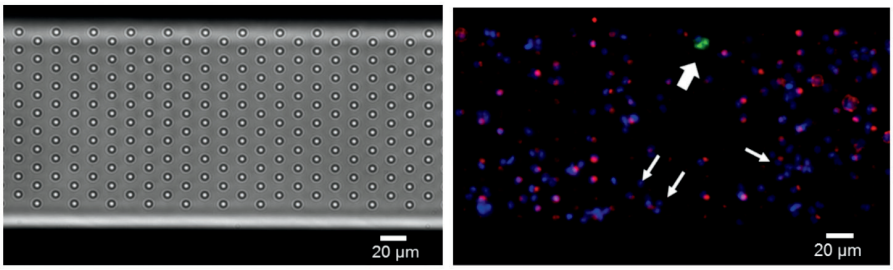

Figure 5. Cells from CellSearch Waste immunostained on a microsieve. Blood from a lung cancer patient was used for a CellSearch assay. After immunomagnetic selection, part of the sample was discarded by the system and used for filtration on a microsieve with 5 µm pores. Brightfield image of the sieve is shown in the left panel. The right panel shows the sieve with filtered sample. Cells were stained for nucleus (blue), cytokeratin C11 (green), and CD45 (red). Fat arrow points to a CTC, positive in CK. Small arrows point to the absent staining of cells, showing the difficulty of accounting for all cells on the sieve. Image taken on a fluorescence microscope with a 10x (0.45NA) objective.

The cells on the filter are immunostained to distinguish CTC from non-CTC and examined by fluorescent microscopy. Figure 5 shows an example of a microsieve; the upper panel shows a bright-field image of a section of a microsieve and the lower panel shows an overlay of fluorescent images of the nucleic acid dye DRAQ5 (blue), CD45-Brilliant Violet staining (red) and cytokeratin-PE staining (green). In the image, a CTC of a lung cancer patient is visible among many other cells. The figure also shows that not all nuclei stain with CD45 or cytokeratin. Currently, efforts are ongoing to identify the tissue of origin of these non-identified cells on the microsieve. These cells could still be leukocytes that either lost the CD45 antigen, or the fluorophore Brilliant Violet does not emits sufficient light to be detected,

or the cell is damaged and lost its cytoplasmic membrane. Other alternative explanations may be that these cells are not of hematopoietic lineage, such as endothelial cells, or that these are CTC that do not express the cytokeratins that are recognized by the C11 clone used to stain the cytokeratins. This lack of cytokeratin expression could be a result of the epithelial-mesenchymal transition (EMT) process[91].

Besides cytokeratins, EpCAM expression is used in the majority of CTC enrichment methods based on antibody-capture[92,93]. Yet EMT could downregulate this protein and other epithelial proteins, leading to a subpopulation of CTC that will be missed during enrichment or detection. CTC that are partially in EMT can co-express mesenchymal proteins, like vimentin, N-cadherin and O-cadherin[94,95]. The CellSearch system only uses a limited panel of cytokeratins for detection and changes in cytokeratin expression during EMT can therefore influence the CTC detection. An expanded panel of cytokeratins is of interest for complete detection and is applied in our search for low EpCAM expressing cells after filtration of the CellSearch waste. To find $EpCAM^{low}$ CTC subpopulations, novel antibodies are of increasing interest to be analyzed as an additional feasible selection marker. CTC populations with expression or lack of expression of epithelial and mesenchymal proteins, characterize the complexity and heterogeneity of CTC. The major challenge in addressing these problems is that it is unknown whether CTC are present in the blood sample. If they are present, their heterogeneity of unknown extend is encountered. It requests an increasing diversity in CTC detection and characterization in current and future methods.

Assessment of treatment targets in CTC

As described earlier, identification of CTC in the CellSearch system uses EpCAM expression for immunomagnetic selection and subsequently DNA, CK and CD45 staining for identification of the enriched cells. Less strict qualifications for CTC definitions, omitting for instance the DNA-positive or CD45-negative qualification, increases the frequency of objects counted as CTC in patients and controls[46]. $EpCAM^{high}/CK^{high}$ CTC can be differentiated into intact CTC, CTC fragments and CTC microparticles. The presence of all these are associated with a relatively short survival in castrate resistant prostate cancer[36]. However, intact CTC containing DNA can provide more information, as they are receptiive to molecular and phenotypic characterization. RNA or DNA from CTC can offer a representation of the genetic composition of the tumor and may be especially

useful when a tumor biopsy is unavailable. Cell sorting of CTC after CellSearch analysis showed that almost 45% of the exomes in single CTC could be sequenced and whole genome amplification allows for variant calling in single CTC[34].

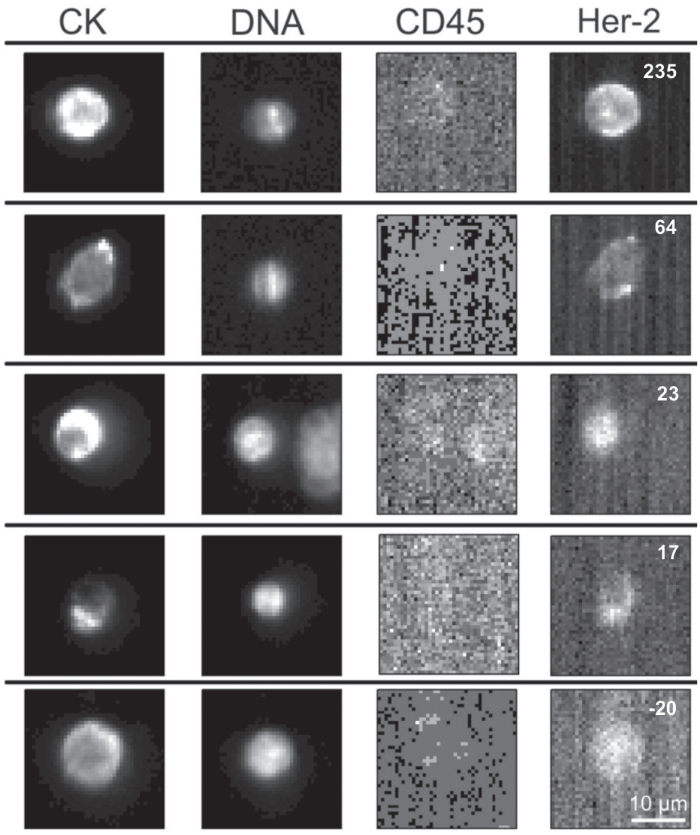

Figure 6. Example of five CTC from five different patients. Fluorescence of CTC Her-2 expression (right column) is quantified by the number in upper right corner. A higher positive number represents a higher Her-2 expression, whereas a negative number (bottom picture) represents no Her-2 expression on that CTC. The scale bar applies to all images. Adapted figure from reference 24.

For breast cancer patients, status of the membrane protein Her-2 may guide their therapy and is of great value for personalized treatment. Usually, tumor biopsies taken at the time of surgery are analyzed for their Her-2 status, but may not be representative for the tumor at the time of metastasis. CTC may circumvent this problem and allows real-time determination of the Her-2 status of the tumor. It can be subjective to determine whether or not a protein like Her-2 is expressed and at what level. Tools will be needed

to quantify the actual expression levels to reliably investigate the relation to the response of therapy targeting the Her-2 receptor. Figure 6 shows an example of an approach to quantify Her-2 expression on CTC. An automated algorithm is used to identify CTC and provides a numerical value to the level of Her-2 expression on CTC. It's quite obvious that the accuracy of Her-2 expression and the ability to assess its heterogeneity will improve with the number of CTC that are detected. Feasibility for assessment of treatment targets on CTC has been demonstrated for a variety of treatment targets at the protein and genetic level. This supports the notion that CTC indeed can be used to guide personalized therapy in the future, provided that CTC indeed can be isolated from the patient[23,25–27,34,39,45].

Outlook

Treatment of cancer is evolving from chemotherapy towards a more personalized approach, with drugs that recognize specific targets. To define the presence of specific targets, an analysis of the tumor is required at the start of therapy. CTC are likely representatives of the tumor to be treated and can therefore be used as a liquid biopsy. However, sufficient numbers of CTC are required to obtain a representative picture. To arrive at a sufficient number of CTC, a new approach is being explored by the European Consortium "CTC Therapeutic APheresis" (*http://www.utwente.nl/tnw/ctctrap/*). The concept of this approach is presented in Figure 7. The CTC-Trap combines immuno-capture and size-based separation of CTC from their hematopoietic background. A large volume of blood is transported through a matrix and then reintroduced in the body, while CTC are captured in the matrix. After elution, CTC can be individually isolated for further characterization. This can, for example, assess the likelihood that certain therapies will be effective. The CTC-Trap is expected to deliver a complete platform to capture, enumerate and characterize CTC. Detection of all CTC in blood will change the current methods of diagnosis and treatment for patients with known and unknown metastatic disease.

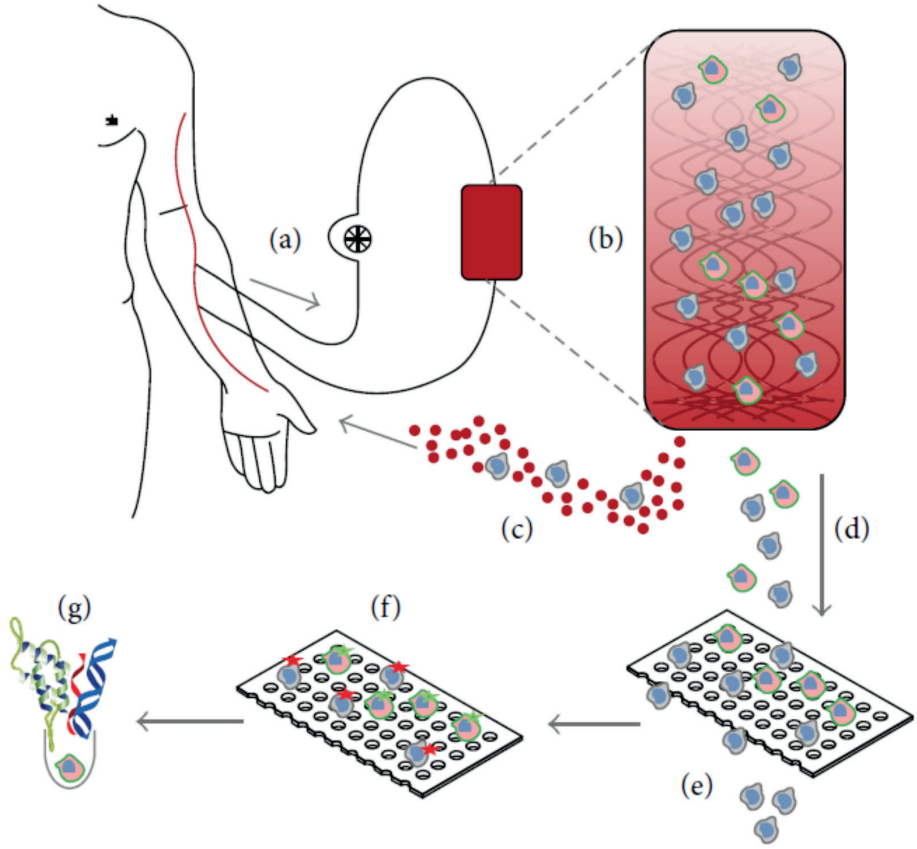

Figure 7. Schematic representation of the CTC-Trap. Blood from a patient (a) is passed through a functionalized 3D matrix (b). The porous matrix can withstand up to 5 L of blood flow. In this matrix are one or more specific antibodies present for CTC capture. A continuous blood flow without cells of interest is circled back to the patient (c). Retained cells are eluted from the matrix (d) and will be filtered through 1-5 µm pores to reduce hematopoietic background (e). Cells retained on the filter can be used for immunofluorescent staining to discriminate CTC from non-CTC (f) and subsequently be used for isolation of single CTC for additional molecular characterization, like protein, RNA and DNA analysis (g).

References

1. Ashworth, T. R. A case of cancer in which cells similar to those in the tumours were seen in the blood after death. Aust Med J 14, 146–147 (1869).
2. Fidler, I. . The pathogenesis of cancer metastasis: the 'seed and soil' hypothesis revisited. Nat Rev Cancer 3, 453–458 (2003).
3. Allard, W. J. et al. Tumor cells circulate in the peripheral blood of all major carcinomas but not in healthy subjects or patients with nonmalignant diseases. Clin. cancer Res. 10, 6897–904 (2004).
4. Cristofanilli, M., Budd, G., Ellis, M. & A. Circulating tumor cells, disease progression, and survival in metastatic breast cancer. Engl. J. 351, 781–791 (2004).

5. Cristofanilli, M. et al. Circulating tumor cells: a novel prognostic factor for newly diagnosed metastatic breast cancer. J. Clin. Oncol. 23, 1420–30 (2005).

6. Hayes, D. F. et al. Tumor Cells at Each Follow-up Time Point during Therapy of Metastatic Breast Cancer Patients Predict Progression-Free and Overall Survival. 12, 4218–4224 (2006).

7. Budd, G. T. et al. Circulating tumor cells versus imaging--predicting overall survival in metastatic breast cancer. Clin. cancer Res. 12, 6403–9 (2006).

8. Cohen, S. J. et al. Relationship of Circulating Tumor Cells to Tumor Response, Progression-Free Survival, and Overall Survival in Patients With Metastatic Colorectal Cancer. J. Clin. Oncol. 26, 3213–3221 (2008).

9. Cohen, S. J. et al. Prognostic significance of circulating tumor cells in patients with metastatic colorectal cancer. Ann. Oncol. 20, 1223–9 (2009).

10. de Bono, J. S. et al. Circulating Tumor Cells Predict Survival Benefit from Treatment in Metastatic Castration-Resistant Prostate Cancer. Clin. Cancer Res. 14, 6302–6309 (2008).

11. Krebs, M. G. et al. Analysis of circulating tumor cells in patients with non-small cell lung cancer using epithelial marker-dependent and -independent approaches. J. Thorac. Oncol. 7, 306–15 (2012).

12. Hiltermann, T. J. N. et al. Circulating tumor cells in small-cell lung cancer: a predictive and prognostic factor. Ann. Oncol. 23, 2937–42 (2012).

13. Hiraiwa, K. et al. Clinical significance of circulating tumor cells in blood from patients with gastrointestinal cancers. Ann. Surg. Oncol. 15, 3092–100 (2008).

14. Kurihara, T. et al. Detection of circulating tumor cells in patients with pancreatic cancer: a preliminary result. J. Hepatobiliary. Pancreat. Surg. 15, 189–95 (2008).

15. Poveda, A. et al. Circulating tumor cells predict progression free survival and overall survival in patients with relapsed/recurrent advanced ovarian cancer. Gynecol. Oncol. 122, 567–572 (2011).

16. Rink, M. et al. Detection of circulating tumour cells in peripheral blood of patients with advanced non-metastatic bladder cancer. BJU Int. 107, 1668–75 (2011).

17. Gazzaniga, P. et al. Prognostic value of circulating tumor cells in nonmuscle invasive bladder cancer: a CellSearch analysis. Ann. Oncol. 23, 2352–6 (2012).

18. Naoe, M. et al. Detection of circulating urothelial cancer cells in the blood using the CellSearch System. Cancer 109, 1439–45 (2007).

19. Strijbos, M. H. et al. Circulating endothelial cells, circulating tumour cells, tissue factor, endothelin-1 and overall survival in prostate cancer patients treated with docetaxel. Eur. J. Cancer 46, 2027–35 (2010).

20. Rowand, J. L. et al. Endothelial Cells in Peripheral Blood of Healthy Subjects and Patients with Metastatic Carcinomas. 113, 105–113 (2007).

21. Damani, S. et al. Characterization of circulating endothelial cells in acute myocardial infarction. Sci. Transl. Med. 4, 126ra33 (2012).

22. Rao, C. et al. Circulating melanoma cells and survival in metastatic melanoma. Int. J. Oncol. 38, 755–60 (2011).

23. Smerage, J. B. et al. Monitoring apoptosis and Bcl-2 on circulating tumor cells in patients with metastatic breast cancer. Mol. Oncol. 7, 680–92 (2013).

24. Ligthart, S. T. et al. Unbiased quantitative assessment of Her-2 expression of circulating tumor cells in patients with metastatic and non-metastatic breast cancer. Ann. Oncol. 1–8 (2012). doi:10.1093/annonc/mds625

25. Swennenhuis, J. F., Tibbe, A. G. J., Levink, R., Sipkema, R. C. J. & Terstappen, L. W. M. M. Characterization of circulating tumor cells by fluorescence in situ hybridization. Cytometry. A 75, 520–7 (2009).

26. Attard, G. et al. Characterization of ERG, AR and PTEN gene status in circulating tumor cells from patients with castration-resistant prostate cancer. Cancer Res. 69, 2912–8 (2009).

27. de Bono, J. S. et al. Potential applications for circulating tumor cells expressing the insulin-like growth factor-I receptor. Clin. cancer Res. 13, 3611–6 (2007).
28. Society, A. C. Cancer Facts & Figures 2013. (2013).
29. Ferlay, J. et al. Estimates of the cancer incidence and mortality in Europe in 2006. Ann. Oncol. 18, 581–92 (2007).
30. Coumans, F. A., Siesling, S. & Terstappen, L. W. Detection of cancer before distant metastasis. BMC Cancer 13, 283 (2013).
31. Rao et al. Expression of epithelial cell adhesion molecule in carcinoma cells present in blood and primary and metastatic tumors. 27, 49–57 (2005).
32. Terstappen, L., Rao, C. & Liberti, P. Increased separation efficiency via controlled aggregation of magnetic nanoparticles. USpatent 6,551,843 B1 (2003).
33. Smirnov, D. a et al. Global gene expression profiling of circulating tumor cells. Cancer Res. 65, 4993–7 (2005).
34. Swennenhuis, J. F., Reumers, J., Thys, K., Aerssens, J. & Terstappen, L. W. Efficiency of whole genome amplification of Single Circulating Tumor Cells enriched by CellSearch and sorted by FACS. Genome Med. 5, 106 (2013).
35. Larson, C. J. et al. Apoptosis of circulating tumor cells in prostate cancer patients. Cytom. Part A 62, 46–53 (2004).
36. Coumans, F. A. W., Doggen, C. J. M., Attard, G., de Bono, J. S. & Terstappen, L. W. M. M. All circulating EpCAM+CK+CD45- objects predict overall survival in castration-resistant prostate cancer. Ann. Oncol. 21, 1851–7 (2010).
37. Tibbe, A. G. J., Miller, M. C. & Terstappen, L. W. M. M. Statistical Considerations for Enumeration of Circulating Tumor Cells. 162, 154–162 (2007).
38. Kraan, J. et al. External quality assurance of circulating tumor cell enumeration using the CellSearch(®) system: a feasibility study. Cytometry B. Clin. Cytom. 80, 112–8 (2011).
39. Ligthart, S. T. et al. Unbiased and automated identification of a circulating tumour cell definition that associates with overall survival. PLoS One 6, e27419 (2011).
40. Ligthart, S. T. et al. Circulating Tumor Cells Count and Morphological Features in Breast, Colorectal and Prostate Cancer. PLoS One 8, e67148 (2013).
41. Racila, E. et al. Detection and characterization of carcinoma cells in the blood. Proc. Natl. Acad. Sci. U. S. A. 95, 4589–94 (1998).
42. Terstappen, L. W. M. M., Rao, C., Gross, S. & Weiss, A. J. Peripheral blood tumor cell load reflects the clinical activity of the disease in patients with carcinoma of the breast. Int. J. Oncol. 17, 573–8 (2000).
43. Meng, S. et al. HER-2 gene amplification can be acquired as breast cancer progresses. Proc. Natl. Acad. Sci. U. S. A. 101, 9393–8 (2004).
44. Meng, S. et al. uPAR and HER-2 gene status in individual breast cancer cells from blood and tissues. Proc. Natl. Acad. Sci. U. S. A. 103, 17361–5 (2006).
45. Hayes, D. F. et al. Monitoring expression of HER-2 on circulating epithelial cells in patients with advanced breast cancer. Int. J. Oncol. 21, 1111–7 (2002).
46. Coumans, F. A. W., Ligthart, S. T., Uhr, J. W. & Terstappen, L. W. M. M. Challenges in the enumeration and phenotyping of CTC. Clin. Cancer Res. 18, 5711–8 (2012).
47. Jiang, Z. F. et al. Circulating tumor cells predict progression-free and overall survival in Chinese patients with metastatic breast cancer, HER2-positive or triple-negative (CBCSG004): a multicenter, double-blind, prospective trial. Ann. Oncol. 24, 2766–72 (2013).

48. Thalgott, M. et al. Detection of circulating tumor cells in different stages of prostate cancer. J. Cancer Res. Clin. Oncol. 139, 755–63 (2013).

49. Resel Folkersma, L., San José Manso, L., Galante Romo, I., Moreno Sierra, J. & Olivier Gómez, C. Prognostic significance of circulating tumor cell count in patients with metastatic hormone-sensitive prostate cancer. Urology 80, 1328–32 (2012).

50. Okegawa, T., Hayashi, K., Hara, H., Nutahara, K. & Higashihara, E. Immunomagnetic quantification of circulating tumor cells in patients with urothelial cancer. Int. J. Urol. 17, 254–8 (2010).

51. Gallagher, D. J. et al. Detection of circulating tumor cells in patients with urothelial cancer. Ann. Oncol. 20, 305–8 (2009).

52. Liu, Y. et al. Circulating tumor cells in HER2-positive metastatic breast cancer patients: a valuable prognostic and predictive biomarker. BMC Cancer 13, 202 (2013).

53. Farace, F. et al. A direct comparison of CellSearch and ISET for circulating tumour-cell detection in patients with metastatic carcinomas. Br. J. Cancer 105, 847–53 (2011).

54. Pierga, J.-Y. et al. Circulating tumor cells and brain metastasis outcome in patients with HER2-positive breast cancer: the LANDSCAPE trial. Ann. Oncol. 24, 2999–3004 (2013).

55. Tryfonidis, K. et al. A multicenter phase I-II study of docetaxel plus epirubicin plus bevacizumab as first-line treatment in women with HER2-negative metastatic breast cancer. Breast 22, 1171–7 (2013).

56. Mostert, B. et al. KRAS and BRAF mutation status in circulating colorectal tumor cells and their correlation with primary and metastatic tumor tissue. Int. J. Cancer 133, 130–41 (2013).

57. Kaifi, J. T. et al. Circulating tumor cells are associated with diffuse spread in stage IV colorectal cancer patients. Cancer Biol. Ther. 14, (2013).

58. Kuboki, Y. et al. Circulating tumor cell (CTC) count and epithelial growth factor receptor expression on CTCs as biomarkers for cetuximab efficacy in advanced colorectal cancer. Anticancer Res. 33, 3905–10 (2013).

59. Sastre, J. et al. Prognostic value of the combination of circulating tumor cells plus KRAS in patients with metastatic colorectal cancer treated with chemotherapy plus bevacizumab. Clin. Colorectal Cancer 12, 280–6 (2013).

60. Juan, O. et al. Prognostic significance of circulating tumor cells in advanced non-small cell lung cancer patients treated with docetaxel and gemcitabine. Clin. Transl. Oncol. (2013). doi:10.1007/s12094-013-1128-8

61. Krebs, M. G. et al. Evaluation and prognostic significance of circulating tumor cells in patients with non-small-cell lung cancer. J Clin Oncol. 29, 1556–63 (2011).

62. Naito, T. et al. Prognostic impact of circulating tumor cells in patients with small cell lung cancer. J. Thorac. Oncol. 7, 512–9 (2012).

63. Poveda, A. et al. Circulating tumor cells predict progression free survival and overall survival in patients with relapsed/recurrent advanced ovarian cancer. Gynecol. Oncol. 122, 567–72 (2011).

64. Khoja, L. et al. A pilot study to explore circulating tumour cells in pancreatic cancer as a novel biomarker. Br. J. Cancer 106, 508–16 (2012).

65. Khan, M. S. et al. Circulating tumor cells and EpCAM expression in neuroendocrine tumors. Clin. Cancer Res. 17, 337–45 (2011).

66. Amato, R. J. et al. Epithelial cell adhesion molecule-positive circulating tumor cells as predictive biomarker in patients with prostate cancer. Urology 81, 1303–7 (2013).

67. Magbanua, M. J. M. et al. Isolation and genomic analysis of circulating tumor cells from castration resistant metastatic prostate cancer. BMC Cancer 12, 78 (2012).

68. Coumans, F. A. W., Ligthart, S. T. & Terstappen, L. W. M. M. Interpretation of changes in circulating tumor cell counts. Transl. Oncol. 5, 486–91 (2012).

69. Hou, H. W. et al. Isolation and retrieval of circulating tumor cells using centrifugal forces. Sci. Rep. 3, 1259 (2013).

70. Ozkumur, E. et al. Inertial focusing for tumor antigen-dependent and -independent sorting of rare circulating tumor cells. Sci. Transl. Med. 5, 179ra47 (2013).

71. Choi, H. et al. Label-Free DC Impedance-based Microcytometer for Circulating Rare Cancer Cell Counting. Lab Chip 13, 970–7 (2013).

72. Coumans, F. A. W., van Dalum, G., Beck, M. & Terstappen, L. W. M. M. Filter characteristics influencing circulating tumor cell enrichment from whole blood. PLoS One 8, e61770 (2013).

73. Park, T. J. et al. Development of label-free optical diagnosis for sensitive detection of influenza virus with genetically engineered fusion protein. Talanta 89, 246–52 (2012).

74. Issadore, D. et al. Ultrasensitive clinical enumeration of rare cells ex vivo using a micro-hall detector. Sci. Transl. Med. 4, 141ra92 (2012).

75. Kim, M. S. et al. SSA-MOA: a novel CTC isolation platform using selective size amplification (SSA) and a multi-obstacle architecture (MOA) filter. Lab Chip 12, 2874–80 (2012).

76. Nagrath, S. et al. Isolation of rare circulating tumour cells in cancer patients by microchip technology. Nature 450, 1235–9 (2007).

77. Stott, S. L. et al. Isolation of circulating tumor cells using a microvortex-generating herringbone-chip. Proc. Natl. Acad. Sci. U. S. A. 107, 18392–7 (2010).

78. Talasaz, A. H. et al. Isolating highly enriched populations of circulating epithelial cells and other rare cells from blood using a magnetic sweeper device. Proc. Natl. Acad. Sci. U. S. A. 106, 3970–5 (2009).

79. Kirby, B. J. et al. Functional characterization of circulating tumor cells with a prostate-cancer-specific microfluidic device. PLoS One 7, e35976 (2012).

80. Lin, H. K. et al. Portable filter-based microdevice for detection and characterization of circulating tumor cells. Clin. Cancer Res. 16, 5011–8 (2010).

81. Hughes, A. D. et al. Microtube device for selectin-mediated capture of viable circulating tumor cells from blood. Clin. Chem. 58, 846–53 (2012).

82. Adams, D., Zhu, P. & Makarova, O. The systematic study of circulating tumor cell isolation using lithographic microfilters. RSC Adv. 4, 4334–4342 (2014).

83. Gorges, T. M. & Pantel, K. Circulating tumor cells as therapy-related biomarkers in cancer patients. Cancer Immunol. Immunother. (2013). doi:10.1007/s00262-012-1387-1

84. Balic, M., Lin, H. & Williams, A. Progress in circulating tumor cell capture and analysis: implications for cancer management. Expert Rev. Mol. Diagn. 12, 303–312 (2012).

85. Pantel, K., Brakenhoff, R. H. & Brandt, B. Detection, clinical relevance and specific biological properties of disseminating tumour cells. Nat. Rev. Cancer 8, 329–40 (2008).

86. Barradas, A. & Terstappen, L. Towards the Biological Understanding of CTC: Capture Technologies, Definitions and Potential to Create Metastasis. Cancers (Basel). 5, 1619–1642 (2013).

87. van Dalum, G., Lenferink, A. T. M. & Terstappen, L. W. M. M. Detection of EpCAM negative circulating tumor cells in CellSearch waste [abstract 3846]. in Proceedings of the 104th Annual Meeting of the American Association for Cancer Research Apr 6-10, (2013).

88. de Wit, S. et al. Circulating Tumor Cells in Metastatic Lung Cancer enriched by EpCAM expression and physical characteristics [abstract 4825]. in Proceedings of the 105th Annual Meeting of the American Association for Cancer Research (2014).

89. Coumans, F. A. W., van Dalum, G., Beck, M. & Terstappen, L. W. M. M. Filtration parameters influencing circulating tumor cell enrichment from whole blood. PLoS One 8, e61774 (2013).

90. van Dalum, G., Lenferink, A. T. M. & Terstappen, L. W. M. M. Detection of EpCAM negative Circulating Tumor Cells in CellSearch waste [abstract 3846]. in Proceedings of the 104th Annual Meeting of the American Association for Cancer Research (2013).

91. Joosse, S. A. et al. Changes in keratin expression during metastatic progression of breast cancer: impact on the detection of circulating tumor cells. Clin. Cancer Res. 18, 993–1003 (2012).

92. Krebs, M. G. et al. Molecular analysis of circulating tumour cells—biology and biomarkers. Nat. Rev. Clin. Oncol. (2014). doi:10.1038/nrclinonc.2013.253

93. Friedlander, T. W., Premasekharan, G. & Paris, P. L. Looking back, to the future of circulating tumor cells. Pharmacol. Ther. (2013). doi:10.1016/j.pharmthera.2013.12.011

94. Kallergi, G. et al. Epithelial to mesenchymal transition markers expressed in circulating tumour cells of early and metastatic breast cancer patients. Breast Cancer Res. 13, R59 (2011).

95. Armstrong, A. J. et al. Circulating tumor cells from patients with advanced prostate and breast cancer display both epithelial and mesenchymal markers. Mol. Cancer Res. 9, 997–1007 (2011).


1

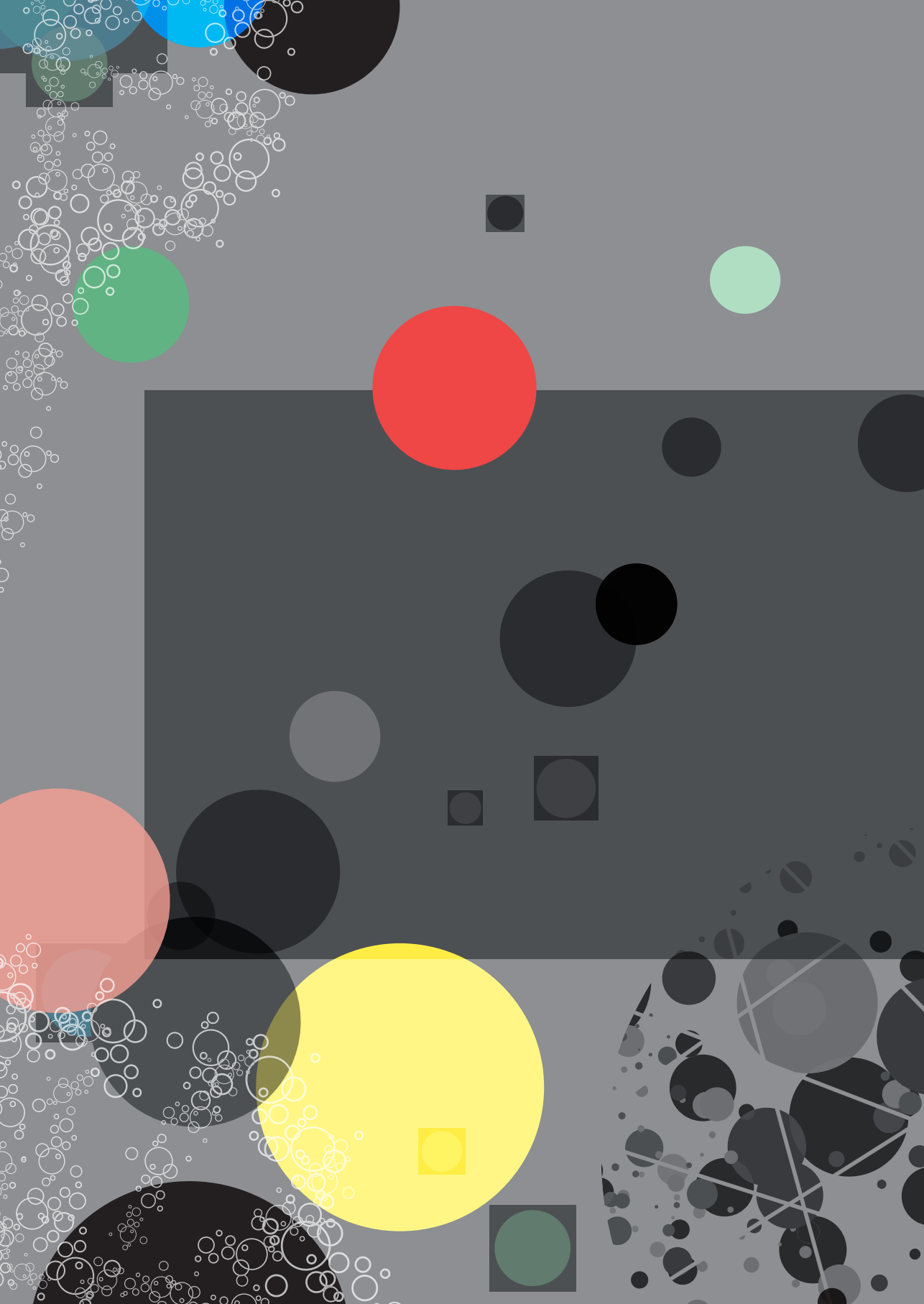

Chapter 2

CTC Therapeutic Apheresis – Novel tools to fight cancer

This dissertation is written during the project Circulating Tumor Cells TheRapeutic APheresis: a novel biotechnology enabling personalized therapy for all cancer patients, or CTC-Trap in short. This four year European project was funded by the FP7-HEALTH-2012-INNOVATION (grant #305341) and comprises of collaboration between 11 universities, research institutions and small & medium-sized enterprises. This consortium shares the common effort to use the therapeutic apheresis to collect circulating tumor cells from peripheral blood in cancer patients.

Background

In order to successfully treat cancer patients, the selected therapy needs to be fitted to each patient personally. During formation, growth and spread of cancer, alterations in the cells develop, creating heterogeneous populations of cancer cells with increasing potential to become resistant to therapy. This demand for personalized therapy raises the need for actual, detailed information about the cancer cells and its heterogeneity. Since circulating tumor cells (CTC) provide a liquid biopsy, with real insight to the current status of the (metastasized) tumor, these cells can meet the necessity for improving personalized therapy. However, since CTC are rare and only found in low numbers in metastatic cancer patients, their detected amount must increase to create a representative picture. To reach these required numbers, the amount of sample volume – which is usually only several mL – must be increased. An analysis of a significant larger blood volume, or even the whole 5 L, will detect CTC in all cancer patients with macro and micro-metastatic disease.

Objectives

The aim of the CTC-Trap project is to increase the blood volume for detection and analysis of all CTC. The intent is to achieve this by therapeutic apheresis. Therapeutic apheresis is used for selectively removing or collecting cells or other components and has a broad application in many (onco) hematologic malignancies. To create a marketable technology from this idea, a large group of companies, research institutes and universities from all over Europe, work together to develop and validate this new therapeutic apheresis device for isolation and molecular characterization of CTC on the single cell level. The application of CTC-Trap could lead to a radical change in the treatment of solid tumors and will provide new insights in the heterogeneity and development of cancer in individual patients and its translation into personalized treatment applications.

To create the CTC-Trap, the project is divided into three objectives:

1. Develop a column that can be attached to the patient via an external apheresis device to remove and harvest CTC. CTC will be captured based on size and/or antigen expression by antibody-coated absorbers and the blood void of tumor cells will be reintroduced back into the patient to maximize CTC recovery from individual patients. Also, increase the number of CTC detected by characterizing CTC that have escaped the EpCAM immunomagnetic detection of the CellSearch system.

2. Develop complete phenotyping and genotyping methods for CTC, which encompasses the isolation of single CTC for proliferation studies and the isolation, amplification and sequencing of DNA and RNA from single CTC. This will show heterogeneity in each individual and cancer type, and might lead to novel treatment or prediction targets.

3. Validate the new CTC-Trap in a clinical setting for safety and efficacy on a group of cancer patients, followed by a clinical pilot study to determine whether CTC can be identified and molecular characterized. Compare the apheresis with the CellSearch system in several cancer types to determine the improvement in the frequency of patients in which CTC can be subjected for molecular analysis.

Work packages and participants

The aim of the CTC-Trap project is to develop new tools to enable the improvement of disease management of cancer patients on a personal level and to improve the quality of care while reducing costs. In four years, the tools to achieve this goal will be developed by the small & medium-sized enterprises (SME) with assistance of the academic institutes and subsequently tested and evaluated in a clinical setting by the academic collaborators.

In total, the project comprises of 9 work packages (WP), dividing the three objectives over the collaborators. The department of Medical Cell BioPhysics of the *University of Twente* (The Netherlands) acts as coordinator for communication and decision making within the consortium and acts as a liaison between the partners and European commission **(WP9)**.

In WP1 and 2, the tools for capturing CTC are developed, thereby addressing the first objective of the project. **WP1**, led by SME *Leukocare* (Germany), focuses on the CTC-apheresis device by coupling a CTC-

trapping molecule to a column. This column captures the CTC and allows the remaining erythrocytes, leukocytes and platelets to be led back to the patient. After one hour, a large volume of blood (at least 2.5 L) passed the column and the captured CTC will be eluted for molecular analysis. Testing of scale models and in-vitro systems will be performed at the *University of Twente*, and testing of the CTC-Trap in-vivo in a clinical setting in collaboration with the clinical partners. In **WP2**, under coordination of SME *Aquamarijn Micro Filtration* (The Netherlands), CTC that are not captured by the CellSearch system are being identified. They will develop a device that can be attached to the CellSearch Autoprep for capturing the blood discarded after EpCAM immunomagnetic selection. After this, systems for filtration of blood and detection of the CTC will be developed to determine the immunophenotype, frequency and molecular profile of these CTC. This will also be used for optimization of the column developed in WP1. Development of these devices and protocols are performed in collaboration with the *University of Twente*. Finally, the complete system will be tested and validated at each clinical site.

In WP3 through 6 the research goals of the second objective are addressed, focusing on characterizing of single CTC. **WP3**, which is led by SME *Asper Biotech* (Estonia), will develop technological tools to profile individual CTC ($EpCAM^{high}$ and $EpCAM^{low}$ CTC) on the molecular level. This encompasses the isolation of single CTC and the DNA amplification from a single CTC. Furthermore, the sequencing of single cell DNA will be developed, optimized and validated. All clinical sites will submit CTC samples from patients for DNA analysis. **WP5**, led by research center *Institute of Cancer Research* – Royal Cancer Hospital (United Kingdom), focuses on processing and analyzing the data gathered from these single CTC. Data tools will be developed to efficiently process and interpret DNA sequencing data by developing quality controls and validation tests of these approaches. In **WP4**, led by SME *AcZon* (Italy), immunophenotyping of CTC is the goal. There is a special emphasis on those antigens that are associated with presently available and new drug targets. This requires first the development of a targeting system, using fluorescent probes based on silica NanoParticles, which will be developed and optimized with intra-laboratory and inter-laboratory validation tests. In **WP6** the aim was to define optimal conditions for proliferation of CTC in animal models to facilitate the ability to test the best treatment choice for the patient. This will be done under coordination of the *Biological Research* Centre – *Hungary Academy of Science* (Hungary). Protocols for handling, freezing and recovering CTC samples from patients will be developed, as well as the optimization of culture conditions for culturing these tumor cells with in-vivo mouse models.

The third objective describes the clinical application of the developed tools in the project. Research institute *Instituto Oncologico Veneto* (Italy) is the leading participant in **WP7**, in close collaboration with the other clinical sites: *Institut Gustave Roussy* (France), the *Heinrich-Heine-Universität Düsseldorf* (Germany), *Ludwig-Maximilians-Universität München* (Germany) and *Institute of Cancer Research – Royal Cancer Hospital*. WP7 focuses entirely on the clinical validation of the developed tools in WP1 (CTC-Trap) and WP2 (detection of $EpCAM^{low}$ CTC) that will be evaluated in a number of patients with metastatic breast and metastatic prostate cancer. Patients undergoing the CTC-apheresis will be tested again sometime after the procedure to determine if therapeutic benefit has been achieved. The CTC-Trap will be compared to the CellSearch in terms of CTC recovery rate, yield, phenotype and genotype. The final work package, **WP8**, led by the department of Health Technology and Service Research of the *University of Twente*, focuses on the impact and the optimal exploitation of the CTC-Trap in health economic models.

Four years later

From 2012 until 2016 the consortium worked on the 9 work packages, which were divided into 32 deliverables and 17 milestones to keep track of the progress over the years. The website *http://www.utwente.nl/tnw/ctctrap/* contains all the tools and protocols developed during the program and is publicly accessible for all interested parties. It is clear that the CTC-Trap project has been a great endeavor in development, research and collaboration. Because of the interesting outlook this project has shown us, part of the research will be continued in the EU IMI program 'CANCER-ID'. On 1 September 2016 the CTC-Trap program came to conclusion and its outcome can be aligned with the premium objectives.

The main goals in the project were the development of a novel CTC capture and identification method and test this in the clinic on metastatic cancer patients. This was aimed by developing a CTC-Trap column attached to an apheresis system in order to capture all CTC that are present in the patient. This outcome would be compared to the CTC from the CellSearch and the newly developed adjacent filtration system to capture the CTC that are missed during CellSearch.

During development of the in-vivo CTC-Trap column it became clear that alternative methods for CTC enrichments had to be pursued. The coupling molecules for capturing CTC in the column itself could not be used for in-vivo diagnostics and two years into the program an alternative in-vitro method

was presented: the Diagnostic LeukApheresis (DLA). This generates a small volume of mononuclear cell fractions – including CTC in a large background of leukocytes – which represents in total 1 to 2 L of blood. The aim was to pass this product over the CTC-Trap column for CTC capture. However, after extensive evaluation, the developed column did not enrich CTC sufficiently enough to proceed to patients. Therefore, an alternative depletion method to remove the major fraction of the leukocytes in the DLA product was evaluated and accepted. This RosetteSep™ depletion method targets the unwanted leukocytes with a cocktail of antibodies to form tetrameric antibody complexes, so-called rosettes, with red blood cells. The increased density of these complexes makes it able to separate them by centrifugation from CTC, which remain untouched and ready for downstream analysis. A more detailed comparison between the three methods used in this program is listed in Table 1.

Table 1. Description of the three methods used in the CTC-Trap program for CTC isolation.

	CellSearch	CTC-Trap	RosetteSep™
Selection	Positive	Positive	Negative
Target	EpCAM	EpCAM (clone VU1D9)	CD2, CD16, CD19, CD36, CD38, CD45, CD66b, glycophorin A
Isolation	Immunomagnetic	Immunophenotypic	Density
Recovery CTC	90% for $EpCAM^{high}$ 2% for $EpCAM^{low}$	2% for $EpCAM^{high}$	60%
Depletion leukocytes	3.5-4 log	1.7 log	3.5-4 log
Enrichment CTC	40x for $EpCAM^{high}$ 4x for $EpCAM^{low}$	1x for $EpCAM^{high}$	10x
Labelling of CTC and cells	Fixed, but one channel remains available for additional labelling	Flexible	Flexible
Primary downstream analysis	Fluorescent microscopy (CellTracks)	Flow cytometry	Flow cytometry
Secondary downstream analysis	Flow cytometry, filtration, fluorescent in situ hybridization	Filtration, CellSearch	Filtration, CellSearch

At the end of the project 30 metastatic breast and prostate cancer patients were processed with DLA at the clinical sites. The amount of CTC detected was indeed larger when compared to 7.5 mL blood, as is being used in CellSearch. However, the recovery percentage in the DLA samples was

relatively low. Various approaches to increase this recovery will be continued in the CANCER-ID program. Additionally, the developed filtration system to isolate and characterize CTC not captured by the CellSearch system was validated at the clinical sites. For this, blood from healthy donors spiked with cells from tumor derived cell lines was used. These spiking experiments showed that the tools and protocols could be executed well at each site and gave an overall recovery of 40%. The fate of the 60% spiked cells that were not recovered has not been unveiled thus far. Also, 22 metastatic breast and 108 metastatic prostate cancer patients were processed with the CellSearch and subsequent filtration system. In these patients nucleated CD45– and CK+ cells were identified, which were either $EpCAM^{high}$ CTC or $EpCAM^{low}$ CTC. The presence of $EpCAM^{low}$ CTC was not associated with a worse prognosis for patients' overall survival, whereas CellSearch $EpCAM^{high}$ CTC were associated with a poor survival.

The second goal of the project was the development of methods for the analysis of single CTC on every molecular level. For analysis on the interior molecular level, tools and protocols were developed to isolate single CTC and subsequently amplify DNA of these cells for molecular profiling, by either array comparative genomic hybridization or whole genome sequencing. Although databases were developed to collect and analyze information received during the project, most of the effort has been dedicated to extract, amplify and analyze the DNA contained in a single CTC. The antigen expression of the CTC was identified and characterized by means of immunophenotyping. Fluorescently labeled reagents and protocols were developed and validated in the consortium to detect CTC from enriched blood samples. Some reagents could be supplied from within the consortium, whereas others were obtained from commercial resources. In addition, to improve the identification of CTC among the fluorescently labeled cells, an image analysis program has been developed. To arrive at a common definition for a CTC, this open source image analysis program 'Automated CTC Classification Enumeration and PhenoTyping' (ACCEPT) is a joint effort between the CTC-Trap and CANCER-ID program. This program detects all events present in the images by an advanced multi-scale segmentation approach and extracts several fluorescence intensities and shape measurements for every event it has found. Also, for proliferation of CTC, animal models were developed to expand CTC derived from prostate and breast cancer patients. In-vitro and in-vivo models were successfully developed and CTC derived from DLA patients were used in these models. NSG mice were injected with non-purified

DLA product containing CTC, leukocytes and, possibly, hematopoietic stem cells. Some mice were found to have human leukemia. Therefore, the protocol was amended to deplete white blood cells in DLA samples prior to xenotransplantation or in-vitro culturing. However, the in-vitro models still showed massive growth of heterogeneous cells, of which the majority was human CD45+ cells. Interestingly, the CellSearch platform showed human CTC (EpCAM+, cytokeratin+, human CD45– and mouse CD45– cells) in blood and bone marrow of the injected NGS mice. However, no metastases were detected in these mice. Therefore, human CTC might survive in the circulation and the hematopoietic compartment of immunodeficient mice; however, they do not seem to be tumorigenic in this developed experimental setup.

Finally, pilot work on the health economic consequences of the use of CTC in cancer disease management has been conducted. Two studies were performed: a model is introduced in breast cancer for the use of CTC to detect early metastases to guide treatment strategies and in metastatic prostate cancer a model for switching therapies is shown. These studies are complemented with an overview of the stakeholder input regarding the requirements for further development and implementation of CTC-Trap. It shows it is very useful to anticipate market access and reimbursement in case of advanced molecular diagnostics, which are developed in the CTC-Trap program.

Outlook

In the CTC-Trap consortium several universities, research institutions and SMEs have explored together various ways to isolate CTC from 1-2 L of blood. The approach ultimately evaluated in numerous cancer patients was the DLA procedure in combination with the CellSearch system, targeting $EpCAM^{high}$ CTC, and technology based on differences in physical characteristics between blood cells and cancer cells, targeting $EpCAM^{low}$ CTC as well. This entire work-flow is visualized in Figure 1. This approach has led to a significant increase in the number of isolated CTC enabling a more comprehensive real-time characterization of the cancer. Development is however still ongoing to further improve the CTC enrichment in conjunction with DLA. Using the technology developed in CTC-Trap, $EpCAM^{high}$ as well $EpCAM^{low}$ CTC were identified in both metastatic prostate and metastatic breast cancer patients. Long-term follow-up will be needed to determine the relation with clinical outcome.

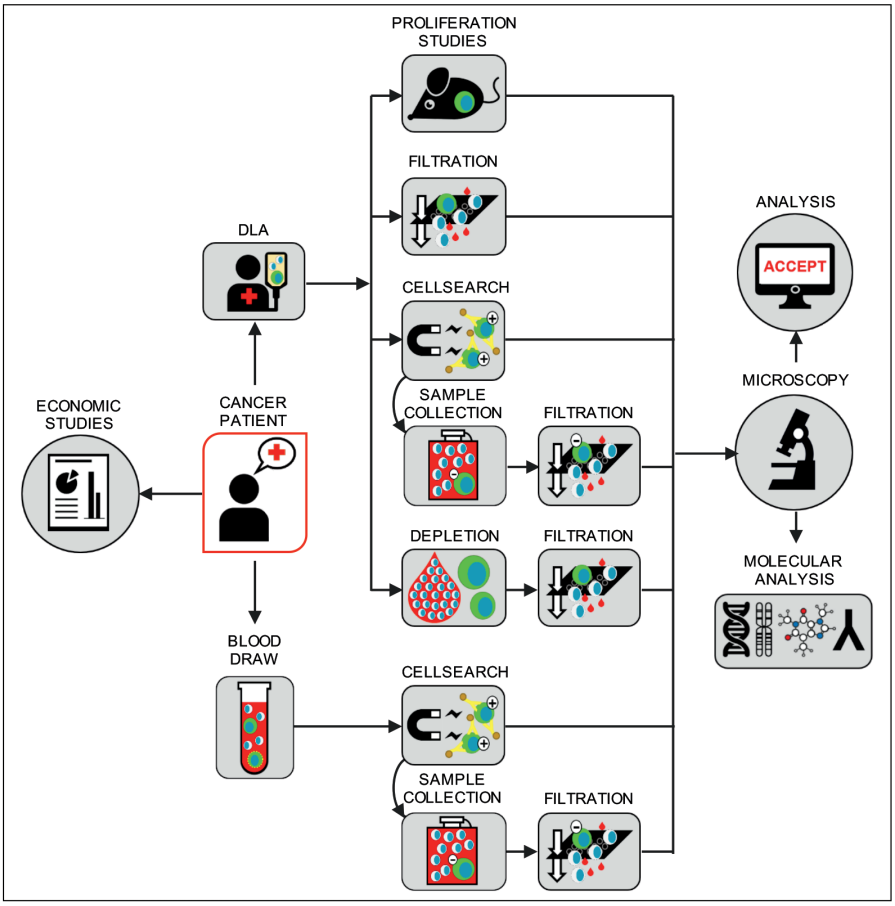

Figure 1. The work-flow of methods for CTC detection and characterization performed in the CTC-Trap project. A cancer patient has blood drawn for CellSearch (EpCAM^{high} CTC) and subsequent collection and filtration (EpCAM^{low} CTC), followed by visualization and analysis. The DLA product of the patient is used for proliferation studies in mice, filtration, CellSearch (EpCAM^{high} CTC) and subsequent collection and filtration (EpCAM^{low} CTC), depletion of leukocytes with the RosetteSep™ and subsequent filtration, all followed by visualization and analysis.

Efforts are still ongoing to gather new knowledge on the differences at both the molecular and protein level of these CTC. These results will provide insight in the mechanism of metastasis, provide a risk assessment and guide the optimal therapy choice for the patients. CTC-Trap is expected to be a door opener for significant revenues in the evolving "personalized medicine" market. During the four years of the project, a lot of scientific output has been generated in the form of papers, abstracts, oral talks and poster presentations.

All CTC-Trap peer reviewed articles are listed at the end of this chapter. This thesis describes the work performed within the CTC-Trap project, dedicated to the identification of CTC. A special emphasis is on EpCAM^{low} CTC: the developed methods for isolation, detection and identification are described in the following chapters, performed in patient studies to determine the relation of these cells to prognosis and survival of these metastatic cancer patients.

Papers published during the CTC-Trap project

The following list presents all peer-review published papers under the CTC-Trap project, which contains reviews about CTC, the CellSearch or DLA[1-6], experimental papers describing isolation of CTC, CTC in a clinical context or CTC in mouse models[7-18] and methodology papers presenting the value of CTC in health economics or personalized medicine[19-22].

References

1. Barradas, A. & Terstappen, L. Towards the Biological Understanding of CTC: Capture Technologies, Definitions and Potential to Create Metastasis. Cancers (Basel). 5, 1619–1642 (2013).
2. de Wit, S., van Dalum, G. & Terstappen, L. W. M. M. Detection of Circulating Tumor Cells. Scientifica (Cairo). 2014, 1–11 (2014).
3. Andree, K. C., van Dalum, G. & Terstappen, L. W. M. M. Challenges in circulating tumor cell detection by the CellSearch system. Mol. Oncol. 10, 395–407 (2016).
4. Swennenhuis, J. F., van Dalum, G., Zeune, L. L. & Terstappen, L. W. M. M. Improving the CellSearch® system. Expert Rev. Mol. Diagn. 16, 1291–1305 (2016).
5. Stoecklein, N. H., Fischer, J. C., Niederacher, D. & Terstappen, L. W. M. M. Challenges for CTC-based liquid biopsies: low CTC frequency and diagnostic leukapheresis as a potential solution. Expert Rev. Mol. Diagn. 16, 147–164 (2016).
6. Allard, W. J. & Terstappen, L. W. M. M. CCR 20th Anniversary Commentary: Paving the Way for Circulating Tumor Cells. Clin. Cancer Res. 21, 2883–2885 (2015).
7. de Wit, S. et al. The detection of EpCAM+ and EpCAM– circulating tumor cells. Sci. Rep. 5, 12270 (2015).
8. de Wit, S. et al. EpCAMhigh and EpCAMlow circulating tumour cells in metastatic prostate and breast cancer patients. submitted (2017).
9. Swennenhuis, J. F., Reumers, J., Aerssens, J. & Terstappen, L. W. M. M. Efficiency of whole genome amplification of Single Circulating Tumor Cells enriched by CellSearch and sorted by FACS. Genome Med.
10. Andree, K. C. et al. Capture of Tumor Cells on Anti-EpCAM-Functionalized Poly(acrylic acid)-Coated Surfaces. ACS Appl. Mater. Interfaces 8, 14349–14356 (2016).
11. Swennenhuis, J. F. et al. Self-seeding microwell chip for the isolation and characterization of single cells. Lab Chip 15, 3039–3046 (2015).
12. Pixberg, C. F. et al. Analysis of DNA methylation in single circulating tumor cells. Oncogene 36, 3223–

3231 (2017).

13. Crespo, M. et al. Androgen receptor expression in circulating tumour cells from castration-resistant prostate cancer patients treated with novel endocrine agents. Br. J. Cancer 112, 1166–74 (2015).
14. Lorente, D. et al. Decline in Circulating Tumor Cell Count and Treatment Outcome in Advanced Prostate Cancer. Eur. Urol. 70, 985–992 (2016).
15. Lorente, D. et al. Interrogating Metastatic Prostate Cancer Treatment Switch Decisions: A Multi-institutional Survey. Eur. Urol. Focus (2016). doi:10.1016/j.euf.2016.09.005
16. Pecze, L. et al. Activation of endogenous TRPV1 fails to induce overstimulation-based cytotoxicity in breast and prostate cancer cells but not in pain-sensing neurons. Biochim. Biophys. Acta - Mol. Cell Res. 1863, 2054–2064 (2016).
17. Jósvay, K. et al. Besides neuro-imaging, the Thy1-YFP mouse could serve for visualizing experimental tumours, inflammation and wound-healing. Sci. Rep. 4, 6776 (2014).
18. Marton, A. et al. Vanillin Analogues o-Vanillin and 2,4,6-Trihydroxybenzaldehyde Inhibit NFKB Activation and Suppress Growth of A375 Human Melanoma. Anticancer Res. 36, 5743–5750 (2016).
19. Schreuder, K., Hummel, J. M., Terstappen, L. W. M. M. & IJzerman, M. J. The Expected Health Economic Value of Using Circulating Tumor Cells to Personalize Cancer Treatment. Value Heal. 16, A424 (2013).
20. Degeling, K. et al. Comparison of Timed Automata with Discrete Event Simulation for Modeling of Biomarker-Based Treatment Decisions: An Illustration for Metastatic Castration-Resistant Prostate Cancer. Value Heal. 20, 1411–1419 (2017).
21. IJzerman, M., Manca, A., Keizer, J. & Ramsey, S. Implementation of comparative effectiveness research in personalized medicine applications in oncology: current and future perspectives. Comp. Eff. Res. 5, 65 (2015).
22. Degeling, K., Koffijberg, H. & IJzerman, M. J. A systematic review and checklist presenting the main challenges for health economic modeling in personalized medicine: towards implementing patient-level models. Expert Rev. Pharmacoecon. Outcomes Res. 17, 17–25 (2017).

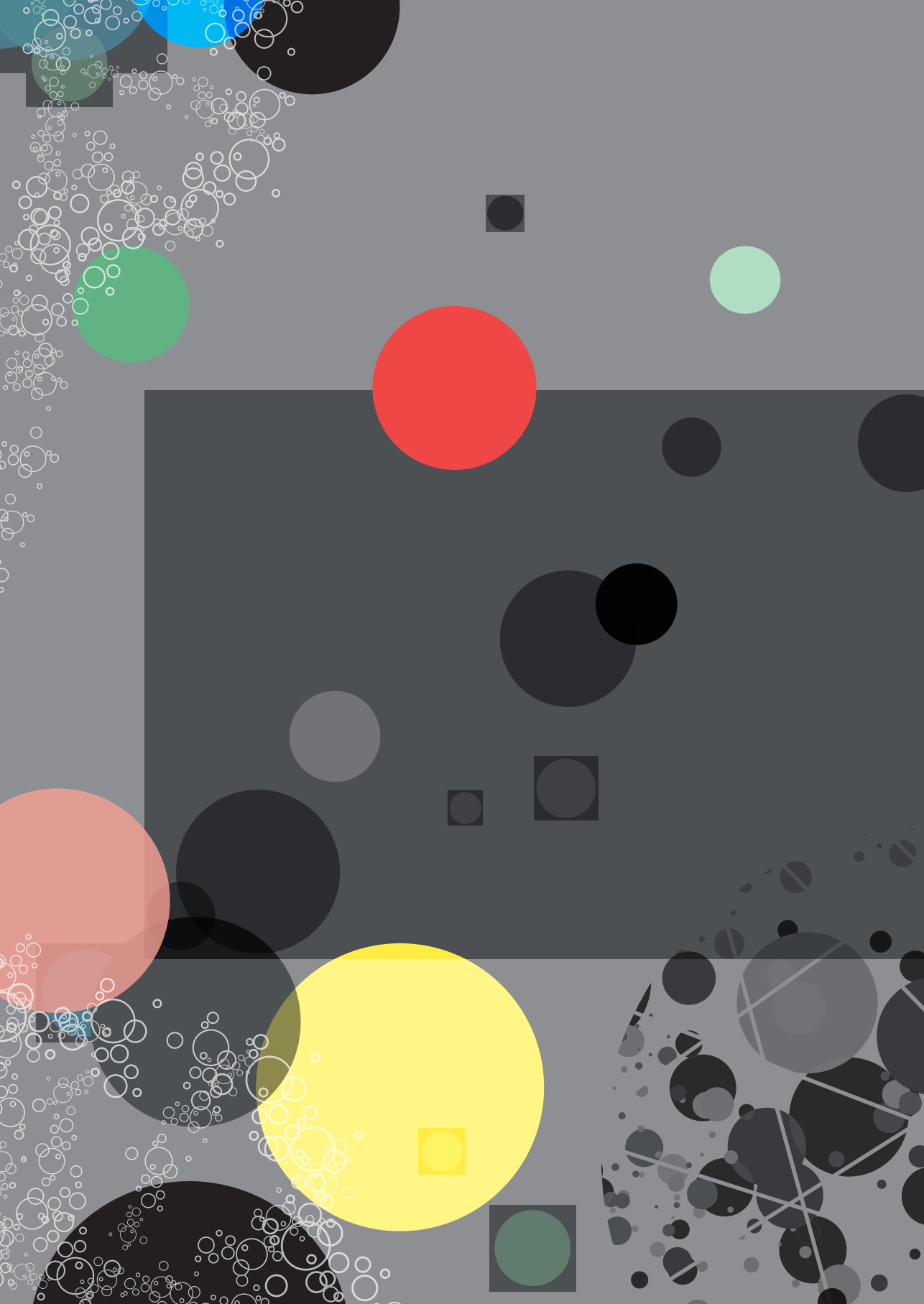

Chapter 3

EpCAM^{high} and EpCAM^{low} circulating tumor cells in metastatic prostate and breast cancer patients

Sanne de Wit, Mariangela Manicone, Elisabetta Rossi, Rita Lampignano, Liwen Yang, Beate Zill, Alvera Rengel-Puertas, Marianne Oulhen, Mateus Crespo, A.M. Sofie Berghuis, Kiki C. Andree, Riccardo Vidotto, Elisabeth K. Trapp, Marie Tzschaschel, Emeline Colomba, Gemma Fowler, Penelope Flohr, Pasquale Rescigno, Mariane Sousa Fontes, Rita Zamarchi, Tanja Fehm, Hans Neubauer, Brigitte Rack, Marianna Alunni-Fabbroni, Françoise Farace, Johann De Bono, Maarten J. IJzerman, Leon W.M.M. Terstappen.

Submitted for publication

Abstract

The presence of high expressing epithelial cell adhesion molecule ($EpCAM^{high}$) circulating tumor cells (CTC) enumerated by CellSearch® in blood of cancer patients is strongly associated with poor prognosis. This raises the question about the presence and relation with clinical outcome of low EpCAM expressing CTC ($EpCAM^{low}$ CTC). In the EU-FP7 CTC-Trap program, we investigated the presence of $EpCAM^{high}$ and $EpCAM^{low}$ CTC, using CellSearch followed by microfiltration of the $EpCAM^{high}$ CTC depleted blood. Blood samples of 108 castration-resistant prostate cancer patients (CRPC) and 22 metastatic breast cancer patients (mBC) were processed at six participating sites, using protocols and tools developed in the CTC-Trap program. 53% of CRPC and 32% of mBC had ≥5 $EpCAM^{high}$ CTC. 28% of CRPC and 36% of mBC had ≥5 $EpCAM^{low}$ CTC. 70% of CRPC and 64% of mBC had in total ≥5 $EpCAM^{high}$ and/or $EpCAM^{low}$ CTC, increasing the number of patients in whom CTC are detected. CRPC patients with ≥5 $EpCAM^{high}$ CTC had shorter overall survival (OS) versus those with <5 $EpCAM^{high}$ CTC ($p<0.000$). However, presence of $EpCAM^{low}$ CTC had no relation with OS. This warrants an in-depth characterization of the $EpCAM^{low}$ CTC to reveal genetic differences with $EpCAM^{high}$ CTC and tumor cells in metastatic sites.

Introduction

The presence of circulating tumor cells (CTC) expressing the cell surface epithelial cell adhesion molecule (EpCAM) as well as intracellular cytokeratins (CK), are associated with poor outcome in patients with metastatic as well as non-metastatic disease[1–8]. In the CellSearch® system, CTC that show no or low expression of EpCAM are discarded during magnetic isolation and their information is lost. This raises the question how many of these EpCAM-negative or EpCAM low expressing CTC (hereinafter referred to as $EpCAM^{low}$ CTC) are present and whether or not their presence is also associated with poor outcome. In the FP7 EU program CTC-Trap (*https://www.utwente.nl/tnw/ctctrap/*) this question was investigated by the collection of the blood discarded by the CellSearch system after immunomagnetic enrichment of $EpCAM^{high}$ cells and passing this sample through a membrane with 111,800 pores with a diameter of 5 μm[9]. Cells were subsequently fluorescently labelled and $EpCAM^{low}$ CTC were scored when cells were 4',6-diamidino-2-phenylindole (DAPI)-positive, CK-positive and CD45-negative.

To validate this method for detection of epithelial EpCAM^{low} CTC, the procedure was tested at six different sites in the CTC-Trap consortium. Healthy donor blood spiked with cells of the prostate cancer cell line PC3 (1.0×10^4 EpCAM antigens, average size 17.7 µm) and the breast cancer cell line MDA-MB-231 (1.5×10^4 EpCAM antigens, average size 15.6 µm) were tested for recovery of EpCAM^{high} and EpCAM^{low} cells. Subsequently, the presence of EpCAM^{high} and EpCAM^{low} CTC was investigated in 108 CRPC patients and 22 metastatic breast patients and their presence was related to overall survival.

Methods

Blood samples

Peripheral blood samples were drawn by venepuncture into 10 mL CellSave Preservative Tubes (Menarini Silicon Biosystems, Huntingdon Valley PA, USA) from healthy donors, metastatic breast and castration resistant prostate cancer patients. All patients and healthy donors provided written informed consent and the study protocol was approved by the medical ethical committee's at each participating site. Patient demographics of patients with known clinical outcome are provided in Table 1. The sites in the CTC-Trap consortium collaborating in this validation study are The Institute of Cancer Research, The Royal Marsden Hospital, NHS Foundation Trust (ICR), United Kingdom; Institute Gustave Roussy (IGR), France, Instituto Oncologico Veneto (IOV), Italy; Ludwig-Maximilians-University Muenchen (LMU), Germany; Universitätsklinikum Düsseldorf (UKD), Germany; and the Universiteit Twente (UT), the Netherlands. CRPC patients (at sites ICR, IGR and IOV) and metastatic breast cancer patients (at sites LMU and UKD) were recruited and processed on site within 96 hours. A schematic overview of the study is shown in Figure 1.

Cell lines and spiking

Spiking experiments were performed with cells from the prostate carcinoma cell line PC3 and the breast carcinoma cell line MDA-MB-231. All cell lines were obtained from ATCC (Manassa VA, USA) and have not been authenticated in the past six months. They were grown at 37°C and 5% CO^2. The PC3 cell line was cultured in RPMI-1640 (Life Technologies Corporation, Carlsbad

CA, USA), and the MDA-MB-231 cell line was cultured in DMEM (Euroclone, Pero MI, Italy); both media were supplemented with 10% fetal bovine serum (GIBCO, Life Technologies Corporation), 2 mM UltraGlutamine (Lonza, Basel, Switzerland) and 10 mM Hepes (Lonza). The median cell size from both cell lines was determined with a Coulter counter pipette (Scepter, Millipore, Billerica, MA, USA). The EpCAM density was determined using a flow cytometer (FACS ARIA II, BD Biosciences, San Jose, CA, USA) and QuantiBrite beads (BD Biosciences). The median size of the MDA-MB-231 cells was 15.6 μm with an average EpCAM density of 1.5×10^4 (165 %CV) antigens. The median size of the PC3 cells was 17.7 μm with an average EpCAM density of 1.0×10^4 (89 %CV) antigens. The histograms showing the distribution of the EpCAM density of the PC3 and MDA-MB-231 cells is shown in Supplementary Figure S1. For comparison, the EpCAM density of the breast cancer cell line MCF-7, expressing EpCAM at much higher density, is shown in the figure as well.

Table 1. Patient demographics in this study of patients with known clinical outcome.

Castration-resistant prostate cancer patients	***n = 85***	***Metastatic breast cancer patients***	***n = 16***
Age (years)		**Age (years)**	
Median (range)	71 (49-84)	Median (range)	63 (37-89)
Unknown	24 (28%)	Unknown	01 (6%)
Status at last follow-up		**Status at last follow-up**	
Alive	38 (45%)	Alive	12 (75%)
Dead	47 (55%)	Dead	04 (25%)
Mean follow-up time in months (min-max)		**Mean follow-up time in months (min-max)**	
Alive	13 (0-28)	Alive	11 (3-17)
Dead	09 (0-27)	Dead	04 (2-8)
Line of therapy		**Line of therapy**	
Before therapy	08 (9%)	Before therapy	05 (31%)
1st line	10 (12%)	1st line	02 (13%)
2nd line	19 (22%)	2nd line	01 (6%)
≥ 3rd line	24 (28%)	≥ 3rd line	07 (44%)
Unknown	25 (29%)	Unknown	01 (6%)

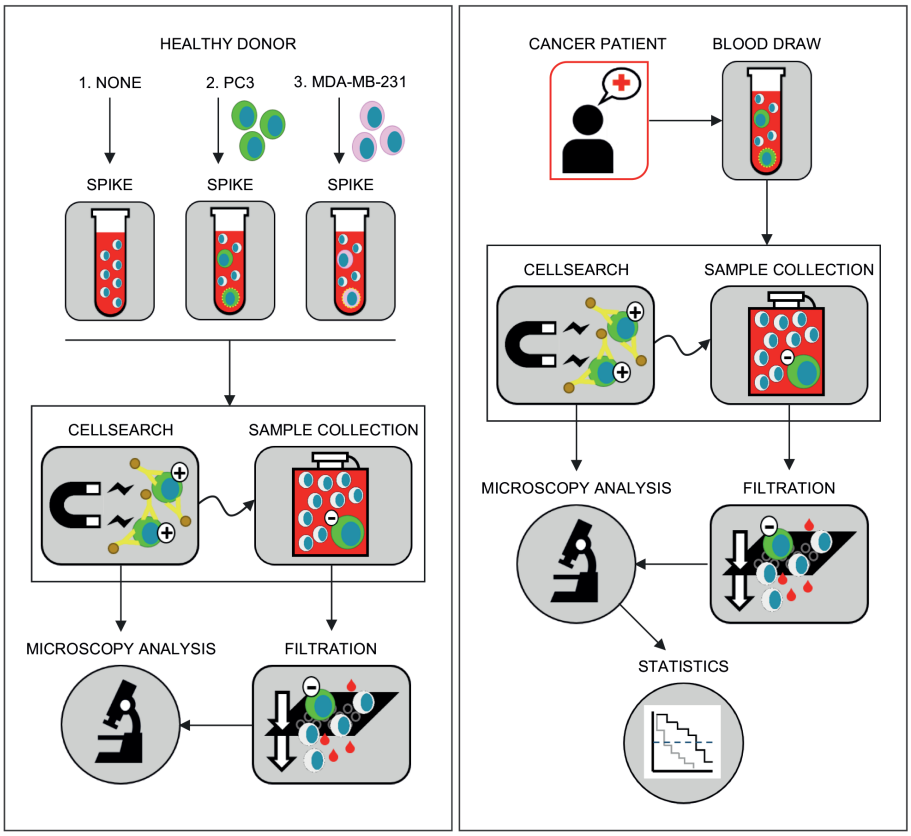

Figure 1. Schematic representation of the study. Left panel: one site collected healthy donor blood and prepared three tubes for each site (*Spike*) to send for enumeration of EpCAM^{high} cell line CTC (*CellSearch*) and EpCAM^{low} cell line CTC (*Sample collection* and *Filtration*): no cells spiked in tube 1, spiked with on average 270 PC3 cells in tube 2 and spiked with on average 270 MDA-MB-231 cells in tube 3. This process was repeated three times with three different healthy donors. Right panel: blood samples collected from castrate-resistant prostate cancer patients and metastatic breast cancer patients (*Blood draw*) at each clinical site were processed for enumeration of EpCAM^{high} CTC (*CellSearch*), followed by detection of EpCAM^{low} CTC (*Sample collection* and *Filtration*). CTC are scored (*Microscopy analysis*) for survival analysis (*Statistics*).

The MDA-MB-231 cells and PC3 cells were spiked in healthy donor CellSave blood. Cell numbers for spiking were counted manually with a fluorescent microscope, using the nuclear dye Hoechst 33342 for visualization on a glass slide. Targeting a spike number of 250 cells in 7.5 mL blood volume, the exact number of cells was counted before adding the cells to the blood and subsequently used to determine the recovery in the CellSearch and on the microsieve. Unspiked blood samples from healthy volunteers were used as a negative control. Spiked samples were prepared at the IOV laboratory and

distributed under temperature control to the six sites to be processed after 48 hours. Each site received a tube of unspiked blood (labelled A), one tube spiked with PC3 cells (labelled B) and one tube spiked with MDA-MB231 cells (labelled C), all from one donor. This was repeated three times with three different donors.

CTC detection by CellSearch

CTC were enumerated in aliquots of 7.5 mL of blood with the CellSearch® Circulating Tumor Cell Kit (Menarini Silicon Biosystems). Analysis was performed within 96 hours of the blood draw. Blood samples were enriched for EpCAMhigh cells and stained with DAPI, Cytokeratin-PE and CD45-APC on the CellTracks Autoprep. Image acquisition of the stained cartridges was performed on the CellTracks Analyzer II. Images of CTC candidates were identified by the CellTracks Analyzer II and presented to experienced operators for classification. Candidates were assigned as CTC when the objects were larger than 4 μm, stained with DAPI and CK, lacked CD45 staining and had morphological features consistent with that of a cell1.

Blood sample collection after EpCAM^{high} CTC enrichment

After immunomagnetic selection of EpCAM^{high} cells, the CellTracks Autoprep aspirates the blood that is void of the selected cells and transports it to a waste container outside the instrument. To enable the investigation of this blood for residual tumor cells, the sample was collected manually or with the specific designed Automated Sample Collection Device (ASCD), as described previously[9]. For manual collection of the Autoprep discarded blood sample, the top of the waste container was removed. After visual inspection of presence of blood in the tubing coming out of the Autoprep, a 50 mL conical tube is placed under the outlet and the sample is collected until no blood can be observed anymore in the tubing. This is repeated for each sample. The first blood arrives at the waste container approximately 1 hour after start of the Autoprep. The protocols and tools are described in more detail at *https://www.utwente.nl/tnw/mcbp/protocolsandtools/*.

Filtration of the discarded CellTracks Autoprep blood sample

To filter tumor cells from the EpCAM^{high} CTC depleted blood sample, microsieve membranes were used (VyCAP, Deventer, The Netherlands). Each microsieve contains 111,800 pores of 5 µm in diameter and these pores are spaced 14 µm apart in lanes with a porosity of 10% on a total surface area of 8 by 8 mm. The specifications of the microsieves were obtained from previous experiments[9–11]. The microsieve is contained in a plastic holder that was placed in a disposable filtration unit, which can be placed on a pump unit that maintained a pressure of –100 mbar across a microsieve during filtration (VyCAP). The CellSearch discarded blood sample was transferred to the filtration unit after which the pump was switched on. The collected blood sample, varying between 25 to 40 mL, was passed through in maximum 10 minutes. After complete filtration of the sample or after 10 minutes, the pump was switched off and if there was any unfiltered sample volume remaining, this was removed with a pipette. Details of the volumes that were not filtered were used to determine how much whole blood volume was processed.

Staining of cells on microsieves

Conditions for staining on microsieves were optimized to assure uniform staining across the microsieve with a minimum of non-specific binding. After filtration, the microsieve was removed and washed once with a permeabilization buffer containing PBS, 1% bovine serum albumin (Sigma-Aldrich, St. Louis MO, USA) and 0.15% saponin (Sigma-Aldrich). Next, this buffer was placed on the sieve and removed after 15 minutes incubation at room temperature. A cocktail of fluorescently labelled antibodies was used to stain the cells on the sieve for 15 minutes at 37°C. The staining solution consisted of the following monoclonal antibodies: three CK antibody clones targeting CK 4, 5, 6, 8, 10, 13, 18 (clone C11), CK 1-8 (clone AE3) and CK 10, 14, 15, 16 and 19 (clone AE1), all conjugated to NTb575 (AcZon s.r.l., Bologna, Italy), and one antibody targeting CD45 (clone HI30) labelled with PerCP (Thermo Fisher Scientific, Waltham MA, USA). The CK-pan cocktail was diluted to a final concentration of 3.5 µg/mL and the anti-CD45 antibody was diluted to 4 µg/mL in PBS/1%BSA/0.05% saponin. After removal of the staining cocktail, the microsieve was washed once and then incubated for 5 minutes at room temperature with PBS/1%BSA. Then the sample was fixed using PBS with 1% formaldehyde (Sigma-Aldrich) for 10 minutes at

room temperature. Removal of the fluid during each of the staining and washing steps was done by bringing the bottom of the microsieve in contact with an absorbing material using a staining holder (VyCAP). The microsieve was subsequently covered with ProLong® Diamond Antifade Mountant with DAPI (Thermo Fisher Scientific). A custom cut 0.85 by 0.85 cm glass coverslip (Menzel-Gläser, Saarbrükener, Germany) was placed on both sides of the microsieve for immediate analysis or storage in the freezer at –30°C.

Detection of cells on microsieves

Microscopes at each site were equipped with a 20× microscope objective with minimal NA0.45 and the same set of filter cubes. The following filters were used: DAPI (DAPI-50LP-A-NQF) with excitation 377/50 nm, dichroic 409 nm LP, emission 409 nm LP; PE (TRITC-B-NQF) with excitation 543/22 nm, dichroic 562 nm LP, emission 593/40 nm and PerCP (FF02-435/40, FF510-Di02 and FF01-676/29 (customized filter cube)) with excitation 435/40 nm, dichroic 510 nm LP, emission 676/29 nm. All cubes were acquired via Nikon (Semrock, Rochester, NY, USA). Images covering the entire 0.64 cm^2 surface of the microsieves were acquired and stored.

Scoring of CTC

Analysis of the fluorescent images generated from the CellSearch cartridges were performed according the instructions of the manufacturer. The fluorescent images from the microsieves were analyzed using the open-source software ICY[12]. Operators were asked to annotate every DAPI+/CK+/CD45– event. In case of clogging of the microsieve, CTC counts were extrapolated to the full volume. Images of CTC were analyzed for their intensity in CK, thereby deducting the background value from the intensity value of CK staining ranging from 0 to 4095 counts.

Statistical analysis

Statistical analysis was performed in SPSS (version 24, SPSS Inc., Chicago IL, USA) and R (version 3.3.0, R Foundation, Vienna, Austria). For survival analysis, patients were divided in two prognostic groups: favorable for less than 5 CTC and unfavorable ≥5 CTC[2,4]. Kaplan-Meier curves for overall survival were generated and compared using the Log-Rank test. A receiver operating characteristic curve was used to determine the $EpCAM^{low}$ CTC

threshold for the highest diagnostic ability. A p-value of <0.05 was considered to indicate a statistical difference.

Results

Validation of CTC detection protocols across sites

On average, 270 PC3 or MDA-MB-231 cells were spiked per tube in fifty-four 7.5 mL blood samples of three healthy donors and sent to the six sites for processing according to the established protocols. The recovery of PC3 and MDA-MB-231 cells was determined using CellSearch (for EpCAM^{high} cells) and on microsieves after filtration of the blood discarded by CellSearch (for EpCAM^{low} cells). The results are illustrated in Figure 2 and a detailed overview of cell recovery per site is provided in Supplementary Figure S2. For EpCAM^{high} CTC detected by CellSearch, the recovery of PC3 cells varied between 11.9% and 40.6% (mean 26.9% ±9 standard deviation (SD)) and for MDA-MB-231 between 2.7% and 39.0% (mean 25.7% ±10 SD). For EpCAM^{low} tumor cells detected on the microsieves after filtration of the CellSearch discarded blood, the recovery of PC3 cells varied between 0.6% and 42.5% (mean 15.1% ±11 SD) and for MDA-MB-231 between 0% and 29.3% (mean 12.8% ±9 SD). In 7.5 mL of blood from three healthy donors, who donated together in total 54 samples, no EpCAM^{high} and no EpCAM^{low} cells were detected.

EpCAM^{high} and EpCAM^{low} CTC in blood from metastatic breast and prostate cancer patients

EpCAM^{high} and EpCAM^{low} CTC were enumerated in 7.5 mL blood obtained from 108 CRPC and 22 mBC patients. EpCAM^{high} CTC in CRPC ranged from 0-3300 with a median of 6 and a mean of 124 (±400 SD). In mBC, EpCAM^{high} CTC ranged from 0-208 with a median of 1 and a mean of 13 (±43 SD). EpCAM^{low} CTC in CRPC ranged from 0-24 with a median of 1 and a mean of 3 (±4 SD) and in mBC EpCAM^{low} CTC ranged from 0-35 with a median of 3 and a mean of 3 (±11 SD). Five or more EpCAM^{high} CTC and ≥5 EpCAM^{low} CTC were detected in 56 (53%) and 26 (28%) CRPC patients, respectively. In the group of mBC patients, 7 (32%) showed ≥5 EpCAM^{high} CTC and 8 (36%) ≥5 EpCAM^{low} CTC. A combination of both ≥5 EpCAM^{high} and EpCAM^{low} CTC was observed in 70% CRPC (n=91) and 64% mBC

patients, increasing the combined CTC-positivity rates by 32% and 100% respectively, in comparison to positivity rates for EpCAM^{high} CTC only. In total, 37% CRPC patients and 23% mBC patients had ≥5 EpCAM^{high} CTC, but <5 EpCAM^{low} CTC. Vice versa, <5 EpCAM^{high} CTC and ≥5 EpCAM^{low} CTC were detected in 10% CRPC and in 18% mBC patients. A more detailed overview of the number of CTC detected in the patients is provided in Table 2 and in Supplementary Figure S3. The complete list of scored CTC for each patient is provided in Supplementary Table S1. Figure 3 presents a representative gallery of EpCAM^{high} and EpCAM^{low} CTC that were found in CRPC and mBC patients, showing CTC of various sizes and staining of CK intensity.

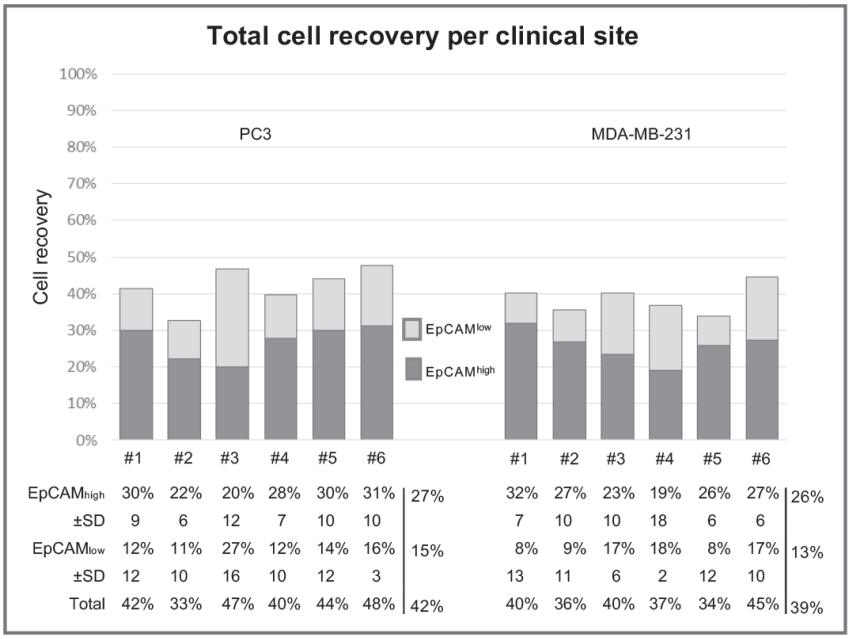

Figure 2. Recovery of PC3 and MDA-MB-231 cancer cells for each clinical site. Recovery of on average 270 PC3 cells and MDA-MB-231 cells spiked in each blood sample, processed with the methods for EpCAM^{high} and EpCAM^{low} CTC detection. To determine the recovery of EpCAM^{high} CTC, the samples were processed with CellSearch and the EpCAM depleted blood was filtered through 5 µm microsieves to determine the recovery of EpCAM^{low} cells. In total, per site (#1-6) three samples per cell line and three controls were processed. The average recovery per three samples is displayed with its standard deviation, followed by an average recovery of all sites per method and cell line.

Table 1. Frequency of CTC in CRPC and mBC patients. Frequency (%) of EpCAM^{high} and EpCAM^{low} CTC in 7.5 mL of blood of 91 castration-resistant prostate cancer patients and 22 metastatic breast cancer patients.

		Prostate cancer % patients with EpCAM^{high} CTC					Breast cancer % patients with EpCAM^{high} CTC				
	# CTC	0	1-4	≥5	≥10	Total	0	1-4	≥5	≥10	Total
% patients with EpCAM^{low} CTC	**0**	12.1	9.9	22.0	18.7	*44.0*	18.2	4.5	9.1	9.1	*31.8*
	1-4	5.5	6.6	15.4	14.3	*27.5*	9.1	9.1	13.6	4.5	*31.8*
	≥5	7.7	2.2	18.7	16.5	*28.6*	13.6	13.6	9.1	4.5	*36.3*
	≥10	1.1	0	5.5	4.1	*6.6*	9.1	9.1	9.1	4.5	*27.3*
	Total	*25.3*	*18.7*	*56*	*49.5*	*100*	*40.9*	*27.3*	*31.8*	*18.2*	*100*

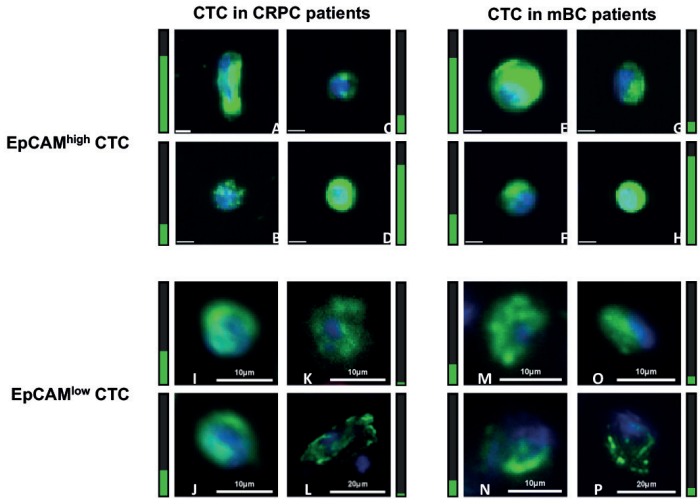

Figure 3. Gallery of captured CTC in CRPC and mBC patients. Display of EpCAM^{high} CTC (CellSearch captured) and EpCAM^{low} CTC (microsieve captured) in castrate-resistant prostate cancer and metastatic breast cancer patients. Cells in panel A-B are from the same patient, as are the cells in C-D, in E-F, in G-H and in I-J. The value for intensity of CK staining (green) is represented in the bar next to the image, visualizing a very high intensity value with maximum 4095 counts as a full green bar. The nucleus is stained with DAPI (blue). The unlabeled scale bar for EpCAM^{high} CTC is 6.4 µm.

Overall survival of CRPC patients with EpCAM^{high} and EpCAM^{low} CTC

Follow-up data from patients that were enrolled in ongoing clinical trials could not be obtained at the time this manuscript was written. Therefore, follow-up data could only be obtained from 85 out of 108 CRPC patients and

16 out of 22 mBC patients. The cohort of mBC patients that remained was too small for survival analysis and this was therefore omitted.

To relate the presence of CTC in CRPC patients to overall survival, the patient cohort was split into a favorable group and an unfavorable group, using 5 CTC as a threshold[2,4]. In Figure 4 the Kaplan-Meier curves for $EpCAM^{high}$ and $EpCAM^{low}$ CTC are shown. A significant difference is observed for the presence of ≥5 $EpCAM^{high}$ CTC in relation to overall survival (p=0.000) (Figure 4A), whereas no significant difference is observed for ≥5 $EpCAM^{low}$ CTC (p=0.317) (Figure 4B). The combination of $EpCAM^{high}$ CTC and $EpCAM^{low}$ CTC was related with overall survival by separating the cohort into four groups: 1. <5 $EpCAM^{high}$ CTC & <5 $EpCAM^{low}$ CTC; 2. <5 $EpCAM^{high}$ CTC & ≥5 $EpCAM^{low}$ CTC; 3. ≥5 $EpCAM^{high}$ CTC & <5 $EpCAM^{low}$ CTC; and 4. ≥5 $EpCAM^{high}$ CTC & ≥5 $EpCAM^{low}$ CTC (Figure 4C). This shows again that the strong correlation with survival can be solely contributed to ≥5 $EpCAM^{high}$ CTC and not to ≥5 $EpCAM^{low}$ CTC (p=0.000). Since ≥5 $EpCAM^{low}$ CTC show no correlation with survival, perhaps a lower CTC cut-off value would show a correlation. The scatter plot of the number of $EpCAM^{low}$ CTC versus survival of these patients in Figure 4D shows no correlation between these two factors. A receiver operating characteristic (ROC) curve was then used to determine the highest diagnostic cut-off value for $EpCAM^{low}$ CTC. Although this calculates a threshold at ≥1 $EpCAM^{low}$ CTC, this value can be considered inconclusive since the separation between sensitivity and specificity is very low (see Supplementary Figure S4A). Using the threshold of ≥1 $EpCAM^{low}$ CTC also no relation can be observed with overall survival (p=0.748) (Supplementary Figure S4B).

Discussion

In this multicenter study we determined the presence of $EpCAM^{high}$ and $EpCAM^{low}$ CTC in castration resistant prostate cancer and metastatic breast cancer patients. Protocols and tools for detection were developed in the FP7-program CTC-Trap and validated at six clinical sites cooperating in the program. The current standard CellSearch method for CTC enumeration was used for the detection of CTC expressing EpCAM, followed by capturing and filtering of the sample depleted of the $EpCAM^{high}$ CTC, and stained for detection of epithelial CTC expressing no or low EpCAM (Figure 1).

To validate the procedure of CellSearch followed by filtration for detection of $EpCAM^{low}$ CTC, samples spiked with cells from the prostate (PC3, on

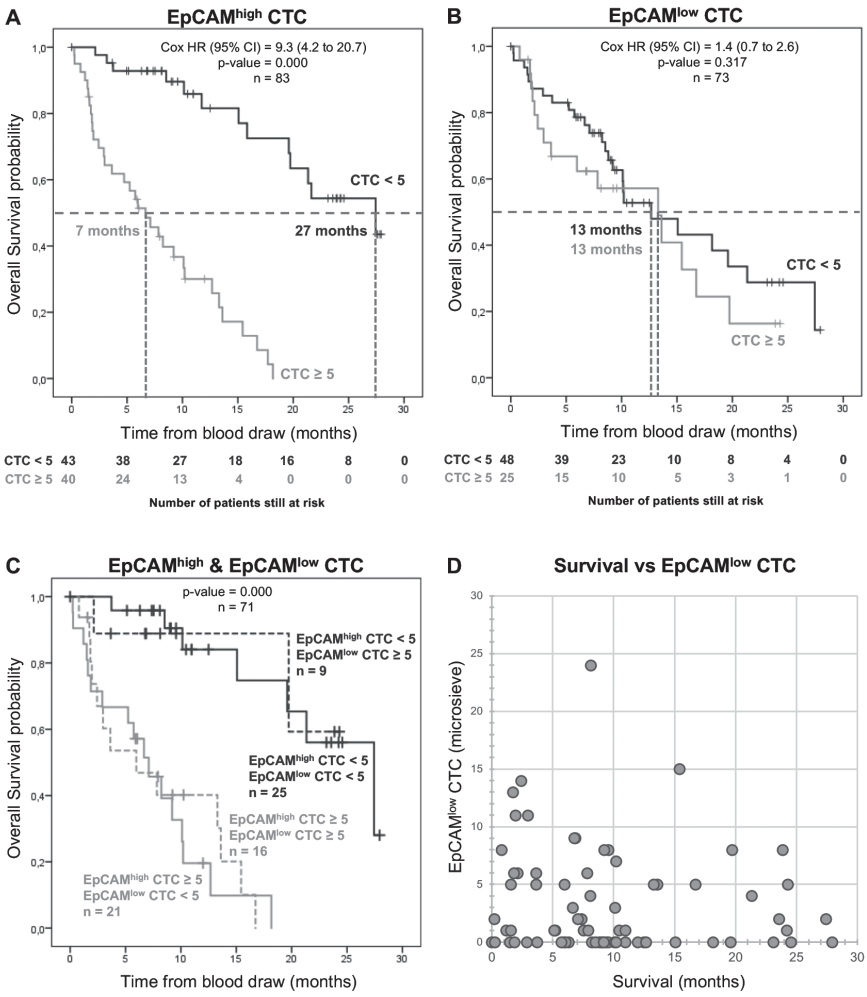

Figure 4. Overall survival for CRPC patients. Kaplan Meier curve of overall survival of patients with EpCAM^{high} CTC from CellSearch (A), EpCAM^{low} CTC from microsieves (B) and separation of the cohort into four groups with both EpCAM^{high} and EpCAM^{low} CTC: <5 EpCAM^{high} CTC & <5 EpCAM^{low} CTC (black solid line); <5 EpCAM^{high} CTC & ≥5 EpCAM^{low} CTC (black dashed line); ≥5 EpCAM^{high} CTC & <5 EpCAM^{low} CTC (grey solid line); and ≥5 EpCAM^{high} CTC and ≥5 EpCAM^{low} CTC (grey dashed line) (C), all show a strong correlation between EpCAM^{high} CTC and survival, but no correlation between EpCAM^{low} CTC and survival. Scatter plot of survival and amount of EPCAM^{low} CTC in patients (n=73) show no correlation (D).

average 1.0×10^4 EpCAM antigens and size of 17.7 μm) or breast (MDA-MB-231, on average 1.5×10^4 EpCAM antigens size 15.6 μm) cancer cell lines were used. The EpCAM density of the cells from both cell lines are an order of magnitude lower as compared to cell lines frequently used for spiking experiments such as cells from the breast cancer cell line MCF-7 (on average 88.0×10^4 EpCAM antigens) (see Supplementary Figure S1). We showed that 27% of the PC3 cells were recovered in the $EpCAM^{high}$ fraction (CellSearch) and 15% in the $EpCAM^{low}$ fraction (microsieve). For MDA-MB-231 26% was recovered in the $EpCAM^{high}$ fraction and 13% in the $EpCAM^{low}$ fraction. The question that arises is: where reside the remaining 58% PC3 spiked cells and 61% MDA-MB-231 spiked cells? Possible answers for this could be found in the filtration process or in the staining procedure of the samples. The most probable answer is that a major part of these cells were lost or destroyed during the filtration process. First, comparing previous reports of cell lines filtered through a microsieve with our results, the recovery of pre-stained bladder cancer cell line T24 (with similar size of 16 μm) shows a loss of 41% by means of merely filtering the cells[9]. Although under slower filtration conditions, a panel of smaller and larger pre-stained cell lines were filtered through a microsieve with the same pore size of 5 μm: among them MDA-MB-231 and PC3-9 (a sub-clone of the PC3 cell line with size of 18.5 μm) were recovered with 38% and 62% efficacy, respectively[10]. In addition, recovery increased with cell size, however with a weak trend due to large variations between technical replicates and between cell lines with similar sizes. Another contributing factor is that the $EpCAM^{low}$ cells that are destroyed during the CellSearch procedure and therefore missed in the total recovery. This can only occur during the removal of $EpCAM^{low}$ cells after immunomagnetic selection. This is however much less likely, since after this step the cells are immediately directed to the waste collection container. Indeed, cell expressing EpCAM at very high density are captured up to 90% in CellSearch, indicating a small loss of cells in the complete CellSearch procedure. Secondly, the immunostaining can also be of influence on the amount of detected cells. Referring to the previously mentioned T24 cells, the recovery of these cells was lower when a staining protocol was included to detect the cells on microsieve: the total combined recovery rate for $EpCAM^{high}$ (CellSearch) and $EpCAM^{low}$ cells (filtration) dropped from 61% to 38%, indicating that not all cells are identified with the immunostaining or are lost during the different steps in the staining procedure[9].

The observed recovery rates retrieved for each cell line includes variation introduced by EpCAM density, by different operators at each clinical site and

by the three measurements for each cell line (Figure 2 and Supplementary Figure 2). Clearly the variation in the obtained results vary a lot between the sites, stressing the need for standardization and proficiency testing to assure accurate reporting of actual CTC numbers. Variation introduced by the interpretation of the images of the CTC can be eliminated by the recently introduced ACCEPT open-source imaging program, which omits the scaling of intensity presented to the operator[13,14].

For PC3 71% and for MDA-MB-231 74% of the total recovered cells were detected in the EpCAM^{high} fraction. Important question is what the actual expression levels of EpCAM is on CTC expressing EpCAM. Rao et al. reported the EpCAM expression on 100 blood samples of metastatic cancer patients in which CTC were detected by flow cytometry and reported an average EpCAM density of 5.0×10^4 EpCAM antigens[15]. This density is fivefold higher than that of the PC3 and MDA-MB-231 cells used in this study. However, these numbers are the average density and the actual distribution of the EpCAM expression can be quite broad, as illustrated in Supplementary Figure S1[15]. The data supports our notion that the majority of CTC with relatively high EpCAM antigen density are captured by CellSearch, while CTC expressing no EpCAM or low EpCAM levels will be present in the EpCAM depleted fraction. After passage of the EpCAM depleted blood through microsieves, only a portion of the spiked cells – and most likely also CTC – will be captured. These observations have to be kept in mind when evaluating our results obtained in CRPC patients and mBC patients discussed below.

In 7.5 mL blood of castration resistant prostate cancer patients EpCAM^{high} CTC were detected in 75% and EpCAM^{low} CTC in 56% of the patients. Either one of these CTC populations was detected in 88% of the patients. For metastatic breast cancer patients, EpCAM^{high} CTC were detected in 59% and EpCAM^{low} CTC in 68% of the patients. One of these CTC populations was detected in 82% of the patients. In 56% of CRPC patients we identified ≥5 EpCAM^{high} CTC in 7.5 mL of blood (Table 2). This can be increased to 66% when both EpCAM^{high} and EpCAM^{low} CTC are used for the ≥5 CTC threshold. For mBC, 32% of the patients had ≥5 EpCAM^{high} CTC, which increased to 60% when patients with ≥5 EpCAM^{low} CTC were included. This corresponds to our previous report of a small pilot study with 28 non-small cell lung cancer (NSCLC) patients, which showed an increase of identified patients from 41% to 74%[9]. Also, these findings fit in the trend of recently published filtration based studies reporting large amounts of CTC detected with high variability[6,16–19]. Many of these studies found larger numbers of

CTC compared to CellSearch, which is not surprising as size exclusion yields CTC regardless of their surface marker expression. The biological reason for this increase in CTC counts is by many thought to be related to epithelial-to-mesenchymal transition (EMT)[20–22]. EMT refers to the complex and heterogeneous process of complete transition from the static, epithelial state to the motile, mesenchymal state of cells[23,24]. Although there is no exact definition of EMT, in tumor cells, this process is believed to be related to the loss of epithelial markers, such as EpCAM and CK, both used in the CellSearch system[20,21,25,26]. However, several studies describe the detection of CTC which co-express epithelial markers and mesenchymal markers at the same time[21,22,26,27]. In this study, only the EpCAM^{low} CTC expressing cytokeratins – and not the EpCAM^{low} CTC not expressing cytokeratins, but for example vimentin – are detected, leaving the question open on the frequency and clinical relevance of this subpopulation of CTC. Whether or not the presence of the different CTC sub-populations correlate with clinical outcome similar to the EpCAM^{high} CTC detected by CellSearch, has barely been addressed[28,29].

To address this question, we investigated the relation between EpCAM^{high} and EpCAM^{low} CTC and survival in CRPC patients. EpCAM^{high} CTC have been correlated with poor outcomes in many studies, and also in this cohort of patients the relation with poor survival is strong (Figure 4A)[1–8]. Interestingly, using the standardized threshold of 5 CTC to distinguish between favorable and unfavorable patient groups for EpCAM^{low} CTC from the same tube of blood, it is clear that they do not correlate with poor survival (Figure 4B). When separating the patients into four groups with combinations of both EpCAM^{high} CTC and EpCAM^{low} CTC, no separation of the four groups was visible, confirming that only the EpCAM^{high} CTC contributed to the strongly correlation with poor overall survival (Figure 4C). Similar observations were made in NSCLC and this prompts the question what type of cells these EpCAM^{low} cells truly are[30]. Here we define them as having no or low EpCAM expression, based on the effective depletion of cells expressing higher levels of EpCAM by the CellSearch system and relatively low capture of cells expressing low levels of EpCAM (Figure 2 and Supplementary Figure 1). The EpCAM^{low} cells have a nucleus identified by DAPI, express CK, but not CD45. The presence of CK shows that these cells are of epithelial origin, but do not proof that they are indeed tumor cells[31]. The CK expression in CTC is variable, even in the same patient (Figure 3A-D and 3E-H). EpCAM^{low} cells that resemble the morphology of EpCAM^{high} CTC have a higher intensity and filamentous pattern of CK (Figure 3I,J), whereas low CK intensity cells show

irregular CK expression (Figure 3K-P). This may indicate that these cells are different subtypes of CTC, where each subpopulation could express its own characteristics and clinical behaviour[32]. Even so, the intensity of CK staining can be very low in some patients (Figure 3K,L,O,P) making it difficult for operators to score CTC. In this study, every operator was asked to annotate every DAPI+/CK+/CD45– event, but this scoring procedure has not been standardized. Even using clearly defined criteria for operators to follow in scoring CTC, the discrepancy between operators can be high and argues for an automated approach to analyze images for cells of interest[13,14].

Definitive proof of the cancerous nature of the EpCAM^{low} cells will need to come from the genetic analysis of the cells, as well as the differences between the genetic and proteomic make-up of the EpCAM^{high} and EpCAM^{low} cells. To accomplish this, technology will need to be developed that can isolate or analyze the individual cells that were captured on the microsieves.

Concluding, in this multicenter study we validated the detection of EpCAM^{high} and EpCAM^{low} CTC from the same blood draw tube by using the CellSearch system for enumeration of the EpCAM^{high} and by microscopic examination of EpCAM^{low} after passage of the blood depleted from EpCAM^{high} cells through microsieves. In metastatic breast cancer, the detection of 5 or more CTC increased from 56% to 66% when including patients with 5 or more EpCAM^{low} CTC. In CRPC this percentage increased from 32% to 60%. However, when the clinical relevance of EpCAM^{high} and EpCAM^{low} CTC in CRPC patients was investigated, only EpCAM^{high} CTC correlated strongly with poor overall survival, whereas EpCAM^{low} CTC did not (Figure 4). This warrants an in-depth characterization of the detected epithelial EpCAM^{low} cells to confirm that they are indeed of cancerous origin and, if so, which differences in genetic or proteomic make-up of this these cells might explain the observed difference in clinical relevance of this subpopulation of CTC.

References

1. Allard, W. J. et al. Tumor cells circulate in the peripheral blood of all major carcinomas but not in healthy subjects or patients with nonmalignant diseases. Clin. cancer Res. 10, 6897–904 (2004).
2. Bidard, F.-C. et al. Clinical validity of circulating tumour cells in patients with metastatic breast cancer: a pooled analysis of individual patient data. Lancet. Oncol. 15, 406–14 (2014).
3. Cohen, S. J. et al. Relationship of Circulating Tumor Cells to Tumor Response, Progression-Free Survival, and Overall Survival in Patients With Metastatic Colorectal Cancer. J. Clin. Oncol. 26, 3213–3221 (2008).

4. de Bono, J. S. et al. Circulating Tumor Cells Predict Survival Benefit from Treatment in Metastatic Castration-Resistant Prostate Cancer. Clin. Cancer Res. 14, 6302–6309 (2008).
5. Hiltermann, T. J. N. et al. Circulating tumor cells in small-cell lung cancer: a predictive and prognostic factor. Ann. Oncol. 23, 2937–2942 (2012).
6. Krebs, M. G. et al. Evaluation and Prognostic Significance of Circulating Tumor Cells in Patients With Non–Small-Cell Lung Cancer. J. Clin. Oncol. 29, 1556–1563 (2011).
7. Janni, W. J. et al. Pooled Analysis of the Prognostic Relevance of Circulating Tumor Cells in Primary Breast Cancer. Clin. Cancer Res. 22, 2583–2593 (2016).
8. van Dalum, G. et al. Importance of circulating tumor cells in newly diagnosed colorectal cancer. Int. J. Oncol. 46, 1361–8 (2015).
9. de Wit, S. et al. The detection of EpCAM+ and EpCAM– circulating tumor cells. Sci. Rep. 5, 12270 (2015).
10. Coumans, F. A. W., van Dalum, G., Beck, M. & Terstappen, L. W. M. M. Filter characteristics influencing circulating tumor cell enrichment from whole blood. PLoS One 8, e61770 (2013).
11. Coumans, F. A. W., van Dalum, G., Beck, M. & Terstappen, L. W. M. M. Filtration parameters influencing circulating tumor cell enrichment from whole blood. PLoS One 8, e61774 (2013).
12. ICY. Available at: http://icy.bioimageanalysis.org/.
13. Zeune, L. L. Evaluating the consensus in circulating tumour cell scoring. in Advances in Circulating Tumour Cells (2017).
14. Zeune, L. L. et al. Quantifying HER-2 expression on circulating tumor cells by ACCEPT. PLoS One 12, e0186562 (2017).
15. Rao et al. Expression of epithelial cell adhesion molecule in carcinoma cells present in blood and primary and metastatic tumors. 27, 49–57 (2005).
16. Farace, F. et al. A direct comparison of CellSearch and ISET for circulating tumour-cell detection in patients with metastatic carcinomas. Br. J. Cancer 105, 847–53 (2011).
17. Pecot, C. V. et al. A Novel Platform for Detection of CK+ and CK- CTCs. Cancer Discov. 1, 580–586 (2011).
18. Schneck, H. et al. EpCAM-Independent Enrichment of Circulating Tumor Cells in Metastatic Breast Cancer. PLoS One 10, e0144535 (2015).
19. Lampignano, R. et al. A Novel Workflow to Enrich and Isolate Patient-Matched EpCAMhigh and EpCAMlow/negative CTCs Enables the Comparative Characterization of the PIK3CA Status in Metastatic Breast Cancer. Int. J. Mol. Sci. 18, 1885 (2017).
20. Krebs, M. G. et al. Analysis of circulating tumor cells in patients with non-small cell lung cancer using epithelial marker-dependent and -independent approaches. J. Thorac. Oncol. 7, 306–15 (2012).
21. Yu, M. et al. Circulating breast tumor cells exhibit dynamic changes in epithelial and mesenchymal composition. Science 339, 580–4 (2013).
22. Kallergi, G. et al. Epithelial to mesenchymal transition markers expressed in circulating tumour cells of early and metastatic breast cancer patients. Breast Cancer Res. 13, R59 (2011).
23. Nieto, M. A., Huang, R. Y.-J., Jackson, R. A. & Thiery, J. P. EMT: 2016. Cell 166, 21–45 (2016).
24. Lamouille, S., Xu, J. & Derynck, R. Molecular mechanisms of epithelial–mesenchymal transition. Nat. Rev. Mol. Cell Biol. 15, 178–196 (2014).
25. Zhang,Y. et al. Patterns of circulating tumor cells identified by CEP8, CK and CD45 in pancreatic cancer. Int. J. cancer 136, 1228–33 (2015).

26. Armstrong, A. J. et al. Circulating Tumor Cells from Patients with Advanced Prostate and Breast Cancer Display Both Epithelial and Mesenchymal Markers. Mol. Cancer Res. 9, 997–1007 (2011).

27. Wu, S. et al. Classification of Circulating Tumor Cells by Epithelial-Mesenchymal Transition Markers. PLoS One 10, e0123976 (2015).

28. Alix-Panabières, C., Mader, S. & Pantel, K. Epithelial-mesenchymal plasticity in circulating tumor cells. J. Mol. Med. 95, 133–142 (2017).

29. Willipinski-Stapelfeldt, B. et al. Changes in cytoskeletal protein composition indicative of an epithelial-mesenchymal transition in human micrometastatic and primary breast carcinoma cells. Clin. Cancer Res. 11, 8006–14 (2005).

30. de Wit, S. Single tube liquid biopsy for NSCLC. in Advances in Circulating Tumour Cells (2017).

31. Moll, R., Franke, W. W., Schiller, D. L., Geiger, B. & Krepler, R. The catalog of human cytokeratins: patterns of expression in normal epithelia, tumors and cultured cells. Cell 31, 11–24 (1982).

32. Adams, D. L. et al. Cytometric characterization of circulating tumor cells captured by microfiltration and their correlation to the CellSearch(®) CTC test. Cytometry. A 87, 137–44 (2015).

Supplementary data

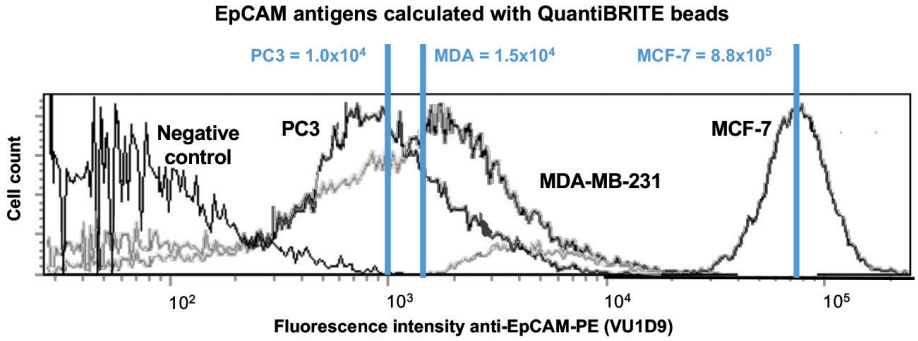

Supplementary Figure S1. Distribution of EpCAM density on cancer cell lines. Histogram showing the distribution of EpCAM density of cancer cell line PC3, MDA-MB-231 and MCF-7 cells, as well as a negative control. The actual number of antigens (blue) was determined by the use of QuantiBRITE beads (BD Bioscience).

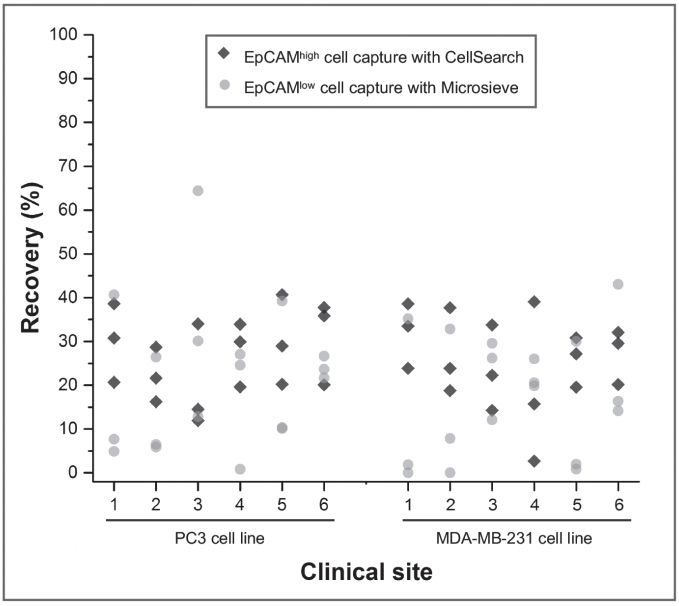

Supplementary Figure S2. Recovery of PC3 and MDA-MB-231 cells per clinical site. Scatter plot displaying the recovery (%) of PC3 and MDA-MB-231 cells of each processed sample with CellSearch and microsieves per clinical site.

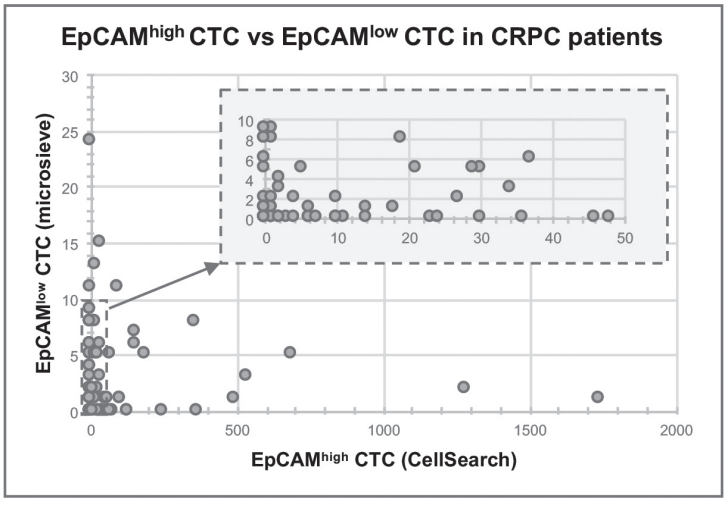

Supplementary Figure S3. CTC counts in 91 CRPC patients. Scatter plot of EpCAM^{high} and EpCAM^{low} CTC counts in 91 castration-resistant prostate cancer patients.

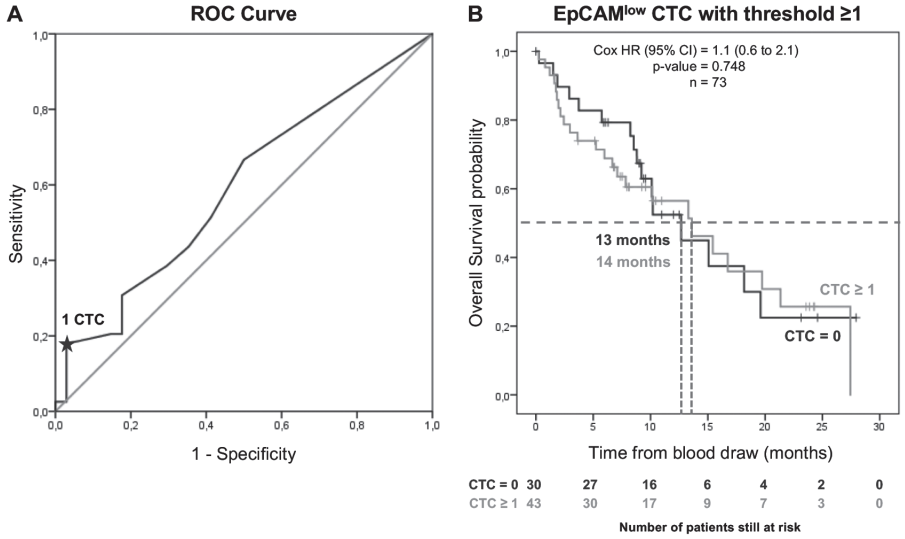

Supplementary Figure S4. Overall survival for EpCAM^{low} CTC with ≥1 CTC cut-off. The ROC curve indicated that the highest diagnostic ability for EpCAM^{low} CTC is with a threshold of 1 CTC (A). The Kaplan Meier curve for overall survival of EpCAM^{low} CTC with 1 CTC threshold shows no correlation with survival (p=0.748) (B).

Supplementary Table S1. Detailed overview of EpCAM^{high} and EpCAM^{low} CTC found in castrate-resistant prostate cancer patients and metastatic breast cancer patients.

Patient #	Cancer location	CellSearch EpCAM^{high} CTC	Microsieve EpCAM^{low} CTC	Patient #	Cancer location	CellSearch EpCAM^{high} CTC	Microsieve EpCAM^{low} CTC
1	Prostate	0	5	**35**	Prostate	66	0
2	Prostate	370	0	**36**	Prostate	71	5
3	Prostate	11	0	**37**	Prostate	24	0
4	Prostate	156	6	**38**	Prostate	0	NA
5	Prostate	0	1	**39**	Prostate	4	0
6	Prostate	30	5	**40**	Prostate	11	NA
7	Prostate	37	6	**41**	Prostate	3	NA
8	Prostate	0	8	**42**	Prostate	2	0
9	Prostate	1	8	**43**	Prostate	10	0
10	Prostate	2	4	**44**	Prostate	2	NA
11	Prostate	955	14	**45**	Prostate	7	0
12	Prostate	97	11	**46**	Prostate	0	NA
13	Prostate	21	5	**47**	Prostate	189	5

Patient #	Cancer location	CellSearch EpCAM^{high} CTC	Microsieve EpCAM^{low} CTC	Patient #	Cancer location	CellSearch EpCAM^{high} CTC	Microsieve EpCAM^{low} CTC
14	Prostate	33	15	**48**	Prostate	29	5
15	Prostate	34	3	**49**	Prostate	6	11
16	Prostate	0	2	**50**	Prostate	731	NA
17	Prostate	2	3	**51**	Prostate	6	0
18	Prostate	1	0	**52**	Prostate	496	1
19	Prostate	27	2	**53**	Prostate	19	13
20	Prostate	0	NA	**54**	Prostate	1	0
21	Prostate	36	0	**55**	Prostate	0	0
22	Prostate	4	NA	**56**	Prostate	686	5
23	Prostate	118	NA	**57**	Prostate	362	8
24	Prostate	65	1	**58**	Prostate	103	1
25	Prostate	0	0	**59**	Prostate	0	1
26	Prostate	23	0	**60**	Prostate	1	0
27	Prostate	NA	0	**61**	Prostate	0	0
28	Prostate	0	0	**62**	Prostate	1740	1
29	Prostate	4	2	**63**	Prostate	130	0
30	Prostate	0	NA	**64**	Prostate	232	NA
31	Prostate	0	0	**65**	Prostate	46	0
32	Prostate	10	2	**66**	Prostate	10	0
33	Prostate	3	0	**67**	Prostate	4	NA
34	Prostate	1	NA	**68**	Prostate	3300	NA
69	Prostate	0	0	**100**	Prostate	0	6
70	Prostate	0	0	**101**	Prostate	0	1
71	Prostate	48	0	**102**	Prostate	2	4
72	Prostate	14	1	**103**	Prostate	0	6
73	Prostate	81	0	**104**	Prostate	1	0
74	Prostate	247	0	**105**	Prostate	156	7
75	Prostate	18	1	**106**	Prostate	0	8
76	Prostate	129	0	**107**	Prostate	0	1
77	Prostate	535	3	**108**	Prostate	0	9
78	Prostate	108	1	**109**	Breast	0	17
79	Prostate	NA	0	**110**	Breast	8	29
80	Prostate	2	0	**111**	Breast	1	35

Patient #	Cancer location	CellSearch EpCAM^{high} CTC	Microsieve EpCAM^{low} CTC	Patient #	Cancer location	CellSearch EpCAM^{high} CTC	Microsieve EpCAM^{low} CTC
81	Prostate	3	NA	**112**	Breast	0	32
82	Prostate	0	0	**113**	Breast	0	0
83	Prostate	19	8	**114**	Breast	0	6
84	Prostate	1	0	**115**	Breast	14	13
85	Prostate	0	0	**116**	Breast	1	7
86	Prostate	5	5	**117**	Breast	1	0
87	Prostate	14	0	**118**	Breast	0	1
88	Prostate	1	2	**119**	Breast	3	15
89	Prostate	0	0	**120**	Breast	1	3
90	Prostate	6	0	**121**	Breast	19	0
91	Prostate	30	0	**122**	Breast	0	0
92	Prostate	65	0	**123**	Breast	208	3
93	Prostate	1281	2	**124**	Breast	0	0
94	Prostate	0	0	**125**	Breast	8	4
95	Prostate	6	1	**126**	Breast	4	3
96	Prostate	51	1	**127**	Breast	17	0
97	Prostate	1	9	**128**	Breast	0	0
98	Prostate	1	1	**129**	Breast	6	2
99	Prostate	0	24	**130**	Breast	0	4

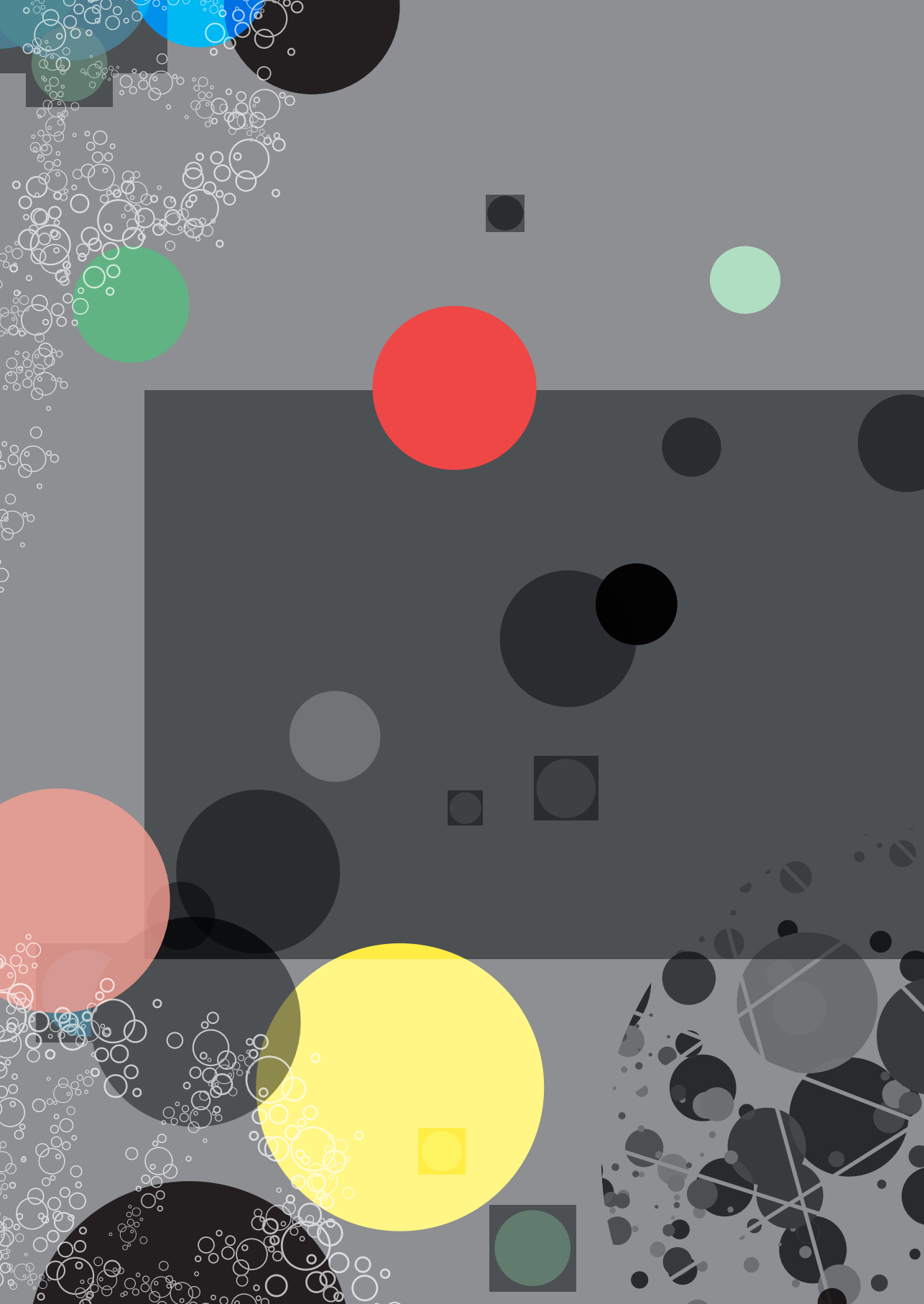

Chapter 4

The detection of EpCAM^{high} and EpCAM^{low} circulating tumor cells

Sanne de Wit*, Guus van Dalum*, Aufried T.M. Lenferink, Arjan G.J. Tibbe,
T. Jeroen N. Hiltermann, Harry J.M. Groen, Cees J.M. van Rijn,
Leon W.M.M. Terstappen

Scientific Reports 5, 12270 (2015); doi10.1038/srep12270

**authors contributed equally*

Abstract

EpCAM expressing circulating tumor cells, detected by CellSearch, are predictive of short survival in several cancers and may serve as a liquid biopsy to guide therapy. Here we investigate the presence of $EpCAM^{high}$ CTC detected by CellSearch and $EpCAM^{low}$ CTC discarded by CellSearch, after EpCAM based enrichment. $EpCAM^{low}$ CTC were identified by filtration and fluorescent labelling. This approach was validated using different cell lines spiked into blood and evaluated on blood samples of 27 metastatic lung cancer patients. The majority of spiked $EpCAM^{high}$ cells could be detected with CellSearch, whereas most spiked cells with low or negative EpCAM expression were detected using filtration. Five or more CTC were detected in 15% of the patient samples, this increased to 41% when adding the CTC detected in the discarded blood. The number of patients with CTC and the number of CTC detected were doubled by the presence of $EpCAM^{low}$ CTC. In this pilot study, the presence of $EpCAM^{high}$ CTC was associated with poor outcome, whereas the $EpCAM^{low}$ CTC were not. This observation will need to be confirmed in larger studies and molecular characterization needs to be conducted to elucidate differences between $EpCAM^{high}$ and $EpCAM^{low}$ CTC.

Introduction

Circulating tumor cells (CTC) are cancer cells disseminated into the blood from primary or metastatic sites. The presence of CTC is predictive of relatively short survival in several types of cancer, including breast, prostate, colon, gastric, bladder, small and non-small cell lung carcinoma and melanoma[1–9]. At a concentration of 1 CTC in 1 mL of blood, they are rare events, especially when compared to 5×10^6 white blood cells and 5×10^9 red blood cells per mL[10,11]. This implies that any assay for CTC enumeration must be able to handle the large number of normal cells. Selection of cells expressing the cell surface epithelial cell adhesion molecule (EpCAM) can be used for CTC enrichment as it has little or no expression on leukocytes and is expressed by the majority of epithelial derived cancers[12–14]. The FDA cleared CellSearch® platform uses CTC enrichment by EpCAM targeted immunomagnetic selection, after which it identifies CTC among the enriched cells by expression of Cytokeratin's 4-6, 8, 10, 13, 18 and 19, lack of CD45 expression, presence of a nucleus and cell like morphology[10]. CTC with this phenotype are associated with poor survival. An unresolved question is

what the frequency and clinical relevance is of CTC, which do not have this phenotype and are thus currently not detected by the CellSearch platform. Here we present a method to investigate the presence of both EpCAM^{high} CTC and EpCAM^{low} CTC. This was achieved by the collection of the blood discarded by the CellSearch after immunomagnetic enrichment of EpCAM^{high} CTC, followed by enrichment of EpCAM^{low} CTC using filtration and immunofluorescent detection. In addition, CTC not expressing cytokeratin 4-6, 8, 10, 13, 18, or 19 were investigated by adding antibodies to cover all cytokeratins. This approach was validated using cells from tumor cell lines with different sizes and EpCAM densities. In a study of 28 metastatic lung cancer patients, we explored the presence of both the EpCAM^{high} CTC and EpCAM^{low} CTC.

Methods

Lung cancer patients and healthy donors

Peripheral blood samples were drawn by venipuncture into 10 mL CellSave Preservative Tubes (Janssen Diagnostics, Huntingdon Valley, PA, USA) from healthy donors and metastatic lung cancer patients treated at the University Medical Center Groningen. Patient demographics are provided in Table 1. All patients provided written informed consent and the study protocol was approved by the medical ethical committee of the University Medical Center Groningen (Groningen, The Netherlands). Blood from healthy volunteers aged 20–55 gave written informed consent before donating blood.

CTC Detection by CellSearch

CTC were enumerated in aliquots of 7.5 mL of blood with the CellSearch system (Janssen Diagnostics). Analysis was performed within 96 hours of the blood draw. Antibodies directed against the epithelial cell adhesion antigen (EpCAM) coupled to ferrofluids were used to enrich CTC. The enriched cells were fluorescently labeled with: the nucleic acid dye 4'6-diaminodino-2-phenylindole (DAPI), phycoerythrin (PE) labeled anti-cytokeratin monoclonal antibodies (mAbs) C11 and A53.B/A2 and Allophycocyan (APC) labeled mAb directed against CD45 (clone HI30) recognizing leukocytes using the CellSearch CTC kit (Janssen Diagnostics). To cover all cytokeratins, the Fluorescein (FITC) labeled anti-cytokeratin mAbs LP5K (Millipore,

Billerica MA, USA) and Ks20.10 (Acris Antibodies, Herford, Germany) were added at 11.2 µg/mL and AE1/AE3 (eBioscience, San Diego CA, USA) was added at 5.6 µg/mL to the extra marker position in the CellSearch Epithelial Cell kit. The extra marker channel was used for the measurement of FITC on the CellTracks Analyzer II. Images of CTC candidates were identified by the CellTracks Analyzer II analyzing the sample twice, using either PE or FITC as the cytokeratin marker and presented to experienced operators for classification. Candidates were assigned as CTC when the objects were larger than 4 µm, stained with DAPI and cytokeratin, lacked CD45 staining and had morphological features consistent with that of a cell[10].

Table 1. Patient demographics of the lung cancer patients in this study.

Lung cancer patients	***(n=27)***
Age (years)	
Average	62
Min-Max	32-82
Gender	
Male	52%
Female	48%
Type	
Adenocarcinoma	18
Squamous Cell carcinoma	4
Small Cell Carcinoma	3
Large Cell Carcinoma	2
Line of therapy	
1st line	74%
≥2 line	26%
Status at last follow-up	
Alive	59%
Dead	41%
Average follow-up time in days (min-max)	
Alive	201 (85-321)
Dead	115 (22-192)

Blood waste collection of CellTracks Autoprep

After immunomagnetic selection of EpCAM^{high} cells, the CellTracks Autoprep aspirates the blood that is void of the selected cells and transports it to a waste container outside the instrument. To enable the investigation of this blood for

residual tumor cells, a device was designed and build to collect this sample waste of the blood samples placed on the CellTracks Autoprep. The device was inserted between the waste tube from the CellTracks Autoprep system and the waste container. The device uses a LED and a photo diode to sense the presence of approaching blood in the waste tube and diverted the samples into standard 50 mL conical sample tubes using an actuated 3-way valve. A motorized rotor holding twelve 50 mL tubes was used to position the correct tube under the valve at the appropriate time. The waste collection device was controlled using a LabView (National Instruments, Austin TX, USA) program on a laptop computer. Figure 1A shows a schematic representation of the waste collection.

Filtration of CellTracks Autoprep blood waste

The system to filter tumor cells from whole blood or the Autoprep waste comprises of a pump unit and a filtration unit holding a slide with a microsieve (VyCAP, Deventer, The Netherlands). The pump unit maintained a pressure of -100 mbar across the microsieve during filtration of the blood. A schematic image of this system is presented in Figure 1B. The microsieve filtration membrane is atomically flat and has a thickness of 1 μm and is supported by 350 μm thick silicon supports. The total surface area is 8 by 8 mm and contains 111,800 pores of 5 μm in diameter which are spaced 14 μm apart in lanes with a porosity of 10%. Specifications of the microsieves were obtained from previous experiments[15,16]. The CellSearch discarded sample was transferred to the filtration unit after which the pump was switched on. The collected sample waste of 35 mL was passed through in 2-15 minutes. This processing time is donor dependent. After completion of the filtration, the pump was switched off and the slide containing the microsieve is removed for staining.

Staining of cells on microsieves

Conditions for staining on microsieves were optimized to assure uniform staining across the microsieve with a minimum of non-specific binding. After filtration the microsieve was removed and washed with PBS-saponin 0.15%. Next, a permeabilization buffer of PBS with 0.15% saponin (Sigma-Aldrich, St. Louis MO, USA) was placed on the sieve and removed after 15 minutes incubation at room temperature. A cocktail of fluorescently labeled antibodies was used to stain the cells on the sieve for 15 minutes at 37°C

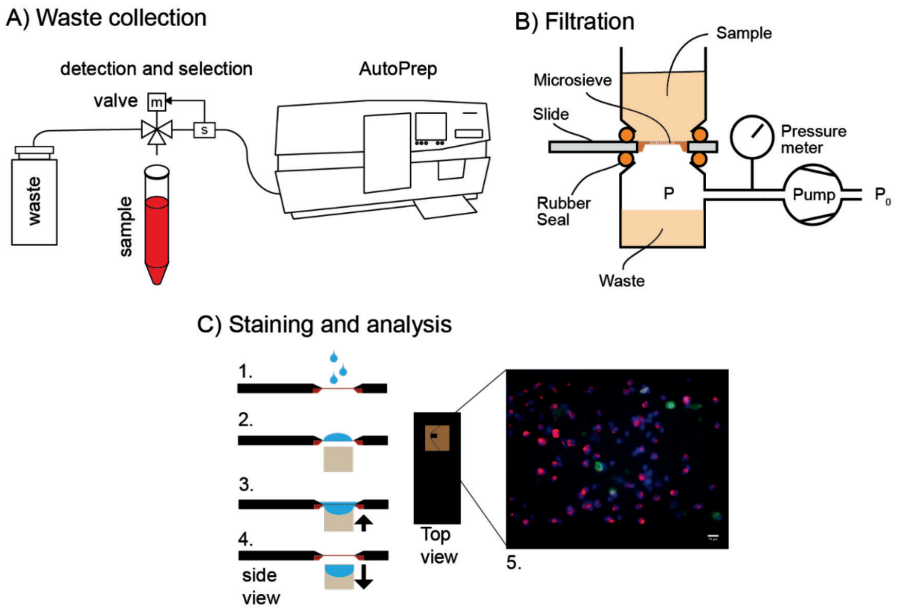

Figure 1. A schematic representation of the waste collection and filtration, followed by analysis of the microsieve with CTC. Blood discarded after immunomagnetic enrichment of EpCAM^{high} cells by CellSearch Autoprep is collected (A). A pump with disposable filtration unit containing a slide with a microsieve filters the discarded blood (B). The staining of the cells is performed directly on the filter (C) by adding a staining cocktail (1), incubating (2) and removing the liquid (3 and 4). The microsieve is analyzed using fluorescence microscopy for detection of EpCAM^{low} CTC (5). Scale bar 10 µm

using a heating plate (StatSpin, Westwood MA, USA). The staining solution consisted of 3 µM of the nucleic acid dye DRAQ5 (CellSignaling, Danvers MA, USA) and the following monoclonal antibodies: two antibodies targeting CK 4-6, 8, 10, 13, 18 and 19 (C11 and A.53B/A2, Janssen Diagnostics) labeled with PE, three antibodies targeting CK 1-8,10,14-16, 19 &20 (AE1/AE3, LP5K and Ks20.10) labeled to FITC and one antibody targeting CD45 (HI30) labeled with Brilliant Violet 421 (Biolegend, San Diego CA, USA). All antibodies were diluted to a final concentration of 1 µg/mL (HI30, C11, A.53B/A2 and AE1/AE3) or 2 µg/mL (LP5K and Ks20.10) in PBS containing 1% bovine serum albumin (Sigma) and 0.05% saponin. After removal of the staining cocktail, the microsieve was washed 2 times with PBS-BSA 1%. Then the sample was fixed using PBS with 1% formaldehyde (Sigma) for 10 minutes at room temperature. Removal of the fluid during each of the staining and washing steps was done by bringing the bottom of the microsieve in contact with an absorbing material using a staining holder (VyCAP), as illustrated in Figure 1C. The microsieve was subsequently covered with PVA-DABCO

(Sigma) mounting medium solution containing 3 µM of DRAQ5. A custom cut 0.85 by 0.85 cm glass coverslip (Menzel-Gläser, Saarbrükener, Germany) was placed on top of the microsieve for immediate analysis or storage in the freezer at –30°C.

Cell lines and spiking

Spiking experiments were performed with cells from the bladder carcinoma cell line T24, the breast carcinoma cell lines SKBR3, the colorectal cancer cell lines Colo-320 and SW480 and the lung cancer cell line NCI-H1650. All cell lines were obtained from ATCC (Manassa, VA, USA) and have not been authenticated in the past six months. They were grown at 37°C and 5% CO^2. SKBR3 and SW480 were cultured in Dulbecco's modified eagle medium (Sigma), NCI-H1650 and Colo-320 were cultured in RPMI-1640 (Sigma) and T24 was cultured in DMEM-F12 (Sigma). Culture media were supplemented with 10% fetal calf serum (Gibco, Invitrogen, Carlsbad CA, USA), 1% L-glutamin (Sigma) and 1% penicillin-streptomycin (Gibco). The median cell size was determined with a Coulter counter pipette (Scepter, Millipore, Billerica, MA, USA). The EpCAM density was determined using a flow cytometer (FACS ARIA II, BD Biosciences, San Jose, CA, USA) and QuantiBrite beads (BD Biosciences). For characterization of the microsieve performance, T24, Colo-320 and NCI-H1650 cells were stained with 5 µM CellTracker Orange CMTMR and SKBR-3 and SW480 cells with 25 µM CellTracker Green BODIPY (Invitrogen). Cells were incubated in culture media for 24 hours at 37°C with CellTracker prior to harvesting with 0.05% Trypsin-EDTA (Gibco). The prestained cells were spiked in healthy donor CellSave blood to determine filtration recovery. Cell numbers for spiking were counted with TruCOUNT Tubes (BD Biosciences) by flow cytometry. To determine the efficiency of the staining solution, spikes of approximately 300 NCI-H1650 cells were counted manually and subsequently added to healthy volunteer blood samples. The exact numbers of cells counted were used to determine the recovery on the sieve. Unspiked blood samples from healthy volunteers were used as a negative control.

Detection of cells on microsieves

A Nikon E400 fluorescence microscope equipped with a Mercury Arc lamp as light source, a 10X (0.45NA) objective (Nikon, Tokyo, Japan), a computer-controlled CCD camera (Hamamatsu Photonics, Hamamatsu, Japan), X,Y,Z

stage and 4-filter cube exchanger (LEP, Hawthorne NY, USA) with filters were used for acquisition of the fluorescent images covering the 0.64 cm^2 surface of the microsieves. The following filters were used: APC with excitation 621/32 nm, dichroic 647 nm LP, emission 682/52 nm (Spectra Physics Newport, Santa Clara, CA, USA); BV421 with excitation 390/40 nm, dichroic 405 nm LP, emission 438/24 nm (Semrock, Rochester, NY, USA); FITC with excitation 480/20 nm, dichroic 495 nm LP, emission 510/20 nm (Spectra Physics Newport); and PE with excitation 547/12 nm, dichroic 560 nm LP, emission 579/25 nm (Spectra Physics Newport). The scanning and image acquisition was controlled by Labview (National Instruments, Austin TX, USA).

Scoring of CTC

The CellSearch cartridges were analyzed twice, first to identify the traditional markers (DAPI+, CK-PE+, CK-FITC–, CD45–) and a dual positive CTC definition (DAPI+, CK-PE+, CK-FITC+, CD45–) after which the sample was reanalyzed for only the additional cytokeratin (DAPI+, CK-PE–, CK-FITC+, CD45–). A previously described image analysis algorithm written in MATLAB® was used to analyze the images taken from the microsieve and select likely CTC candidates by using a broader CTC classifier[17]. The actual scoring of CTC was performed by a trained operator.

Statistical analysis

Statistical analysis was done using R[18]. A p-value less than 0.05 was considered to indicate a significant difference. Patients were divided into two prognostic groups: favorable for zero CTC and unfavorable for those with CTC. Kaplan-Meier curves for overall survival were generated and compared using the Log-Rank test.

Results

Capture efficiency of fluorescently labeled spiked cell lines

Two aliquots of 7.5 mL of peripheral blood from five healthy donors were spiked with approximately 500 pre-labeled cells from the tumor cell lines T24, SKBR3, Colo-320, SW480 and NCI-H1650. The EpCAM antigen density of cells of each cell line was determined by flow cytometry and varied from

hundreds of molecules to millions. The size was determined by Coulter counter pipette and was 11-12 µm for smaller cells and 16 µm for larger cells. When each sample was run in the CellTracks Autoprep, the blood discarded by the system was collected and passed through the filtration device as illustrated in Figure 1. The numbers of T24, SKBR3, Colo-320, SW480 and NCI-H1650 on the microsieves and inside the CellSearch cartridges were counted. The average number of cells counted and the standard deviation in the CellSearch cartridge and on the microsieves for each of the cell lines are provided in Table 2. The EpCAM^{high} cells show a high recovery of cells in the cartridge, whereas the EpCAM^{low} cells are mainly recovered on the microsieve. Because all samples travel through the same waste tubing, this could be a theoretical cause for carryover between collected samples. To determine this carryover on the CellTracks Autoprep, a blood sample of a healthy donor without tumor cells was placed after each sample spiked with T24 and SKBR3 cells and run through the complete protocol. The waste of these samples was also collected and filtered to determine the carryover between samples. The average percentage of the spiked cells found in six healthy donor samples was 0.3% (±0.3) for T24 cells and 1% (±0.3) for the SKBR3.

Capture and staining efficiency of unlabeled spiked cell lines

To evaluate the staining efficiency of the captured cells, cells from the T24 bladder cancer cell line and NCI-H1650 lung cancer cell line were spiked in blood of healthy donors. The average number of spiked cells identified in the CellSearch cartridge and on the microsieve is shown in Table 2. This also shows the percentage of identified cells being significantly lower as compared to the pre-stained cells; 23% versus 59% for T24 and 27% versus 60% for NCI-H1650. To evaluate the background of CTC identified by CellSearch and on the microsieves in the CellSearch Waste, blood samples of eleven healthy controls were used and minimal CTC (on average less than 1) were detected in these unspiked samples, also shown in Table 2.

Identification of CTC in blood from metastatic lung cancer patients by CellSearch with additional cytokeratin antibodies

To determine whether or not additional anti-cytokeratin antibodies increased the number of detected CTC, the images were reanalyzed using cytokeratin FITC and DAPI as the primary threshold to generate images of CTC candidates

for review in the CellTracks Analyzer II, instead of the traditional cytokeratin PE and DAPI as the primary threshold. By combining the two reviews of each sample, the CTC were divided into three groups: 1. CTC only positive for CK-PE in the original CellSearch test; 2. CTC only positive for CK-FITC; and 3. CTC positive for both CK-PE and CK-FITC. Of all the CTC that were detected, 50% were stained with the added CK-FITC markers and this additional CK-FITC was the only CK stain present in 15% of these CTC. The percentage of patient samples with ≥1 CTC in 7.5 mL of blood increased from 41% to 52%, when adding the number of CTC identified by the extra CK. A comparable increase was shown for a threshold of ≥3 CTC from 19% to 26% and for ≥5 CTC from 15% to 19%. The results of these analyses are summarized in Table 3 and the number of cells scored in each sample can be found in Supplementary Table S1.

Table 2. Recovery of cell lines in healthy donor blood. Recovery of cell lines spiked in blood of healthy donors and processed by CellSearch (CS) and the blood discarded by CS was collected and filtered through a microsieve (MS). The cells in the CS cartridges were counted on the CellTracks Analyzer II and the cells on the MS by standard fluorescent microscope.

	Relatively large		Relatively small			Healthy Control
	T24	**SKBR3**	**Colo-320**	**SW480**	**NCI-H1650**	**(N=11)**
Classification	$EpCAM^{low}$	$EpCAM^{high}$	$EpCAM^{low}$	$EpCAM^{high}$	$EpCAM^{neg}$	
EpCAM molecules	4.9×10^3	1.5×10^6	2.0×10^3	2.3×10^6	1.4×10^2	
Size	16 µm	16 µm	11 µm	11 µm	12 µm	
Average recovery of pre-stained cells ± standard deviation (N=5)						
CS recovery	2% (±1)	87% (±12)	2% (±2)	91% (±13)	0.2% (±0.3)	nd
MS recovery	59% (±9)	2% (±1)	18% (±6)	6% (±7)	60% (±7)	nd
Average recovery of cells not pre-stained ± standard deviation (N=4)						
CS recovery	15% (±5)	nd	nd	nd	0.1% (±0.1)	0.3 (±0.9)
MS recovery	23% (±7)	nd	nd	nd	32% (±7)	0.3 (±0.6)

Identification of CTC in blood from metastatic lung cancer patients discarded by CellSearch

The number of CTC in the blood discarded by the CellTracks Autoprep was analyzed in blood from 27 patients. The waste that belongs to a single blood sample of 7.5 mL, that is processed and then discarded by the Autoprep,

has a volume of approximately 35 mL because of dilution with the system buffer during the CTC isolation process. Filtration of this waste volume of 35 mL takes 2-15 minutes. Figure 2A shows typical examples of images of CTC and leukocytes identified by CellSearch, whereas Figure 2B displays typical images of CTC and leukocytes collected on the microsieve after filtration. The colors and scaling of the images was kept the same to obtain a fair comparison. When adding the number of CTC found in the waste by filtration, the percentage of patient samples with ≥1 CTC in 7.5 mL of blood increased from 41% to 74%. A similar increase was shown for a threshold of ≥3 CTC from 19% to 52%, for ≥5 CTC this increased from 15% to 41%, and for ≥10 CTC this increased from 11% to 26%. In the discarded blood, ≥1 CTC were detected in 33% of lung cancer patients in which no CTC were detected by CellSearch. This frequency decreases to 33%, 22% and 15% when thresholds were increased to ≥3, ≥5 and ≥10 CTC respectively. CTC were found by CellSearch in 41% of the samples, while in 52% CTC were found in the waste using microsieve filtration. In 19% of the samples, CTC were detected by CellSearch and in the CellSearch Waste. There is no correlation between the number of both types of CTC in each sample with a Spearman's Rho of 0.009. The number of cells found is summarized in Table 3 and can be found in more detail in Supplementary Table S1.

Table 3. Overview of patients (n=27) with detected number of CTC. Overview of CTC that are detected in 27 lung cancer patients. For detection with CellSearch, extra CTC with additional cytokeratin are separately included. CTC detected on the microsieves after filtration of the discarded blood from CellSearch are separately included as well. The final percentage of patients show the detected CTC from all above categories in total.

	% Patients with CTC			
Method	**≥1**	**≥3**	**≥5**	**≥10**
CellSearch CTC	41%	19%	15%	11%
CellSearch CTC & additional CellSearch CK-marker CTC	52%	26%	19%	11%
CellSearch CTC & filtered CTC from CellSearch Waste	74%	52%	41%	26%
All types of CTC	**81%**	**56%**	**41%**	**26%**

CTC and overall survival

To relate the presence of CTC to overall survival, the patient group was split into those with and those without detectable CTC. In Figure 3 the Kaplan-Meier for the different CTC definitions are shown. Panel A shows

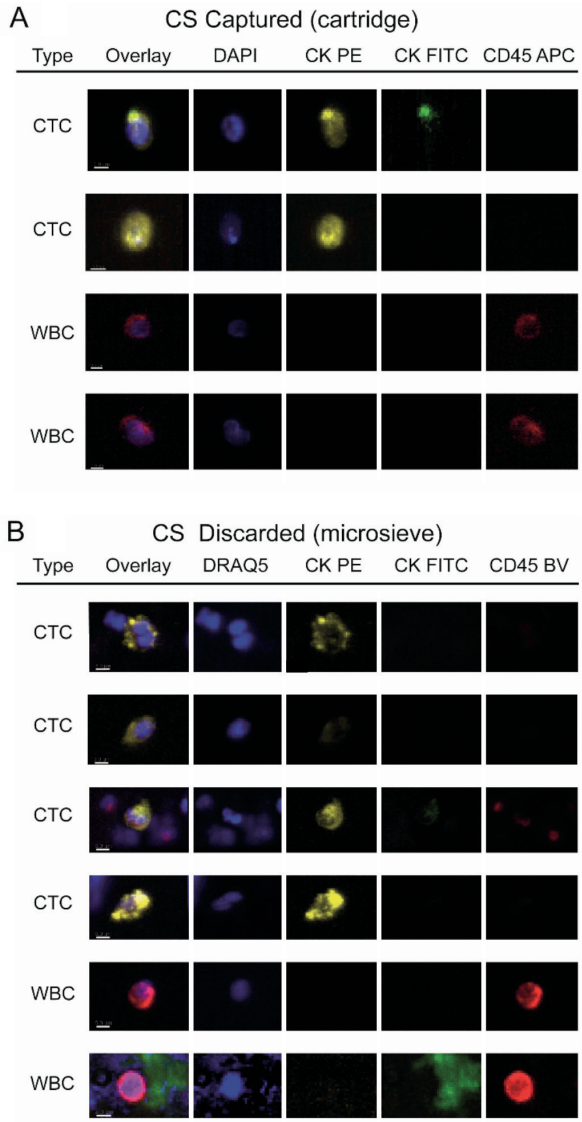

Figure 2. Thumbnail gallery of CTC and leukocytes in a lung cancer patient identified by CellSearch and in the blood discarded by CellSearch after filtration.

a significant difference (p=0.006) in overall survival when using CTC defined by CellSearch (41% patients with ≥1 CTC). Panel B also shows a significant difference (p=0.007) in overall survival when using CTC defined by CellSearch with the addition cytokeratin coverage (52% patients with ≥1 CTC). Panel C shows no significant difference (p=0.308) in overall

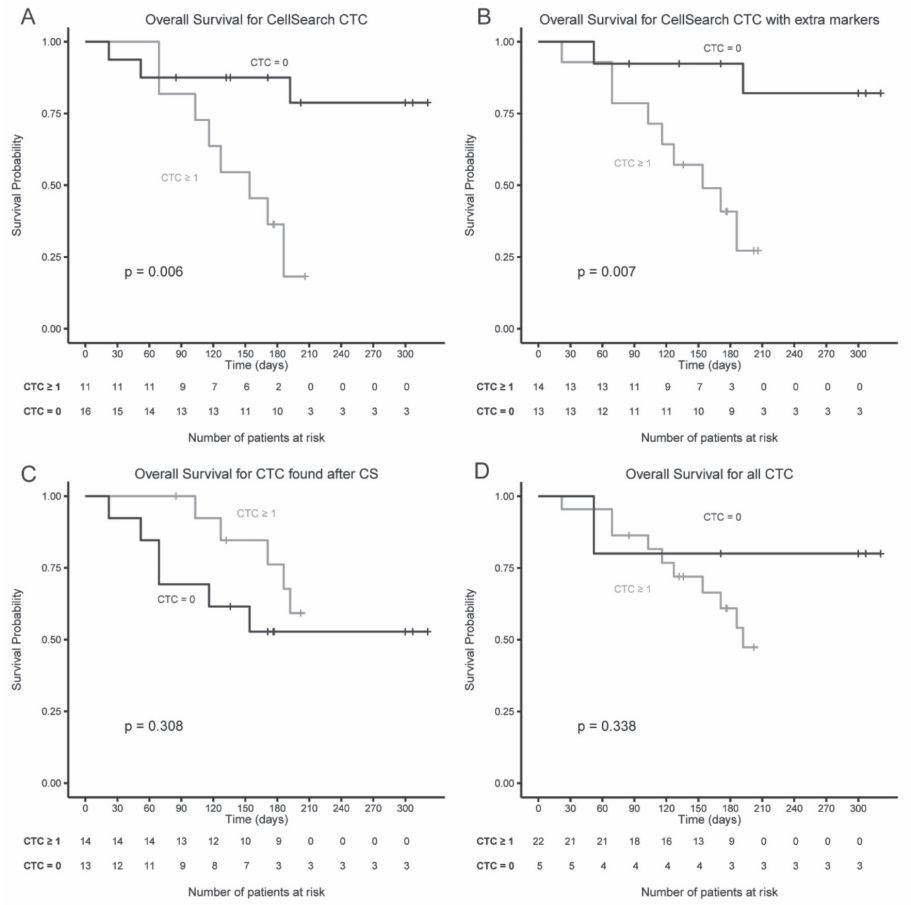

Figure 3. Kaplan-Meier curves for overall survival for CTC subpopulations with a cut-off of 1 CTC or more. Panel A: EpCAM^{high}/CK 8,18,19+ CTC detected by CellSearch. Panel B: EpCAM^{high}/panCK+ CTC detected by CellSearch. Panel C: EpCAM^{low}/panCK+ CTC after filtration of blood discarded by CellSearch (CS). Panel D: all populations of EpCAM^{high}/panCK+ CTC and EpCAM^{low}/panCK+ CTC.

survival when using the EpCAM^{low} CTC detected in the blood discarded by CellSearch (74% patients with ≥1 CTC). Panel D also shows no significant difference (p=0.338) in overall survival when all types of CTC detected were evaluated (81% patients with ≥1 CTC). These results change slightly when the threshold was set at ≥5 CTC (see Supplementary Figure S1 and Table 3). For CellSearch, 15% of patients had ≥5 CTC with a significant difference in overall survival (p=0.007). The significant association between CTC with additional cytokeratin coverage and overall survival is dependent

on the threshold, 19% of patients had ≥5 CTC, but there was no longer a significant difference in overall survival (p=0.075). For EpCAM^{low} CTC, 26% of patients had ≥5 CTC and no significant difference in overall survival was found (p=0.526). Finally, for all types of CTC detected, 41% of patients had ≥5 CTC and no significant difference was noted (p=0.118).

Discussion

Treatment options for patients with metastatic cancer are increasing and create a need for biomarkers to determine whether the tumor will respond to the intended therapy. To enable quantitative real-time drug responsiveness, biomarkers need to be determined at multiple time points. The ability to obtain tumor cells from the blood would enable the ability to assess the presence of treatment targets on tumor cells real time. Prerequisite to achieve this goal is the presence of CTC in blood, which can be isolated, their identity verified and their composition determined. The heterogeneity of CTC within individual patients imposes the need for analysis of multiple CTC. Ten or more CTC are detected in 7.5 mL of blood in 11% of metastatic colorectal, 32% of metastatic breast and 40% of metastatic prostate cancer cases, using the CellSearch system, which is the current standard for CTC enumeration[11]. Although processing larger blood volumes could circumvent this issue, the presence of CTC with a different phenotype, as those identified with the CellSearch system, may also increase the number of CTC detected[11,19,20]. Requirement is that these CTC are also representative of the tumor and their presence is associated with poor outcome. Many alternative technologies have been introduced and compared with the results of the CellSearch system[21–31]. Most of these studies show the presence of more CTC, but do not address the question whether these identified cells have clinical relevance or the difference between the detected cells and the CellSearch CTC. To address the question which "CTC" are not detected by the CellSearch approach, we expanded the coverage of the cytokeratins used in the CellSearch system and we captured the blood discarded by the CellSearch system after immunomagnetic depletion of the EpCAM expressing cells in the blood and investigated the presence of CTC after filtration.

Cell lines with different sizes, EpCAM expression and cytokeratin expression were spiked in blood to determine the proportion of each cell type that can be detected. The capture efficiency of fluorescently pre-labeled spiked cell lines shows the expected results; recovery of the cells with CellSearch is proportional to the density of the EpCAM antigen and recovery of the cells on the microsieve

after filtration is related to the size of the cells[16]. The experiments confirm that the CellSearch system is very efficient in recovery of cells with relatively high EpCAM expression. Cells with low or no EpCAM expression significantly decreases the efficiency and a large portion of these cells can be captured in the blood discarded by the CellSearch system using filtration. Filtration efficiency, however, depends on the size of the cells and smaller tumor cells will still be missed using this approach. The configuration of the microsieves used for filtration was previously optimized for the filtration of whole blood[15,16]. The approximately 5-fold increase in volume by the dilution of the blood discarded by the CellSearch Autoprep does not seem to have a negative effect on the enrichment of cell lines by filtration, since the capture efficiency of cells from different cell lines was similar in whole blood[15].

To investigate the influence of the staining protocol and microscopic examination on cell identification, unlabeled cells of different sizes were spiked in blood. Compared to the pre-stained cells, the percentage of identified cells was significantly lower (see Table 2). This observation demonstrates that improvements in CTC detection can be obtained by improving the staining and detection of these cells on microsieves.

Carryover between collected samples in the CellSearch Autoprep could theoretically occur, since all samples travel through the same waste tubing. Spiking experiments showed only a carryover of 1% and less, which is approximately one magnitude larger than with the CellSearch test, where carryover is possible when samples have a CTC count higher than 5000 cells. A maximum of 30 CTC were found in the CellSearch Waste of patient samples, therefore we do not expect carryover to have influenced our results. Control samples containing higher number of spiked cell lines were always placed at later positions in the CellSearch Autoprep when processed with patient samples in the same run, to make sure that patient samples would be collected first.

The percentage of patient samples with ≥1 CTC in 7.5 mL of blood increased from 41% to 81%, when adding the number of CTC found in the waste by filtration and adding the CTC identified by the extra cytokeratins. A similar increase was shown for a threshold of ≥3, ≥5 and ≥10 CTC. This increase in detected CTC number can be contributed mainly to the presence of CTC in the blood discarded by the CellSearch system, as can be seen in Table 3. It is likely these CTC express very little or no EpCAM. This was demonstrated by the processing of blood of healthy donors spiked with cell lines, and are therefore not detected by the CellSearch system.

The urging question is whether this increase in the number of CTC is also reflected in the clinical outcome of the patients. To start addressing this question, we asked the treating physicians after the study was completed for the last date of contact with the patients and the date of death, if that had occurred. The relation between overall survival and the type of CTC detected was determined and displayed using Kaplan-Meier curves, as shown in Figure 3. We confirmed the relation between EpCAM^{high}/CK 8,18,19+ CTC detected by CellSearch and poor outcome (Figure 3A). This relation was maintained by increasing the coverage of the cytokeratins, which resulted in more patients having CTC detected in blood (Figure 3B). The level of significance depended on the CTC threshold and clearly shows the limitations of the small patient cohort, which were also diverse with respect to cancer type and line and type of therapy (see Table 1 and Supplementary Table S1). We did not find a significant relation between the presence of EpCAM^{low}/panCK+ CTC and overall survival (Figure 3C) and also no relation between overall survival and all types of CTC detected (Figure 3D). The number of patients is too small in numbers to make any definitive conclusions. Still, this pilot study warrants a larger study to confirm the findings. It also urges for an in-depth characterization of the EpCAM^{high} and EpCAM^{low} CTC to confirm by molecular analysis that the EpCAM^{low}/panCK+ cells are indeed cancerous cells, as well as identifying antigens that may explain the difference in clinical behavior, for example the means for CTC to extravasate and form distant metastasis.

References

1. Racila, E. et al. Detection and characterization of carcinoma cells in the blood. Proc. Natl. Acad. Sci. U. S. A. 95, 4589–4594 (1998).
2. Cristofanilli, M. & Budd, G. Circulating tumor cells, disease progression, and survival in metastatic breast cancer. Engl. J. Med. 351, 781–791 (2004).
3. de Bono, J. S. et al. Circulating tumor cells predict survival benefit from treatment in metastatic castration-resistant prostate cancer. Clin. cancer Res. 14, 6302–9 (2008).
4. Cohen, S. J. et al. Relationship of Circulating Tumor Cells to Tumor Response, Progression-Free Survival, and Overall Survival in Patients With Metastatic Colorectal Cancer. J. Clin. Oncol. 26, 3213–3221 (2008).
5. Hiltermann, T. J. N. et al. Circulating tumor cells in small-cell lung cancer: a predictive and prognostic factor. Ann. Oncol. 23, 2937–2942 (2012).
6. Krebs, M. G. et al. Evaluation and Prognostic Significance of Circulating Tumor Cells in Patients With Non–Small-Cell Lung Cancer. J. Clin. Oncol. 29, 1556–1563 (2011).

7. Matsusaka, S. et al. Circulating tumor cells as a surrogate marker for determining response to chemotherapy in patients with advanced gastric cancer. Cancer Sci. 101, 1067–71 (2010).
8. Rao, C. et al. Circulating melanoma cells and survival in metastatic melanoma. Int. J. Oncol. 38, 755–60 (2011).
9. Gazzaniga, P. et al. Prognostic value of circulating tumor cells in nonmuscle invasive bladder cancer: a CellSearch analysis. Ann. Oncol. 23, 2352–6 (2012).
10. Allard, W. J. et al. Tumor cells circulate in the peripheral blood of all major carcinomas but not in healthy subjects or patients with nonmalignant diseases. Clin. cancer Res. 10, 6897–904 (2004).
11. Coumans, F. A. W., Ligthart, S. T., Uhr, J. W. & Terstappen, L. W. M. M. Challenges in the Enumeration and Phenotyping of CTC. Clin. cancer Res. 18, 5711–8 (2012).
12. Herlyn, D. et al. Efficient selection of human tumor growth-inhibiting monoclonal antibodies. J. Immunol. Methods 73, 157–167 (1984).
13. Stahel, R., Gilks, W., Lehmann, H. & Schenker, T. Third international workshop on lung tumor and differentiation antigens: overview of the results of the central data analysis. Int. J. cancer 6–26 (1994).
14. Rao, C. G. et al. Expression of epithelial cell adhesion molecule in carcinoma cells present in blood and primary and metastatic tumors. Int. J. Oncol. 27, 49–57 (2005).
15. Coumans, F. A. W., van Dalum, G., Beck, M. & Terstappen, L. W. M. M. Filtration parameters influencing circulating tumor cell enrichment from whole blood. PLoS One 8, e61774 (2013).
16. Coumans, F. A. W., van Dalum, G., Beck, M. & Terstappen, L. W. M. M. Filter characteristics influencing circulating tumor cell enrichment from whole blood. PLoS One 8, e61770 (2013).
17. Ligthart, S. T. et al. Unbiased and automated identification of a circulating tumour cell definition that associates with overall survival. PLoS One 6, e27419 (2011).
18. R Core Team. R: A Language and Environment for Statistical Computing. (2013).
19. van Dalum, G. et al. Importance of circulating tumor cells in newly diagnosed colorectal cancer. Int. J. Oncol. 46, 1361–8 (2015).
20. van Dalum, G. et al. Circulating tumor cells before and during follow-up after breast cancer surgery. Int. J. Oncol. 46, 407–413 (2014).
21. Rosenberg, R. et al. Comparison of two density gradient centrifugation systems for the enrichment of disseminated tumor cells in blood. Cytometry 49, 150–8 (2002).
22. Hsieh, H. Ben et al. High speed detection of circulating tumor cells. Biosens. Bioelectron. 21, 1893–9 (2006).
23. Nagrath, S. et al. Isolation of rare circulating tumour cells in cancer patients by microchip technology. Nature 450, 1235–9 (2007).
24. Lin, H. K. et al. Portable filter-based microdevice for detection and characterization of circulating tumor cells. Clin. Cancer Res. 16, 5011–8 (2010).
25. Stott, S. L. et al. Isolation of circulating tumor cells using a microvortex-generating herringbone-chip. Proc. Natl. Acad. Sci. U. S. A. 107, 18392–7 (2010).
26. Williams, A. et al. Reporting the capture efficiency of a filter-based microdevice: a CTC is not a CTC unless it is CD45 negative--letter. Clin. Cancer Res. 17, 3050–3050 (2011).

27. Khoja, L. et al. A pilot study to explore circulating tumour cells in pancreatic cancer as a novel biomarker. Br. J. Cancer 106, 508–16 (2012).
28. Krebs, M. G. et al. Analysis of circulating tumor cells in patients with non-small cell lung cancer using epithelial marker-dependent and -independent approaches. J. Thorac. Oncol. 7, 306–15 (2012).
29. Hou, H. W. et al. Isolation and retrieval of circulating tumor cells using centrifugal forces. Sci. Rep. 3, 1259 (2013).
30. Adams, D. L. et al. The systematic study of circulating tumor cell isolation using lithographic microfilters. RSC Adv. 4, 4334 (2014).
31. Adams, D. L. et al. Circulating giant macrophages as a potential biomarker of solid tumors. Proc. Natl. Acad. Sci. U. S. A. 111, 3514–9 (2014).

Supplementary Data

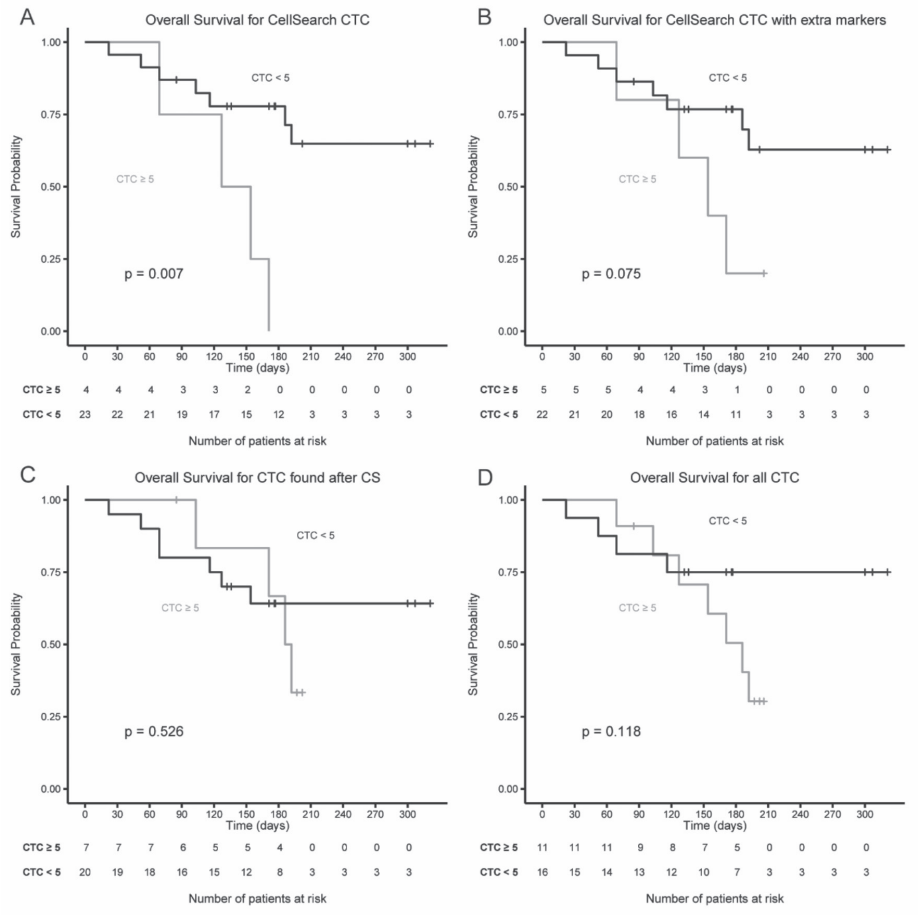

Supplementary Figure S1. Overall survival for CTC subpopulations with a ≥5 CTC cut-off. Kaplan-Meier curves for overall survival for CTC subpopulations with a cut-off at 5 or more CTC. Panel A: EpCAM^{high}/CK 8,18,19+ CTC detected by CellSearch. Panel B: EpCAM^{high}/panCK+ CTC detected by CellSearch. Panel C: EpCAM^{low}/ panCK+ CTC after filtration of blood discarded by CellSearch (CS). Panel D: all populations of EpCAM^{high}/ panCK+ CTC and EpCAM^{low}/panCK+ CTC.

Supplementary Table S1. Detailed overview of CTC found in lung cancer patients. The left part shows the total number of CTC found using the traditional CellSearch count and the CTC found in waste filtration. The right part lists the CTC found using the FITC labeled CK-cocktail. The events scored as CK-FITC+ are the results of a reanalysis on the CellTracks of the same sample using the FITC channel for CK detection.

	CellSearch & EpCAM^{low} CTC			CellSearch extra cytokeratin markers				Cancer
Patient #	**Total CTC**	**CTC CellTracks**	**CTC Waste**	**CK PE+**	**CK PE+, CK FITC+**	**CK FITC+**	**Total**	**type**
1	0	0	0	0	0	0	0	Adeno
2	0	0	0	0	0	0	0	Squamous
3	2	2	0	0	2	0	2	Adeno
4	0	0	0	0	0	2	2	Squamous
5	0	0	0	0	0	0	0	Adeno
6	11	11	0	2	9	0	11	Adeno
7	2	2	0	1	1	0	2	Adeno
8	31	1	30	1	0	1	2	Squamous
9	43	29	14	15	14	3	32	Adeno
10	16	2	14	2	0	0	2	Adeno
11	6	0	6	0	0	0	0	Adeno
12	1	0	1	0	0	0	0	Adeno
13	3	0	3	0	0	0	0	Adeno
14	6	2	4	2	1	2	5	Large cell
15	16	0	16	0	0	0	0	Adeno
16	2	0	2	0	0	0	0	Adeno
17	1	0	1	0	0	0	0	Adeno
18	5	0	5	0	0	1	1	Small cell
19	13	10	3	10	1	1	12	Small cell
20	0	0	0	0	0	0	0	Adeno
21	1	1	0	0	1	2	3	Adeno
22	4	4	0	4	0	0	4	Adeno
23	0	0	0	0	0	0	0	Squamous
24	6	6	0	6	1	0	6	Small cell
25	0	0	0	0	0	1	1	Adeno
26	3	0	3	0	0	0	0	Adeno
27	2	0	2	0	NA	NA	0	Adeno
28	10	0	10	0	0	0	0	Large cell


4

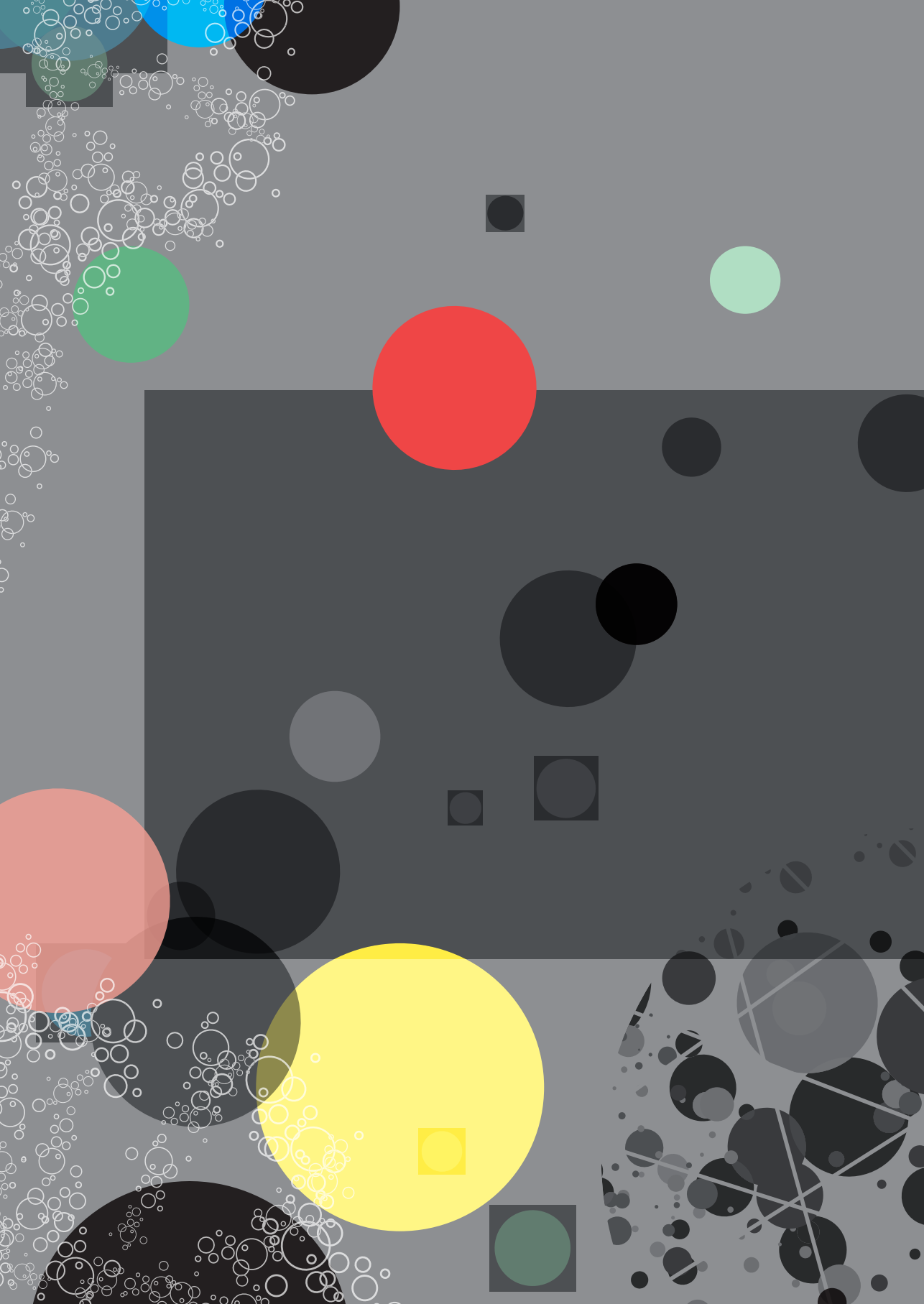

Chapter 5

Genetic confirmation of cancerous origin of EpCAM^{low} circulating tumor cells in a non-small lung cancer patient

Sanne de Wit, Heleen W. Mulder, Joost F. Swennenhuis, T. Jeroen N. Hiltermann, Harry J.M. Groen, Leon W.M.M. Terstappen

Submitted for publication

Clinical Practice Points

Treatment options for non-small cell lung cancer (NSCLC) patients are rapidly increasing. Biomarkers to accurately predict the response to therapy are however lacking. The heterogeneity of the cancer cells within a patient and the changes that occur during the course of therapy complicate the choice of the optimal therapy for the individual patients. Liquid biopsies such as CTC can offer the opportunity to assess the molecular composition of the tumour at the time a switch of therapy is needed. In a 65 year old women with metastatic NSCLC genetically aberrant EpCAM^{low} CTC, but not EpCAM^{high} CTC were detected and 43% of these CTC had an ALK-rearrangement. The patient showed progressive disease while on two different ALK-TKI inhibitors, suggesting that the presence of ALK rearrangements in only EpCAM^{low} CTC without having EpCAM^{high} CTC may be a novel mechanism of ALK resistance. Systematic longitudinal assessment of biomarkers during the course of therapy of NSCLC patients can however shed some light on what the important factors are to guide therapy.

Abstract

EpCAM expressing circulating tumor cells (CTC) captured by CellSearch® are predictive for poor overall survival in many cancers, including non-small cell lung cancer (NSCLC). We have investigated the presence of EpCAM low or negative (EpCAM^{low}) cells in NSCLC patients by analyzing the blood that is discarded after EpCAM enrichment for CTC in CellSearch. EpCAM^{low} cells are captured on a microsieve after filtration and identified by cytokeratin (CK) expression. The presence of these EpCAM^{low} cells was not related to poor overall survival and the cancerous origin was questioned. Therefore, to determine whether these EpCAM^{low}/CK+ cells are cancer cells, we developed a fluorescent in situ hybridization (FISH) procedure on microsieves. We analyzed the ALK-status in the EpCAM^{low} cells from one NSCLC patient who showed an ALK-rearrangement by FISH on a biopsy at the time of progressive disease that was not present on the primary tumor. We were able to genetically confirm the cancerous origin of EpCAM^{low} CTC on the microsieve by showing the presence of the ALK-rearrangement in 43% of the CTC and chromosomal aberrations in all EpCAM^{low} CTC. This calls for an in-depth characterization of these EpCAM^{low} CTC to determine which differences in genetic or proteomic make-up might explain the observed difference for clinical relevance.

Introduction

Circulating tumor cells (CTC) are epithelial cells disseminated into the blood from primary or metastatic sites. At a concentration of 1 CTC in 1 mL of blood they are rare events; they are surrounded by 5×10^6 white blood cells and 5×10^9 red blood cells per mL[1]. The presence of CTC expressing the cell surface epithelial cell adhesion molecule (EpCAM) as well as intracellular cytokeratins (CK), are associated with poor outcome in patients with metastatic as well as non-metastatic disease in several cancers, including non-small cell lung cancer (NSCLC)[2–5]. In the CellSearch® system, CTC that show no or low expression of EpCAM (EpCAM^{low} CTC) are discarded during magnetic isolation and their information is lost. EpCAM expressing CTC have shown to be highly clinically relevant for survival and the prognostic and predictive value has been assessed by several studies[6–10]. However, recently, the relevance of the presence of CTC expressing no or low EpCAM in cancer patients, is the subject of debate. While many subpopulations can be described, the clinical utility of these cells is barely addressed[11–15]. Previously, we developed a method to capture and identify these EpCAM^{low} CTC, discarded by the CellSearch system[16]. After magnetic enrichment for EpCAM expressing CTC, the discarded blood sample was captured and filtered through a microsieve. EpCAM^{low} CTC were identified through an antibody cocktail recognizing CK and the nucleus. In our non-small cell lung cancer pilot study we have processed in total 28 patients for detection of EpCAM^{high} and EpCAM^{low} CTC and it was assessed if the presence of these CTC related to overall survival. It confirmed that the presence of EpCAM^{high} CTC was correlated with poor overall survival, but showed that the presence of EpCAM^{low} CTC was not correlated with overall survival[16]. One of the questions raised is whether these EpCAM^{low} cells are indeed cancer cells. To confirm the cancerous heritage of these EpCAM^{low} cells, we developed a fluorescent in situ hybridization (FISH) procedure that can be performed on the microsieve. After the procedure, the EpCAM^{low} cells can be revisited and analyzed for genetic aberrations. Previously, with a similar approach the cancerous origin of EpCAM^{high} CTC present in the CellSearch cartridges was proven with FISH[17,18]. With this new microsieve FISH procedure, the cancerous origin of the EpCAM^{low} cells in one NSCLC patient with a known ALK-gene rearrangement on the metastatic tumor was analyzed.

Methods

Patient characteristics

The mutation status of the primary tumor from the 28 patients in our pilot study was retrieved from the patient records[16]. In total, nine patients showed mutations in the primary tumor, however, eight patients had point mutations which are not suitable for FISH analysis. One patient had an ALK rearrangement established by FISH in the primary tumor and mediastinal lymph nodes and thereby eligible for FISH analysis on the detected CTC. This patient was diagnosed with stage IV adenocarcinoma in 2012 (see Figure 1). At that time no driver mutations were detected from her primary tumor and therefore chemotherapy was administered. In 2014, when patient developed bone metastases again, tumor tissue was procured with oesophageal and endobronchial ultrasound endoscopy for mutational analysis. No mutations were found, however ALK rearrangements were detected with Vysis ALK Break Apart FISH probe (Abbott 06N38-020)[19]: 64% of 100 tumor cells showed an ALK-translocation and the patient started treatment with crizotinib. Unfortunately, the tumor response was short-lasting due to the development of small brain metastases. Subsequently she was treated with pemetrexed and before starting ceritinib, blood was drawn for CTC analysis with CellSearch (Menarini Silicon Biosystems, Huntingdon Valley PA, USA). She had no $EpCAM^{high}$ CTC detected with the CellSearch, however, 16 $EpCAM^{low}$ CTC were scored on the microsieve, originating from 7.5 mL whole blood. After providing ceritinib without tumor response the patient passed away, surviving 250 days after CTC analysis.

Preparation of microsieves

For development of the FISH procedure on microsieves, cell line cells spiked in healthy donor blood was used. The lymphoma cell line Karpas 299 contains the ALK-translocation and was used for testing the procedure[20]. These cells were grown in RPMI-1640 medium (Gibco™, ThermoFisher Scientific, Waltham MA, USA), supplemented with 10% FBS (Sigma-Aldrich, St. Louis MO, USA) and 5000 U Penicillin-Streptomycin (Sigma-Aldrich) at 37°C with 5% CO^2. Approximately 4,000 cells were spiked in CellSave fixed whole blood and passed through a microsieve as described before[16]. Immunostaining on these cells was not performed, since these lymphoma cells do not express cytokeratin and are positive for CD45. They can only be

distinguished from leukocytes by their ALK-translocation. The cells were fixed on the microsieve by incubation with 4% formaldehyde for 10 minutes. The formaldehyde solution was removed using 70% ethanol and followed by the remaining dehydration steps in the FISH procedure.

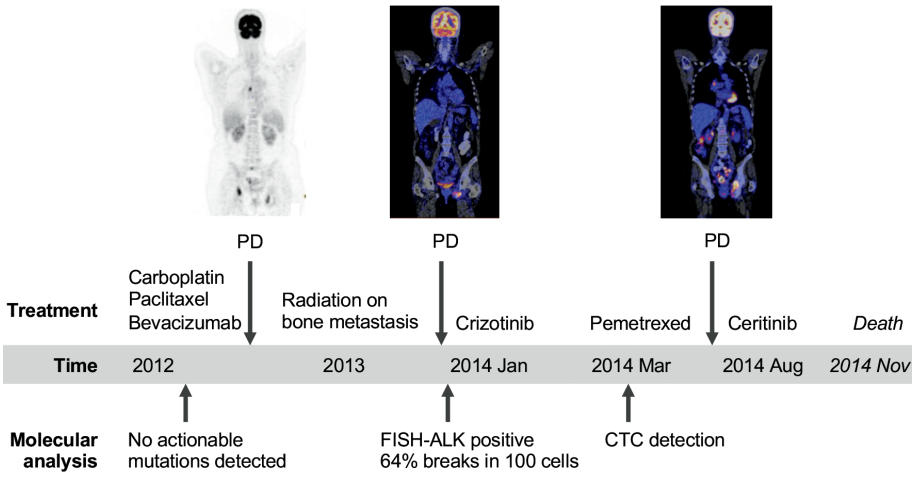

Figure 1. Pretreated patient with adenocarcinoma from lung with bone metastases, who became quickly resistant to subsequent ALK inhibitors. Blood was drawn for CTC enrichment before starting second line ALK-inhibitor ceritinib. FDG-PET/CT scans show left pelvic metastasis and a small mediastinal lymph node that was positive for adenocarcinoma by endoscopic ultrasound needle aspiration at first and third scan.

FISH procedure

The microsieve was soaked for 0-30 minutes in 2X SSC/0.1% Tween (Sigma-Aldrich and Fisher Scientific Netherlands, Landsmeer, The Netherlands) until the coverslip fell off by itself. When it took longer than 30 minutes, the coverslip was gently removed using tweezers. The microsieve was dehydrated for 1 minute in sequential ethanol solutions: 70%, 85% and 100%. After this, the microsieve was completely dried by air. The ALK 2p23 probe was diluted 10 times in hybridization buffer (Leica Biosystems, Amsterdam, The Netherlands). Ten microliter of this mixture was applied to the top of the microsieve. Then, the top was covered with a custom cut 0.85 by 0.85 cm glass coverslip (Menzel-Gläser, Saarbrükener, Germany). Next, 10 µL was applied to the bottom of the microsieve and covered with a glass coverslip. A generous amount of fixogum (Leica Biosystems) was used to seal the

edges of the coverslip and dried for 30 minutes. First the bottom coverslip was sealed and dried, then the top coverslip. The microsieve was put onto a humidified ThermoBrite StatSpin (Leica Biosystems) hot plate. Denaturation for 10 minutes at 85°C was followed by overnight hybridization at 37°C. The fixogum and coverslips were removed manually. The microsieve was incubated for 2 minutes in pre-warmed Wash Buffer I (0.4X SSC/0.3% Igepal) (Sigma-Aldrich) at 72°C (±1). After this, the microsieve was incubated for 1 minute in Wash Buffer II (2X SCC/0.1% Igepal) at room temperature. Then, the microsieve was dehydrated in 70%, 85% and 100% ethanol for 1 minute each and dried by air. Five microliter counterstain with DAPI (Leica Biosystems) was applied to the top and the bottom of the microsieve and covered with a glass coverslip. The counterstain was incubated for 30 minutes in the dark at room temperature.

Image acquisition

First, the complete microsieve was automatically scanned with a 10X objective. All images were merged and locations of previously scored EpCAM^{low} CTC and other aberrant FISH signals were located. These locations were then analyzed with a 40X objective and the images were used for determining the ALK-status of these cells. For image acquisition of the FISH signals, the Nikon E400 fluorescence microscope equipped with a Mercury Arc lamp as light source, a 10X (0.45NA) and 40X (0.45NA) objective (Nikon, Tokyo, Japan) and a computer-controlled CCD camera (Hamamatsu Photonics, Hamamatsu, Japan) was used. The following filters were used: DAPI (DAPI-50LP-A-NQF) with excitation 377/50 nm, dichroic 409 nm LP, emission 409 nm LP; FITC with excitation 480/20 nm, dichroic 495 nm LP, emission 510/20 nm (Spectra Physics Newport); and PE with excitation 547/12 nm, dichroic 560 nm LP, emission 579/25 nm (Spectra Physics Newport). Integration times were 100 ms for DAPI, 500 ms for FITC and 500 ms for PE. Hokawo Hamamatsu imaging software (version 2.1) and ICY[21] was used for visualization and merging of the images.

Single cell FISH analysis

The ALK 2p23 probe was used for detection of the translocation in the ALK-gene on chromosome 2. In NSCLC, the EML4-gene is the most common translocation partner, but many other partners have been described as well[22]. The ALK 2p23 FISH probe contains two short fluorescently labelled oligo's

that hybridize on two locations of the p-arm 23 of chromosome 2 (2p23) that are close together in healthy cells. The FITC labelled probe (visualized as a green dot) attaches to the ALK-gene, whereas the PE labelled probe (visualized as a red dot) hybridizes to a piece of DNA adjacent to the ALK-gene. If these two signals are very close together (fusion) this can be visualized as a yellow dot. When a translocation of the ALK-gene has taken place, the locations of these two signals are further apart and the signals are visualized as a separate green and red dot. In healthy cells, two fusions are present, whereas ALK-translocated cells show one fusion and one red and green signal separated. More than two copies of each signal (with or without ALK-translocation) shows a duplication of the gene or chromosome and indicates a cancerous origin of a cell as well. For interpretation of the signals present in cells after the FISH procedure, the images were manually analyzed by an operator. The amount of signal and the separation of these signals was taken into account and judged to the best effort. For validation of this analysis, six independent operators were asked to score 45 randomized cells, including the 5 CTC that were found on previously scored locations. Operators were asked to determine if the cell contained: a 'normal' ALK-translocation (1 fusion: 1 translocation), a healthy ALK-gene pattern (2 fusions), an aberrant FISH signal (with or without ALK-translocation) or an incomplete FISH signal, making it not possible to annotate a lineage to this cell. The inter-operator agreement was calculated with the Fleiss' Kappa, thereby determining the agreement between operators and ruling out agreement by chance.

Results

ALK-translocation in cell lines

The FISH procedure was first tested and optimized on cell lines spiked in healthy donor blood and filtered with a microsieve. Figure 2 shows results of an experiment in which cells of the Karpas 299 lymphoma cell line were spiked into blood. The lymphoma cells express CD45 and are only distinguishable from normal leukocytes by their ALK translocation. Cells in panel A show four leukocytes, which have the normal ALK pattern: two signals close together for each chromosome. The cell in panel B however, shows a translocation and duplication of the ALK gene; one fusion and two translocations.

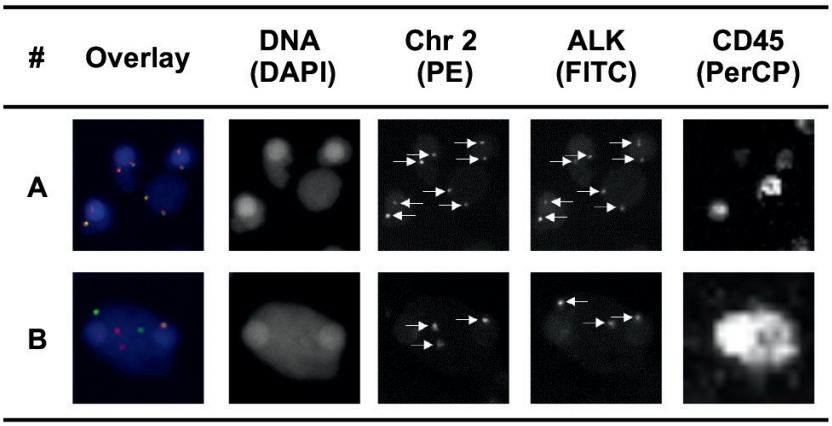

Figure 2. Karpas 299 cells spiked in blood and filtered on a microsieve, followed by FISH for the ALK-translocation. All cells are positive for CD45 with immunostaining. In panel A four normal leukocytes are visible, showing two fusions per cell, whereas the cell in panel B is a Karpas 299 cell with two translocations of the ALK-gene and one fusion (arrows). The more intense circular area in the nuclei is caused by the accumulation of some of the nuclear DNA in the pores of the microsieve.

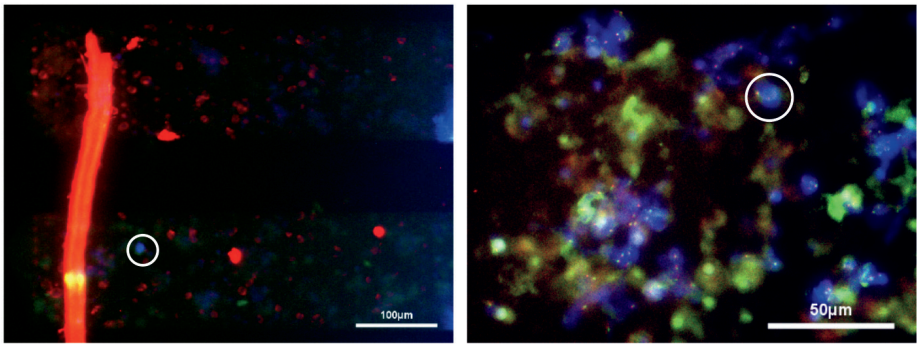

Figure 3. Images of cells and EpCAM^{low} CTC (white circle) on a microsieve after filtration and immunostaining (left) and after FISH for the ALK-translocation (right).

ALK-translocation in EpCAM^{low} CTC

To confirm the cancerous origin of the detected EpCAM^{low} CTCs, a FISH procedure on the microsieve was developed. In one patient, the ALK-rearrangement was found in 64% of the tumor cells in a biopsy from the primary tumor and FISH analysis was performed on EpCAM^{low} CTC on the microsieve was used. During the FISH procedure, the immunostaining

is washed away and only DAPI can be used to locate the nuclei. In Figure 3 two images are presented that show the microsieve after filtration and immunostaining (panel A) and after the FISH procedure (panel B). Encircled is an EpCAM^{low} CTC that was analyzed for its ALK status.

After the FISH procedure, the locations of the 16 scored CTC were revisited and on five locations the FISH status of the cells could be assessed. Figure 4 panel A-E, shows the characteristics of these five cells that were found on the location of the microsieve that were scored as CTC after immunostaining. In Figure 4 panel A, B and C, the cells are positive for a translocation of the ALK gene. This is visualized by the separation of the two FISH signals for chromosome 2 (PE, red) and the ALK-gene (FITC, green); designated by arrows in the corresponding channels. Panel D shows a cell, which is negative for the ALK-translocation, visualized by the fusion of the FISH signals. However, three copies of chromosome 2 and three copies of the ALK gene are visible. Since leukocytes always contain two copies of chromosome 2, this cell can be considered as a CTC. In panel E is a cell presented that is in the telophase of cell division, containing two nuclei (designated by arrows in the DNA channel). Because of the high background noise in the FITC channel, it was not possible to detect a FISH signal. However, leukocytes do not divide in the bloodstream, but only divide from precursor cells that are present in the bone marrow. Therefore, this cell could also be considered as a CTC.

ALK-translocation status in leukocytes

To prove the reliability of the FISH signals, FISH signals of 50 cells identified as leukocytes were analyzed. These cells were all negative for cytokeratin staining, but positive for CD45 and nuclear staining after the immunostaining. Examples of FISH signals in leukocytes are visible in Figure 4, panel F and G. This shows that every chromosome 2 signal (red) is located in close proximity to the ALK-gene signal (green). In none of the 50 cells that were analyzed, a translocation of the ALK gene or multiple copies of chromosome 2 were detected.

Agreement in scoring FISH signals

Before definitive conclusions about cells with abnormal FISH signals can be drawn, the reliability of FISH-signal interpretations was validated. In total, 45 images of FISH signals in cells were shown to a panel of six independent operators. These images contained randomized images of the FISH signals

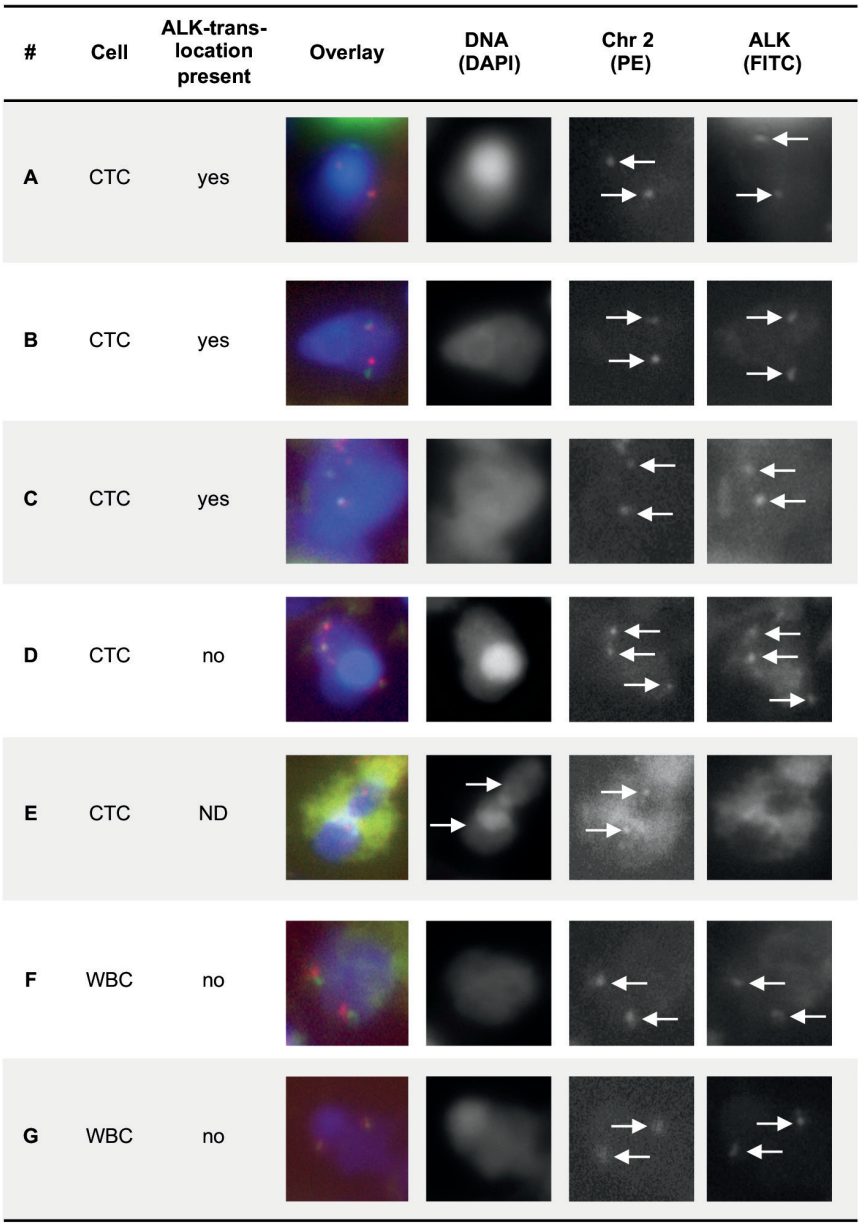

Figure 4. Gallery of five CTC scored as DAPI+/CK+/CD45– after microsieve filtration of the EpCAM depleted blood and analyzed with FISH for genetic analysis for ALK-translocation (A-C), other genetic aberrances (D, E) or the normal ALK-gene pattern (F, G). Cells are stained with DAPI for the nucleus and fluorescent signals of the ALK-gene are in green and the control FISH signals of chromosome 2 are in red. When these signals are in very close proximity, the signals
are overlaid and can appear as a yellow dot.

detected in the five CTC from Figure 4 and 40 other cells. Of the five CTC presented in Figure 4, the CTC in panel A was interpreted as a cell with an ALK-translocation by all operators. The CTC in panel C was interpreted as a cell with a normal ALK-translocation, but also as a cell with additional aberrancies, whereas the CTC in panel D was uniformly scored as a cell with genetic aberrancies, but not with the ALK-translocation. The CTC in panel B was interpreted as a cell with the ALK-translocation, but also by one operator as a cell with the healthy ALK-gene pattern. The CTC in panel E was uniformly identified as a cancer cell. In total, 23 of the 45 cells were scored uniformly by all operators, of which 16 as a normal cell and 2 of which the FISH signal was incomplete. The remaining 22 cells were scored in all categories, and in 15 of these cells, only one operator disagreed with the others. In addition, two cells were scored uniformly as aberrant with multiple copies of chromosome 2, that contains the ALK-gene (see Figure 5). The Fleiss' Kappa value, displaying the inter-operator agreement, was 0.62. This can be interpreted as a substantial agreement (Fleiss' Kappa value between 0.61-0.80)[23].

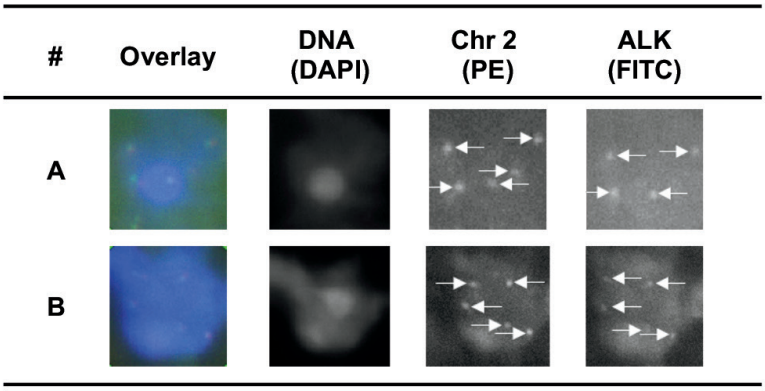

Figure 5. The two cells with genetic aberrancies that were found on the microsieve, but not on a location that was scored after immunostaining. Both cells show multiple copies of chromosome 2, that also contains the ALK-gene, but no ALK-translocation.

Discussion

After EpCAM^{high} CTC isolation by CellSearch, the remaining blood sample is discarded. This blood is now filtered and immunofluorescently stained for detection of EpCAM^{low} CTC. These CTC were defined by the presence of

cytokeratin expression, only expressed in epithelial cells, the presence of a nucleus and the absence of CD45, a leukocyte marker. To confirm these epithelial cells are of cancerous origin, a FISH procedure was developed that could be performed on the captured cells on the microsieve itself. After the procedure, the location of the scored CTC could be revisited with the fluorescence microscope and analyzed for FISH signals. However, since the FISH procedure entails several washing steps, it is possible that cells will not remain on the same location or are lost after immunostaining. Also, the conditions in the procedure can be quite harsh for cells. This results in a loss of fluorescent signal from the prior immunostaining, making it harder to locate the scored CTC on microsieves. Also, these harsh conditions can destroy the nuclear membrane, thereby diffusing its DNA content and losing the possibility for effective probe hybridization. This can result in a lower or complete loss of FISH signal, usually accompanied with high non-specific background noise that covers the actual FISH signal. In cytopathology, the morphology of the nuclei, background and probe signal intensity should pass the quality criteria before a reliable FISH assessment can be performed[24]. It is therefore important to make sure the cells are properly fixed before the procedure on microsieve. In the entire workflow, cells are fixed first with CellSave directly after blood draw, followed by fixing with 1% formaldehyde after immunostaining. The loss of many cells on the microsieve could be explained because cells are also permeabilized during the immunostaining. For future experiments, it might be beneficial to add an extra fixation step before the FISH procedure to ensure that the nuclei remain intact.

In total 16 CTC were scored on the microsieve, but only 5 CTC could be relocated. The remaining 11 locations were unsuitable to determine a FISH status, mostly because high background noise prevented analysis of the FISH signals. On several locations it was clear that cells had shifted and the previously scored $EpCAM^{low}$ CTC could not be relocated. Even though the entire microsieve was scanned and analyzed on a low resolution, analyzing all cells present on the microsieve is laborious work and prone to error. However, an approach to analyze all cells would be favorable, since it is possible that more CTC are present, yet not identified, because they contain a different phenotype. Cells low in EpCAM expression could also be low or negative for CK and would therefore be missed with our current immunostaining reagents. A more automated approach to analyze all images and to rule out subjectivity would therefore be required.

For the validation of interpretation of FISH signals, six operators independently scored 45 randomized images of cells. Of the five CTC that

were found on their previous annotated location, the cell in panel A of Figure 4 was scored as a CTC with the ALK-translocation. The cell in panel C was interpreted as a CTC with an ALK-translocation, but also as a cell with additional genetic aberrancies. Therefore, this cell is considered by none of the operators as a leukocyte and can be considered a CTC. The cell in panel D was judged to have multiple copies of the ALK-gene and is therefore also aberrant and can be considered as a CTC. The CTC in panel E was uniformly interpreted as a cell that could not be annotated to a lineage, because the FISH signal was incomplete. This is in concordance with our previous conclusion that this cell does not contain a genetic aberrancy, but was designated as a CTC because it contained two nuclei. The cell in panel B was scored as a cell with the ALK-translocation by five operators, while one operator thought the signals of chromosome 2 and the ALK-gene were not sufficiently separated and scored this cell as a normal leukocyte.

For 15 cells there was one operator that disagreed with the other five operators. This shows that analyzing these signals is a very subjective matter and that reaching a complete agreement will be very hard. For five cells, the majority of the operators designated these cells as a normal cell, whereas one operator judged the signals to be translocated. This shows that operators interpret the signals by their own standards and that they require suitable training to set the same standards for analysis. The analysis of FISH status in cytopathology tumor samples is performed according international guidelines using information from 50 cells presented independently to two experienced evaluators[19,25]. In tumor biopsies a case is considered ALK-FISH positive when more than 15% of the evaluated 100 neoplastic nuclei have the break-apart pattern. This 15% cut-off value in 100 cells may not always be applicable when scoring EpCAM^{low} CTC, since CTC occur in low numbers and fewer cells are present for evaluation. Therefore, new ways of interpreting the results from this FISH procedure have to be developed to ensure a standardized approach.

The overall agreement between the reviewers was calculated with Fleiss' Kappa. This showed that the agreement was 0.62, indicating a substantial agreement. A Kappa-value below 0.20 is accepted as a poor agreement, whereas a Kappa value above 0.80 to 1.00 is almost a perfect agreement[23]. However, it should be kept in mind that the value of the Kappa is highly subjective to the number of subjects that are compared (in this case 45 cells), the number of categories (here: four) and the amount of referees (six operators) and the categorizing of these values is not fixed.

In addition to the five CTC that were found on the same location after immunostaining, two other cells were scored uniformly as an aberrant cell (Figure 5), which we can consider as a CTC. These cells were positioned on a different location on the microsieve. Because 11 immunostained CTC could not be relocated, it is possible one of these cells has moved during the FISH procedure and was found during the analysis of leukocytes. It is also possible these cells were missed during the immunostaining because they contain a different phenotype that expresses no of low CK. If this is the case, it is conceivable that more CTC are present on the microsieve that have not been scored as such. This shows an expansion of the immunostaining might be required to identify these CTC as well[13,15,26,27].

The patient that was analyzed with our developed FISH procedure on circulating epithelial cells, showed 64% of ALK-translocated tumor cells in the biopsy of the metastatic tumor. In total, seven CTC were found on the microsieve during FISH analysis. Of these seven cells all were genetically aberrant and in three cells (43%) the ALK-translocation was found. This confirms that the $EpCAM^{low}$ CTC are indeed cancerous and that the occurrence of the ALK translocation is present in a roughly similar proportion of the CTC as compared to cells in the metastatic tumor[28,29].

Previously, we have shown the relation of $EpCAM^{high}$ and $EpCAM^{low}$ CTC with overall survival in 28 NSCLC patients[16]. This showed that $EpCAM^{high}$ CTC are predictive for poor overall survival ($p=0.004$), whereas $EpCAM^{low}$ CTC show no relation with overall survival ($p=0.271$). This could be due to the fact that most of these so-called CTC were of epithelial origin without being cancerous. However, this patient had no $EpCAM^{high}$ CTC in her blood, but 16 $EpCAM^{low}$ CTC scored on the microsieve. She was pre-treated with chemotherapy and palliative radiotherapy on her bone lesions. Afterwards she did not response to crizotinib or later to ceritinib, neither on her brain or bone lesions. Resistance mechanisms are described as ALK dependent or independent. In this case, we observed ALK translocations in $EpCAM^{low}$/CK+ CTC, while in most cases these aberrations occur in EpCAM positive tumor cells, but can also be detected in $EpCAM^{low}$ cells[30]. With the developed FISH protocol on a microsieve after filtration, we have shown that all located $EpCAM^{low}$/CK+ cells with interpretable FISH signals are of cancerous origin. Also, some cells that were not detected with the immunostaining showed genetic aberrancies. This conclusion demonstrates the need to improve the detection of all $EpCAM^{low}$ CTC and to include $EpCAM^{low}$/CK– CTC as well. Our outcome warrants a larger study to confirm that all subpopulations of $EpCAM^{low}$ CTC in patients are of cancerous origin. For this, technology needs to be developed

to isolate these cells from the microsieve and sensitively detect other genetic mutations in these cells[31–33]. This genetic information is required for the clinic to use this test for clinical decisions. For instance, the digital droplet PCR could be used to detect point mutations, whereas copy number variances could be used for a more general analysis of amplifications and deletions throughout the genome[31,32]. The difference in clinical relevance between the EpCAM^{high} and EpCAM^{low} cells also raises the question whether these EpCAM^{low} cells belong to a subpopulation of CTC that has its own characteristics and clinical relevance. Or that EpCAM^{low} CTC with ALK rearrangements confer resistance towards ALK-TKI inhibitors. This calls for an in-depth characterization of these EpCAM^{low} CTC to determine which differences in genetic or proteomic make-up might explain the observed difference in clinical relevance.

Acknowledgements

Special thanks to Kiki Andree, Anouk Mentink-Leusink, Afroditi Nanou and Niels van der Velde for taking part in the validation of FISH signals by scoring the 45 cells as independent operators.

References

1. Allard WJ, Matera J, Miller MC, et al. Tumor cells circulate in the peripheral blood of all major carcinomas but not in healthy subjects or patients with nonmalignant diseases. Clin cancer Res. 2004;10(20):6897-6904. doi:10.1158/1078-0432.CCR-04-0378.
2. Krebs MG, Hou J-M, Sloane R, et al. Analysis of circulating tumor cells in patients with non-small cell lung cancer using epithelial marker-dependent and -independent approaches. J Thorac Oncol. 2012;7(2):306-315. doi:10.1097/JTO.0b013e31823c5c16.
3. Janni WJ, Rack B, Terstappen LWMM, et al. Pooled Analysis of the Prognostic Relevance of Circulating Tumor Cells in Primary Breast Cancer. Clin Cancer Res. 2016;22(10):2583-2593. doi:10.1158/1078-0432.CCR-15-1603.
4. de Bono JS, Scher HI, Montgomery RB, et al. Circulating Tumor Cells Predict Survival Benefit from Treatment in Metastatic Castration-Resistant Prostate Cancer. Clin Cancer Res. 2008;14(19):6302-6309. doi:10.1158/1078-0432.CCR-08-0872.
5. Cohen SJ, Punt CJ a, Iannotti N, et al. Prognostic significance of circulating tumor cells in patients with metastatic colorectal cancer. Ann Oncol. 2009;20(7):1223-1229. doi:10.1093/annonc/mdn786.
6. Gallo M, De Luca A, Maiello MR, et al. Clinical utility of circulating tumor cells in patients with non-small-cell lung cancer. Transl lung cancer Res. 2017;6(4):486-498. doi:10.21037/tlcr.2017.05.07.
7. Krebs MG, Sloane R, Priest L, et al. Evaluation and prognostic significance of circulating tumor cells in patients with non-small-cell lung cancer. J Clin Oncol. 2011;29(12):1556-1563. doi:10.1200/JCO.2010.28.7045.

8. Tamminga M, Groen HHJM, Hiltermann TJN. Investigating CTCs in NSCLC-a reaction to the study of Jia-Wei Wan: a preliminary study on the relationship between circulating tumor cells count and clinical features in patients with non-small cell lung cancer. J Thorac Dis. 2016;8(6):1032-1036. doi:10.21037/jtd.2016.04.17.

9. Tartarone A, Rossi E, Lerose R, et al. Possible applications of circulating tumor cells in patients with non small cell lung cancer. Lung Cancer. 2017;107:59-64. doi:10.1016/j.lungcan.2016.05.027.

10. Tong B, Xu Y, Zhao J, et al. Prognostic significance of circulating tumor cells in non-small cell lung cancer patients undergoing chemotherapy. Oncotarget. 2017;8(49):86615-86624. doi:10.18632/oncotarget.21255.

11. Lustberg MB, Balasubramanian P, Miller B, et al. Heterogeneous atypical cell populations are present in blood of metastatic breast cancer patients. Breast Cancer Res. 2014;16(2):R23. doi:10.1186/bcr3622.

12. Armstrong AJ, Marengo MS, Oltean S, et al. Circulating tumor cells from patients with advanced prostate and breast cancer display both epithelial and mesenchymal markers. Mol Cancer Res. 2011;9(8):997-1007. doi:10.1158/1541-7786.MCR-10-0490.

13. Alix-Panabières C, Mader S, Pantel K. Epithelial-mesenchymal plasticity in circulating tumor cells. J Mol Med. 2017;95(2):133-142. doi:10.1007/s00109-016-1500-6.

14. Hanssen A, Wagner J, Gorges TM, et al. Characterization of different CTC subpopulations in non-small cell lung cancer. Sci Rep. 2016;6(1):28010. doi:10.1038/srep28010.

15. Hanssen A, Loges S, Pantel K, Wikman H. Detection of Circulating Tumor Cells in Non-Small Cell Lung Cancer. Front Oncol. 2015;5:207. doi:10.3389/fonc.2015.00207.

16. de Wit S, van Dalum G, Lenferink ATM, et al. The detection of EpCAM+ and EpCAM– circulating tumor cells. Sci Rep. 2015;5(1):12270. doi:10.1038/srep12270.

17. Swennenhuis JF, Tibbe AGJ, Levink R, Sipkema RCJ, Terstappen LWMM. Characterization of circulating tumor cells by fluorescence in situ hybridization. Cytometry A. 2009;75(6):520-527. doi:10.1002/cyto.a.20718.

18. Gasch C, Oldopp T, Mauermann O, et al. Frequent detection of PIK3CA mutations in single circulating tumor cells of patients suffering from HER2-negative metastatic breast cancer. Mol Oncol. 2016;10(8):1330-1343. doi:10.1016/j.molonc.2016.07.005.

19. Thunnissen E, Bubendorf L, Dietel M, et al. EML4-ALK testing in non-small cell carcinomas of the lung: a review with recommendations. Virchows Arch. 2012;461(3):245-257. doi:10.1007/s00428-012-1281-4.

20. Fischer P, Nacheva E, Mason DY, et al. A Ki-1 (CD30)-positive human cell line (Karpas 299) established from a high-grade non-Hodgkin's lymphoma, showing a 2;5 translocation and rearrangement of the T-cell receptor beta-chain gene. Blood. 1988;72(1):234-240.

21. ICY. http://icy.bioimageanalysis.org/.

22. ALK (2p23), Leica Biosystems. http://www.leicabiosystems.com/ihc-ish-fish/ish-probes-molecular-pathology/kreatech-fish-probes/solid-tumors/products/alk-2p23/. Published 2017.

23. Landis JR, Koch GG. The Measurement of Observer Agreement for Categorical Data. Biometrics. 1977;33(1):159. doi:10.2307/2529310.

24. Zneimer SM. Cytogenetic Laboratory Management: Chromosomal, FISH and Microarray-Based Best Practices and Procedures. Wiley; 2016.

25. Leonard DGB. Molecular Pathology in Clinical Practice. Springer International Publishing; 2016. doi:10.1007/978-3-319-19674-9.

26. Manicone M, Poggiana C, Facchinetti A, Zamarchi R. Critical issues in the clinical application of liquid biopsy in non-small cell lung cancer. J Thorac Dis. 2017;9(Suppl 13):S1346-S1358. doi:10.21037/jtd.2017.07.28.

27. O'Flaherty L, Wikman H, Pantel K. Biology and clinical significance of circulating tumor cell subpopulations in lung cancer. Transl lung cancer Res. 2017;6(4):431-443. doi:10.21037/tlcr.2017.07.03.

28. Pailler E, Oulhen M, Borget I, et al. Circulating Tumor Cells with Aberrant ALK Copy Number Predict Progression-Free Survival during Crizotinib Treatment in ALK -Rearranged Non–Small Cell Lung Cancer Patients. Cancer Res. 2017;77(9):2222-2230. doi:10.1158/0008-5472.CAN-16-3072.

29. Faugeroux V, Pailler E, Auger N, Taylor M, Farace F. Clinical Utility of Circulating Tumor Cells in ALK-Positive Non-Small-Cell Lung Cancer. Front Oncol. 2014;4:281. doi:10.3389/fonc.2014.00281.

30. Manicone M, Scaini MC, Rodriquenz MG, et al. Liquid biopsy for monitoring anaplastic lymphoma kinase inhibitors in non-small cell lung cancer: two cases compared. J Thorac Dis. 2017;9(Suppl 13):S1391-S1396. doi:10.21037/jtd.2017.08.151.

31. Swennenhuis JF, de Wit S, Terstappen LWMM. Digital droplet PCR test for detection of low abundant CTC captured on microsieves. In: International Symposium on Minimal Residual Cancer. ; 2018.

32. Neves RPL, Raba K, Schmidt O, et al. Genomic High-Resolution Profiling of Single CKpos/CD45neg Flow-Sorting Purified Circulating Tumor Cells from Patients with Metastatic Breast Cancer. Clin Chem. 2014;60(10):1290-1297. doi:10.1373/clinchem.2014.222331.

33. Marchetti A, Del Grammastro M, Felicioni L, et al. Assessment of EGFR mutations in circulating tumor cell preparations from NSCLC patients by next generation sequencing: toward a real-time liquid biopsy for treatment. PLoS One. 2014;9(8):e103883. doi:10.1371/journal.pone.0103883.

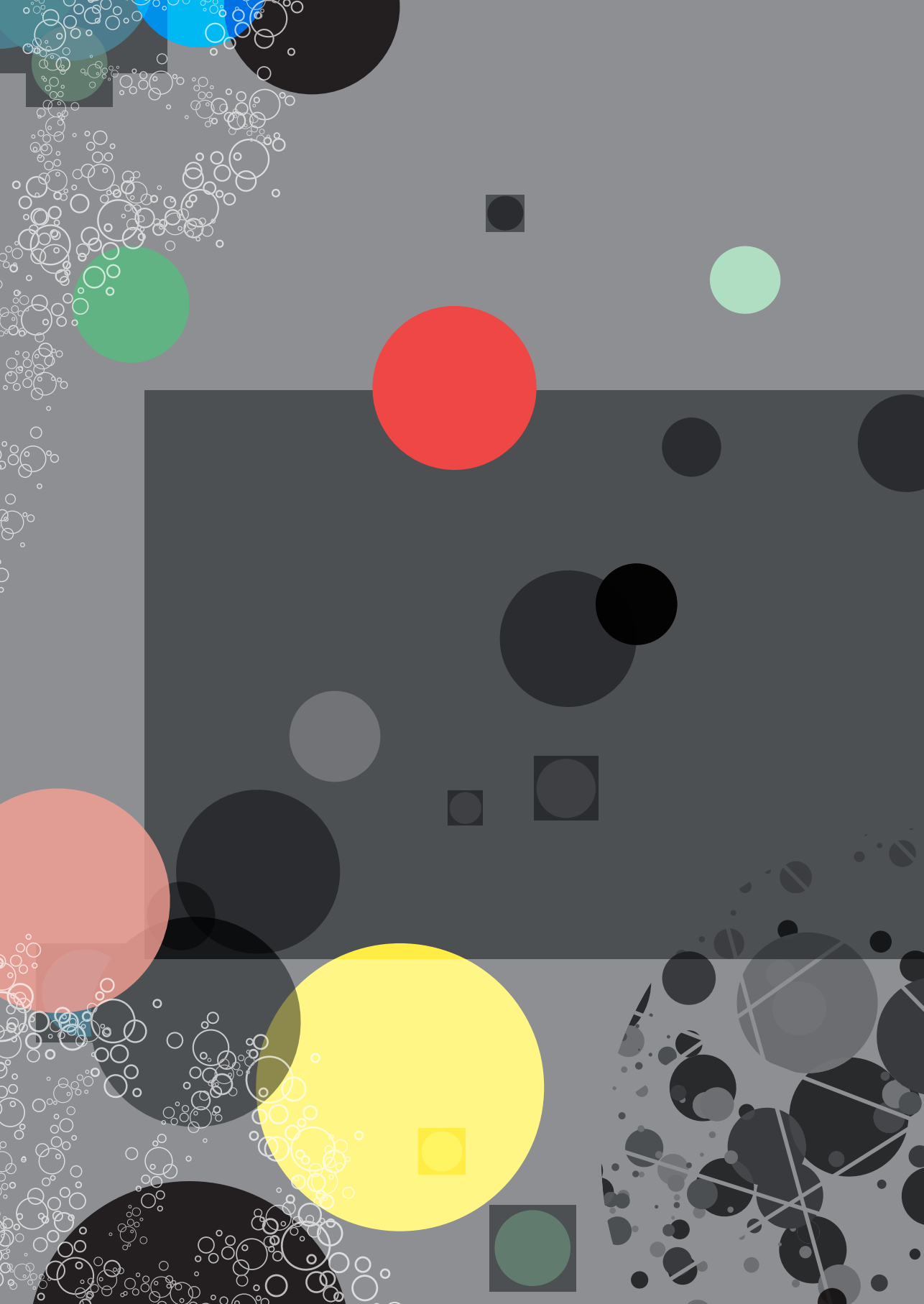

Chapter 6

Single tube liquid biopsy for advanced non-small cell lung cancer

Sanne de Wit, Elisabetta Rossi, Sabrina Weber, Menno Tamminga, Mariangela Manicone, Joost F. Swennenhuis, Catharina G.M. Groothuis-Oudshoorn, Riccardo Vidotto, Antonella Facchinetti, Leonie L. Zeune, Ed Schuuring, Rita Zamarchi, T. Jeroen N. Hiltermann, Michael R. Speicher, Ellen Heitzer, Leon W.M.M. Terstappen, Harry J.M. Groen

Submitted for publication

Translational Relevance

EpCAM^{high} CTC, EpCAM^{low} CTC, tdEV and plasma ctDNA were detected in a single tube of blood of 97 metastatic NSCLC patients. The presence of EpCAM^{high} CTC and elevated levels of tdEV and ctDNA, but not the presence of EpCAM^{low} CTC, was associated with a poor overall survival in these NSCLC patients. This single tube approach enables simultaneous analysis of several biomarkers; however, the added predictive value of the combined markers was low. Known mutations from the primary tumor could be detected in 11 of 16 (69%) patients in plasma ctDNA. Single circulating epithelial cell sequencing may be the next step in the diagnostic technologies to be developed.

Abstract

The need for a liquid biopsy in non-small cell lung cancer (NSCLC) patients is rapidly increasing. We studied the relation between overall survival (OS) and the presence of EpCAM^{high} circulating tumor cells (CTC), EpCAM^{low} CTC, tumor derived extracellular vesicles (tdEV) and cell-free circulating tumor DNA (ctDNA) from a single blood draw. EpCAM^{high} CTC were detected with CellSearch, tdEV in the CellSearch images and EpCAM^{low} CTC with filtration after CellSearch. ctDNA was isolated from plasma and mutations present in the primary tumor were tracked with deep sequencing methods. Discriminative and predictive abilities were studied by Cox hazard regression and C-index. In 97 patients, 21% had ≥2 EpCAM^{high} CTC, 15% had ≥2 EpCAM^{low} CTC, 27% had ≥18 tdEV and 19% had ctDNA with ≥10% mutant allele frequency. Either one of these biomarkers was detected in 45% of the patients. EpCAM^{high} CTC was associated with worse OS ($p=0.012$; hazard ratio (HR) 2.1), as did tdEV ($p=0.012$; HR 2.0) and ctDNA ($p=0.029$; HR 1.9). However, EpCAM^{low} CTC ($p=0.578$; HR 1.2) was not associated with OS. In 11 out of 16 patients (69%) mutations were detected in the ctDNA. Two or more unfavorable biomarkers were associated with poor OS; however, the added predictive value of each biomarker was small. A single tube approach enables simultaneous analysis of EpCAM^{high} CTC, EpCAM^{low} CTC, tdEV and ctDNA. EpCAM^{high} CTC, tdEV and ctDNA were significantly associated with poor OS, whereas EpCAM^{low} CTC was not. The added predictive value of the combined markers was low.

Introduction

Advanced non-small cell lung cancer (NSCLC) patients are characterized by gradual growing metastases in different organs, increasing tumor load and comorbidities that grimly determines their fate. Invasive diagnostics are often difficult by inability to perform invasive procedures or due to inaccessible metastases. Liquid biopsies may provide a convenient and patient-friendly approach to obtain information on prognosis and prediction of the best treatment management[1]. Liquid biopsy approaches include the sampling and analysis of circulating components from blood and other body fluids[2]. While the clinical utility of circulating tumor cells (CTC) and cell-free circulating tumor DNA (ctDNA) has been extensively investigated in recent years, other components, such as tumor derived extracellular vesicles (tdEV), have only recently been put to the focus of research[3–7].

CTC are epithelial cells disseminated into the blood from primary or metastatic sites. The presence of CTC is predictive of relatively short survival in several types of cancer, including breast, prostate, colon, small and non-small cell lung carcinoma[8–14]. CTC are rare events; they are surrounded by 5×10^6 white blood cells and 5×10^9 red blood cells per mL[15]. For this reason the appropriate marker selection for enrichment is a crucial factor. In most cases, CTC detection is based on the expression of the cell surface epithelial cell adhesion molecule (EpCAM), as it is expressed by the majority of epithelial derived cancers, while hematopoietic cells show no or only very little expression[16,17]. However, the sole use of EpCAM for CTC isolation might lead to an underestimation of CTC numbers because tumor cells expressing low amounts of EpCAM might be missed by the system. While EpCAM expressing CTC have shown to be highly clinically relevant, recently, the relevance of the presence of CTC expressing no or low EpCAM in cancer patients, is the subject of debate. While many subpopulations can be described, the clinical utility of these cells is barely addressed[18–22].

The use of ctDNA as a clinical response marker for NSCLC patients has already moved into the clinical routine and EGFR T790M testing from plasma has been proven to complement tissue-based testing[5]. However, this can be applied to only a subset of patients harboring an activating EFGR mutation, while an untargeted approach, which does not require prior knowledge of the mutation status the tumor, would facilitate a more widespread application.

Tumor derived Extracellular Vesicles (tdEV) comprise of a variety of vesicles secreted or budded of from cancer cells and are known to play an important role in many tumor biological processes[7,11,23,24]. In a previous work

we have demonstrated that a subset of tdEV, which expresses both EpCAM and cytokeratin but not CD45 or DNA, can be enriched and enumerated using the CellSearch and their presence was strongly associated with poor overall survival[25].

While all of these biomarkers are promising for predicting survival, the predictive ability of the combined biomarkers may yield complementary information and thereby improve diagnostic sensitivity. We hypothesized that a comprehensive, multi-parameter approach with different highly specific tumor shedding products will predict those patients with a relative good prognosis from those with a poor prognosis. Therefore, we determined the presence of four biomarkers in one tube of blood in advanced NSCLC patients. Two CTC subpopulations were discriminated: EpCAM expressing CTC (referred to as $EpCAM^{high}$ CTC) detected using the CellSearch® system and no or low EpCAM expressing CTC (referred to as $EpCAM^{low}$ CTC) detected on microsieves after filtration[20]. The tdEV were identified in the images from the CellSearch using the open source imaging program ACCEPT, whereas plasma from the same tube was used for cell-free ctDNA extraction followed by tumor allele fraction analysis[26–28]. For tracking of tumor-specific mutations in plasma DNA, deep sequencing or Safe-SeqS was used[29]. In total 97 NSCLC patients were included and the presence of these different biomarkers in an all-in-one liquid biopsy was explored.

Methods

Patients and healthy donors

Patients with stage IIIB and IV NSCLC were staged and diagnosed using FDG-PET/CT imaging and different techniques to procure tumor tissue. Sixty patients were enrolled at University Medical Center Groningen (UMCG, Netherlands) and 37 patients at Institute Oncology Venice (IOV, Italy) (Table 1). All patients provided written informed consent and the study protocol was approved by the medical ethical committees. Healthy donors – used as control – provided informed consent prior to blood donation, in accordance to the study protocol approved by the METC Twente ethics committee.

Table 1. Patient characteristics of the patients enrolled in this study.

Metastatic non-small lung cancer patients	***N = 97***
Site location	
UMCG, the Netherlands	60 (62%)
IOV, Italy	37 (38%)
Age (years)	
Median (range)	65 (40-82)
Gender	
Male	47 (48%)
Female	50 (52%)
Smoking	
Never	19 (20%)
Smoker	59 (60%)
Unknown	19 (20%)
ECOG Performance Status	
0	54 (56%)
1	34 (35%)
2	6 (6%)
3	2 (2%)
4	1 (1%)
Therapy type	
Chemotherapy	41 (42%)
Targeted therapy	23 (23%)
Immunotherapy	24 (25%)
Unknown	10 (10%)
Cancer type	
Adenocarcinoma	59 (61%)
Squamous cell carcinoma	38 (39%)
Mean follow-up time in months (min-max)	
Alive	16 (4-30)
Dead	7 (1-25)
Status at last follow-up	
Alive	36 (37%)
Dead	61 (63%)

Blood and plasma collection

Peripheral blood samples were drawn by vena puncture into 10 mL CellSave blood collection tubes (Menarini Silicon Biosystems, Huntingdon Valley PA, USA) and in an additional EDTA blood collection tube for 59 patients. For CellSearch analysis, the blood from patients was processed within 96 hours, whereas blood samples from healthy donors were processed within 24 hours. Blood from the CellSave tube was transferred to a CellSearch conical tube and centrifuged for 10 minutes at 800g without using the brake. Thereafter, plasma was aspirated without disturbing the buffy coat into a sterile 2 mL Eppendorf tube and stored at –80°C. For CellSearch CTC enumeration the same volume of plasma was replaced with CellSearch Dilution buffer and again centrifuged at 800g for 10 minutes without using the brake. Finally, the sample was placed on the CellTracks Autoprep for CTC analysis. Blood from EDTA collection tubes was transferred to 15 mL Falcon polypropylene tubes. Samples were centrifuged for 10 minutes at 200g at room temperature with both brake settings set to slow and followed by a second centrifugation step at 1,600g for 10 minutes. The upper plasma layer was transferred to a Falcon polypropylene tube, avoiding contact with the buffy coat layer and again centrifuged at 1,600g for 10 minutes. Afterwards, the supernatant was transferred to Eppendorf tubes without disturbing the cell pellet and stored at –80°C.

Plasma DNA extraction

Plasma DNA from 97 samples was extracted using the QIAamp Circulating Nucleic Acid Kit (Qiagen) from EDTA plasma (n=59) (mean 1.0 mL, range 0.5-2.0 mL) or CellSave plasma (n=54) (mean 1.7 mL, range 0.8-2.0 mL) and eluted in 60 µL to 90 µL nuclease-free H_2O, depending on the input volume of plasma. Plasma from both CellSave and EDTA tubes from 31 patients was available for comparison of ctDNA levels. Plasma DNA was quantified using the Qubit dsDNA HS Assay Kit (ThermoFisher Scientific, Waltham MA, USA).

Stratification of plasma DNA samples based on tumor fraction using mFAST-SeqS

Tumor fractions were assessed using the mFAST-SeqS assay, which is based on the selective amplification of uniquely mappable LINE1 (L1) sequences and can be used as an overall measure of aneuploidy and therefore corresponds to

the plasma tumor fraction. L1 amplicon libraries were prepared as previously described[28]. Briefly, using target-specific L1 primers, 5 µL plasma DNA was amplified with Phusion Hot Start II Polymerase for 8 PCR cycles. PCR products were purified with AMPure Beads (Beckman Coulter, Brea CA, USA), and 10 µL was directly used for a second PCR with 18 cycles to add Illumina specific adaptors and indices. L1 amplicon libraries were pooled equimolarly and sequenced on an Illumina MiSeq generating 150 bp single reads aiming for at least 100,000 reads. Aligned sequence reads were counted and normalized using an in-house script. In order to assess over- and under-representation of read counts of each chromosome arm, a Z-score statistic was applied by comparing read counts to a set of healthy individuals. In order to get a general overview of aneuploidy, a genome-wide Z-score was calculated by normalizing read counts per chromosome arms and squaring and summing them up. Based on previous comparisons with genome-wide Z-scores and mutant allele frequencies of somatic mutations, a Z-score of 5 correlated with a tumor allele frequency of approximately 10%[28]. Plasma DNA-samples were stratified based on genome-wide Z-scores with high tumor allele frequency (Z-score $\geq$5) and low tumor allele frequency (Z-score $<$5).

Primary tumor mutations and detection of plasma circulating tumor DNA

For 16 patient samples, the mutational status of the primary tumor was available. In these samples somatic mutations were tracked using either Safe-SeqS (for KRAS and BRAF mutations) or Deep-Seq (for EGFR mutations). For Safe-SeqS, on average 11.7 ng plasma DNA (range 7.9-20.0 ng) was amplified by Phusion polymerase (Thermo Fisher) using amplicon specific primers whereby the sense primer contains a 12-base unique molecular identifier (UMI). After 12 cycles of PCR, products were purified using Ampure XP beads (Beckman Coulter) and eluted in nuclease-free H_2O. In a second PCR with 35 cycles, Illumina specific adapters and indices were added. Products were again purified and subjected to quality control and quantification on an Agilent Bioanalyzer DNA 7500 chip (Agilent Technologies). All samples were pooled equimolarly and sequenced on an Illumina MiSeq in a 2x 150 bp paired-end run. Generated reads were then grouped to read families according to the UMI. A consensus sequence of each read family and a FastQ-file from this sequence was generated and aligned to the human reference genome (hg19) using Burrows-Wheeler transformation, SAMtool and alignments visualized in the "Integrative Genomes Viewer" to detect variants. For Deep-Seq, on

average 5.2 ng (range 3.3-9.6 ng) was used for a target-specific PCR and amplified in 25 cycles using FastStart HiFi Polymerase (5 U/µL) followed by a Ampure XB beads (Beckman Coulter) purification. Illumina specific adapters and indices were added in a second PCR for 25 cycles. Analysis was performed as described above but without collapsing the read to a consensus sequence.

EpCAM^{high} CTC detection by CellSearch

CTC were enumerated in aliquots of 7.5 mL of blood with CellSearch® Circulating Tumor Cell Kit (Menarini Silicon Biosystems). Blood samples were enriched for EpCAM^{high} cells and stained with DAPI, Cytokeratin-PE and CD45-APC on the CellTracks Autoprep. Image acquisition of the stained cartridges was performed on the CellTracks Analyzer II and all images were stored for review by an independent trained operator.

EpCAM^{low} CTC detection by filtration after CellSearch

After immunomagnetic selection of EpCAMhigh cells, the CellTracks Autoprep transports the remaining blood sample to a waste container. These samples can be used for identification of residual tumor cells, as described previously[20]. In short, microsieves (VyCAP, Deventer, The Netherlands) were used to filter tumor cells from these samples, containing mostly leukocytes and EpCAM^{low} CTC. The microsieves contain 111,800 pores of 5 µm in diameter and are spaced 14 µm apart on a total surface area of 8 by 8 mm. After filtration, the microsieve was washed once with a permeabilization buffer containing PBS, 1% bovine serum albumin (Sigma-Aldrich, St. Louis MO, USA) and 0.15% saponin (Sigma-Aldrich) and was incubated in this buffer for 15 min at room temperature. Subsequently, a cocktail of fluorescently labeled antibodies was used to stain the cells on the microsieve for 15 min at 37°C. The staining solution consisted of the following monoclonal antibodies: three CK antibody clones targeting CK 4, 5, 6, 8, 10, 13, 18 (clone C11) conjugated to PE (not commercialized), CK 1-8 (clone AE3) and CK 10, 14, 15, 16 and 19 (clone AE1), both conjugated to eFluor570 (ThermoFisher Scientific, Waltham, MA, USA), and one antibody targeting CD45 (clone HI30) labeled with PerCP (Themo Fisher Scientific). After removal of the staining cocktail, the microsieve was washed once and then incubated for 5 min at room temperature with PBS/1%BSA and fixed using PBS with 1% formaldehyde (Sigma-Aldrich) for 10 min at room temperature. Removal

of the fluid during each of the staining and washing steps was performed by bringing the bottom of the microsieve in contact with an absorbing material using a staining holder (VyCAP). The microsieve was subsequently covered with ProLong® Diamond Antifade Mountant with DAPI (Thermo Fisher Scientific). A custom cut glass coverslip of 0.85 by 0.85 cm (Menzel-Gläser, Saarbrükener, Germany) was placed on both sides of the microsieve for immediate analysis or stored at –30°C awaiting further analysis.

Images covering the entire 0.64 cm^2 surface of the microsieves were acquired on a Nikon fluorescence microscope equipped with computer controlled X, Y, Z stage, a 20X microscope objective with a NA of 0.45 and a LED as a light source. The following filters were used: DAPI (DAPI-50LP-A-NQF) with excitation 377/50 nm, dichroic 409 nm LP, emission 409 nm LP; PE (TRITC-B-NQF) with excitation 543/22 nm, dichroic 562 nm LP, emission 593/40 nm and PerCP (FF02-435/40, FF510-Di02 and FF01-676/29 (customized filter cube)) with excitation 435/40 nm, dichroic 510 nm LP, emission 676/29 nm. All cubes were acquired via Nikon (Semrock, Rochester, NY, USA).

Scoring of CTC by CellSearch and on microsieves

Analysis of the fluorescent images generated from the CellSearch cartridges was performed according the instructions of the manufacturer. Images of $EpCAM^{high}$ CTC candidates were identified by the CellTracks Analyzer II and presented to an operator for CTC classification. Cell candidates were assigned as "CTC" when the objects were larger than 4 μm in diameter, stained with DAPI and CK, lacked CD45 staining and had morphological features consistent with that of a cell[17]. The fluorescent images from the microsieves were analyzed for identification of $EpCAM^{low}$ CTC using a plugin for the open-source software ICY[30]. Operators were asked to annotate every DAPI+/CK+/CD45– event and classify the event as a CTC when morphological features were consistent with that of a cell.

Analysis of tdEV with ACCEPT

The CellTracks images from every cartridge were analyzed with the open source image analysis program ACCEPT (*www.github.com/LeonieZ/ACCEPT*)[26,27]. The ACCEPT toolbox detects all events present in the images by an advanced multi-scale segmentation approach and extracts several fluorescence intensities and shape measurements for every event it has found.

The tdEV identified here are relatively large as they have been pelleted with the blood cell fraction after centrifugation at 800g. The selection criteria used for tdEV were: CK mean intensity ≥60, CK maximum intensity ≥90, CK standard deviation of intensity ≥0.15, CK size <150 μm^2, CK perimeter ≥3.2 μm (≥5 pixels), CK roundness <0.80 (where 0 is perfectly round and 1 is a perfect line), CK perimeter to area <1.1, DNA mean intensity <5, CD45 mean intensity <5. Objects that fit the selected definition are depicted in blue, whereas all other objects present in the cartridge are depicted in grey. Scatter plots of all parameters for tdEV are presented in Supplementary Figure 1.

Statistical analysis

Patient variables and EpCAM^{high} CTC, EpCAM^{low} CTC, tdEV and ctDNA data were gathered in an independent way and blindly merged into one data set. For EpCAM^{high} and EpCAM^{low} CTC a cut-off of 2 CTC was used as threshold[17,31]. For tdEV the cut-off threshold was 18 (see results). A previously established cut-off of 5 was used for the genome-wide mFAST-SeqS Z-score to estimate high versus low tumor allele frequency[28]. To determine associations between biomarkers, the non-parametric Spearman's Rho correlation coefficient was used. Kaplan-Meier curves for overall survival (OS) were constructed and differences between groups were tested by the Log-Rank test. Subsequently, a multivariable Cox regression analysis was used to evaluate the discriminative power of favorable (above cut-off threshold) versus unfavorable (below cut-off threshold) biomarkers. To analyze the added predictive value of the biomarkers a multivariable analysis of changes in concordance index (C-index) was used[32]. Statistical analysis was performed in SPSS (version 24, SPSS Inc., Chicago IL, USA) and R (R Foundation, Vienna, Austria). A nominal p-value <0.05 was considered to be significant.

Results

Patients and healthy donors

In this study 97 patients with advanced NSCLC were included, with median age of 65 years, 91% ECOG performance score 0-1 and 20% non-smokers (Table 1). No difference in survival was found between the two locations; the median survival of IOV was 10.2 months and the median survival of UMCG

was 9.9 months (p=0.693). Healthy donors (n=36) aged 20–55 years and without prior history of cancer or blood transmittable disease were used as controls.

Classification of EpCAM^{high} CTC, EpCAM^{low} CTC and tdEV

EpCAM^{high} CTC were identified in the thumbnail images presented to the operator by the CellTracks Analyzer II. The EpCAM^{low} CTC were manually identified in the images scanned from the microsieves with the open source imaging ICY software. Three typical images of EpCAM^{high} CTC (panel A), EpCAM^{low} CTC (panel B) and tdEV (panel C) are displayed using the ACCEPT software in Figure 1. A total of 40,094 events were detected by ACCEPT in this patient sample. After application of the criteria for an event to be assigned as a tdEV, 113 objects were identified as tdEV (panel D).

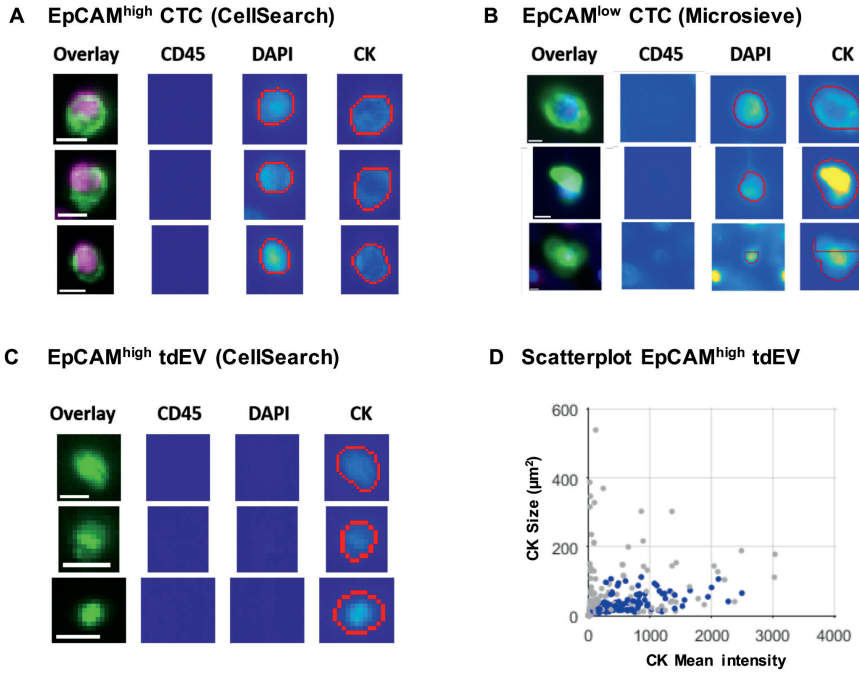

Figure 1. Thumbnail gallery of EpCAM^{high} CTC from CellSearch (A), EpCAM^{low} CTC from microsieves (B) and EpCAM^{high} tdEV from CellSearch (C), showing fluorescent signal for DAPI and/or CK (red circle drawn by the ACCEPT software). The scale bar in the overlay thumbnails is 6.4 µm. Panel D shows a scatter plot of every object present in the cartridge for characteristics in size (y-axis) and fluorescent mean intensity (x-axis). The tdEV are identified with a multi parameter gate and are visualized as blue dots. The remaining objects that do not fit the multi parameter gate are visualized as grey dots.

Presence of CK positive EpCAM^{high} and EpCAM^{low} cells and tdEV in healthy donors

In order to assess the specificity of our classification system, blood of 36 healthy donors were processed for the detection of CK-positive EpCAM^{high} and EpCAM^{low} cells and tdEV. While only one EpCAM^{high} cell was found in a single control sample (2.8%), EpCAM^{low} cells were detected in five of the 36 samples (13.8%) (mean 0.7, standard deviation 2.3, range 0-12). The mean tdEV count in these samples was 4.7 (median 3, range 0-36) with a standard deviation of 6.6. For tdEV the cut-off threshold was established at 18 based on the mean tdEV plus two standard deviations.

Presence of EpCAM^{high} CTC, EpCAM^{low} CTC, tdEV and ctDNA in NSCLC patients

In 20 patients (21%) ≥2 EpCAM^{high} CTC were detected, in 15 patients (15%) ≥2 EpCAM^{low} CTC, in 26 patients (27%) ≥18 tdEV and 18 patients (19%) showed high (>10%) tumor allele frequency with genome-wide mFAST-SeqS. EpCAM^{high} CTC, tdEV and ctDNA were significantly correlated with each other, but not with EpCAM^{low} cells. The frequency distribution is illustrated in Figure 2 and in more detail in Supplementary Table 1. The ctDNA fraction was determined in the plasma from either the CellSave tube (n=23) used for CTC enumeration or from an additional EDTA tube (n=74). Concentration of plasma total DNA ranged from 11.9 to 407 ng per mL plasma (mean 69.87 ng/mL) for CellSave tubes and 4.6 to 780.3 ng per mL plasma (mean 98.7 ng/mL) for EDTA tubes. ctDNA extracted from EDTA and CellSave collection tubes from 31 patients were significantly correlated ($r=0.493$, $p=0.005$); ≥10% tumor allele frequencies measured with mFAST-SeqS were always detected in corresponding tubes.

Primary tumor mutation detection

In 46 of the 97 advanced NSCLC patients molecular analysis of the primary tumor was performed and in 16 patients a specific mutation was detected. The number of EpCAM^{high} CTC, EpCAM^{low} CTC, tdEV and plasma ctDNA and the mutations identified in the primary tumor is shown in Table 2. The plasma tumor allele frequency was low (<10%) in all of the 16 samples. However, using the high-resolution methods Safe-SeqS or Deep-Seq, mutations could be successfully tracked in 11 samples (69%). In three of

these patients, no CTC were detected. As expected by the low mFAST-SeqS Z-scores, the variant allele frequencies (VAF) detected with the sensitive sequencing methods were low, ranging from 0.1-5.3%.

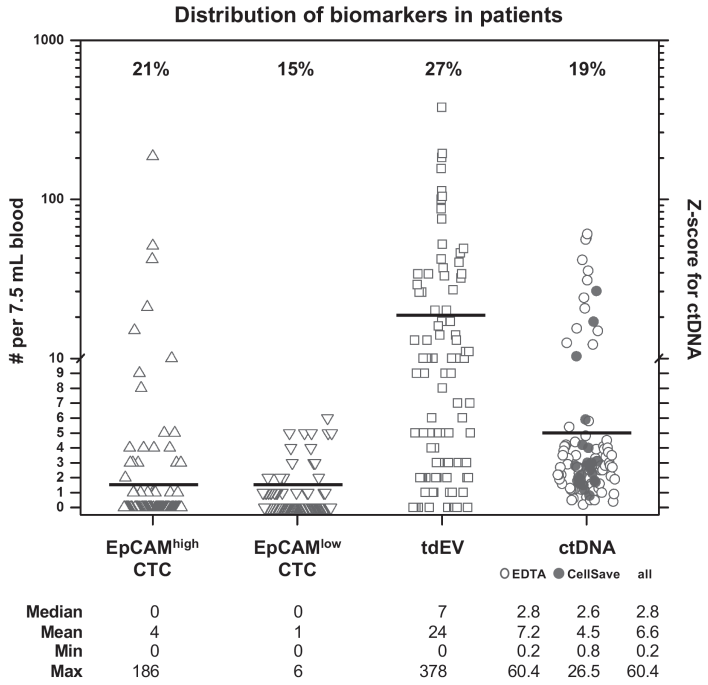

Figure 2. Frequency distribution of EpCAM^{high} CTC, EpCAM^{low} CTC, tdEV and Z-score for ctDNA of 97 NSCLC patients. Percentages displayed above the black bar represent the patients that score above the threshold for that biomarker. Thresholds are: two CTC for EpCAM^{high} and EpCAM^{low}, 18 vesicles for tdEV and a Z-score of 5 for ctDNA, representing 10% tumor allele frequency. Z-score was determined in 74 samples from EDTA tubes (open circle) and in 23 samples from CellSave tubes (filled circle).

Single blood biomarkers and overall survival of NSCLC patients

To study the discriminative value of the biomarkers NSCLC patients were stratified in those with favorable and unfavorable biomarker status according to the threshold cut-off values (Figure 3). EpCAM^{high} CTC was associated with prolonged overall survival (HR 2.1, 95% CI 1.2-3.7; p=0.014) with a median OS of 4.2 months (range 1-21) for the unfavorable group (≥2 CTC) and 12.2 months (range 1-30) for the favorable group (<2 CTC) (panel A).

Secondly, tdEV was associated with overall survival (HR 2.0, 95% CI 1.2-3.5; p=0.014) with a median OS of 4.2 months (range 1-19) for the unfavorable group (≥18) versus 12.2 months (range 1-30) for the favorable group (<18)

Table 2. Primary tumor mutations and the presence of CTC, tdEV and ctDNA in sixteen patients with adeno-carcinoma of the lung.

Pt	Mutation primary tumor	EpCAM^{high} CTC	EpCAM^{low} CTC	tdEV	Z-score	WT reads	Mutated reads	VAF %*	Method
1	KRAS: c.37 G>T; p.G13C	3	0	52	0.91	16,577	476	2.79	SS
2	EGFR: p.L747_P753delinsS EGFR: c.2369 C>T; p.T790M	1	6	9	2.06	179,591	0	0.00	DS
3	KRAS: c.38 G>A; p.G13D	1	3	33	3.99	60,274	2,911	4.61	SS
4	KRAS: c.35 G>C; p.G12A**	0	5	5	1.95	48,546	151	0.31	SS
5	ALK: c.3616 T>G;p.S1206A	0	3	2	2.23	410,108	1,179	0.29	DS
6	EGFR: c.2315_2316insGTT; p.P772_H773insF	0	3	0	1.15	430,091	611	0.14	DS
7	BRAF: c.1406 G>T; p.G469V	0	1	17	0.49	45,137	459	1.01	SS
8	NRAS: c.182 A>G; p.Q61R	0	1	1	1.23	36,371	52	0.14	SS
9	KRAS: c.34 G>T; p.G12C EGFR: c.2305 G>T; p.V769L	0	1	0	2.18	203,640	177	0.09	SS
10	KRAS; c.34 G>T; p.G12C	0	0	14	2.96	166	0	0.00	SS
11	EGFR: c.2573 T>G; p.L858R EGFR: c.2369 C>T; p.T790M	0	0	14	0.57	37,493	0	0.00	SS
12	EGFR: c.2126 A>C; p.E709A EGFR: c.2156 G>C; p.G719A	0	0	10	2.00	619,082 620,329	1,489 474	0.24 0.10	DS
13	KRAS: c.183 A>C; p.Q61H	0	0	5	2.63	10,980	0	0.00	SS
14	EGFR: c.2236_2250del15; p.E746_A750del	0	0	5	0.54	514,839	29,039	5.34	DS
15	EGFR: c.2236_2250del15; p.E746_A750del	0	0	3	0.96	527,145	3,715	0.70	DS
16	EGFR: c.2240_2254del15; p.L747_T751delLREAT	0	0	2	0.47	503,499	5	0.00	DS

* VAF (%) indicates the percentage of variant allele frequency found among the wild type alleles in ctDNA.

** Additional KRAS mutation: c.35G>T; p.G12A was found with 2.50 VAF%;

SS = Safe-SeqS; DS = Deep Sequencing ; WT = wild type.

(panel C). Thirdly, ctDNA was associated with overall survival (HR 1.9, 95% CI 1.1-3.4; p=0.032) with a median OS of 5.2 months (range 1-26) for the unfavorable group with high tumor allele frequency (≥10%) versus 11.5 months (range 1-30) for the favorable group (tumor allele frequency <10%) (panel D). However, the presence of EpCAM^{low} CTC did not associate with

overall survival (HR 1.2, 95% CI 0.6-2.3, p=0.579) with a median OS of 6.8 months (range 1-30) for the unfavorable group (≥2 CTC) versus 11.0 months (range 1-29) for the favorable group (<2 CTC) (panel B). To study the predictive ability of the four biomarkers, the concordance index was calculated. For EpCAM^{high} CTC the C-index was 0.561, for EpCAM^{low} CTC this was 0.512, for tdEV 0.565 and for ctDNA 0.551.

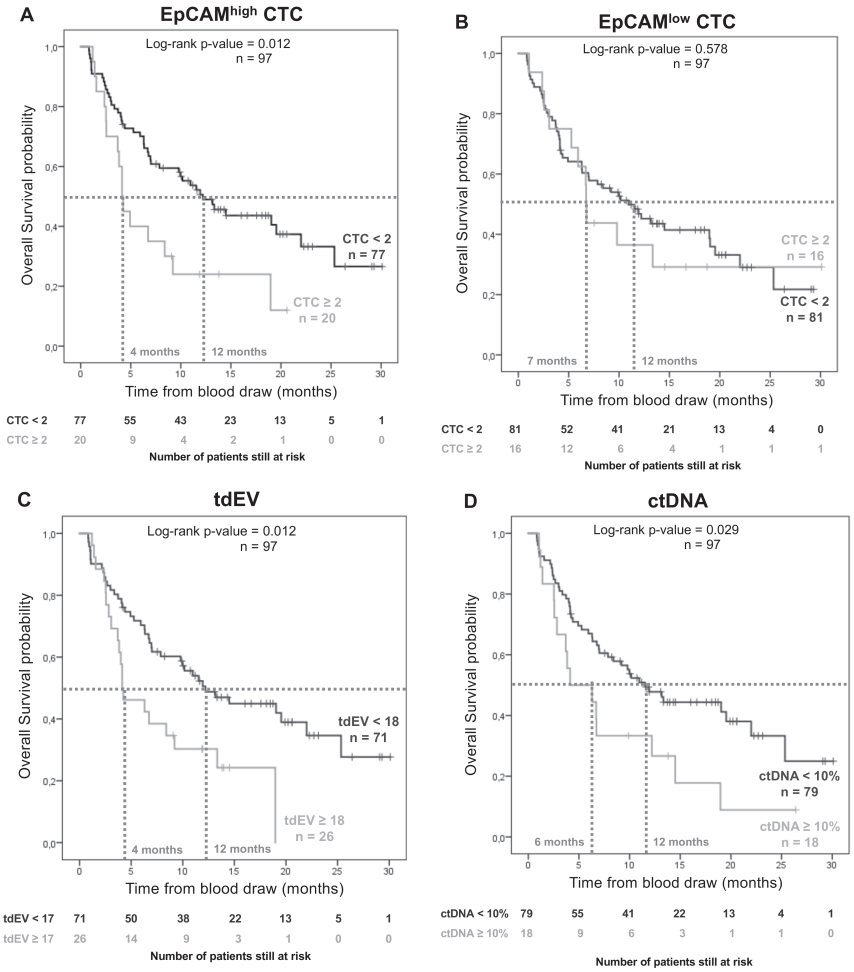

Figure 3. Kaplan-Meier plots of probabilities of overall survival of 97 metastatic NSCLC patients with favorable or unfavorable EpCAM^{high} CTC (A), EpCAM^{low} CTC (B), tdEV (C) and ctDNA (D). To separate between favorable and unfavorable groups, the threshold for CTC was 2, for tdEV 18, and for ctDNA 10% mutant alleles (Z-score of 5).

Comprehensive multi-parameter blood biomarker

The significant biomarkers from the univariate analysis were EpCAM^{high} CTC, tdEV and ctDNA, but not EpCAM^{low} CTC. The values of EpCAM^{high} CTC were correlated with those of tdEV (0.66), ctDNA (0.35) but not with EpCAMlow CTC (0.08). The correlation between tdEV and ctDNA was low (0.25). EpCAM^{low} CTC was not correlated with tdEV (0.05) or ctDNA (–0.02). To study the discriminative power of the three significant biomarkers from the univariate regressions, all were simultaneously included as categorical values (favorable and unfavorable) in a multivariable Cox proportional regression model. In the model none versus one unfavorable biomarker was not significantly different from each other (HR 1.0, 95% CI 0.4-2.1, p=0.909), whereas two (HR 2.3, 95% CI 1.0-5.0, p=0.038) or all three (HR 2.9, 95% CI 1.4-6.0, p=0.005) unfavorable biomarkers were significantly different compared to none unfavorable biomarkers (panel A in Figure 4). Therefore, we stratified the patients based on the presence of none and one unfavorable biomarker versus two and three unfavorable biomarkers and determined the OS of these two groups (panel B). The patients with none and one unfavorable biomarker had a median OS of 12 months (range 1-30) versus 6 months (range 1-19) for the patients with two and three unfavorable biomarkers (HR 2.6, 95% CI 1.5-4.6, p=0.001). The predictive ability of all three biomarkers in the multivariable C-index model provides a significant contribution of 0.575 (p=0.047), but the biomarkers themselves become non-significant. When each of the biomarkers were removed from the model, a drop in C-index after removing them was extremely small; for EpCAM^{high} CTC this was 0.002 (from 0.575 to 0.573); for tdEV 0.000 (from 0.575 to 0.575) and for ctDNA 0.005 (from 0.575 to 0.570). Moreover, the effect size of each biomarker in the combined model became smaller and non-significant (EpCAM^{high} CTC HR 1.4; tdEV HR 1.5 and ctDNA HR 1.5).

Discussion

Blood may contain different tumor derived cells, vesicles and DNA molecules that offer a simple, patient friendly approach, to study clone diversity that may be most relevant to determine treatment options for patients with advanced NSCLC. In the CANCER-ID consortium (*www.cancer-id.eu*) CTC and tumor related nucleic acids in blood are being extensively explored for their potential to serve as a predictive or prognostic factor in advanced

NSCLC. In this study, members of this consortium explored CTC, tumor derived extra cellular vesicles and plasma nucleic analysis of 97 NSCLC patients to determine whether a combined analysis of multiple liquid biopsy components is feasible on the same tube of blood and what information could be obtained from such analysis. From the blood collected in 10 mL CellSave tubes for subsequent CTC analysis, on average 1.7 mL (0.8-2.0 mL) of

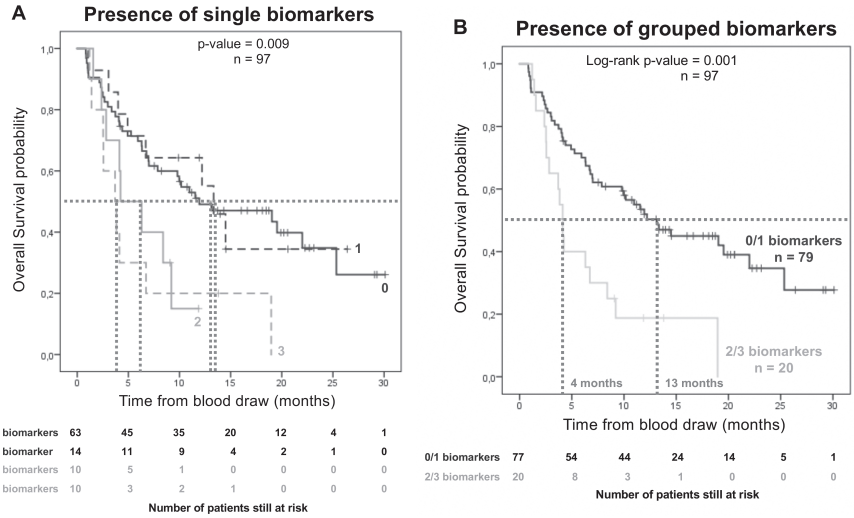

Figure 4. Kaplan Meier plot of probabilities of overall survival of 97 metastatic NSCLC patients stratified for the amount of unfavorable biomarkers (EpCAM^{high} CTC ≥2, tdEV ≥18 and ctDNA ≥10%). Group 0 includes patients with no unfavorable biomarkers, group 1 with one unfavorable biomarker, group 2 with two unfavorable biomarkers, and group 3 with all unfavorable biomarkers (A). Two groups stratified for the presence of either none and one unfavorable biomarkers or two and three unfavorable biomarkers (B).

plasma could be harvested and stored for ctDNA analysis before processing the samples on the CellSearch system. Comparison of the CellSave plasma for ctDNA analysis with plasma from EDTA blood showed a strong correlation, indicating that all tests can be reliably obtained from CellSave tubes.

For CTC analysis, the FDA cleared CellSearch system was used and in 21% of the advanced NSCLC patients CTC were detected. These CTC are referred here as EpCAM^{high} CTC and their presence has been reported to be associated with poor survival which was confirmed in this study[14,20]. We also confirmed previous findings that the presence of EpCAM^{low} CTC, present in 15% of the patients, after filtration of the EpCAM depleted blood was not significantly associated with survival[20]. This may question the cancerous origin of the

EpCAM^{low} CTC. For single cell analysis of these EpCAM^{low} CTC, technology will need to be developed that can determine the molecular composition of these CTC on the microsieves.

In metastatic prostate cancer, objects smaller than cells expressing cytokeratin and lacking CD45 in the EpCAM enriched cell suspensions were associated with poor survival, similarly with CTC in these patients[25]. Using the recently introduced open source imaging program ACCEPT, the identification of these objects in CellSearch image sets was automated and in our NSCLC cohort these objects were identified with a relatively high density, with elevated levels in 27% of the patients. Moreover, patients with elevated tdEV numbers showed significantly worse survival, confirming the earlier observations of a strong relation between poor outcome and the presence of tdEV[33].

For ctDNA analysis we determined the tumor allele frequency in plasma DNA using mFAST-SeqS assay, which measures the aneuploidy fraction of circulating DNA[28]. It is of note that mFAST-SeqS has a limited analytical sensitivity and a correlation of Z-scores with tumor allele frequency can only be provided in patients with high tumor allele frequency (≥10%). mFAST-SeqS Z-scores in the lower range are not informative and indicate low tumor DNA content. Nevertheless, the intent of this study was not an absolute quantification of tumor-derived fragments in plasma but rather the assessment of a fast and cost-effective method to stratify patients into groups of high and low tumor allele frequencies and to combine these data with other liquid biopsy components. Patients with high tumor allele frequencies (19%) had significantly poor survival, similar to elevated EpCAM^{high} CTC and tdEV.

Blood derived tumor markers EpCAM^{high} CTC, tdEV and ctDNA in advanced NSCLC were each associated with poor survival. Two or three unfavorable biomarkers – all shedding from the tumor – discriminates poor prognosis better than one biomarker, but the predictive contribution of each biomarker is small, as was shown by the drop in C-index after removing each biomarker from the model. We questioned whether there is still room for their own contribution to survival since serious collinearity arises with higher correlations between biomarkers. In other words, these biomarkers come from the same underlying biological processes but still may have their own dynamics that may influence survival. However, the lack of power – that is the low number of patients where all three biomarkers were present – prohibited significance for the predictive accuracy.

Although EpCAM^{high} CTC, tdEV and ctDNA may be useful to identify a subset of NSCLC patients with a relatively poor prognosis, it does not address the question whether information can be retrieved to predict whether patients are eligible for targeted therapy. Expression of mutated proteins, such as EGFR, can be assessed on CTC and tdEV, but only in those harboring such mutations (i.e. approximately 20% of patients with advanced NSCLC). In this cohort of patients, mutations in the primary tumor were identified in 16 of the 46 NSCLC patients (35%). However, the mutation status of a tumor can easily be tracked with ctDNA, even in those with low tumor fractions since a variety of high resolution methods are now available[34–36]. Indeed, in 11 of the 16 patients (69%) the tumor-specific mutations could be tracked with ultra-deep sequencing methods. As expected from the low mFAST-SeqS Z-scores, the observed variant allele frequencies ranged from 0.09 to 5.34%, which is indeed below the dynamic range of mFAST-SeqS.

The true potential of a liquid biopsy lies in determining genetic alterations associated with therapy resistance or new mutations occurring during the course of the disease. A variety of different liquid biopsy approaches have been evaluated for their clinical potential in NSCLC. Due to the low efficiency to retrieve high CTC numbers (30% of the patients have 1 or more CTC; 8% with >5 CTC per 7.5 mL blood) and elevated plasma DNA tumor fractions all fall short when it comes to a broad patient coverage[31,37–39]. In this study we detected one of the biomarkers in 45% of the patients, whereas each individual biomarker was detected in 15-27% of the patients. A potential solution to increase these percentages even further is to increase the blood volume that can be analyzed which can be obtained through a diagnostic leukapheresis[40]. Studies in advanced NSCLC are currently being conducted in the CANCER-ID consortium to evaluate whether this approach can yield sufficient number of CTC or ctDNA to yield a liquid biopsy for the majority of NSCLC patients[41].

Taken together, here we report for the first time a single tube approach enabling a simultaneous analysis of EpCAM^{high} CTC, EpCAM^{low} CTC, tdEV and ctDNA. Except for EpCAM^{low} CTC, the presence of each component was associated with a poor clinical outcome in advanced NSCLC patients. Two or more biomarkers discriminated an unfavorable subgroup of advanced NSCLC, but the predictive accuracy could not be determined.

References

1. Tang, Y. et al. Biomarkers for early diagnosis, prognosis, prediction, and recurrence monitoring of non-small cell lung cancer. Onco. Targets. Ther. Volume 10, 4527–4534 (2017).
2. Siravegna, G., Marsoni, S., Siena, S. & Bardelli, A. Integrating liquid biopsies into the management of cancer. Nat. Rev. Clin. Oncol. 14, 531–548 (2017).
3. Heitzer, E., Auer, M., Ulz, P., Geigl, J. B. & Speicher, M. R. Circulating tumor cells and DNA as liquid biopsies. Genome Med. 5, 73 (2013).
4. Gallo, M. et al. Clinical utility of circulating tumor cells in patients with non-small-cell lung cancer. Transl. lung cancer Res. 6, 486–498 (2017).
5. Singh, A. P., Cheng, H., Guo, X., Levy, B. & Halmos, B. Circulating Tumor DNA in Non–Small-Cell Lung Cancer: A Primer for the Clinician. JCO Precis. Oncology (2017). doi:10.1200/PO.17.00054
6. Reclusa, P. et al. Exosomes as diagnostic and predictive biomarkers in lung cancer. J. Thorac. Dis. 9, S1373–S1382 (2017).
7. Cui, S., Cheng, Z., Qin, W. & Jiang, L. Exosomes as a liquid biopsy for lung cancer. Lung Cancer 116, 46–54 (2018).
8. Cristofanilli, M., Budd, G., Ellis, M. & A. Circulating tumor cells, disease progression, and survival in metastatic breast cancer. Engl. J. 351, 781–791 (2004).
9. Janni, W. J. et al. Pooled Analysis of the Prognostic Relevance of Circulating Tumor Cells in Primary Breast Cancer. Clin. Cancer Res. 22, 2583–2593 (2016).
10. de Bono, J. S. et al. Circulating Tumor Cells Predict Survival Benefit from Treatment in Metastatic Castration-Resistant Prostate Cancer. Clin. Cancer Res. 14, 6302–6309 (2008).
11. Cohen, S. J. et al. Relationship of Circulating Tumor Cells to Tumor Response, Progression-Free Survival, and Overall Survival in Patients With Metastatic Colorectal Cancer. J. Clin. Oncol. 26, 3213–3221 (2008).
12. van Dalum, G. et al. Importance of circulating tumor cells in newly diagnosed colorectal cancer. Int. J. Oncol. 46, 1361–8 (2015).
13. Hiltermann, T. J. N. et al. Circulating tumor cells in small-cell lung cancer: a predictive and prognostic factor. Ann. Oncol. 23, 2937–42 (2012).
14. Krebs, M. G. et al. Evaluation and prognostic significance of circulating tumor cells in patients with non-small-cell lung cancer. J. Clin. Oncol. 29, 1556–63 (2011).
15. Andree, K. C., van Dalum, G. & Terstappen, L. W. M. M. Challenges in circulating tumor cell detection by the CellSearch system. Mol. Oncol. 10, 395–407 (2016).
16. Rao, C. G. et al. Expression of epithelial cell adhesion molecule in carcinoma cells present in blood and primary and metastatic tumors. Int. J. Oncol. 27, 49–57 (2005).
17. Allard, W. J. et al. Tumor Cells Circulate in the Peripheral Blood of All Major Carcinomas but not in Healthy Subjects or Patients With Nonmalignant Diseases. Clin. Cancer Res. 10, 6897–6904 (2004).
18. Lustberg, M. B. et al. Heterogeneous atypical cell populations are present in blood of metastatic breast cancer patients. Breast Cancer Res. 16, R23 (2014).
19. Armstrong, A. J. et al. Circulating tumor cells from patients with advanced prostate and breast cancer display both epithelial and mesenchymal markers. Mol. Cancer Res. 9, 997–1007 (2011).
20. de Wit, S. et al. The detection of EpCAM+ and EpCAM– circulating tumor cells. Sci. Rep. 5, 12270 (2015).

21. Francart, M.-E. et al. Epithelial-mesenchymal plasticity and circulating tumor cells: Travel companions to metastases. Dev. Dyn. (2017). doi:10.1002/dvdy.24506
22. Alix-Panabières, C., Mader, S. & Pantel, K. Epithelial-mesenchymal plasticity in circulating tumor cells. J. Mol. Med. 95, 133–142 (2017).
23. van der Pol, E., Boing, A. N., Harrison, P., Sturk, A. & Nieuwland, R. Classification, Functions, and Clinical Relevance of Extracellular Vesicles. Pharmacol. Rev. 64, 676–705 (2012).
24. Azmi, A. S., Bao, B. & Sarkar, F. H. Exosomes in cancer development, metastasis, and drug resistance: a comprehensive review. Cancer Metastasis Rev. 32, 623–642 (2013).
25. Coumans, F. A. W., Doggen, C. J. M., Attard, G., de Bono, J. S. & Terstappen, L. W. M. M. All circulating EpCAM+CK+CD45- objects predict overall survival in castration-resistant prostate cancer. Ann. Oncol. 21, 1851–7 (2010).
26. Zeune, L. L., van Dalum, G., Terstappen, L. W. M. M., van Gils, S. A. & Brune, C. Multiscale Segmentation via Bregman Distances and Nonlinear Spectral Analysis. SIAM J. Imaging Sci. 10, 111–146 (2017).
27. Zeune, L. L. et al. Quantifying HER-2 expression on circulating tumor cells by ACCEPT. PLoS One 12, e0186562 (2017).
28. Belic, J. et al. Rapid Identification of Plasma DNA Samples with Increased ctDNA Levels by a Modified FAST-SeqS Approach. Clin. Chem. 61, 838–849 (2015).
29. Kinde, I., Wu, J., Papadopoulos, N., Kinzler, K. W. & Vogelstein, B. Detection and quantification of rare mutations with massively parallel sequencing. Proc. Natl. Acad. Sci. 108, 9530–9535 (2011).
30. ICY. Available at: http://icy.bioimageanalysis.org/.
31. Krebs, M. G. et al. Analysis of circulating tumor cells in patients with non-small cell lung cancer using epithelial marker-dependent and -independent approaches. J. Thorac. Oncol. 7, 306–15 (2012).
32. Kattan, M. W. Evaluating a new marker's predictive contribution. Clin. Cancer Res. 10, 822–4 (2004).
33. Nanou, A. et al. Circulating tumor cells, tumor-derived extracellular vesicles and plasma cytokeratins in castration-resistant prostate cancer patients. Oncotarget Press (2018).
34. Forshew, T. et al. Noninvasive Identification and Monitoring of Cancer Mutations by Targeted Deep Sequencing of Plasma DNA. Sci. Transl. Med. 4, 136ra68-136ra68 (2012).
35. Dietz, S. et al. Low Input Whole-Exome Sequencing to Determine the Representation of the Tumor Exome in Circulating DNA of Non-Small Cell Lung Cancer Patients. PLoS One 11, e0161012 (2016).
36. Newman, A. M. et al. Integrated digital error suppression for improved detection of circulating tumor DNA. Nat. Biotechnol. 34, 547–555 (2016).
37. Hanssen, A. et al. Characterization of different CTC subpopulations in non-small cell lung cancer. Sci. Rep. 6, 28010 (2016).
38. Tong, B. et al. Prognostic significance of circulating tumor cells in non-small cell lung cancer patients undergoing chemotherapy. Oncotarget 8, 86615–86624 (2017).
39. Pailler, E. et al. Circulating Tumor Cells with Aberrant ALK Copy Number Predict Progression-Free Survival during Crizotinib Treatment in ALK -Rearranged Non–Small Cell Lung Cancer Patients. Cancer Res. 77, 2222–2230 (2017).
40. Stoecklein, N. H., Fischer, J. C., Niederacher, D. & Terstappen, L. W. M. M. Challenges for CTC-based liquid biopsies: low CTC frequency and diagnostic leukapheresis as a potential solution. Expert Rev. Mol. Diagn. 16, 147–164 (2016).
41. Andree, K.C., et al. Circulating tumor cells in the peripheral blood and leukapheresis product of non-small cell lung cancer patients. in American Association for Cancer Research (2018).

Supplementary data

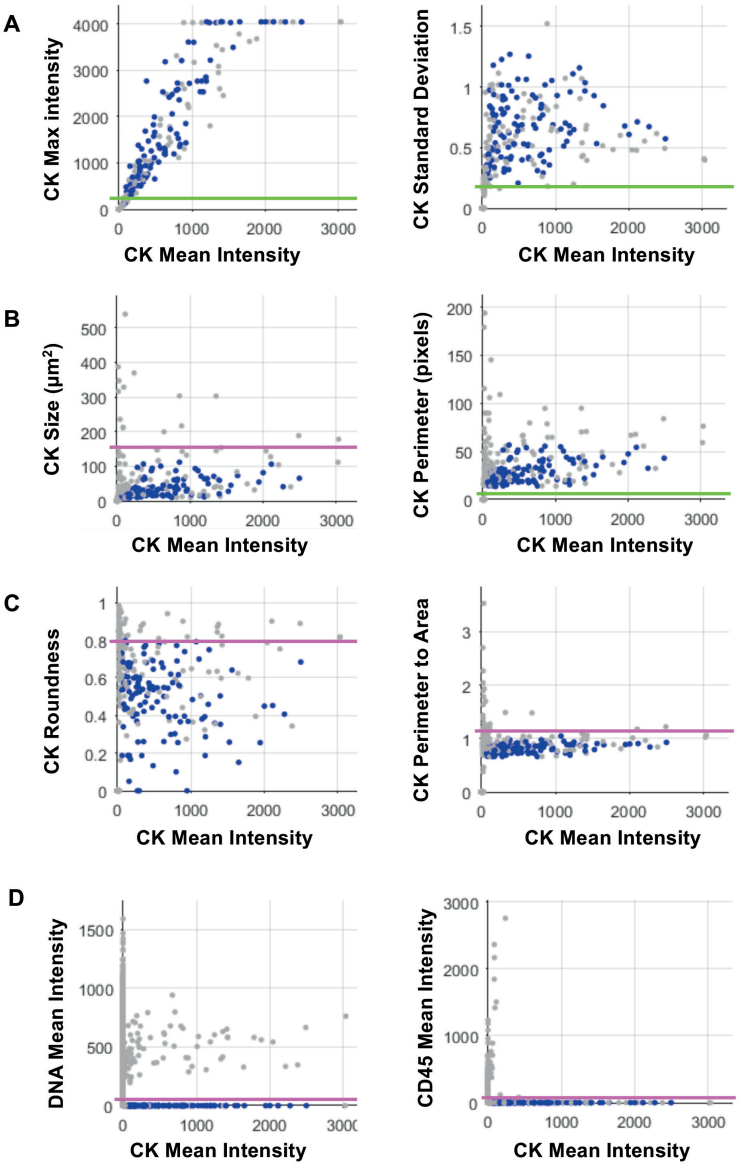

Supplementary Figure S1. ACCEPT plots of each parameter for defining tdEV. Events that fit the definition of tdEV are depicted as blue dots and all other events present in the sample are depicted as grey dots. A pink bar represents the restriction value for that parameter, whereas the green bar represents the minimal value for that parameter.

Supplementary Table S1. Number of patients positive for each biomarker combination in 97 advanced NSCLC patients.

EpCAM^{high} CTC	EpCAM^{low} CTC	tdEV	ctDNA	NSCLC patients
-	-	-	-	No biomarker: 53
+	-	-	-	2
-	+	-	-	8
-	-	+	-	6
-	-	-	+	4
				One biomarker: 20
+	+	-	-	0
+	-	+	-	7
+	-	-	+	0
-	+	+	-	2
-	+	-	+	2
-	-	+	+	2
				Two biomarkers: 13
+	+	+	-	1
+	+	-	+	0
+	-	+	+	8
-	+	+	+	0
				Three biomarkers: 9
+	+	+	+	Four biomarkers: 2

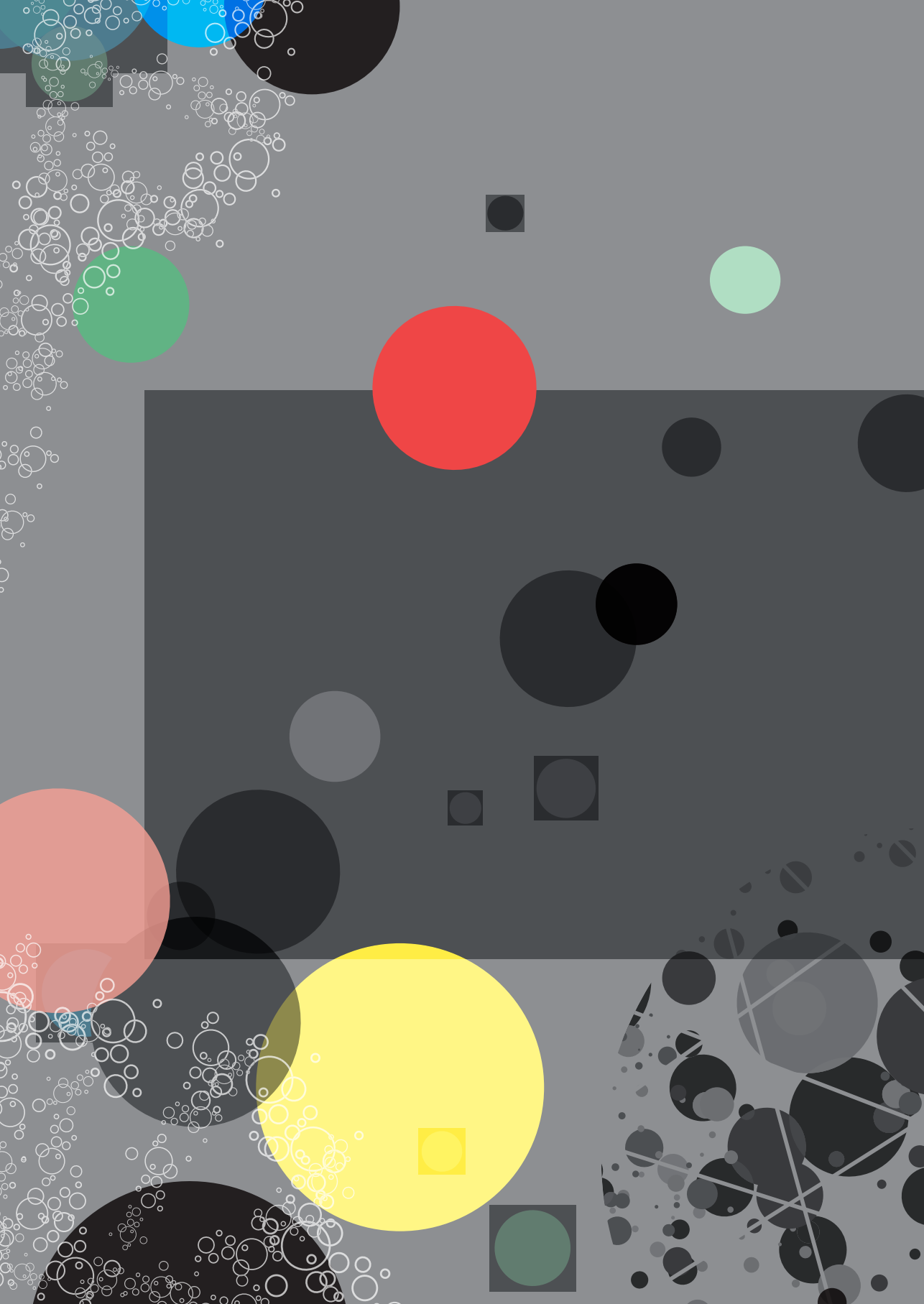

Chapter 7

Classification of cells in CTC enriched samples by advanced image analysis

Sanne de Wit*, Leonie L. Zeune*, Christoph Brune, Guus van Dalum, T. Jeroen N. Hiltermann, Harry. J.M. Groen, Leon W.M.M. Terstappen

**authors contributed equally*

Abstract

In the CellSearch® system blood is immunomagnetically enriched for EpCAM expression and cells are stained with the nucleic acid dye DAPI, Cytokeratin-PE (CK) and CD45-APC. Only DAPI+/CK+ objects are presented to the operator to identify circulating tumor cells (CTC) and the identity of all other cells remains unrevealed. Here, we used the open source imaging program ACCEPT to analyze all DAPI+ nuclei in 659 EpCAM enriched blood samples from 162 controls and 192 metastatic non-small cell lung (NSCLC) cancer patients. Significantly larger number of nuclei were detected in the 300 patient samples ranging from 433-384,015 with a mean of 73,570 ±74,948, as compared to the 359 control samples ranging from 50-33,600 with a mean of 4,191 ±4,463 ($p<0.001$). With CellSearch, in patients only 18% ±21 and in controls 23% ±15 of the nuclei were identified as leukocytes or CTC. Adding CD16-PerCP increased the leukocyte population to 80% in patients and to 84% in controls. The use of a LED as light source for CD45-APC excitation increased the percentage of nuclei identified as leukocytes from 8% (±7) to 16% (±9), whereas the CD45+/CD16+ leukocytes increased from 1% (±0) to 59% (±25) (n=10). Plasma membrane staining obtained with wheat germ agglutinin (wga) showed that 48% (±23) of unstained cells are simply bare nuclei. Addition of CD16 and wga to the antibody cocktail and the use of a LED light source improve the classification of EpCAM enriched cells. However, especially in patients, the origin of a portion of the cells remains unknown. Further studies are needed to determine if EpCAM+/DAPI+/CK–/CD45– CTC are present among the nucleated cells with unknown origin.

Introduction

Circulating Tumor Cells (CTC) are cells disseminated from the primary or metastatic tumor site into the blood stream. In several cancer types, including non-small and small cell lung, prostate, breast, colon, bladder, gastric carcinoma and melanoma, the presence of CTC in circulation is associated with the poor survival of the patients[1–9]. With many blood cells circulating in our cardiovascular system, CTC are rare events. A concentration of 1 CTC per mL of blood is already high, while the concentration of white blood cells is around $5 \cdot 10^6$ cells and red blood cell concentrations reach up to $5 \cdot 10^9$ cells per mL. When detecting CTC, it is therefore of utmost importance

to have an extremely sensitive and specific assay to discriminate between the tumor cells and blood cells. In the CellSearch® system Epithelial Cell Adhesion Molecule (EpCAM) antibodies coupled to ferrofluids are used for immunomagnetic enrichment of cells thereby removing the bulk of leukocytes. After this, CTC are fluorescently labeled with: DAPI to stain the nucleus; Phycoerythrin (PE) labeled antibodies recognizing cytokeratins (CK) 4-6, 8, 10, 13, 18 and 19 – which are present in the majority of cells derived from epithelial cancers – and Allophycocyan (APC) labeled CD45 – present on the cell surface of leukocytes[10]. Images covering the surface of the CellTracks cartridge are acquired by the CellTracks Analyzer II and all events positive for both DAPI and CK are presented as thumbnail images to the operator, who will decide which cells fit the CTC criteria. The identity and number of all other nucleated cells is not provided, but can now be explored using the open source image analysis program ACCEPT (*https://github.com/LeonieZ/ACCEPT*). The ACCEPT program is an open source toolbox designed to analyze and characterize all objects present in the fluorescent images. With this program we explored the identity of all cell populations present in the acquired images to assess the number of cells that potentially are CTC and missed by the current staining cocktail.

Previously, we observed that the number of cells identified as leukocytes in the EpCAM enriched fraction was too low and addition of CD16 recognizing the FcgIIIa to the staining cocktail improved the identification of nuclei as granulocytes, since they express CD45 at a lower level compared to lymphocytes and monocytes[11]. We also explored a LED as an alternative light source on a fluorescence microscope to improve the efficiency of excitation of the fluorochromes, as opposed to the CellTracks which uses a mercury arc lamp as light source. The LED lamp used for APC excitation has an excitation peak at 635 nm, close to the excitation maximum of 650 nm for APC and therefore dramatically improves the excitation of APC compared to the mercury arc lamp[12]. Hence, we hypothesized we would detect more CD45-APC positive cells with the LED light. In addition, wheat germ agglutinin (wga), a lectin that binds to sialic acid and N-acetylglucosamine residues, was explored because it is present on cellular plasma membranes[13–18]. We examined the presence of a cell membrane by using wga conjugated to AlexaFluor-488 and adding it to the CellSearch immunostaining cocktail.

Methods

Cancer patients and controls

Peripheral blood samples were drawn by venipuncture into 10 mL CellSave Preservative Tubes (Menarini Silicon Biosystems, Huntingdon Valley PA, USA) from healthy donors and metastatic NSCLC patients. 300 blood samples from 192 NSCLC patients were obtained and all patients provided written informed consent and the study protocol was approved by the medical ethical committee of the University Medical Centre Groningen (Groningen, The Netherlands). Blood draw from patients occurred before and/or during their treatment. 127 blood samples from 20 healthy volunteers aged 20–55 were obtained from the TNW-ECTM-donor services at the University of Twente and all donors gave written informed consent before donating blood. All healthy donor samples were processed 1 day after blood draw, whereas patient samples were processed after 1-4 days. Digitally stored images from 232 samples from 142 patients with benign disease processed with CellSearch from previous studies were included for ACCEPT analysis[10,19]

Cell lines and spiking

For testing wheat germ agglutinin (wga) staining of cancer cells, blood from a healthy donor was spiked with cells from the breast cancer cell line MCF-7. The MCF-7 cell line was obtained from ATCC (Manassas, VA, USA) and has not been authenticated in the past six months. The cells were grown at 37°C and 5% CO2 and cultured in RPMI-1640 (Sigma-Aldrich, St. Louis MO, USA). Culture media was supplemented with L-Glutamine (Sigma), 10% fetal bovine serum (Gibco, Invitrogen, Carlsbad CA, USA) and 1% penicillin-streptomycin (Gibco).

Processing blood with CellSearch

Aliquots of 7.5 mL of blood were processed with the CellSearch® system (Menarini Silicon Biosystems) for CTC detection. CellSearch analysis was performed within 96 hours after the blood draw. Antibodies directed against the epithelial cell adhesion antigen (EpCAM) coupled to ferrofluids were used to enrich CTC from the background of leukocytes. The enriched cells were fluorescently labeled with the CellSearch CTC kit (Menarini Silicon Biosystems) using the nucleic acid dye 4'6-diaminodino-2-phenylindole

(DAPI) for DNA staining, anti-cytokeratin monoclonal antibodies (mAbs) C11 and A53.B/A2 labelled with phycoerythrin (PE), and anti-CD45 mAb (clone HI30) labeled with Allophycocyan (APC) recognizing leukocytes. Peridinin Chlorofyll A Protein (PerCP) labeled mAb anti-CD16 (clone 3G8, Biolegend, San Diego CA, USA) directed against granulocytes and Alexa-Fluor488 conjugated to the lectin wga (Thermo Fisher Scientific, Waltham MA, USA) was added to the extra marker position in the CellSearch Epithelial Cell kit with an end concentration of 2 µg/mL and 3 µg/mL respectively. This extra marker channel was used for the measurement of PerCP and DIOC on the CellTracks Analyzer II, which generates images of the complete cartridge for all channels.

Image acquisition

Fluorescent microscopy images were acquired using a modified CellTracks Analyzer II, which included – next to the standard instruments – a 20X and 40X objective and in total 6 filter cubes. Besides the acquisition of the standard channels DAPI, PE, DIOC and APC, the images with PerCP staining were acquired with a customized PerCP filter cube (excitation 435/40 nm; dichroic 510 nm; emission 676/29 nm (Semrock, Rochester NY, USA)) using an integration time of 400 ms. When wga was used in the immunostaining, the integration time of the DIOC filter was also 400 ms. To determine if another light source detects weakly stained leukocytes better than the mercury arc lamp of the CellTracks, 10 cartridges were automatically scanned with an inverted Nikon Ti-E microscope with filter cube and objective changer (Nikon, Tokyo, Japan). The light source of this microscope is the Lumencor Sola SE II 365 LED. A 10X (0.45NA) objective (Nikon), a computer controlled CCD camera (C114400, Orca Flash 4.0LT, Hamamatsu Photonics, Hamamatsu, Japan), an ASI MS-2500 XY stage and filters optimized for LED illumination were used for the acquisition of fluorescent images of the cartridge. The following filters (all from Semrock) were used: DAPI with excitation 377/50 nm, dichroic 409 nm, emission 409 nm/LP; FITC with excitation 482/18 nm, dichroic 495 nm, emission 520/28 nm; PE with excitation 543/22 nm, dichroic 562 nm, emission 593/40 nm; APC with excitation 635/18 nm, dichroic 652 nm, emission 680/42 nm; and PerCP with excitation 435/40 nm, dichroic 510 nm, emission 676/29 nm. The integration times were the same as used in the CellTracks: for DAPI 30 ms, FITC 100 ms, PE 200 ms, APC 600 ms and for PerCP 400 ms. The scanning and image acquisition was controlled by

a software program written in Labview (National Instruments, Austin TX, USA).

Image analysis with ACCEPT

In CellSearch, CTC are annotated when the objects are stained with DAPI and CK, but lack CD45 staining and are larger than 4 μm with morphological features consistent with that of a cell[10]. In the ACCEPT (Automated CTC Classification, Enumeration and PhenoTyping) toolbox, every event in the images is analyzed using an advanced multi-scale segmentation approach and several intensity and shape measurements are extracted for every event found[20,21]. ACCEPT is developed in the EU funded "CANCER-ID" and "CTC-Trap" programs, as an open source toolbox for CTC analysis and can be downloaded from *https://github.com/LeonieZ/ACCEPT*. New tools and features for ACCEPT are being developed and made available in the downloadable version at regular intervals.

For this study the fluorescent images from all samples were uploaded and all events present in the images were detected. To enhance the detection of cells, especially in areas where the cells formed large cell clusters, we added a background subtraction to the ACCEPT toolbox. Before images are segmented, a Fourier filtering is applied and large and very fine scales are filtered by multiplying the filtered signal with two Gaussian kernels before the signal is back-transformed by an inverse Fourier transformation. In this way the background is removed, which enhances the detection in very crowded areas, as well as areas with inhomogeneous illumination.

Fragmented fluorescent signals make a segmentation with an intensity based segmentation method difficult, which is now implemented in the downloadable version of the ACCEPT toolbox. In this study, this was especially observed in the fluorescent images obtained from the CD16-PerCP stained cells. We therefore decided to explore Deep Learning approaches to determine if this limitation could be overcome. For this approach all thumbnail containing nucleated cells in the cartridge were found using ACCEPT and a random selection of these thumbnails was used for further evaluation. Per sample we exported 10% of the found events, but minimally 1,000 (if the total amount was high enough) and maximally 5,000 thumbnails. Moreover, we exported 759 thumbnails with 5 fluorescent channels each where the segmentation method of ACCEPT gave satisfactory results. We used these thumbnails (split into single channels) to train a Deep Learning network to segment the cells. The implementation was done in Keras and we used the U-net architecture

with skip connections[22,23]. The set of 3,796 thumbnail images was split into a training set of 3,037 images (80%) and a validation set of 759 images (20%). The images were preprocessed in the following way: each thumbnail exported from the ACCEPT toolbox was transformed into a thumbnail of 80x80 pixels by adding a padding at all four sides with the median intensity of the pixels at the image boundary. Moreover, all images scanned with CellTracks were cast from double to uint8 arrays by first dividing by 4,095 (the maximum value in Celltracks) and then multiplying by 255 and converting the results to uint8. Images scanned with the inverted Nikon Ti-E microscope were recorded as uint16, thus having a theoretical maximum value of 65,535. However, during our analysis we noticed that this range was not used and that the range of intensity values used strongly differs between the fluorescent channels. Therefore, we calculated for each fluorescent channel the intensity value that is higher than 99.9% of the measured intensities over all images in all samples. The images were then divided by the resulting intensity per channel, multiplied by 255 and casted to uint8. By taking the value that is above 99.9 % instead of the maximum we accounted for individual saturated pixels, where the incident light caused the camera sensor to respond with the highest possible value. To train the Deep Learning network, we used a batch size of 16 and the network was trained for 10 epochs. The resulting convolutional network was then used to segment the exported thumbnails for each sample. The original thumbnails together with the segmentation derived by Deep Learning was fed back into the ACCEPT algorithm by using the Marker Characterization processor for further analysis and visualization of results.

Statistical analysis

Statistical analysis was performed using SPSS (version 24, SPPS Inc., Chicago IL, USA). A p-value below 0.05 was considered significant. The non-parametric Mann-Whitney U test with significance level $\alpha = 0.05$ was used to determine if there was a difference in nucleated cell numbers between cohorts of patients and controls. The total nucleated cell amounts were log-transformed for normality. With multiple regression analysis we determined the association of several variables with the total nucleated cell count, such as age, treatment, CTC score and sample age before processing. The confounding effect of each variable was determined as well.

Results

Enumeration of nucleated cells in the EpCAM enriched cells

The image analysis program ACCEPT was used to enumerate the total number of nucleated cells in the image files after EpCAM enrichment. Panel A in Figure 1 shows an example of the ACCEPT analysis in which the nucleated cells (blue dots) are identified among the other objects in the images (grey dots). To identify nucleated cells in the cartridge images the following criteria for DNA staining were used: 1. Mean fluorescence intensity ≥50; 2. Standard deviation of the fluorescence intensity ≥20; 3. Size <500 μm^2, and 4. Eccentricity <0.95 (0 is perfect circle). To identify single cells, a perimeter to area (P2A) of <1.5 was used, for doublets a P2A between ≥1.5 and <2.5, for small clusters P2A between ≥2.5 and <4 and for large clusters a P2A ≥4. For enumeration of nucleated cells, the doublets and clusters were counted as one. An example of the single cells, double cells and clusters that were identified in this manner are illustrated in panel B of Figure 1. Figure 2 shows the nucleated cell count from 300 samples from 192 NSCLC patients (range 433-384,015, mean 73,570 ±74,948, median 47,192) and from 359 samples from 162 controls (range 50-33,600, mean 4,191 ±4,463, median 2,729). The number of nucleated cells was significantly larger in the patient samples as compared to the control samples (Mann-Whitney U test: $p<0.001$).

To investigate potential causes for the larger differences in nucleated cell count after EpCAM enrichment, we investigated several factors that could influence the nucleated cell count. First, we evaluated the influence of the assay itself by determining the nucleated cell count from 30 controls from which four blood tubes were obtained and processed subsequently. The nucleated cell count in these samples ranged from 50 to 33,600 (mean 5,541; median 3,237), as illustrated in Figure 3. The CV of the nucleated counts of the 4 samples from the 30 controls ranged from 9.9%-77.6% (mean 25.6% ±14.6%) implying that a variation of 40.2% (mean + 1 standard deviation) of the nucleated cell count cannot be attributed to assay variation with a 97% certainty. Second, the nucleated cell count of 64 NSCLC patients with sample drawn before and after initiation of therapy was determined and these results are also illustrated in Figure 3. In 30 (46%) of the 65 NSCLC patients an increase of more than 10% in nucleated cell count was observed, in 31 (48%) a decrease of more than 10% and in 3 (5%) patients the change in the nucleated cell count was not more than 10% and therefore not considered as a significant change (2 decreases and 1 increase). Third, we examined the

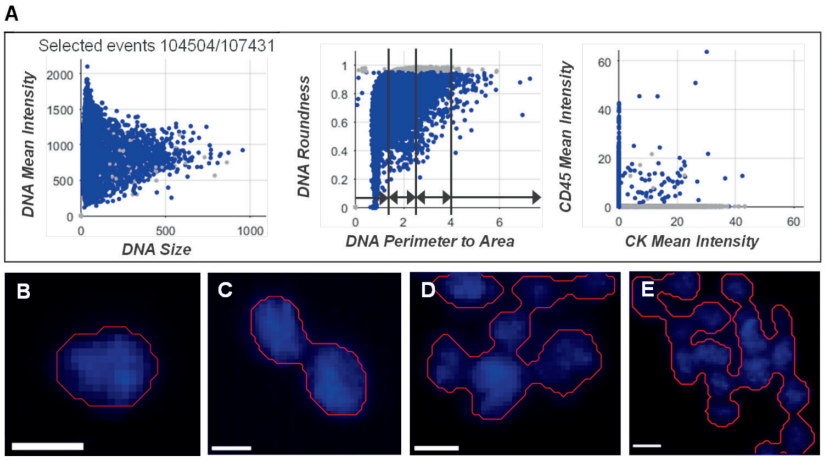

Figure 1. ACCEPT identification of nucleated cells. Panel A shows three scatter plots defining nucleated cells (depicted in blue) by ACCEPT. In total, 104,504 events were detected and 107,431 of them were classified as nucleated cells, whereas the other events are depicted as grey dots. The division into single cells, doublets, small and large clusters was based on DNA Perimeter to Area ratio, as illustrated in the middle scatter plot. In the bottom scatter plot the mean fluorescence intensity of the Cytokeratin-PE (CK Mean Intensity) is plotted against the mean fluorescence intensity of the CD45-APC (CD45 Mean Intensity). Panels B through E illustrate typical examples of the segmentation (red line) around the nucleus of a single cell (B), a doublet (C), a small cluster (D) and a large cluster (E). The white scale bar represents 10 pixels, which corresponds to a size of 6.4 µm.

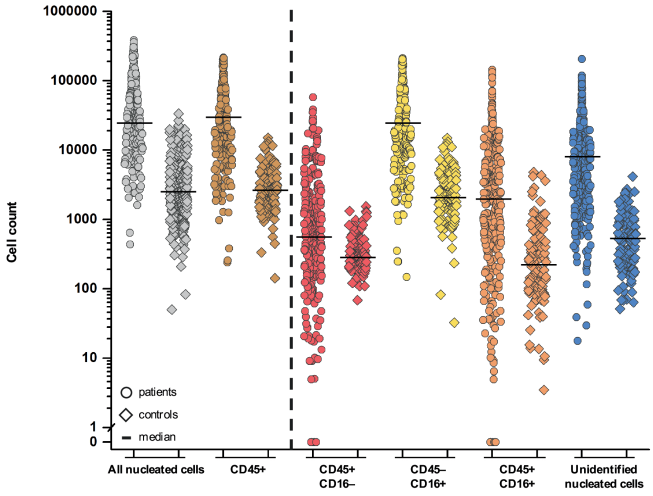

Figure 2. Frequency distribution and median of several cell populations after EpCAM immunomagnetic enrichment of 300 blood samples from 192 NSCLC patients and blood samples from controls. The differences in cell count between the patients and controls in the same cell classification is significant for all ($p<0.001$). Nucleated cells are in grey and all CD45+ leukocytes (CD16 undefined) are in brown. This last population can be split in C45+/CD16– leukocytes (red), CD45–/CD16+ leukocytes (yellow) and CD45+/CD16+ leukocytes (orange). The population of unidentified cells is shown in blue.

influence of sample age before processing it with CellSearch. The nucleated cell count of 149 samples processed at one day ranged from 433-272,010 (mean 55,987, ±56,706), while the nucleated count of 151 samples processed at 2 to 4 days ranged from 2,048-384,015 (mean 90,917 ±85,914). Fourth, the influence of gender was examined. However, no influence of the gender (133 male patients, 127 female patients and 40 patients unknown) on the nucleated cell count was observed (p=0.237).

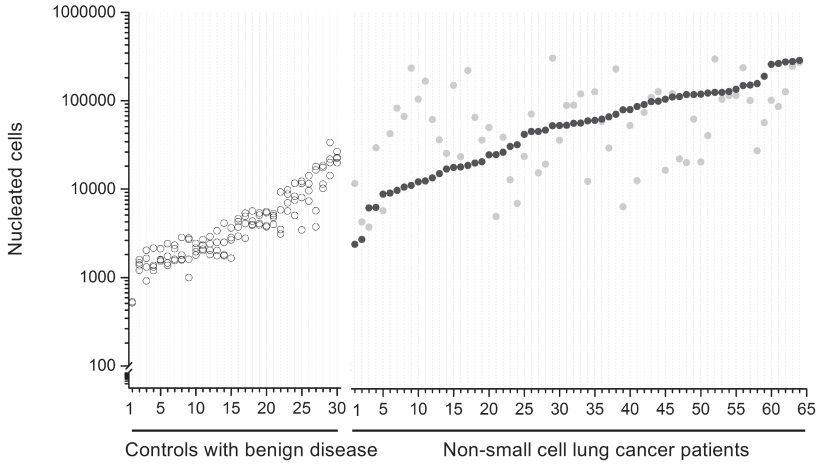

Figure 3. Nucleated cell count in controls with benign disease and NSCLC patients. Counts for four blood samples drawn at the same time in 30 controls with benign disease (A, open circle) and in 64 NSCLC patients with two blood samples (B): one drawn before initiation of therapy (right, dark circle) and one during therapy (light circle).

Table1. Multiple regression analysis for association between sample type and nucleated events corrected for several patient variables.

	Regression coefficient	95% Confidence Interval	P-value
Crude analysis	17.030	14.111 – 20.553	<0.001
Corrected analysis for age	19.202	15.256 – 24.192	<0.001
Corrected analysis for age, and patient variables (sample age, CTC count and treatment)	12.404	9.359 – 16.428	<0.001

For a complete analysis, a multiple regression analysis was used to determine the association between the number of nucleated cells and the sample type (patients vs. controls), with inclusion of the previous mentioned factors, except for gender, since this was only available for most of the NSCLC

patients. For this analysis, 300 samples from metastatic NSCLC patients and 359 control samples were used. In the crude analysis, the relation between sample types was established. This was followed by an analysis to correct for age (younger vs. older than 55 years). As a third analysis, we corrected for the patient variables: CTC count (continuous variable), treatment (during treatment vs. before or no treatment) and sample age at the time of processing (1 day vs. 2 to 4 days). The result of this multiple regression analysis is presented in Table 1. Each variable was analyzed for its confounding effect on the number of nucleated events. This showed that age of the patient, treatment and CTC count had little confounding effect (below 5%). The sample age showed a confounding effect of 11.7%.

High nucleated cell counts and poor cell distribution

The number of nucleated events present in some cartridges can be enormous (over 100,000 for 27% of the patients), covering the whole detection surface, while some cartridges barely hold any cells (less than 5,000 for 6% of the patients). The high number of cells creates a large area of packed cells, which increases the difficulty to define borders for each cell, either manually or by image analysis algorithms. In very full regions the signal is frequently either very bright or fragmented. In both cases it is difficult to find the correct contours surrounding single cells, also when this is performed manually. In Figure 4 the images of nuclear staining of three cartridges are presented: one with approximately 1,000 cells (panel A), one with approximately 10,000 cells (panel B) and one with over 100,000 cells (panel C). While single cells can easily be detected in panels A and B, the example in panel C demonstrates the effect that a high cell density makes the separation of cell boundaries nearly impossible. It is also visible that the cells are not uniformly distributed over the cartridge but there are areas were only very few events are visible (dark areas on the left and right site of the cartridge) and other areas where the cells are very densely packed (bright area in the center and enlarged in panel E). Apart from the cell count, the segmentation quality in the ACCEPT toolbox is highly influenced by the signal quality. In several samples we noticed an illumination bias as illustrated by panel D, an enlargement of a section from panel C. In panel D the background intensity, averaged over a small square of 5 by 5 pixels, is 2.3 times brighter on the right side of the image compared to the left one. In relation to the overall intensity range of 4095 intensity values, this is an increase of 18%. The segmentation model used assumes a nearly homogeneous background, but this assumption fails in case of an illumination

bias and leads to segmentation errors. These errors can either be cells that are missed in the dark half of the image or noise that is segmented in the bright half of the image. Another difficulty is the segmentation of very fragmented signals, especially in combination with very packed areas as shown in panel F. We do see a fluorescent signal, but it is impossible to distinguish single cells, apart from a few locations with a homogenous bright staining. This motivated the use of a segmentation approach based on Deep Learning.

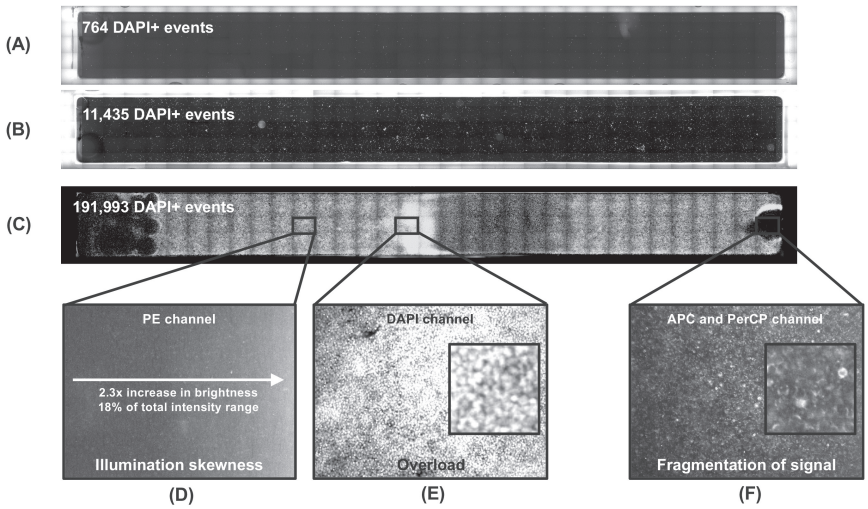

Figure 4. In total, 175 images of DAPI staining covers the surface of CellSearch cartridges for each sample. Panel A shows a cartridge containing less than 1,000 DAPI+ events, Panel B a cartridge containing around 10,000 DAPI+ events and Panel C a cartridge containing much more than 100,000 DAPI+ events. Three of the 175 images of the very full cartridge are shown at a higher magnification to illustrate the three main difficulties for an image analysis program to identify objects. Panel D shows the illumination skewness of the PE channel corresponding to the DAPI image shown in Panel C. Panel E shows an overload of signal because the cartridge is too full with cells. Panel F shows the fragmentation of signal, which makes it for the software hard to accurately segment a cell and extract correct parameters. The segmentation results in case of overload (E) or fragmentation of signal (F) can be improved with a Deep Learning segmentation approach.

As opposed to model-based approaches as currently implemented in the ACCEPT toolbox, Deep Learning approaches do not make any model assumptions about the signal (e.g. a nearly homogenous background and cell intensity), but learn a model just based on the data used for the training. A drawback of Deep Learning approaches in biomedical applications is often the lack of sufficient ground-truth data, but we could export ground-truth data from the ACCEPT toolbox by exporting thumbnails with cells where

the segmentation was successful. Thereby we could train the algorithm to segment also very fragmented signals. Another advantage is that the algorithm also learns that we are looking for a "cell-like" morphology and therefore it tends to autocomplete the segmentation for only partially stained cells. In that way the algorithm mimics what the human visual system is doing. By using this segmentation as a basis for the feature extraction we derived more reliable features for each cell, which facilitated the definition of gates to identify different cell populations.

Assignment of nucleated cells to a cell lineage

In the CellSearch system CD45-APC is used to identify leukocytes and Cytokeratin-PE to identify CTC among the nucleated cells. Nucleated cells expressing both CD45-APC and Cytokeratin-PE are assigned as cells binding non-specifically to at least one of the antibodies. The number of CTC identified by the classical CellSearch method in the 300 samples of 192 NSCLC patients ranged from 0-186 (mean 2, median 0) and represent only a very small portion of the nucleated cells identified in the samples from these patients. To determine whether the identity of the majority of nucleated cells could be assigned to the hematopoietic cell lineage by their expression of CD45, the thumbnails of the nucleated cells were put into a trained Deep Learning network for segmentation and the segmented images were fed back into the ACCEPT toolbox. Using the Marker Characterization processor tool, the results could be visualized and analyzed. The improved segmentation allowed for a relatively simple definition of cell subpopulations and in most cases a simple yes or no could be used to define the presence or absence of a marker. The actual definitions of the different cell populations are listed in Table 2. In this manner nucleated cells were classified as CD45+, CD45– & CK– or CK+ in 300 samples from NSCLC patients and 127 control samples.

As described in the method section, for this analysis 10% of the nucleated cells – found by the ACCEPT toolbox – up to a maximum number of 5000 were analyzed and the results were extrapolated to the full amount of nucleated events to arrive at the cell numbers. The amount of nucleated cells that could be identified as leukocytes in CellSearch was only 18% ±21 (range 0-89%, median 9%) in patients and 23% ±15 (range 2-68%, median 19%) in controls (Figure 5). To be able to assign the cell lineage of origin of the nucleated cells on which no CD45– or CK-expression could be detected, several approaches were pursued.

Table 2. The definition of cell populations used to classify cells in ACCEPT after Deep learning segmentation in 300 NSCLC patient samples and 127 control samples.

		Mean Intensity value					Overlay nucleus			Size (µm²)
		DAPI	CD45	CK	CD16*	wga*	with CK	with CD45	with CD16	CK
CTC	CK+/CD45–	>0	0	≥50	0	>0	>0.4	ND	ND	>9
Leukocytes	CD45+/CD16–	>0	>0	0	0	>0	ND	>0	ND	ND
	CD45+/CD16+	>0	>0	0	>0	>0	ND	>0	>0	ND
	CD45–/CD16+	>0	0	0	>0	>0	ND	ND	>0	ND
Nucleus	Bare nucleus	>0	0	0	0	0	ND	ND	ND	ND
	Unstained cell	>0	0	0	0	>0	ND	ND	ND	ND

*only for those experiments in which CD16 or wga was added to the immunostaining cocktail

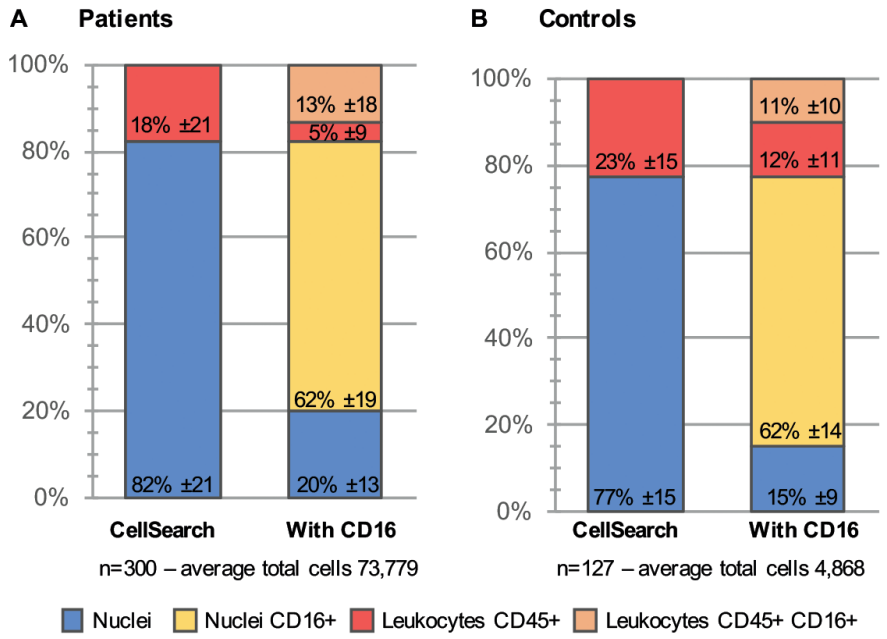

Figure 5. Cell population distribution in patients (A) and controls (B) using the CellSearch definition (left bar) and using CD16 expression (right bar) for further classification of the cells.

Increasing leukocyte identification by adding CD16 immunostaining

Whereas CD45 is basically present on all human leukocytes, it is strongest expressed on lymphocytes and monocytes, but at a relatively low density expressed in granulocytes. CD16 identifies the FcgIII receptor present on granulocytes and Natural Killers cells. We added anti-CD16 labeled to PerCP to the CellSearch staining cocktail to improve the identification of especially granulocytes, using 300 blood samples of 192 NSCLC patients and 127 blood samples of 20 healthy controls. Thumbnail images of the nucleated cells identified by ACCEPT were fed into the trained Deep Learning network as described above. Figure 6 shows typical thumbnail images of nucleated events identified by ACCEPT using the presence of the different markers for classification. Classified CTC with expression of CD45 or CD16 can either be CTC nonspecifically binding to CD16 or CD45 antibodies, or leukocytes non-specifically binding to the cytokeratin antibodies. The distribution of these cell populations in the patient and control samples is shown in Figure 5. From the 82% (±21) unidentified nucleated cells in 192 NSCLC patients, 62% (±19) are identified as granulocytes through CD16-expression. This decreases the number of unidentified cells to 20% (±13) of the total nucleated cells present in the cartridge. The percentage of CD45-expressing leukocytes that express CD16 as well is 13% (±18). These are most likely Natural Killer cells that express CD45 in higher density as compared to granulocytes. In 20 healthy controls, 77% (±15) of the cells are unidentified which was decreased to 15% (±9) when CD16 was used. The actual number of nucleated cells identified by either CD45 or CD16 for patients and controls is shown in Figure 2. The number of all classifications of nucleated cells was significantly larger in patients as compared to controls ($p<0.001$). Figure 2 and 5 show there is still a large number of nucleated cells, especially in the patients, that remain unidentified.

LED as light source to improve excitation efficiency of CD45-APC and CD16-PerCP

For five NSCLC patients and five healthy donors, cartridges were scanned first with the CellTracks – equipped with a mercury arc lamp as a light source – followed by scanning on a microscope equipped with a LED light source. The objectives and filter cubes were kept the same in both systems. The mean percentage of CD45+/CD16– leukocytes found by the CellTracks

was 8% (±7) and this increased to 16% (±9) when a LED light source was used (Figure 7, panel A). More pronounced was the increase for CD45+/CD16+ leukocytes, which increased from 1% (±0) to 59% (±25) with the LED light source. Whereas the population of CD16+/CD45– cells comprise a large population of the cells when a mercury arc lamp is used, these cells appear to be CD45+ as well when the LED light source was used for analysis; CD16+/CD45– leukocytes decreased from 58% (±17) to 19% (±15). In total, the number of unidentified cells was reduced from 33% (±14) to 6% (±5) when a LED light source was used instead of a mercury arc lamp.

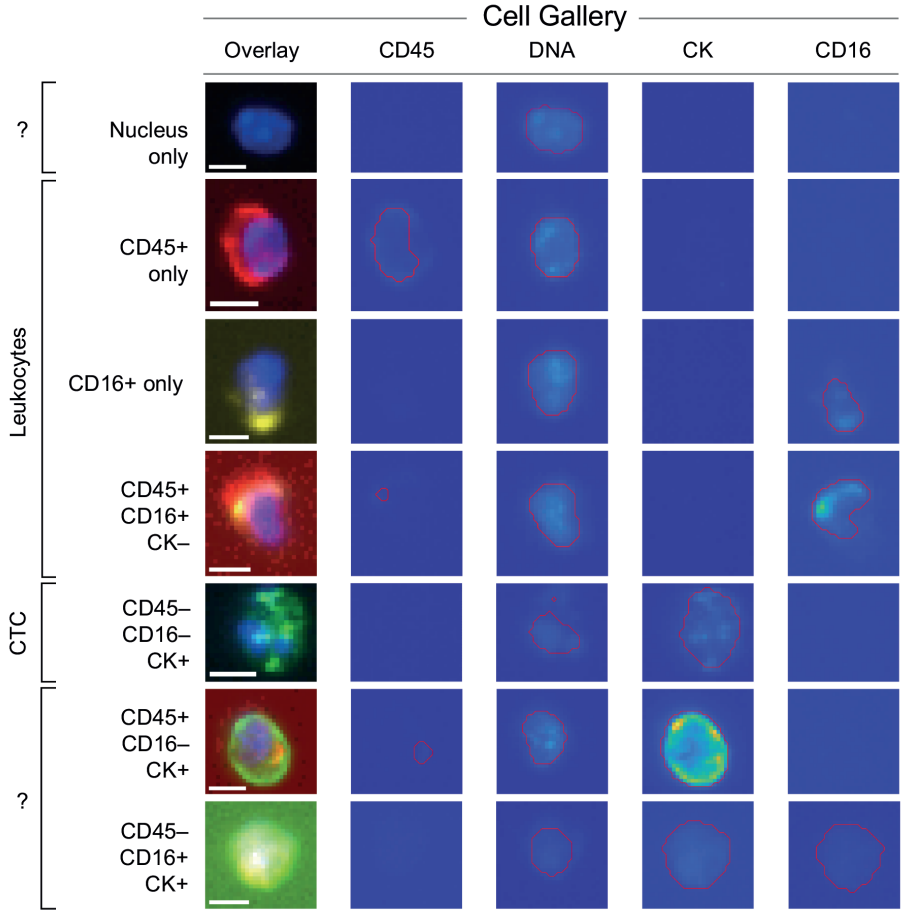

Figure 6. ACCEPT gallery showing cells from all classifications using the presence or absence of several markers. The scale bar is 10 pixels, representing 6.4 mm.

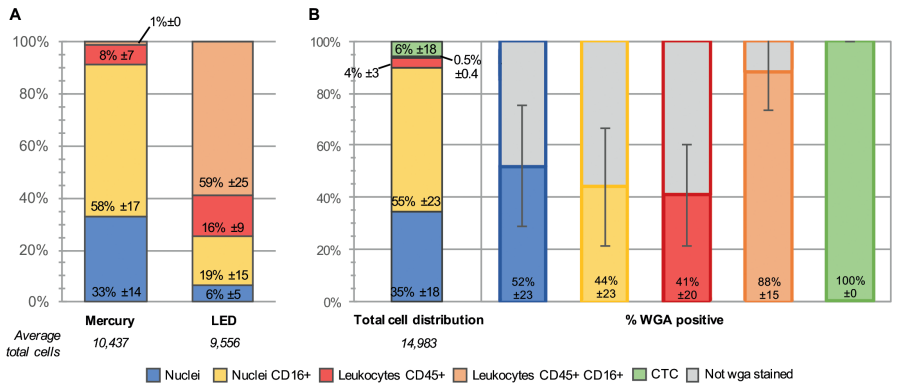

Figure 7. Improved identification of cells. Comparison of cell population distributions analyzed with the mercury arc light source in CellSearch, followed by analysis with a LED light source on a separate microscope (A). Distribution of cell populations in samples with wheat germ agglutinin (wga)-AlexaFluor488 staining (B). The stacked bar represents the five cell populations present in these cartridges. One healthy control sample was spiked with MCF-7 cancer cells, which are represented in the "CTC" category (6%). Of each population, the percentage of cells that stained positive for wga is displayed in the right side of the image, whereas the population remaining unstained with wga is visualized in grey.

Identification of unstained nuclei by adding wheat germ agglutinin immunostaining

In samples from 5 NSCLC patients and 5 healthy controls, the lectin wga conjugated to Alexa-Fluor488 was added to the CellSearch staining cocktail for the identification of cellular plasma membranes. In Figure 8 an ACCEPT gallery shows the staining of wga present on all cell classifications. The absence of wga on a nucleus, classifies this event as a "bare nucleus". The presence of wga on already identified cells was 41% (±20) for CD45+ leukocytes, 44% (±23) for CD16+ granulocytes and 52% (±23) for the unidentified cell population (Figure 7, Panel B). One healthy donor sample was spiked with MCF-7 cells and 100% of these spiked CTC were stained with wga. By adding CD16 for improved identification of leukocytes, there still are 48% (±23) of the nuclei in these samples that remain unidentified. In the entire population, on average 17% nuclei appear to be without a cell membrane, suggesting they are simply bare nuclei, which cannot be identified through immunofluorescence staining.

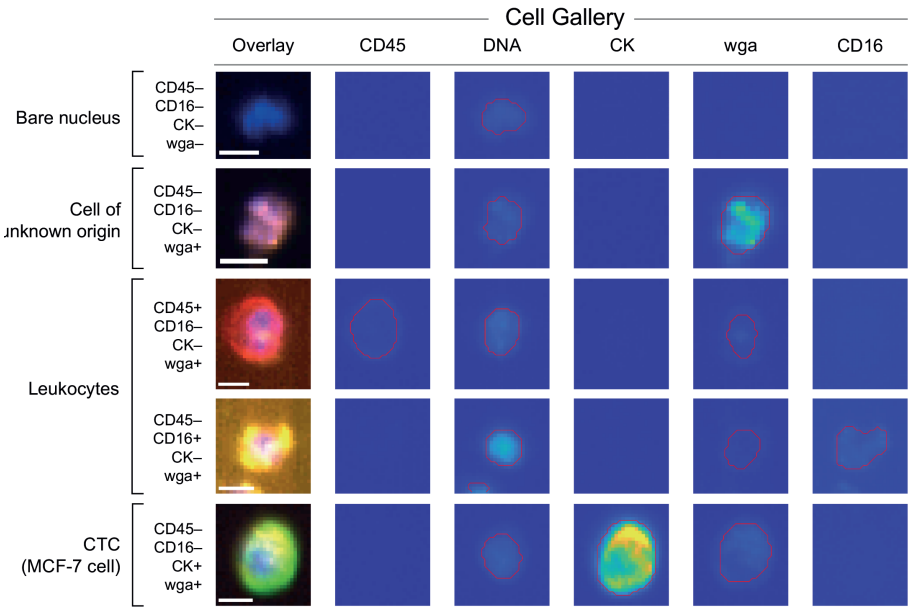

Figure 8. ACCEPT gallery of cells stained with the membrane lectin wheat germ agglutinin (wga). The cell with wga-staining, but without the presence of any other markers remains without determined origin, whereas the nucleus without wga-staining appears to be a bare nucleus. The scale bar is 10 pixels, representing 6.4 mm.

Discussion

In this study, we investigated the cell populations present in 659 cartridges after immunomagnetic EpCAM enrichment by the CellSearch system, gathered from 162 controls and 192 NSCLC patients. Stored fluorescent microscope images of the surface of the cartridges were analyzed by image analysis for the presence of different cell populations. Most of the image analysis tools that were used, are already assembled in the open source imaging program ACCEPT[20,21]. Through analysis of large sets of image data, such as described here, new challenges arise. First, we will address these challenges and how we overcame these and then we will discuss our finding of the analysis of the large image data set.

In this image data set we had to deal with samples of low image quality, unequal distribution of the illumination and extremely crowded images containing many clustered events. Addition of a Fourier filtering as a pre-processing step before segmentation, clearly improved the ability to identify

individual objects in the images, even in case of very packed areas. The analysis of CD16-PerCP images, the antibody that was added to improve the identification of leukocytes, created a new challenge. The fragmented CD16 signals on the surface of the cells could not be segmented well enough and alternatives to Fourier filtering were therefore explored. Experiments with a Deep Learning based approach appeared to be a good solution since it could easily be adapted to a certain type of signal to segment by feeding it with enough training data. The Deep Learning based segmentation algorithm was programmed in Python® using the Keras[22] framework and is not yet linked to the ACCEPT toolbox, which is developed in MATLAB®. To be able to use the Deep Learning based segmentation, we exported thumbnails identified by ACCEPT after Fourier filtering and used them as input for the Deep Learning segmentation network. After segmentation of the thumbnails by the network, the segmentation results, together with the original thumbnails, were fed back into the ACCEPT toolbox for further analysis. For samples with thousands of nucleated events (up to 300,000 with 5 fluorescent channels each), saving all images twice is a huge computational task. Therefore, for the current analysis we restricted that part of our analysis to only 10% of the nucleated events which were randomly selected. Experience obtained with the Deep Learning based classification algorithm we developed[24], showed very promising results and the new segmentation method also showed that it is often superior to the more traditional segmentation approach currently used in ACCEPT. Thus, in the future, we would like to incorporate a semantic Deep Learning segmentation into the ACCEPT toolbox to automatically detect and classify CTC, tumor derived extra cellular vesicles, leukocytes and other cell populations for which reagents are added.

The analysis of the images by ACCEPT provided not only insight in the composition of the EpCAM enriched cells, but also provided means to assess the quality of the sample such as an overload of nucleated cells, an uneven distribution of the cell suspension or uneven illumination of the cartridge. In a future release of ACCEPT we plan to incorporate quality control warnings to alert the user that the quality of the sample is not sufficient to obtain reliable results. Samples can be discarded from further analysis or, in case of too many cells, diluted and reanalyzed or rescanned after adjustment of the microscope.

In total, 300 samples from 192 metastatic lung cancer patients, 232 samples from 142 patients with benign tumors and 127 samples from 20 healthy donors were investigated for the presence of nucleated events. The number of nucleated events was significantly higher in cancer patients (mean 73,568

±74,949) as compared to the controls (mean 4,191 ±4,463; $p<0.001$). In only 37% of the patient samples CTC were detected by traditional CellSearch scoring and in these samples, the CTC number ranged from 1-186 (mean 3 ± 13, median 0) and this amount surely could not account for the large differences in nucleated events detected. The nucleated cell count in patients with and without CTC detected was not significantly different and showed very little confounding effect (Table 1). The nucleated cell count increased with sample age, but could not account for the difference in the nucleated cell count between patients and controls. Knowledge of the composition of these nucleated cells is needed to be able to hypothesize about this difference. Most likely, these nucleated events originate from hematopoietic cells that are captured along with the EpCAM enrichment in CellSearch. The fraction of nucleated cells on which the leukocyte marker CD45 was detected, was however remarkably low both in healthy donors (mean 23% ±15) and metastatic cancer patients (mean 18% ±21) (Figure 5). Since the excitation of CD45-APC with a mercury arc lamp used in the CellTracks system is not optimal, we first looked into a way to increase the detection of especially granulocytes that express the CD45 antigen in relatively low antigen density compared to leukocytes.

We evaluated this by adding anti-CD16-PerCP antibody to the immunostaining in the CellSearch system. All 300 samples from metastatic lung cancer patients and 127 samples from healthy donors were processed with this extra marker. The leukocytes and granulocytes that were identified indeed increased from to 80% in patients and 85% in the controls (Figure 5). However, still a considerable number of nucleated cells remained unidentified: 20% ±13 and 15% ±9, respectively. Next, we looked into the role of ferrofluids, which are used at a concentration of 40 µg/mL in CellSearch and are present on the imaging surface of the cartridge[25,26]. The ferrofluids reduce the fluorescence intensity, and effect which is most obvious in the blue region (400-460 nm). Therefore, we looked into an improvement of the excitation of the fluorophores. For this, a microscope equipped with a LED light source to improve the APC fluorophore excitation was tested on samples from five patients and five controls[12]. This resulted in a clear improvement of the number of unidentified nucleated cells, reducing this from 33% to 6% (Figure 7A). Also, to determine whether these remaining nuclei were enclosed by a cellular plasma membrane, we added wheat germ agglutinin conjugated to Alexa-Fluor488 to the CellSearch cocktail in five patients and five controls[13,14]. This showed that 52% of the unidentified nucleated cells did not stain with wga, suggesting they are "bare"-like nuclei (Figure 7B). Whether or not these bare

nuclei were actually present in the blood, or if they represent cells that have been damaged through the immunomagnetic selection or staining process, remains an outstanding question. However, a large fraction of leukocytes identified with the current immunostaining are not stained with wga as well. This could suggest that the wga-staining assay is not sufficiently sensitive to stain all membranes or that the imaging method is not sufficiently sensitive to detect dim wga fluorescence. High concentration of wga added to the CellSearch cocktail caused aggregation of blood cells and therefore a lower concentration was chosen for this assay. It might however be possible that a higher concentration of wga is necessary to locate all membranes present in the blood sample. Also, all samples were analyzed on the CellTracks, but improved identification will be observed when the LED light source is used. Another option is that the leukocyte membranes are damaged to a point that the agglutinin cannot bind to the residues on the membrane anymore. This might be caused during the 15 minute permeabilization process to open the membranes. The CellSearch permeabilization agent is saponin, a detergent which interacts with membrane cholesterols by selectively removing them to form pores, which enables antibodies to enter[27]. Notable is, that the fraction of the spiked MCF-7 cancer cells that were stained with wga, was a full 100%. Compared to cancer cell line cells, possibly the leukocytes are more fragile and susceptible to damage caused during permeabilization.

The wga+/DNA+/CD45–/CD16–/CK– cells are potentially CTC not expressing the cytokeratins. However, our observation that a similar population was detected in blood of healthy donors makes this explanation less likely. Confirmation whether or not CTC are among the unidentified nucleated cells likely will have to come from DNA or RNA assays. Removing the cells from the cartridge might allow them to be selected based on their absence of fluorescence markers and subsequently sorted with fluorescence-activated cell sorting (FACS). Quantitative PCR after DNA isolation and amplification could reveal the presence of mutations, indicating one of the cells is in fact a tumor cell. Digital-droplet PCR has a higher sensitivity and could be applied on the whole cell suspension from a cartridge, although the multiplex analysis of mutations is less feasible in this assay. With these approaches, the number of tumor cells will have to be compared to the number of CTC scored on the CellTracks (if present at all) to determine if more or equal tumor cells are present in the cell suspension. Also, analysis of mRNA after FACS isolation might be feasible for the unidentified cells with a cellular membrane present. Quantification of a selection of proteins can indicate if the cells are of hematopoietic of epithelial lineage. However, the

permeabilization of cells in the CellSearch might complicate this approach and therefore, the CellSearch Epithelial Cell Profile Kit should be used. This kit is designed for RNA analysis and enriches EpCAM+ cells without subsequent permeabilization and staining.

Possible identities for the cells that remain unidentified thus far might be: 1. Hematopoietic cells not identified through damage incurred during the procedure or inaccessible antigens through the ferrofluids[25,26]; 2. Hematopoietic cells without sufficient expression of CD45 and CD16: this suggests they would need additional CD markers for identification or an improved labelling method that amplifies low signals, which might yield increased detection of these very dim stained cells and separate the fluorescent signal of densely packed cells[11,28-30]; 3. CTC with no or low expression of the CK antigens detected by the C11 and A53.B/A2 clones: since these clones only recognize a subset of the CK present in a cell, it might be beneficial to include antibody clones that recognize all CK. Previously, we have shown that adding several CK clones to the CellSearch antibody cocktail improved detection of CTC positive patients with 11%[31]. Also, it might be possible EpCAM+/CK– CTC are present, remaining undetected because of downregulation of epithelial markers through epithelial-to-mesenchymal transition[32–34]. In order to detect these cells, antibodies specific for this process could be added to the CellSearch immunostaining[35–37]; or 4. Cells of other origin: such as circulating stromal, endothelial or stem cells[38]. Detection of these cells would also require the addition of other antibodies to the assay.

In conclusion, we used advanced image analysis to identify the cell populations present after immunomagnetic EpCAM enrichment by the CellSearch system from 659 cartridges and found a significant larger number of nucleated cells from which the origin could not be identified in NSCLC patients compared to controls. A large portion of the unidentified nucleated cells could be identified by adding CD16 to improve the identification of granulocytes, the use of a LED light source and the addition of wga to discriminate between bare nuclei and cells. However, there is still much to gain in the identification of the cells that still remain anonymous. These observations have to be confirmed in patients with other cancers as well. The question remains: what are these cells? Going forward, it is most important to determine if all tumor cells have been located or if some are still missed. Therefore, further studies are needed to determine if EpCAM+/CK– CTC are present among the nucleated cells of which the origin is not known.

References

1. Racila, E. et al. Detection and characterization of carcinoma cells in the blood. Proc. Natl. Acad. Sci. U. S. A. 95, 4589–94 (1998).
2. Cohen, S. J. et al. Relationship of Circulating Tumor Cells to Tumor Response, Progression-Free Survival, and Overall Survival in Patients With Metastatic Colorectal Cancer. J. Clin. Oncol. 26, 3213–3221 (2008).
3. Cristofanilli, M., Budd, G., Ellis, M. & A. Circulating tumor cells, disease progression, and survival in metastatic breast cancer. Engl. J. 351, 781–791 (2004).
4. de Bono, J. S. et al. Circulating Tumor Cells Predict Survival Benefit from Treatment in Metastatic Castration-Resistant Prostate Cancer. Clin. Cancer Res. 14, 6302–6309 (2008).
5. Hiltermann, T. J. N. et al. Circulating tumor cells in small-cell lung cancer: a predictive and prognostic factor. Ann. Oncol. 23, 2937–42 (2012).
6. Krebs, M. G. et al. Evaluation and Prognostic Significance of Circulating Tumor Cells in Patients With Non–Small-Cell Lung Cancer. J. Clin. Oncol. 29, 1556–1563 (2011).
7. Hiraiwa, K. et al. Clinical significance of circulating tumor cells in blood from patients with gastrointestinal cancers. Ann. Surg. Oncol. 15, 3092–100 (2008).
8. Rao, C. et al. Circulating melanoma cells and survival in metastatic melanoma. Int. J. Oncol. 38, 755–60 (2011).
9. Gazzaniga, P. et al. Prognostic value of circulating tumor cells in nonmuscle invasive bladder cancer: a CellSearch analysis. Ann. Oncol. 23, 2352–6 (2012).
10. Allard, W. J. et al. Tumor cells circulate in the peripheral blood of all major carcinomas but not in healthy subjects or patients with nonmalignant diseases. Clin. cancer Res. 10, 6897–904 (2004).
11. van Dalum, G. The role and definition of cancer cells in blood - The identity of nucleated cells enriched by CellSearch. (University of Twente, 2015). doi:10.3990/1.9789036538312
12. Lumencore, I. SOLA Light Engine. (2017). Available at: http://lumencor.com.
13. Chazotte, B. Labeling Membrane Glycoproteins or Glycolipids with Fluorescent Wheat Germ Agglutinin. Cold Spring Harb. Protoc. 2011, pdb.prot5623-prot5623 (2011).
14. Legant, W. R. et al. High-density three-dimensional localization microscopy across large volumes. Nat. Methods 13, 359–365 (2016).
15. Solórzano, C. et al. Isolation and characterization of the potential receptor for wheat germ agglutinin from human neutrophils. Glycoconj. J. 23, 591–598 (2006).
16. Sharon, N. & Lis, H. Lectins. (2007). doi:https://doi.org/10.1007/978-1-4020-6953-6
17. Emde, B., Heinen, A., Gödecke, A. & Bottermann, K. Wheat germ agglutinin staining as a suitable method for detection and quantification of fibrosis in cardiac tissue after myocardial infarction. Eur. J. Histochem. 58, 2448 (2014).
18. Adair, W. L. & Kornfeld, S. Isolation of the receptors for wheat germ agglutinin and the Ricinus communis lectins from human erythrocytes using affinity chromatography. J. Biol. Chem. 249, 4696–4704 (1974).
19. van Dalum, G. et al. Importance of circulating tumor cells in newly diagnosed colorectal cancer. Int. J. Oncol. 46, 1361–8 (2015).
20. Zeune, L. L., van Dalum, G., Terstappen, L. W. M. M., van Gils, S. A. & Brune, C. Multiscale Segmentation via Bregman Distances and Nonlinear Spectral Analysis. SIAM J. Imaging Sci. 10, 111–146 (2017).
21. Zeune, L. L. et al. Quantifying HER-2 expression on circulating tumor cells by ACCEPT. PLoS One 12, e0186562 (2017).

22. Chollet, F. et al. Keras. (2015).

23. Ronneberger, O., Fischer, P. & Brox, T. U-Net: Convolutional Networks for Biomedical Image Segmentation. in 234–241 (Springer, Cham, 2015). doi:10.1007/978-3-319-24574-4_28

24. Zeune L.L. et al. Deep Learning to identify circulating tumor cells by AACEPT. In: International Symposium on Minimal Residual Cancer. ; 2018.

25. Scholtens, T. M. Automated clissification and enhanced characterization of circulating tumor cells by image cytometry - Quantitative and qualitative effect of free ferrofluid on cell analysis. (University of Twente, 2012). doi:10.3990/1.9789036534215

26. Coumans, F. & Terstappen, L. Detection and Characterization of Circulating Tumor Cells by the CellSearch Approach. Methods Mol. Biol. 1347, 263–78 (2015).

27. Jamur, M. C. & Oliver, C. Permeabilization of Cell Membranes. in Methods in molecular biology (Clifton, N.J.) 588, 63–66 (2010).

28. Faget, L. & Hnasko, T. S. Tyramide Signal Amplification for Immunofluorescent Enhancement. in Methods in molecular biology (Clifton, N.J.) 1318, 161–172 (2015).

29. Zhou, S., Yuan, L., Hua, X., Xu, L. & Liu, S. Signal amplification strategies for DNA and protein detection based on polymeric nanocomposites and polymerization: A review. Anal. Chim. Acta 877, 19–32 (2015).

30. Gustafsdottir, S. M. et al. Proximity ligation assays for sensitive and specific protein analyses. Anal. Biochem. 345, 2–9 (2005).

31. de Wit, S. et al. The detection of EpCAM+ and EpCAM– circulating tumor cells. Sci. Rep. 5, 12270 (2015).

32. Serrano, M. J. et al. EMT and EGFR in CTCs cytokeratin negative non-metastatic breast cancer. Oncotarget 5, 7486–7497 (2014).

33. Willipinski-Stapelfeldt, B. et al. Changes in cytoskeletal protein composition indicative of an epithelial-mesenchymal transition in human micrometastatic and primary breast carcinoma cells. Clin. Cancer Res. 11, 8006–14 (2005).

34. Krebs, M. G. et al. Analysis of circulating tumor cells in patients with non-small cell lung cancer using epithelial marker-dependent and -independent approaches. J. Thorac. Oncol. 7, 306–15 (2012).

35. Kallergi, G. et al. Epithelial to mesenchymal transition markers expressed in circulating tumour cells of early and metastatic breast cancer patients. Breast Cancer Res. 13, R59 (2011).

36. Armstrong, A. J. et al. Circulating Tumor Cells from Patients with Advanced Prostate and Breast Cancer Display Both Epithelial and Mesenchymal Markers. Mol. Cancer Res. 9, 997–1007 (2011).

37. Wu, S. et al. Classification of Circulating Tumor Cells by Epithelial-Mesenchymal Transition Markers. PLoS One 10, e0123976 (2015).

38. Chen, Y. et al. Rare cell isolation and analysis in microfluidics. Lab Chip 14, 626–45 (2014).


7

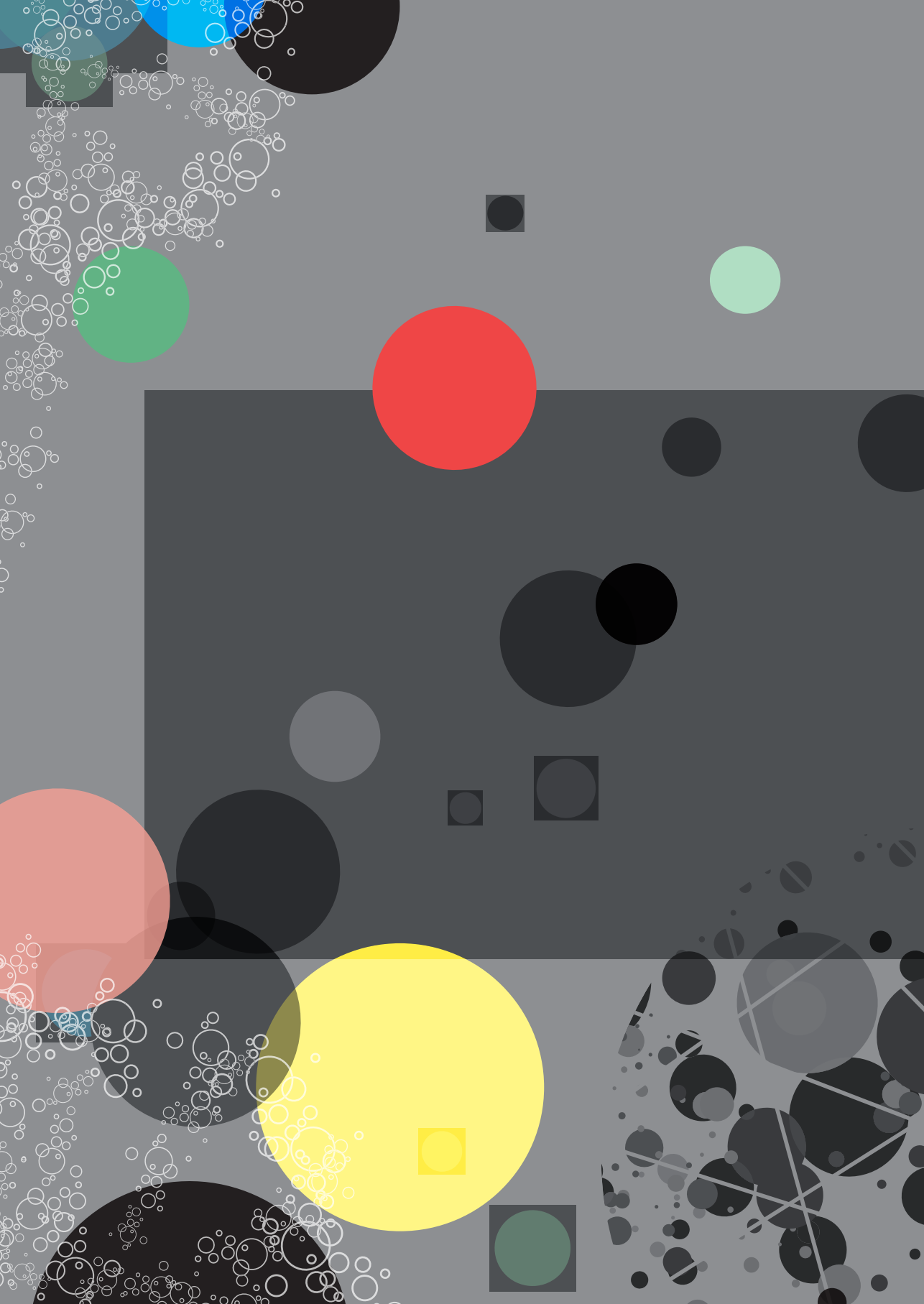

Chapter 8

Developing protocols in CTC-Trap

CTC-Trap aims to isolate and characterize all tumor cells circulating in blood to enable a real-time liquid biopsy for all cancer patients with metastatic disease regardless whether or not the disseminated disease has been clinically detected. The CTC-Trap consortium consists of 11 academic institutions or small businesses. To conduct the studies at different institutions, unified protocols and analysis methods are required. Detecting circulating tumor cells (CTC) require the fluorescently labeling of cells after filtration, followed by microscopic analysis of the microsieves. All these protocols have been developed into standard operating procedures (see Appendix of this thesis). During the development of these protocols, the performance of antibodies and microscope systems were tested and compared in order to determine which antibody-cocktail would perform best and if each clinical site would be able to deliver comparable images for unified analysis. In Part I of this chapter, the comparison of antibodies used for the immunophenotypic labeling of CTC and leukocytes is described. This research was performed over the years during the project and reported in several reviews for the EU. The most important results are presented here. This is followed by Part II, where the microscopy scanning system of each clinical site is discussed in order to determine if these systems are comparable and can be used in the CTC-Trap protocols.

Part I: Antibodies

Introduction

In CTC-Trap, detection of CTC will be achieved by fluorescent labeling of the cells with antibodies. This immunophenotyping was developed throughout the first years of the program, in which the antibodies produced by AcZon were tested and their performance compared with other available fluorescently labeled antibodies.

AcZon is a small-medium enterprise located in Italy, which specializes in biotechnology to develop, produce and commercialize silica NanoParticles conjugated to antibodies for diagnostic, clinical and research purposes. Silica NanoParticles are spherical, water-soluble and between 10 and 100 nm in size. Each NanoParticle consists of two compartments: a shell that surrounds and protects the core, which can be doped with fluorescent molecules. This core can be filled with a high concentration of molecules which are protected from any external contact with the surrounding environment, thereby aiming to create a stronger and more stable signal (see Figure 1).

The NanoParticles will be compared with commercially available antibodies and tested for their optimal performance in signal strength, a-specific staining and population separation. The type of antibodies are focused on white blood cell exclusion with anti-CD45 and epithelial cell inclusion with cytokeratin (CK), conjugated to fluorescent labels fluorescein isothiocyanate (FITC), phycoerythrin (PE) or peridinin-chlorophyll-protein complex (PerCP).

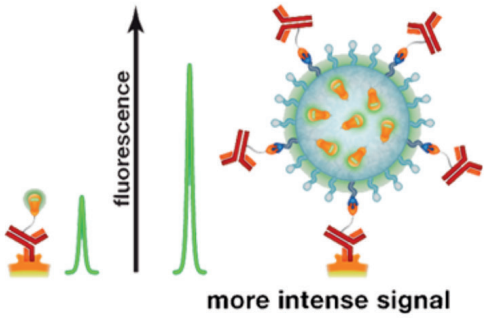

Figure 1. Comparison between an antibody conjugated with a traditional fluorophore (left) and with a silica NanoParticle, which is doped with fluorescent molecules, functionalized externally and conjugated with antibodies (right)[1].

Methods

Antibodies tested in the CTC-Trap

Table 1 provides an overview of the antibodies that were tested in the CTC-Trap and discussed in this report. Each AcZon antibody was compared to a commercial available antibody of the same clone, conjugated with either NanoParticles or traditional fluorophores, respectively.

Fluorescent immunostaining of cells in solution

EDTA blood was run with the haematology analyzer for a specific count of white blood cells (WBC). Approximately 0.5×10^6 WBC were used per test, measured on the same day as the blood draw. Also, 0.5×10^6 cells of the non-small lung cancer cell line NCI-H1650, fixed for 24 hours in CellSave, were used per test. Whole blood was stained with antibodies at 37°C for 30 minutes, followed by red blood cell lysis and fixation with 1x BD FACS Lysing Solution (cat.no. 349202) at RT until measurement. NCI-H1650 cells were

stained for 30 min at 37°C with antibodies, after 15 minutes permeabilization with 0.15% saponin in PBS/BSA1%. Next, these cells were fixed with 1% formaldehyde and resuspended in PBS/BSA1% until measurement.

Table 1. Antibodies and concentrations that were tested in the CTC-Trap. *recommend concentration by manufacturer.

Antibody	Conjugate	Manufacturer	Clone	Reference # Lot #	Concentrations tested (µg/mL)
CD45	FITC	AcZon	GA90	130131H-2746	1, 2.5, 5*
CD45	NP_{520}	AcZon	GA90	13014NH-2747	1, 2.5, 5*
CD45	PerCP	Life Technologies	HI30	MHCD4531 1433681C	1, 2, 5*, 10
CD45	NP_{678}	AcZon	HI30	HI30-13F000T 15019BS-3915	1, 2, 5*, 10
CD45	NP_{678}	AcZon	GA90	CD45 13F000T 15025BS-3960	1, 2, 5*, 10
C11	PE	Not commercialized	C11	-	1*, 2, 5, 10
C11	NP_{575}	AcZon	C11	PANCK02F000T 15017BS-3913	0.9, 2.3, 4.6*, 9.3
AE-pan	eFluor570	eBioscience	AE1/AE3	41-9003-80 E16301-104	1*, 2, 5, 10
AE-pan	NP_{575}	AcZon	AE1/AE3	AE1-302F00T 15018BS-3914	1, 2, 5*, 10

Fluorescent immunostaining of cells on a microsieve

After filtration, the microsieve was removed and washed once with a permeabilization buffer containing PBS, 1% bovine serum albumin (Sigma-Aldrich, St. Louis MO, USA) and 0.15% saponin (Sigma-Aldrich). Next, this buffer was placed on the sieve and removed after 15 minutes incubation at room temperature. A cocktail of fluorescently labeled antibodies was used to stain the cells on the sieve for 15 minutes at 37°C using a cell culture incubator. The staining solution consisted of the following monoclonal antibodies: one cocktail of three CK antibody clones targeting CK 4, 5, 6, 8, 10, 13, 18 (clone C11), CK 1-8 (clone AE3) and CK 10, 14, 15, 16 and 19 (clone AE1), all conjugated to NTb575 (AcZon s.r.l., Bologna, Italy), and one antibody targeting CD45 (clone HI30) labeled with PerCP (Themo Fisher Scientific, Waltham, MA, USA). The CK-pan cocktail was diluted to a final concentration of 3.5 µg/mL and the anti-CD45 antibody was diluted to 4 µg/mL in PBS/1%BSA/0.05% saponin. After removal of the staining cocktail, the microsieve was washed once and then incubated for 5 minutes at room temperature with PBS/1%BSA. Then

the sample was fixed using PBS with 1% formaldehyde (Sigma) for 10 minutes at room temperature. Removal of the fluid during each of the staining and washing steps was done by bringing the bottom of the microsieve in contact with an absorbing material using a staining holder (VyCAP). The microsieve was subsequently covered with ProLong® Diamond Antifade Mountant with DAPI (ThermoFisher Scientific, Waltham MA, USA). A custom cut 0.85 by 0.85 cm glass coverslip (Menzel-Gläser, Saarbrükener, Germany) was placed on the upside and on the downside of the microsieve for immediate analysis or storage in the freezer at -30°C.

Analysis of fluorescent cells

The flow cytometer (BD FACS ARIA II from BD Bioscience) was used to measure fluorescence intensity on labeled cells. At least 500 µL with approximately 0.5×10^6 cells was used for each measurement. For fair comparison, the settings of the lasers were held constant in each individual experiment. Also, cells were analyzed with the fluorescent microscope. The Nikon E400 microscope was equipped with a mercury arc lamp as a light source, a 10X/NA0.45 and a 20X/NA0.45 objective (both Nikon, Tokyo, Japan), a computer-controlled CCD camera (Hamamatsu Photonics, Hamamatsu, Japan) and an X,Y,Z-stage. The following filters (Semrock, Rochester, NY, USA) were used: DAPI with excitation 377/50 nm, dichroic 409 nm, emission 409 nm LP; FITC with excitation 480/20 nm, dichroic 495 nm LP, emission 510/20 nm; PE with excitation 543/22 nm, dichroic 562 nm, emission 593/40 nm and customized PerCP with excitation 435/40 nm, dichroic 510 nm LP, emission 676/29 nm.

Image analysis

For measuring of fluorescence intensity loss during bleaching of the fluorophore, an ImageJ script was used to analyse the raw, grey value images. This script segmented the cells from the background and calculated the mean intensity of all segments in each image. By comparing these values with the intensity values of images without bleaching, the loss of fluorescent intensity can be calculated. For compiling merged images, the Hamamatsu software and open-source software ICY was used. Lookup tables (LUT) for intensities of each channel in a merged image was kept the same to compare the fluorescent intensity between different experimental settings.

Results

Comparing NanoParticles with traditional fluorophores

CD45-FITC

First, CD45 was used to compare between the traditional fluorophore FITC and AcZon's silica NanoParticle$_{520}$. AcZon conjugated supplied CD45 from clone HI30 with both fluorophores and they were tested at the University of Twente by flow cytometry. In all the tests that were performed, the side and forward scatter plots, distinguishing lymphocytes and granulocytes, are similar for the conventional FITC and the NP$_{520}$ (see Figure 2, panel A). Three concentrations were tested –1 µg/mL, 2.5 µg/mL and 5 µg/mL– and they all show sufficient signal for detection. With a lower concentration of antibody (1 µg/mL), there is barely any difference in intensity between conventional and NP$_{520}$. However, a higher concentration (5 µg/mL) shows that NP$_{520}$ have a stronger intensity (panel B). Unfortunately, the 5 times increase in antibody concentration only shows a 1.62 times increase in signal intensity, indicating a saturation of the antigens on the cell membrane. A triplicate experiment staining three times with 5 µg/mL conventional fluorophore and NP520 concentration was performed. It showed that the average mean intensity of those samples was 1,031 for the conventional fluorophore, and 1,578 for the NP520 (Δ547, 53% increase). To identify the two populations of blood cells –lymphocytes and granulocytes– the intensity distance between the two peaks in the histogram signal should be as large as possible. For the conventional FITC, this distance was 1,400 on average. For the NP520, this was 2,067 on average (Δ667, 48% increase) (panel C).

CD45-PerCP

During the course of CTC-Trap it became clear that PerCP was the most likely candidate for the staining of CD45, because the fluorophore FITC or APC would be too weak to pose as an exclusion marker, whereas the bright PE would be used for the essential inclusion markers. Therefore the conventional fluorophore PerCP would be compared to its NanoParticle equivalent NP$_{678}$. Four concentrations (1, 2, 5 and 10 µg/mL) were tested with the traditional PerCP and NP$_{678}$ (clone HI30) and this shows that the mean intensity of both conjugates is similar at every concentration (see Figure 3). On average, the intensity is 2% higher for NP$_{678}$ in the lymphocyte population. For conventional PerCP, there is a slight total increase of 13% intensity when the antibody concentration increases from 1 to 10 µg/mL.

For NP_{678}, this is 6%. For the granulocyte population, the difference between PerCP and NP_{678} intensity is on average 5% higher with NanoParticles. This intensity increases when doubling concentrations and has increased for 52% and 42% with traditional and NP_{678}, respectively, at 10 µg/mL. Figure 4 shows the side scatter (SSC-A) plots of these white blood cell populations (CD45 as 488-695/40-A). The lymphocytes (green) can be divided in three subpopulations; lymphocytes ($CD45^{high}/SSC^{low}$), monocytes ($CD45^{high}/SSC^{med}$) and basophils ($CD45^{low}/SSC^{low}$)[2]. For both conjugates the separation of populations looks similar.

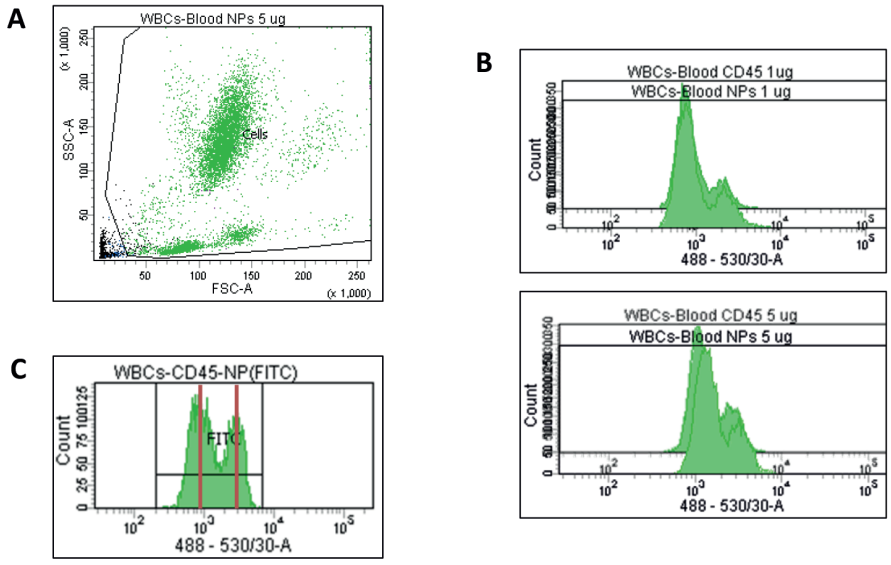

Figure 2. Flow cytometry measurements of CD45-FITC and CD45-NP($FITC_{520}$) (clone HI30). **A** – Side scatter vs. forward scatter plot of lysed white blood cells stained with 5 µg/mL CD45-NP($FITC_{520}$). The granulocytes (upper population) and lymphocytes (lower population) are easily distinguishable. **B** – Intensity comparison between the conventional fluorophore ("CD45") and the NanoParticles ("NPs") with different concentrations. The mean intensity using 1 µg/mL antibody is similar for both fluorophore, with a difference of only 137 in intensity. The mean intensity of 5 µg/mL antibody shows a higher intensity for CD45-NP($FITC_{520}$) with 1,917, while CD45-FITC shows 1,562. **C** – Histogram of CD45-NP($FITC_{520}$) with red bars indicating the average intensity to establish the distance between the two populations.

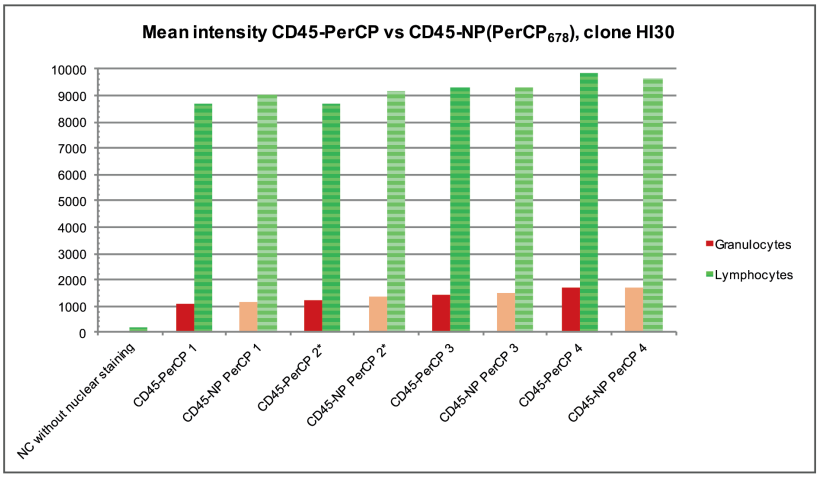

Figure 3. Comparing mean intensity values for CD45 conjugated antibodies (clone HI30) against white blood cells, divided in granulocytes and lymphocytes, measured by flow cytometry. Four concentrations were used: 1, 2, 5 and 10 µg/mL for the numbers 1, 2, 3 and 4 respectively. On average, the NP(PerCP$_{678}$) is 2% higher in intensity for lymphocytes and 5% higher for granulocytes. *Comparison between two unequal concentrations: 2.0 µg/mL for PerCP and 2.5 µg/mL for NP(PerCP$_{678}$).

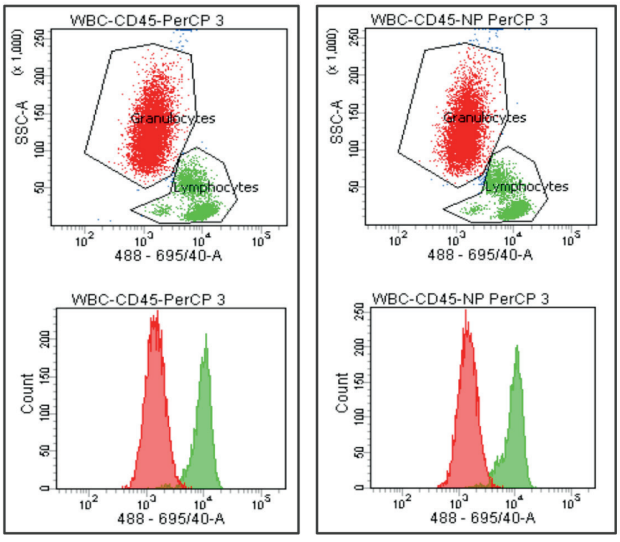

Figure 4. Flow cytometry plot showing the side scatter and CD45 fluorescence intensity of the two blood cell populations stained with 5.0 µg/mL for anti-CD45-PerCP (left) and anti-CD45-NP(PerCP$_{678}$) (right). Granulocytes are in red and lymphocytes in green

Cytokeratin-pan PE

In addition to excluding white blood cells, the inclusion of cytokeratin positive cells are used for detection of CTC. For this marker the yellow channel will be used and conventional PE and commercial eFluor570 will be compared to AcZon's NP_{575}. The non-small cell lung cancer NCI-H1650 cells were used for testing the cytokeratin-pan staining. Two cytokeratin clones, C11 and AEpan (consisting of clone AE1 and clone AE3), were used for comparison at concentration 1, 2, 5 and 10 µg/mL (see Figure 5). The anti-C11 mean intensity (orange bars) shows a higher staining with the traditional fluorophore PE compared to the NP_{575}. For the first three concentrations, the NP_{575} intensity is below 50% of the intensity of the traditional fluorophore. At the highest concentration this intensity has increased to 75% of PE.

The commercial fluorophore eFluor570, conjugated to the AE-pan cytokeratins, is not compatible with the flow cytometer. This fluorophore needs an excitation of 555 nm, whereas the flow cytometer excites at 488 nm[3]. As a consequence, the intensity is very low in these measurements (Figure 5, blue bars). The AEpan-NP_{575} therefore shows a higher intensity, which starts at 1.6 times for 1 µg/mL, increasing to 7.9 times at 10 µg/mL. The right panel in Figure 6 shows a fluorescence microscope picture of NCI-H1650 cells stained with anti-AE1/AE3-eFluor570, which shows a bright signal, in contrast to the flow cytometry data (left panel). Flow cytometry is therefore unfit to be used for comparison between eFluor570 and NP_{575}, and the fluorescent microscope measurements are the only measurements that can be used in reaching a decision.

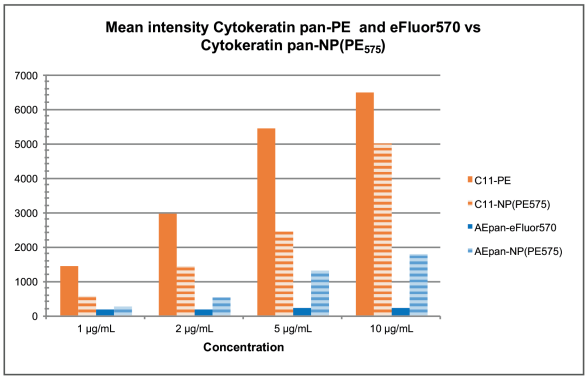

Figure 5. Comparing mean intensity values for cytokeratin conjugated antibodies against NCI-H1650 cells, divided in clone C11-pan (orange bars) and clone AE1/AE3-pan (blue bars), measured by flow cytometry. Four concentrations – 1, 2, 5 and 10 µg/mL – were used to compare the fluorophores PE and eFluor570 (filled bars) with AcZon's NP_{575} (dashed bars).

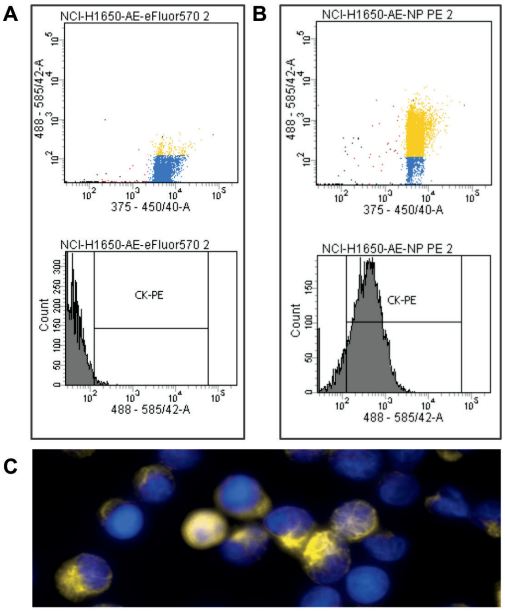

Figure 6. Comparing fluorophores eFluor570 and NP575 with flow cytometry, which is an unsuitable method and does not show the same signal as fluorescent microscopy. A – Flow cytometry plots showing the fluorescence intensity of NCI-H1650 stained with AEpan, conjugated to fluorophore eFluor570 (488-585/42-A) with a concentration of 2.0 µg/mL. B – NCI-H1650 stained with 2.5 µg/mL anti-AEpan-NP575, which shows a higher signal. C – Fluorescence image of NCI-H1650 stained with 2 µg/mL anti-AE1/AE3-eFluor570 (yellow) and DAPI (blue), with an exposure time of 1 second for eFluor570 with 10x/0.45NA objective (Nikon).

Comparing CD45 clones for population separation

To determine the suitability of a CD45 clone, the separation based on the larger density of the CD45 antigen on lymphocytes as compared to granulocyte is important. Separation of lymphocytes $CD45^{high}/SSC^{low}$, monocytes $CD45^{high}/SSC^{med}$) and basophilic granulocytes ($CD45^{low}/SSC^{low}$) should also be clearly visible. The clone that provides the better separation of these cell populations is the preferred one.

Anti-CD45 clone GA90, in possession by AcZon, was compared to clone HI30, which had to be acquired commercially. Again, four concentrations of each clone was tested and compared by their mean intensity values (see Figure 7). The ratio between the two white blood cell populations is presented in Table 2 and visualized in Figure 8. For clone HI30, both the traditional fluorophore and NP_{678} were compared again as well. In contrast to the previous experiment (see Figure 3), the intensity of NP($PerCP_{678}$) antibodies

is now slightly lower than the traditional conjugated antibodies. However, on average they are only 6% lower in intensity, for both lymphocyte and granulocyte populations, which is a similar to previous experiments (2-5% increase). On average, you can say that there is no real difference between the conventional PerCP and AcZon's NP_{678}.

When comparing the two anti-CD45 antibodies clone types, it can be seen that the intensity with clone GA90 is higher and increases during the titration, in contrast to clone HI30. Whereas the lymphocyte intensity increases with only 6% on average in both NP_{678} HI30 tests, the GA90 intensity increases with 72% with doubled concentration, and increases another 45% and 13% with each doubling of concentration. For the granulocytes, the intensity increases 96%, 114% and 65% with a doubling of concentration. Compared to the NP_{678} antibody from clone HI30, clone GA90 has 17%, 92%, 139% and 246% more intensity respectively. Since the increase of signal continues with increasing concentration, it appears the optimal concentration of CD45-NP($PerCP_{678}$) from clone GA90 is not yet reached when using 10 µg/mL.

It can be noted that the overall intensity of Figure 7 is lower than the intensity in Figure 3, while the same concentrations were used. However, these were separate experiments, and the settings on the flow cytometer were different between these experiments in order to create the best measurement.

To visualize the population separation of clone GA90, flow cytometry SSC is plotted against anti-CD45-NP($PerCP_{678}$) (Figure 8). The two populations, granulocytes in red and lymphocytes in green, can be clearly distinguished. However, the three subpopulations –lymphocytes, monocytes and basophils– cannot be distinguished at all antibody concentrations. The basophils are not visible using 1, 2 and 5 µg/mL (panel A, B and C), and are starting to become visible at 10 µg/mL (panel D) as a separate population in the SSC plot. In the histogram, the tiny bump before the major peak of lymphocytes (green) indicates the basophils, which is only visible in 5 and 10 µg/mL (C and D). This separation is less distinct than the separation of clone HI30 in this and previous experiments (see Figure 3). The ratio between the staining intensity in lymphocytes and granulocytes is shown in Table 2. This ratio goes down for 39% for the GA90 clone as the antibody concentration goes up. This indicates unspecific staining of the antibody. With clone HI30, this decrease in ratio is only 15 to 19%.

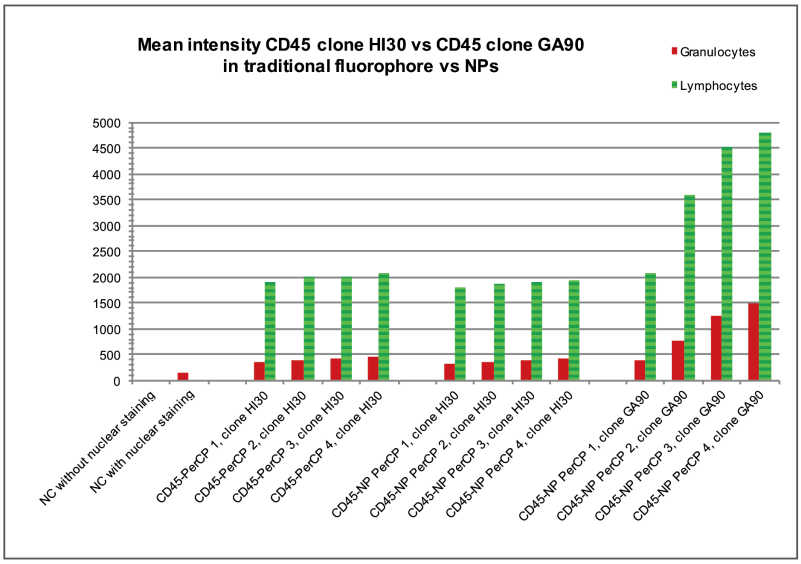

Figure 7. Comparing mean intensity values for CD45 conjugated antibodies (clone HI30) with CD45 NanoParticle antibodies (clone HI30 and GA90), divided in granulocytes and lymphocytes, measured by flow cytometry. Four concentrations were used: 1.0, 2.0, 5.0 and 10.0 µg/mL for the numbers 1, 2, 3 and 4 respectively.

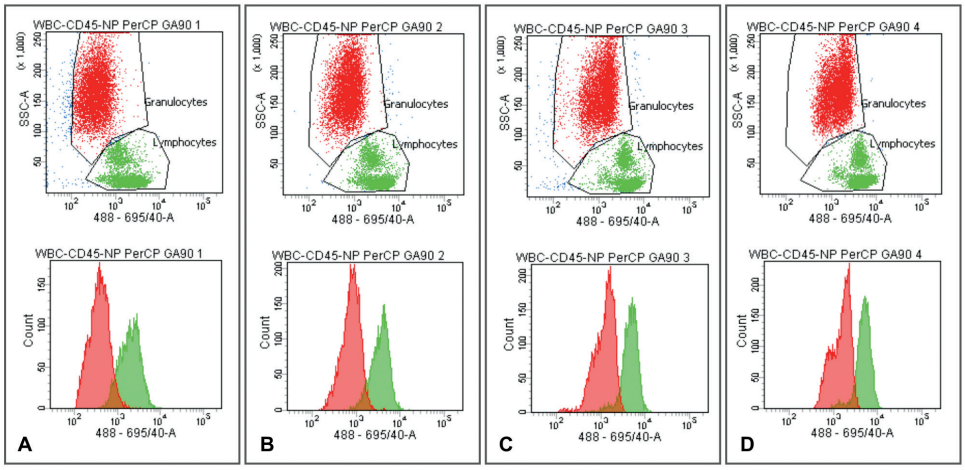

Figure 8. Overview of flow cytometry plot showing the side scatter and fluorescence intensity of the two blood cell populations in a concentration titration of anti-CD45-NP(PerCP$_{678}$) from clone GA90. Concentrations were **A** 1 µg/mL, **B** 2 µg/mL, **C** 5 µg/mL and **D** 10 µg/mL. Red are the granulocytes and green are the lymphocytes, divided in three subpopulations: lymphocytes (CD45^{high}/SSC^{low}), monocytes (CD45^{high}/SSC^{med}) and basophils (CD45^{low}/SSC^{low}). The basophils are only visible in the plots with highest antibody concentration.

Table 2. Lymphocyte/granulocyte ratio in WBC staining with anti-CD45 conjugated to traditional fluorophore PerCP or NP678 from clone HI30 or GA90.

Sample	Concentration	Ratio
CD45-PerCP, clone HI30	1 µg/mL	5.55
	2 µg/mL	5.12
	5 µg/mL	4.72
	10 µg/mL	4.52
CD45-NP(PerCP$_{678}$), clone HI30	1 µg/mL	5.39
	2 µg/mL	5.11
	5 µg/mL	4.77
	10 µg/mL	4.58
CD45-NP(PerCP$_{678}$), clone GA90	1 µg/mL	5.21
	2 µg/mL	4.57
	5 µg/mL	3.65
	10 µg/mL	3.19

Fluorescent bleaching measured with fluorescent microscopy

Cells stained with traditional fluorophores and NanoParticles were used for a bleaching experiment to determine the loss of fluorescent signal after exposure to a light source. The cells were continuously exposed to the mercury arc lamp, and images were snapped at several time intervals: directly after 1 second of exposure, after 3 seconds, 5, 10, 20, 30, 60, 90 and finally at 120 seconds. Of each image the mean intensity of all cells were determined with an ImageJ script. The first image at 1 second was taken as a reference with 0% loss of intensity (see Figure 9). It shows that the PerCP fluophore and NanoParticle$_{678}$ suffer very little loss over time. The commercial eFluor570 fluorphore is very stable and loses only 2% of its intensity after 2 minutes. The NanoParticle PE$_{575}$ suffers great losses; around 40% in both samples after 120 seconds. But, in the first five seconds, the loss is less than 10%. This kind of exposure time is more likely during scanning or manual analysis. However, the traditional PE loses only 1.5% of its intensity in the first 5 seconds.

The three most bleached samples (AEpan-NP(PE$_{575}$), C11-NP(PE$_{575}$) and C11-PE) are visualized in Figure 10, showing time interval 1, 10 and 120 seconds. This clearly shows that, by eye, the intensity is practically the same between 1 second and 10 seconds. A clear difference is visible after 120 seconds.

Immunostaining with NanoParticles on a microsieve

As part of the CTC-Trap program, the goal of the immunostaining cocktail is to use it on a microsieve after filtration of a blood sample. Important features here are the performance of the antibodies and fluorophores in the presence of non-target cells, the recovery of cells in comparison with the traditional fluorophores and the compatibility of the fluorophores with the fluorescent microscope filters.

Non-specific staining

In order to determine the non-specific binding of the NanoParticle antibodies, PC3 cells were spiked in healthy donor blood and processed with the CellSeach Autoprep. CellSearch Waste was collected, filtered with VyCAP microsieves and stained as described in the CTCTrap 'Protocol Staining Of

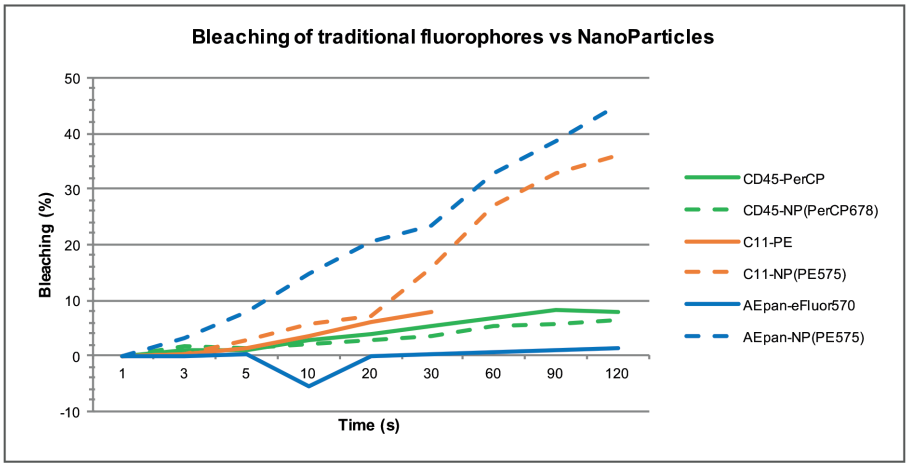

Figure 9. Graph showing the percentage of bleaching in different samples after 3 seconds, 5 seconds, 10, 20, 30, 60, 90 and 120 seconds. The green lines shows the white blood cells that were stained with 2 µg/mL anti-CD45-PerCP (solid line) and 5 µg/mL anti-CD45-NP(PerCP$_{678}$) (dashed line). The orange lines shows the NCI-H1650 cells, stained with 1 µg/mL anti-C11-PE (solid line) and 4.6 µg/mL anti-C11-NP(PE$_{575}$) (dashed line). In the last three images (60 seconds, 90 seconds and 120 seconds) for the mean intensity value of C11-PE could not be determined. The blue lines show the staining of NCI-H1650 cells with 2 µg/mL anti-AE1/AE3-eFluor570 (solid line) and 5 µg/mL anti-AE1/AE3-NP(PE$_{575}$) (dashed line). Concentration of the commercial antibodies in this experiment were as they were used in the staining cocktail at the moment. Concentration of the NPs from AcZon were the recommended concentrations.

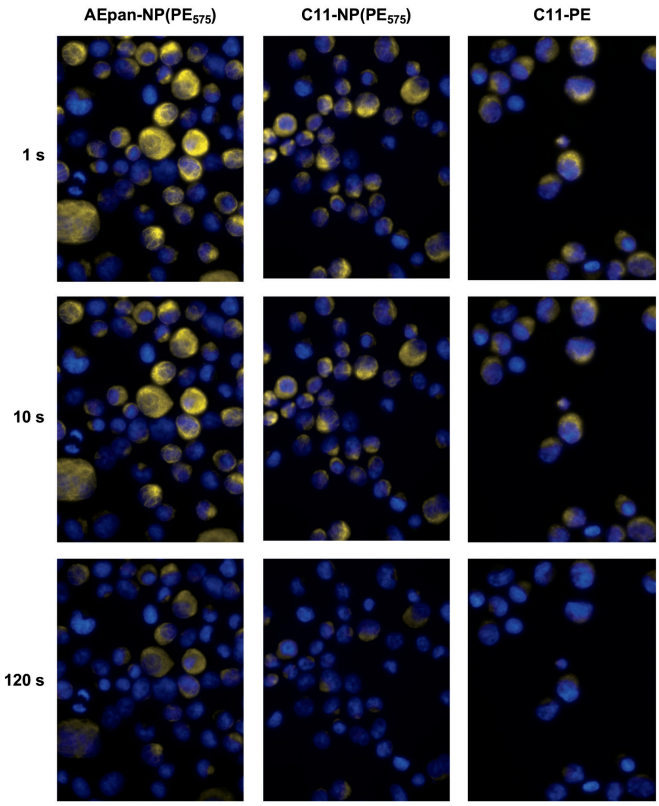

Figure 10. NCI-H1650 cells during bleaching of the fluorophore with 5 µg/mL anti-CKpan antibodies. All images are taken with 1 second exposure time for PE with a 10x/0.45NA objective (Nikon). Between the same sample, all LUT-values were kept the same, but not necessarily between the different samples. In the top row, three samples without bleaching (1 s), in the middle row after 10 seconds of bleaching, and in the last row after 120 seconds. Blue is the nuclear staining DAPI and yellow the cytokeratin staining.

Cells After Filtration With Microsieves', where the antibodies in the staining cocktail were replaced by the AcZon NanoParticle antibodies for CKpan and CD45. The recommended concentration prescribed by AcZon in the technical data (see Table 1) was used for staining of the cells (Figure 11, panel A). As expected, NanoParticle cytokeratin anibodies stain the spiked PC3 cells (white arrows). However, also strong non-specific staining of leukocytes is visible in the figure (grey arrows). Most likely these cells are granulocytes, which can be subject to unspecific staining of cytokeratins. Leukocytes are visible with the CD45-NanoParticles, however, small white arrows show unstained nuclear cells, which could be either cancer cells or blood cells.
After scanning, these samples were stored in the freezer, as is the protocol for

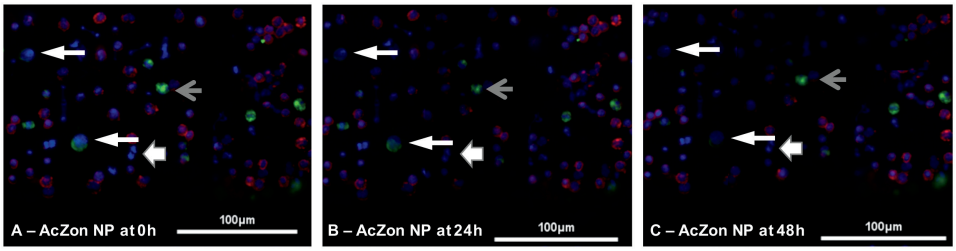

Figure 11. Images of PC3 cells (white arrows) spiked in healthy donor blood, processed with the CellSearch followed by CellSearch Waste filtration and staining with AcZon NanoParticles for CKpan (green) and CD45 (red) at recommended concentration. **A** – The microsieve was scanned directly. **B** – The microsieve was stored in the freezer for 24 hours and thawed once. **C** – The microsieve was stored for 48 hours and thawed twice. Small white arrow shows unstained nucleated cells and the small grey arrow shows a-specific stained white blood cells. Images were taken with a 20X/0.45NA objective (Nikon) with exposure times of 20ms for DAPI (blue), 100ms for anti-C11-NP(PE_{575}) (green), anti-AE1/AE3-NP(PE_{575}) (green) and 400ms for anti-CD45-NP($PerCP_{678}$) (red). LUT values are the same for all images.

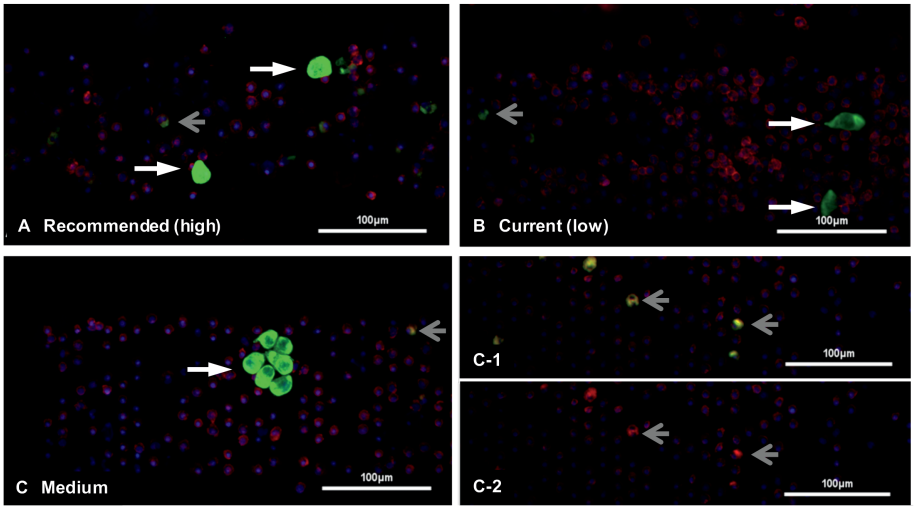

Figure 12. Microsieves with SK-BR-3 cells which were spiked in healthy donor blood, diluted 1:4 with CellSeach Instrument Buffer to mock the waste composition, filtered and stained for CKpan (green) and CD45 (red) with the AcZon NanoParticle antibodies at three concentrations (see Table 3). White arrows indicate SK-BR-3 cells. Grey arrows show non-specific stained white blood cells. Panel C1 shows brightly PE-stained cells in yellow, which also show CD45 staining in red (C-2), indicating this is non-specific cytokeratin staining of granulocytes. Images were taken with a 20X/0.45NA objective (Nikon) with exposure times of 2ms for DAPI (blue), 100ms for anti-C11-NP(PE575) (green), anti-AE1/AE3-NP(PE575) (green) and 400ms for anti-CD45-NP(PerCP678) (red). LUT values are the same for all images.

all patient samples. The microsieve was scanned again after 24h (thawed once) and 48h of storage (thawed twice), to determine the loss of fluorescence signal over time (Figure 11, panel B and C). The two PC3 cells are visible in all images, yet with a much lower intensity after 48h storage compared to direct scanning. Non-specific staining of cells with cytokeratin are also still visible after 48h of storage. The decrease in signal could still be overcome by changing picture settings, since the LUT-values are the same in all panels for comparison.

In order to decrease the amount of non-specific stained white blood cells, two lower concentrations were tested as well (Table 3). Again, at recommended concentration, there is a lot of non-specificity (Figure 12, grey arrows). This is also visible at lower concentrations, but in a much lesser amount. Instead of clone HI30, clone GA90 was used for anti-CD45 staining with a medium concentration staining cocktail (panel C). The only notable difference were the bright cytokeratin positive cells (grey arrows, panel C-1), which are also brightly stained with CD45 (panel C-2), thereby probably being granulocytes stained a-specific for cytokeratin .

Table 3. Concentrations of NanoParticle-antibodies used for staining on a microsieve (images in Figure 11).

Panel	Name	Concentration C11-NP(PE_{575})	Concentration AE1/AE3-NP(PE_{575})	Concentration CD45-NP($PerCP_{678}$)	Anti-CD45 clone
11.A	Recommended staining concentration	5.0 µg/mL	4.5 µg/mL	5.0 µg/mL	HI30
11.B	Current staining concentration	2.0 µg/mL	1.0 µg/mL	2.0 µg/mL	HI30
11.C	Medium staining concentration	3.5 µg/mL	3.5 µg/mL	2.0 µg/mL	GA90

Recovery

To compare recovery of cells on the microsieve, spiked healthy donor samples were stained with a cocktail with either antibody-NanoParticles or commercial available antibodies (see Table 1). In Table 4 the results of 10 samples labeled with each cocktail is presented. PC3 cells are medium EpCAM positive with mean 1.0×10^4 (89 %CV) EpCAM antigens on the cell surface (measured with FACS ARIA II flow cytometer (BD Biosciences, San Jose, CA, USA) and QuantiBrite beads (BD Biosciences)), resulting in a

selection being captured with CellSearch, while the rest of the cells is filtered through the microsieve with 5µm pores. PC3 cells have a medium cell size of 17.7µm (Coulter counter pipette (Scepter, Millipore, Billerica, MA, USA)). Recovery with each cocktail is approximately the same: around 30%. The variation with the AcZon cocktail is larger, however. The percentage of missing cells is also similar in both cocktails, indicating there are still cells that are missed in the antibody staining.

Table 4. Recovery of PC3 in CellSearch and on microsieve.

#	Amount of spiked cells	Recovery in CellSearch	Staining cocktail	Recovery on microsieve	Missing cells
1	325	64%	ACZON	102%*	-1%
2	296	55%	ACZON	71%	13%
3	233	21%	ACZON	29%	57%
4	315	39%	ACZON	15%	51%
5	468	29%	ACZON	38%	44%
6	228	30%	ACZON	16%	58%
7	311	26%	ACZON	15%	63%
8	306	39%	ACZON	13%	53%
9	331	47%	ACZON	15%	45%
10	447	41%	ACZON	15%	50%
		Mean (±SD): 33% (±29) Min-max: 13-102 Median: 16			**Mean (±SD): 43% (±20) Min-max: -1-63 Median: 51**
11	328	51%	Commercial	16%	41%
12	334	44%	Commercial	22%	44%
13	331	45%	Commercial	14%	47%
14	346	48%	Commercial	13%	45%
15	304	12%	Commercial	22%	69%
16	233	24%	Commercial	41%	45%
17	232	27%	Commercial	40%	44%
18	280	52%	Commercial	67%	16%
19	276	15%	Commercial	43%	48%
20	303	41%	Commercial	12%	52%
		Mean (±SD): 29% (±17) Min-max: 12-67 Median: 22			**Mean (±SD): 45% (±12) Min-max: 16-69 Median: 45**

*Extrapolated number because of clogging of the filter.

Spectra

Figure 13 displays the spectra characteristics of the fluorescent antibodies and the microscope filters. It compares the traditional PE and PerCP fluorophore with the AcZon NanoParticles, using the set of filter cubes used at the MCBP laboratory at the University of Twente.

Summary

- With the CD45 antibodies from clone HI30 two tests were performed which showed a similar intensity on the flow cytometer. The separation of populations is good for both the traditional fluorophore and NanoParticles. The bleaching of both fluorophores is also similar.
- For the CD45 antibodies from clone GA90 flow cytometry data showed that the intensity of clone GA90 is much higher than clone HI30, both conjugated to NanoParticles. The optimal concentration of this antibody is not yet reached at 10 µg/mL, whereas the ratio between antibody and NanoParticle is the same for both clones. The GA90 clone showed a decline in staining ratio between de granulocytes and lymphocytes, this is usually due to non-specific staining. A hypothesis for the cause of this non-specific staining might be the presence of the isotype control in the same staining reagent.
- CD45-NanoParticle$_{678}$ (PerCP-like) staining on microsieve appears similar to traditional CD45-PerCP. Clone GA90 on microsieve shows a high intensity in blood cells, which are positive as well for cytokeratin.
- For the Cytokeratin antibodies from clone C11, the traditional PE has a higher intensity than the NanoParticles in flow cytometry experiments. The NanoParticles bleach slightly faster than the traditional PE, however, staining on a fluorescent microscope showed very similar intensities.
- For the Cytokeratin antibodies from clone AE1/AE3, the eFluor570 is not compatible with the flow cytometer and can therefore not be compared to the NanoParticles. The eFluor570 is less susceptible to bleaching than the NanoParticles under a fluorescent microscope.
- The cytokeratin NanoParticle antibodies show non-specific staining of white blood cells on the microsieve at the recommended concentration. Lower concentrations of NanoParticle antibodies show less non-specificity of the antibody.

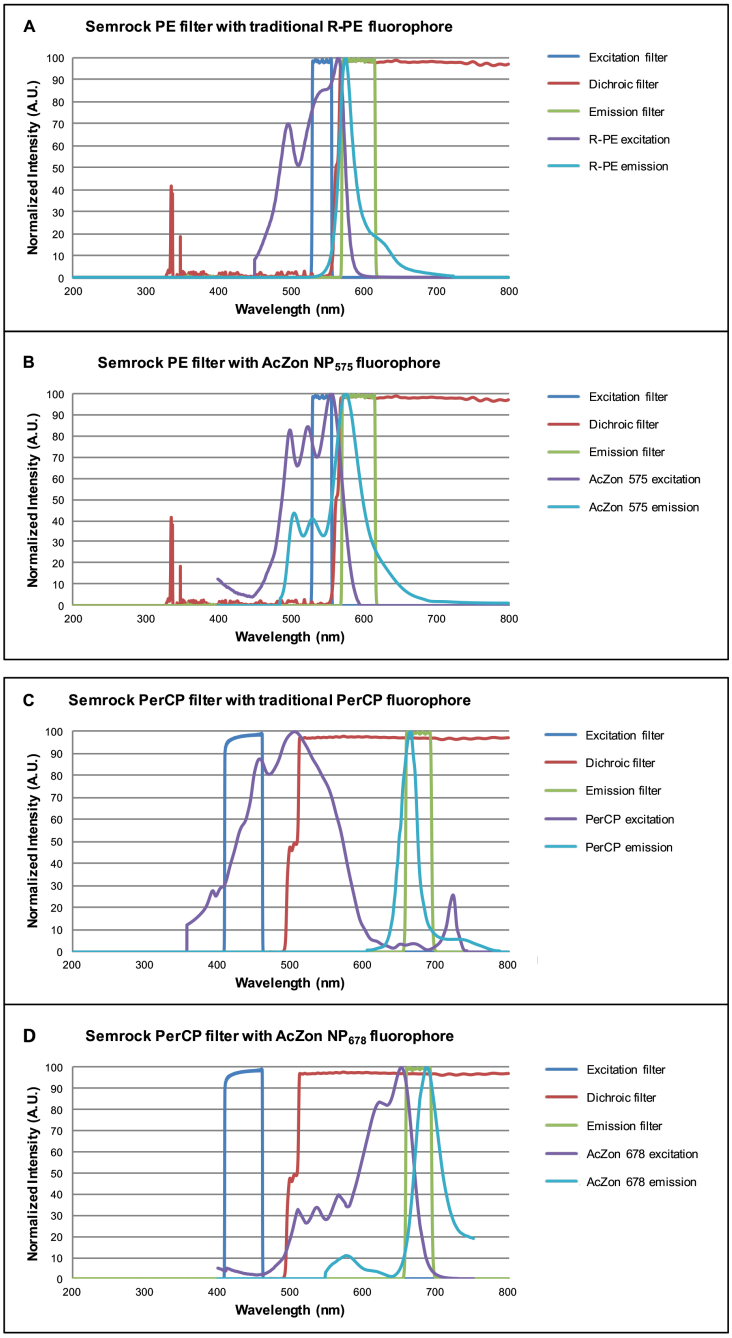

Figure 13. Spectra of Semrock filters are compared with the traditional fluorphore and NanoParticle PE-fluorophore. **A** – Traditional PE fluorophore. **B** – AcZon NP_{575} fluorophore. **C** – Traditional PerCP fluorophore. **D** – AcZon NP_{678} fluorophore.

- Loss of fluorescence for NanoParticles or traditional fluorophores during storage in the freezer appear to be minimal. Visible loss can be overcome by image analysis settings. Recovery of CTC with NP or traditional labeled antibodies is approximately for both around 30%. However, the variation with the NP antibodies is larger. The percentage of missing cells is also similar for both, indicating there are still cells that are missed in the antibody staining.
- $NanoParticle_{575}$ (PE-like) is compatible with the PE cube from Semrock recommended for use by the consortium. $NanoParticle_{678}$ (PerCP-like) is not compatible with the recommended PerCP cube, since the excitation of the NP-fluorophore (~650 nm) falls outside the excitation filter of the cube (415-455 nm).

Outlook

The CTC-Trap consortium chose to go forward with the CKpan-NP_{575} (PE-like) antibody conjugation (consisting of clone C11 and AE1/AE3). The concentration used was 3.5 µg/mL per test on a microsieve. AcZon supplied every clinical partner with sufficient antibody for all tests and patients, in a convenient aliquot concentration that required only 1 µL antibody to be added to the staining mix.

Acknowledgements

Special thanks to Christian Breukers for writing the ImageJ script used for the bleaching experiments and preparing Figure 13 by measuring the fluorophores for comparison with our microscope filters.

References

1. AcZon, silica NanoParticles (2017) http://www.aczonpharma.com/
2. Fujimoto H., et al., Flow cytometric method for enumeration and classification of reactive immature granulocytepopulations. Cytometry, 2000, Dec 15;42(6):371-378.
3. Pan Cytokeratin Monoclonal Antibody (AE1/AE3), eFluor 570, eBioscience™ (2017) https://www.thermofisher.com/

Part II: Microsieves and microscopy

Introduction

In November 2014 the University of Twente (UT, Enschede) prepared three microsieve slides and shipped these to the laboratories of Institute of Cancer Research (ICR, London), Institut Gustave Roussy (IGR, Paris), Instituto Oncologico Veneto (IOV, Padova) and Heinrich-Heine-Universität (HHU, Düsseldorf).

The goal of sending these three microsieves was to determine if all samples can be scanned and analyzed at each site in a comparable manner and to determine loss of staining intensity during transport and scanning.

Each clinical site completed a questionnaire about the settings, characteristics of their microscope and scanning system and the procedure of scanning multiple slides. This report describes the important results and the encountered issues.

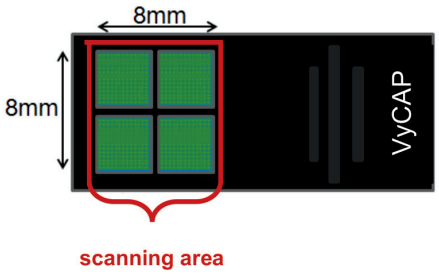

Figure 1. VyCAP microsieve in a slide.

Methods

Microsieves

- Microsieve A was scanned at the UT prior to sending and was also scanned at the clinical site after shipment.
- Microsieve B was not scanned at the UT, but at the clinical site.
- Microsieve C was not scanned prior to sending, not scanned at the clinical site, but stored at -20°C while the other slides were processed at the clinical site.
- All microsieves were scanned at the UT upon return.

Fluorescent immunostaining on a microsieve

The microsieves (VyCAP, Deventer) were prepared at the UT by spiking ~500 SK-BR-3 cells in 1 mL healthy donor blood. Blood was filtered with –40 mbar through the microsieve. After 15 minutes permeabilization at room temperature with 0.15% saponin in PBS/1%BSA, cells were stained with 4 µg/mL Hoechst 33342 (Invitrogen, Carlsbad CA, USA), 10 µg/mL C11-FITC (not commercially available), 5 µg/mL AE1/AE3-AlexaFluor488 (eBioscience™, ThermoFisher Scientific, Waltham MA, USA), 10 µL EpCAM-PE (Sigma-Aldrich, St. Louis MO, USA) and 2 µg/mL CD45-PerCP (Invitrogen). The antibodies were dissolved in 0.05% saponin/PBS/1% BSA for incubation at room temperature for 15 minutes. After staining, cells were fixed in 1% formaldehyde and covered with a glass coverslip with PVA-DABCO mounting medium.

Scanning at MCBP

A Nikon E400 fluorescence microscope equipped with a Mercury Arc lamp as light source, a 10X (0.45NA) objective (Nikon, Tokyo, Japan), a computer-controlled CCD camera (Hamamatsu Photonics, Hamamatsu, Japan), X,Y,Z stage and 4-filter cube exchanger (LEP, Hawthorne NY, USA) with filters were used for acquisition of the fluorescent images covering the entire 0.64 cm2 surface of the microsieves. The following filters were used: DAPI with excitation 377/50 nm and emission 409 nm LP (Spectra Physics Newport, Santa Clara, CA, USA); FITC with excitation 480/20 nm, dichroic 495 nm LP, emission 510/20 nm (Spectra Physics Newport); PE with excitation 547/12 nm, dichroic 560 nm LP, emission 579/25 nm (Spectra Physics Newport); and a customized PerCP filter with excitation 435/40 nm, dichroic 510 nm LP, emission 676/29 nm (Semrock, Rochester, NY, USA) . The scanning and image acquisition was controlled by Labview (National Instruments, Austin TX, USA).

Sample shipment

After preparation and scanning, the microsieves were stored at –80 °C for one night until shipment at room temperature with cold packages inside the foam box. Each site returned the microsieves in this way as well.

Processing samples at the clinical sites

Each clinical site scanned the microsieves according their protocols. Microsieves were stored at –20°C in the meantime until return shipment.

Image analysis

All images were analyzed and compiled with the open source programs ICY or ImageJ.

Results

Scanning systems at each site

This section describes the different technical systems that are available at each clinical site.

Filter cubes

Every site has different cubes for the Hoechst, PE (-like), FITC (-like) and PerCP (-like). Except for the University of Twente, none of the sites have a cube for the PerCP fluorophore. Figure 2 shows the comparison of the cubes of every site, visualized on the spectra of the four fluorophores. With these cubes, the generated data is not comparable. It shows the importance of the correct cubes to ensure maximum coverage of the fluorophores and avoid signal leaking into different channels.

Objectives, light source and camera

The design for the microscope and its technical attributes are summarized in Table 1. Every site has a similar fluorescent light source. However, the objectives and camera are of different qualities yielding different quality images for analysis.

Scanning software

Automatically scanning the microsieves is performed differently at each site (see Table 2a). For most of the sites, the edge definition and focus plan is set manually, while the scanning goes automatically. IGR addressed some issues with focus on the borders of the microsieve and had to use a different magnification to scan the areas in focus. IOV addressed focus issues as well; during scanning the focus plane is lost in both big and small areas. HHU, IGR and IOV have a second system that can scan microsieves as well.

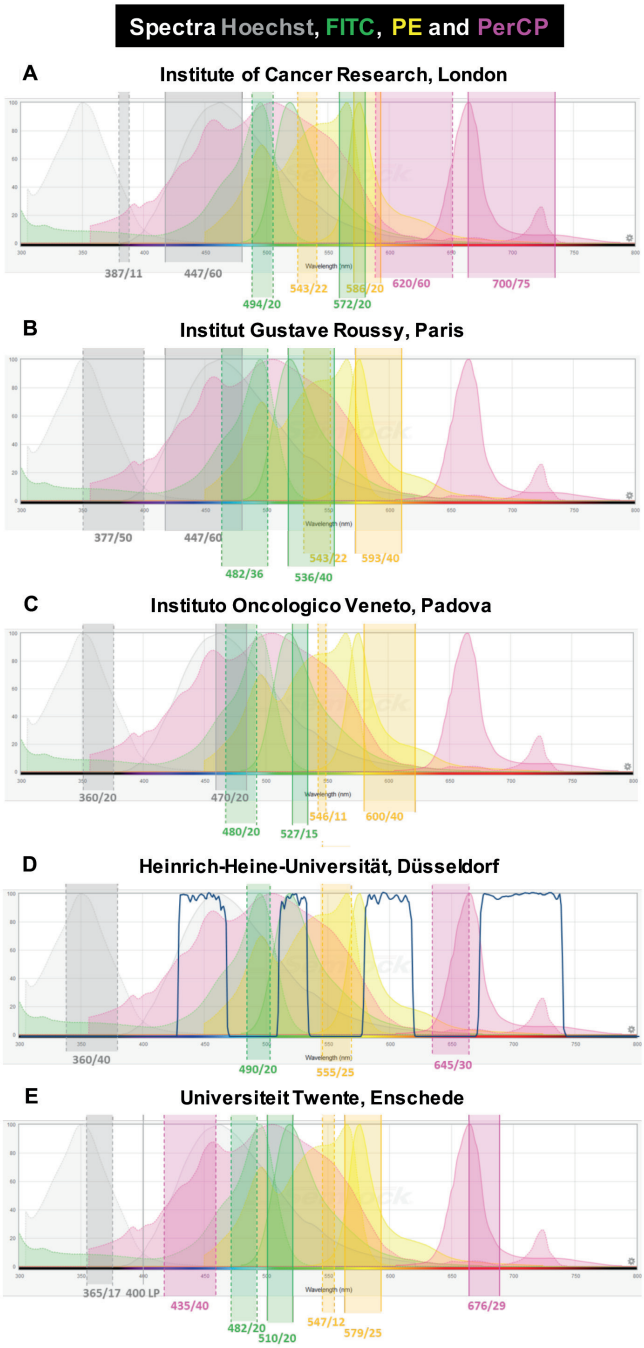

Figure 2. The spectra of Hoechst (grey), FITC (green), PE (yellow) and PerCP (pink) with corresponding cube characteristics of each site in the same color.

Table 1. Technical details of the microscope systems used in all the sites.

Site	Microscope	Light source	Objective	Camera	Resolution (µm) objective & camera	
ICR, London	Bioview Duet (Olympus)	Metal halide arc lamp 120W	10X/NA 0.45	8 bit, 2048x2048	0.6	1.4
IGR, Paris	Nikon Eclipse Ti-E	Nikon Intensilight 130W	10X/NA 0.30 20X/NA 0.75*	Nikon, 12 bit, 1080x1024	0.9 0.4	1.3 0.6
IOV, Padova	Leica DM 6000B	Leica mercury arc lamp	10X/NA 0.30 20X/NA 0.40 40X/NA 0.60	Leica, 12 bit, 1392x1040	0.9 0.7 0.5	1.3 0.6 0.6
HHU, Düsseldorf	Olympus CKX41	Prior Lumen metal arc lamp 200W	20X/NA 0.45	Olympus XM20	0.6	0.6
UT, Enschede	Nikon Eclipse E400	Mercury arc lamp 130W	10X/NA 0.45 20X/NA 0.45	Hamamatsu, 12 bit, 1280x1024	0.6 0.6	1.3 0.6

* Also available in long distance objective

Table 2a – The manual and automatic part of the scanning software of each system.

Site	Software	Edge definition	Focus plane	Scanning	Switching cubes
ICR, London	Duet	Manual	Manual	Automatic	Automatic
IGR, Paris	NIS Elements	Manual	Manual	Manual	Manual
IOV, Padova	Leica LMD	Manual	Manual	Automatic	Manual
HHU, Düsseldorf	ALS CellCollector	Manual	Manual	Automatic	Automatic
UT, Enschede	Labview	Manual	Manual	Automatic	Automatic
2nd system					
IGR, Paris	ARIOL	Manual	Manual	Automatic	Automatic
IOV, Padova	LAS AF	Manual	Manual	Manual	Manual
HHU, Düsseldorf	Axioplan	Manual	Manual	Automatic	Automatic

Scanning times vary between each site, which has an influence on the mounting medium and the fluorescence of the fluorophores (see Table 2b). The scanning of one microsieve takes a long time at IOV. However, between the exposure times of each channel, the fluorescent source is shuttered in order to prevent bleaching. This is the same for the secondary system at IGR. Other primary systems take under 30 minutes to scan one microsieve completely. The data outputs are generally able to be viewed in common licensed or free programs. However, there is a big difference in the amount of files that is generated at each site (see Table 3).

Table 2b. The scanning time of the software of each system.

Site	Primary system	Secondary system
ICR, London	15 min	-
IGR, Paris	15 min	75 min
IOV, Padova	90 min	60 min
HHU, Dusseldorf	30 min	30 min
UT, Enschede	7 min	-

Table 3. Data output of each system.

Site		Files	Format
ICR, London	-	32 for each channel	JPEG
IGR, Paris (ARIOL)*	primary system	1 for each channel	JPEG2000
IOV, Padova	primary system secondary system	4 for each channel 32 for each channel	JPEG TIFF
HHU, Dusseldorf	primary system	1 for each channel	LZW compressed TIFF
UT, Enschede	-	98 for each channel	TIFF

* NIS Elements cannot scan automatically, so images of interest are gathered manually

Fluorescent intensity of cells

During scanning

To observe the loss of fluorescence during scanning, a microsieve with blood and spiked SK-BR-3 cells was filtered and stained according protocol. After this, the microsieve was scanned several times in a row. Figure 3 shows some of these scans, which shows the decrease of fluorescent intensity by bleaching. In the first three scans, the PE fluorophore slowly fades, while FITC remains behind and is visible throughout all the scans. PerCP is bleached very fast. After more than 10 scans, the Hoechst and FITC is still visible, though more faint. Increasing the exposure time during scanning, increases the signal again to a bright signal which can still be used for analysis. After scan 8, the PVA mounting medium layer was dried out and air bubbles prevented focused images over the entire microsieve. Therefore, the PVA layer was washed away and replaced by a new layer (scan 9). It appears this fresh layer has less background than a dried PVA layer (scan 8). These images show that it is important to protect the fluorophores from bleaching before the scan is taken that will be used for analysis. Scanning multiple times is possible, but signal will be lost. In order to prevent loss of signal after two or three scans,

a mounting medium that protects the signal better against bleaching could be considered.

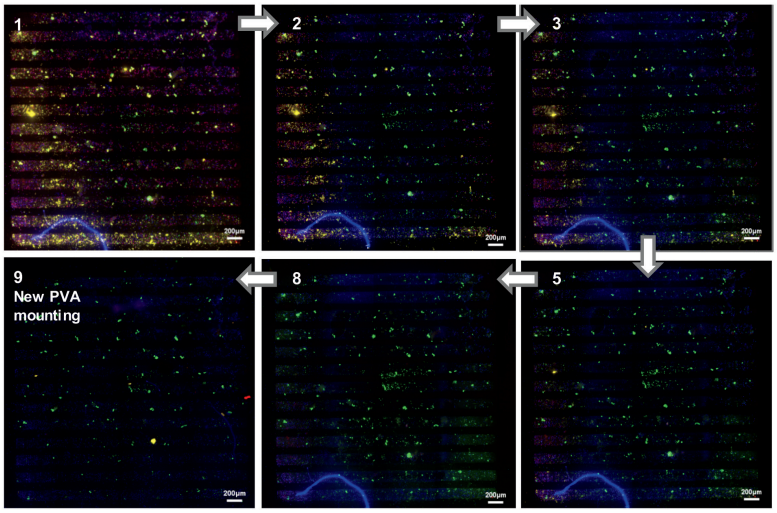

Figure 3. Multiple scans of the same microsieve, SK-BR-3 cells spiked in blood, filtered and stained with CD45-PerCP (red, 400 ms), EpCAM-PE (yellow, 200 ms), CK-FITC (green, 300 ms) and nuclear dye Hoechst 33342 (blue, 20 ms). Depicted are scan 1, 2, 3, 5, 8 and 9 at the same scan and image settings. Between scan 8 and 9, the PVA mounting medium layer was removed and replaced. Scale bar is 200µm.

During shipping

At the UT, shipments of microsieves were mimicked to create similar environments for the cells as it would during real shipments. Shipment boxes were filled with deep frozen icepacks and stored at room temperature for either 24 or 72 hours. These represent a shipment that arrives the next day and a shipment that is transported over the weekend. Microsieves were either scanned directly after staining or directly "shipped", to compare the loss of fluorescence during shipment. Microsieves were scanned after their shipment of 24 hours and/or 72 hours to compare the fluorescent loss as well.

Figure 4 shows images of the microsieves that were shipped and scanned. The scanning and image settings were the same for each microsieve; with LUT values from 200 to 2040, scanned at 20 ms for DAPI, 200 ms for PE, 300 ms for FITC and 400 ms for PerCP. From these images the following remarks can be made:

- Scanned directly after staining yields the brightest fluorescence (A, E).
- After a cold shipment, stored at room temperature, loss of fluorescence can already be detected (B, F).

- Fluorophore PE bleaches faster than FITC, clearly visible throughout all images.
- Fluorophore PerCP is barely visible anymore after 24h (B).
- Hoechst is stable throughout the process.
- The fluorescent intensity can be very variable, visible in picture A and E, which technically the same, yet E is oversaturated using the same picture settings.

During storage

Figure 5 shows some microsieves that have been stored in different environments: at room temperature (panel A), in the refrigerator at 4°C (panel B) and in the freezer at -20°C (panel C). It shows that the dried PVA mounting medium layer gives a high background signal (see panel A). This is less in colder and more humidified environments (see panels B and C). Also visible in this figure, is that the PerCP quickly loses its signal, whereas FITC and Hoechst are more stable.

Discussion and recommendations

Scanning systems

Here follow the recommendations to optimize the scanning systems.

- The cubes at each site are not comparable with each other. The solution for this is that each site obtains the same cubes with the same parameters.
- The fluorescent light sources are comparable with each other and can be used for exchangeable data. The spectral distribution of metal halide arc lamps and mercury lamps are highest at the same wavelength.
- The cameras and the objectives are comparable. We recommend to obtain an objective with 20X/NA 0.45 long working distance and a camera with ~6.4µm pixels in order to obtain the maximal resolution of 0.64 µm.
- A complete manual scanning is subject to bias and generally takes longer to complete, exposing the sample to bleaching of the fluorophores. It is therefore recommended to use an automated scanning system.

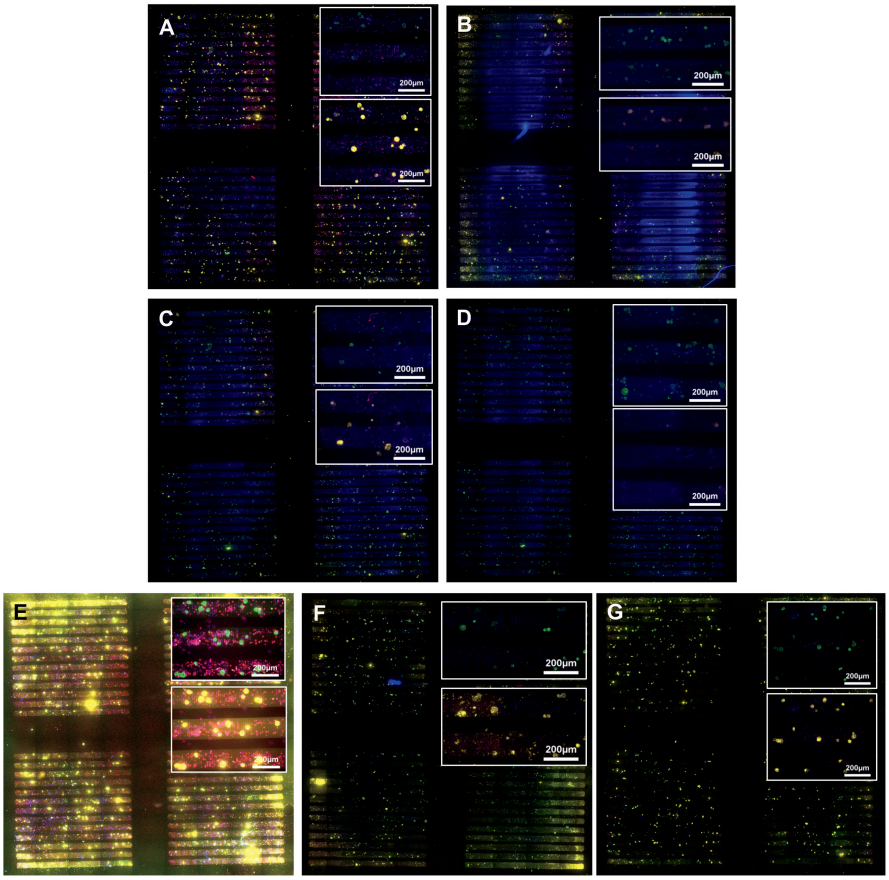

Figure 4. Shipments inside the University of Twente of microsieves with fluorescent cells, with (A) direct scanning after staining compared to (B) scanning after a shipment of 24 hours, (C) scanned directly after staining and shipped for 24 hours and scanned, and (D) scanned directly after staining and shipped for 24 hours, scanned, followed by a another shipment of 72 hours and scanned again. Also, (E) direct scanning after staining compared to (F) scanning after a shipment of 72 hours and (G) scanned directly after staining and shipped for 72 hours and scanned (shown) All pictures have the same exposure times and intensity settings of the colors. Blue = nuclear dye Hoechst, green = CK-FITC, yellow = EpCAM-PE, red = CD45-PerCP.

- The output of the system should be in a platform independent, easy accessible data format. All data should be raw images per frame, without compression, to yield high resolution.
- Analysis of the microsieves was performed manually at each site. Some sites perform the analysis with the microscope. However, this bleaches the sample and information for further analysis can be lost. For direct results, images can be analyzed with free available programs like ImageJ or ICY,

which can load separate channels. For future use, raw images should be archived for automated analysis of the images.

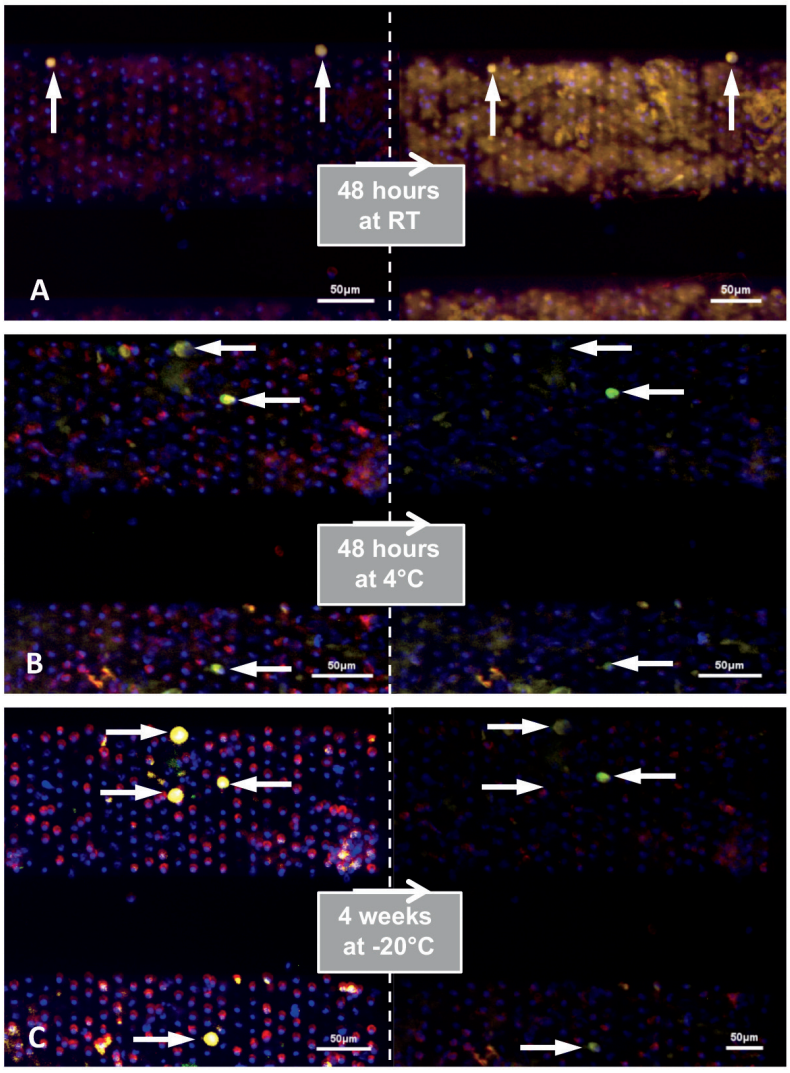

Figure 5. Overview of the fluorescent intensity during storage at room temperature (panel A), in the refrigerator (panel B) and in the freezer (panel C). The left side of the panel is an image of the microsieve before storage and right side the same image area after storage. Scanning and image settings are the same within each panel. Arrows indicate CTC. Blue = nuclear dye Hoechst, green = CK-FITC (only in panel B and C), yellow = EpCAM-PE, red = CD45-PerCP.

Preserving fluorescent intensity

In order to prevent signal loss during scanning, shipping and storage, it is important to have a mounting medium that protects the signal as best as possible. Storage in the freezer loses the least signal, compared to storage at room temperature or at refrigerator temperature. All pictures show that the best signal is recorded with the scan right after staining. Therefore, in order to ensure the possibility to scan multiple times, using a mounting medium that protects against bleaching and stabilizes the fluorophores during storage is required.

Options for scanning

There are several options in the approach to scan the patient samples in the CTC-Trap for consistent analysis material at each site.

Option A – Same settings at each site

In this option every site creates a similar set-up for the scanning of the microsieves. Every site already has a similar fluorescent light source and when every site uses the same filter cubes with designated exposure times, theoretically comparable results could be reached. However, the scan procedures are different and some sites cannot scan the complete microsieve in focus. Downside for this option as well, are the costs for the cubes (approximately €1,000,- per cube).

Option B – Scan at sites with appropriate scanning system

Here, all microsieves will be shipped to one site, which performs the scanning and distributes the images. The microsieve can be shipped back to the original site for additional analysis. Shipping each slide separately will be costly; therefore once or twice per month a shipment could be arranged. However, in this approach the slides will be stored for a longer period before the first scan and lose signal. The temperature and storage still has a large influence on the fluorescent signal, so it is important to stabilize and minimize the loss in signal during the shipment and storage and resolve this issue beforehand.

Option C – Stain and scan at sites with appropriate scanning system

In order to prevent the loss of fluorescent signal, microsieves could be shipped after filtration, but before staining of the cells. One site can stain and scan the microsieves and distribute the images. Microieves can be shipped back to the original site for further analysis and storage. This option however,

increases the workload in that one site that will perform the staining. Also, the loss of cells during shipment and removal of a cover slip to proceed to the staining has not been tested. Fixation before staining can result in loss of fluorescent intensity and low expressed markers can be missed.

Option D – Process complete sample at sites with appropriate scanning system

To prevent the loss of cells and fluorescent intensity, blood samples can be shipped to sites with a scanning system. That site can process the sample in CellSearch and filter, stain and scan the sample. Downside is the shipment of the blood samples, which have to be at the site that processes them within 96 hours after blood draw. This requires fast processing and transport and increases the risk of samples that cannot be included in the clinical studies due to late arrival. Also, this approach increases the workload at those sites with scanning systems enormously.

Option E – Fluorophores are adapted to individual system at each site

In order to avoid any costs for the improvement of the fluorescent and scanning system, the fluorophores in the staining can be adapted to each setting at the sites. However, this would make it not possible to compare and combine results from patients gathered at all the clinical sites.

Discussing the options

If sites are willing and have a possibility to adapt their cube setting to the standard that will be used in the CTC-Trap (plan A), minor issues like a long scanning time or compressed images, can be resolved in another way. This way the microsieves can be scanned right after staining, which yields the best fluorescent intensity for all channels.

Next best option is to ship the microsieves after scanning to the closest site, that has an adequate system for scanning (plan B), on the condition that the intensity of the fluorophores is more stable during storage and shipment. Fluorescent signal is quickly lost during storage and scanning, so it is important to use a mounting medium that protects the signals.

Plan C and D increase the workload in the sites with an adequate system for scanning. Also, these approaches require rearrangements of CellSearch kits and antibodies between sites, and this requires fast transport in order to ensure a timely arrival of samples. For now, it appears realizing other options are reasonable in execution.

For plan E, the original idea of using multiple sites in order to create large patient cohorts will be nullified. Therefore, this option is least favorable.

Conclusions

At the moment we cannot proceed with the scanning of patient samples at all the sites. The current settings at each site are incomparable with each other (see Table 4). If we are to proceed with plan A, the purchase of the cubes will take some time and this will require some funding in the budget. If we are to proceed with plan B, the issue with the stability of the fluorophores needs to be addressed and resolved first. The other options require several resolutions in shipping and budget as well, before it is possible to proceed.

Outlook

On Wednesday January 14, 2015 from 11:00AM-12:15PM (Amsterdam time) the CTC-Trap consortium had a conference call to discuss this report and reach a conclusion on the approach for the scanning of filtered patient samples.

We agreed to use Option A: we will use the same settings at each clinical site. This embodies the adaptation of the scanning set-up with similar filter cubes to yield the same fluorescent signals.

The following agreements were made:

- The following filter cubes will be used and need to be purchased: DAPI cube, FITC cube, PE cube and a PerCP cube. The University of Twente will determine which filter cubes will have to be acquired by all the sites and give this information to each site.
- The University of Twente will continue experiments to find out if other mounting media with anti-fade properties perform better in persevering fluorescent signal then the current mounting medium.
- Every site will scan with a 20X objective, with minimal 0.45NA, to reach maximum resolution with the current cameras and light source.
- The format of the scan pictures will be in TIFF files for future analysis.

Table 4. Overview of the technical components for each site, compared with the recommended technical settings. In green are comparable settings, whereas in red the settings are displayed that do not meet the recommendations.

Sites	ICR, London	IGR, Paris	IOV, Padova	HHU, Dusseldorf	UT, Enschede
Cubes	No PerCP cube, overlay FITC and PE	No PerCP cube	No PerCP cube	No PerCP cube, one emission filter (CellSelector)	
Light source					
Camera					
Objective	20X available?				
Automatic scanning		ARIOL	Leica		
Scanning time		> 30 min (ARIOL)	> 30 min		
Data output				Compression of images	Lot of data with 20X
Conclusion	Adapt cubes	Adapt cubes, increase stability fluorophores	Adapt cubes, increase stability fluorophores	Adapt cubes, use raw images. Switch to Axioplan?	

Acknowledgements

Special thanks to Anouk Mentink-Leusink for helping prepare and scan the microsieves before shipment to all the clinical sites.

Supplementary data

From four clinical site one image of (part of) a microsieve is displayed in the figure below.

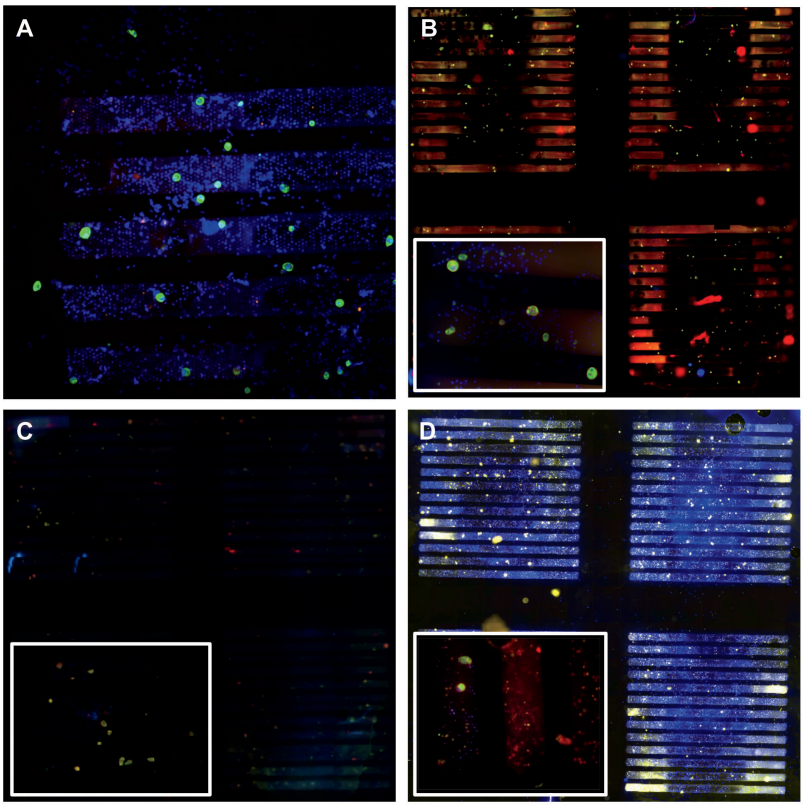

Figure 7. Images from microsieves processed and imaged at the four clinical sites. (A) ICR, Londen: merged image with DAPI, Spectrum Green, Spectrum Orange and Cy5. Image taken with Olympus Bioview microscope with 10X objective. (B) IGR, Paris: merged image with DAPI, FITC, Texas Red and Cy5. Image taken with Ariol microscope with 20X objective. Inserted image is made with the manual Nikon microscope with 20X objective. (C) IGR, Paris: merged image with DAPI, FITC, Texas Red and Cy5. Image taken with Ariol microscope with 20X objective. Inserted image is made with the manual Nikon microscope with 20X objective. (D) HHU, Düsseldorf: merged image with DAPI, FITC, TRITC and Cy5. Image taken with Olympus CellSelector with 20X objective. Inserted image is made with the Axioplan microscope (unknown objective).


8

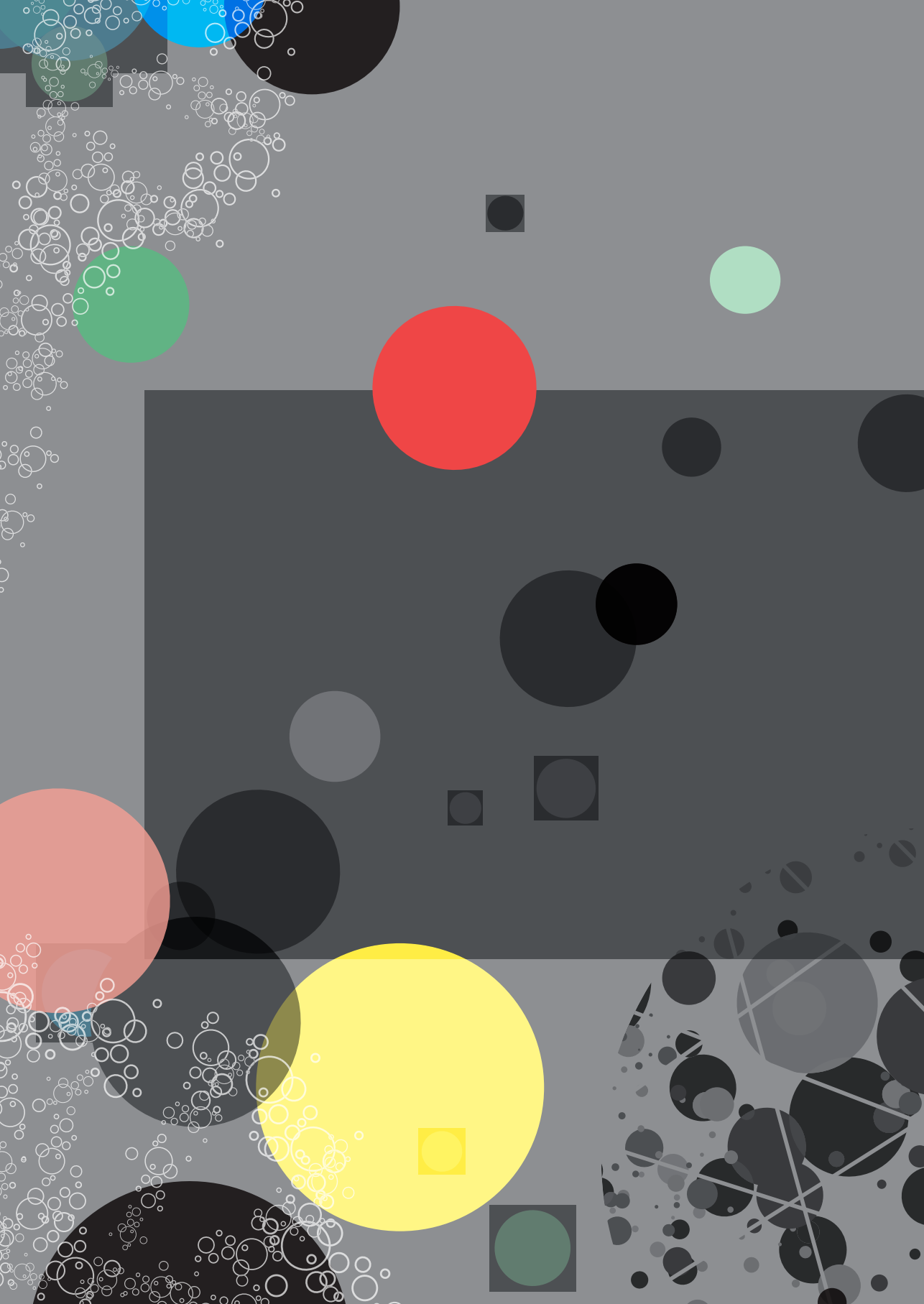

Chapter 9

Looking beyond

In this thesis

The main focus of the research described in this thesis is the detection of EpCAM^{high} and EpCAM^{low} circulating tumor cells (CTC) in blood of metastatic cancer patients. Our approach was to collect the blood discarded after immunomagnetic selection of cells expressing EpCAM with CellSearch® and the use of size selection by means of filtration to enrich CTC. The relation between patient outcome and CTC detected by CellSearch has already been established and in this manner we could investigate the relation of CTC not captured with the CellSearch system with clinical outcome. Of course, this procedure can also be reversed and we passed blood through the microsieves, followed by CellSearch analysis. However, the leukocytes were quite damaged after filtration and the leukocyte carry-over during EpCAM enrichment increased tremendously, which led to a discontinuation of the experiments. Isolation methods based on the size or deformability of CTC, like the microsieves used in this research or other available systems like ISET®[1], Parsortix™[2] and ClearCell® FX1[3], will also discard the smaller or more flexible CTC. However, this subpopulation of CTC, consisting of small cells or cell fragments, can also provide valuable information for the patient[4]. These cells can be isolated with immuno-capture methods, for instance by selecting for EpCAM or other surface markers. The concept of analyzing discarded cells shows that it is possible to gather more information from the same blood tube and highlights what can be missed when only one population of cells is analyzed. The limitation however remains that the process of cell enrichment can alter or damage the cells, with the consequence that the procedure used to analyze the discarded cells may no longer be optimal for CTC selection. Procedures with or without a minimal pre-enrichment procedure, such as the enrichment free Epic Sciences™ system[5], may be more suitable to answer these questions. However, the volume of blood that can be analyzed and the specificity of CTC detection at extreme low frequencies will remain a challenge (**Chapter 1**).

The question that remains is whether it is possible to reach 100% detection of CTC or 100% identification of all cells that are present in the sample. With advanced image analysis, we have shown that a part of the cells after CellSearch enumeration remains unidentified; suggesting that addition of several other markers will be needed to determine the identity of all cells and perhaps unveil a yet unidentified subpopulation of CTC (**Chapter 7**). The immunostaining protocol developed during this research aimed for the identification of EpCAM^{low} CTC with the same epithelial identification

markers as used in CellSearch (**Chapter 2 and 8**). The antibodies now used can be expanded, since only three fluorescent channels are currently being used (DAPI, PE and PerCP)in the protocol. Identification of markers labeled with AQUA, FITC or PerCP are therefore open for inclusion, for instance for mesenchymal or stem cell markers. Since EpCAM is low in these cells, mesenchymal markers like Vimentin or Cadherin-11, might be up-regulated and a good candidate for identification of additional CTC subpopulations. Research on this subject has been extensively pursued by bachelor and master students during the course of this thesis. These students developed immunostaining for the identification of EpCAM^{low} CTC by exploring several novel, mesenchymal and epithelial markers[6,7].

Downstream analysis of cells present on the microsieves has also been investigated. We have developed a procedure on the microsieve for fluorescent in situ hybridization (FISH) (**Chapter 5**). However, we noticed that, for a more optimal application of this technique, it is very important to retain the morphology of cells on the microsieve. Therefore, a stronger fixation of the cells is recommended directly after filtration of the cells to ensure the morphology is preserved for FISH analysis. An updated commercialized protocol, including this fixation step, has been made available by VyCAP, the developer of the microsieves in the CTC-Trap project[8]. While we show in one patient that the detected EpCAM^{low} CTC are of cancerous origin, we still need to determine if this is also true for all EpCAM^{low} CTC detected in all patients. For this purpose we have developed a method to release all cells from the microsieve using Proteinase K and sonication. From this mixture of cell debris, DNA is isolated and can be used for mutation analysis with the digital droplet PCR (ddPCR)[9]. The sensitivity of the ddPCR is sufficiently high to detect one mutated allele in a high background of leukocyte DNA and the entire DNA sample can be analyzed in independent runs. Similar to the FISH on microsieve, it is necessary to have prior knowledge of the patient mutation status. However, detection of mutated DNA will not prove they originate from the EpCAM^{low} CTC that were identified on the microsieve, since the single cell level in this approach is lost, but it will give a good indication if EpCAM^{low}/Cytokeratin– CTC are present and missed with our immunostaining when the mutation count in the sample exceeds the EpCAM^{low} CTC count.

In CTC-Trap we developed and implemented the procedure of collecting CellSearch discarded CTC and identification on a microsieve. To validate this procedure, we spiked tumor cells derived from cancer cell lines into blood at one clinical site and distributed these samples to the other clinical sites in

the CTC-Trap consortium for CTC enumeration (**Chapter 3**). This clearly demonstrated the importance of testing protocols at multiple sites in order to get a sense of the variation in the results obtained and identify bottlenecks in the procedures. With three samples per site, the results in CTC recovery already varied noticeably, indicating that patient samples might show an even larger variation. However, when planning to use such applications on a large scale, the validation and standardization of the developed technique is required.

The main focus of cancer type in this thesis has been metastatic non-small cell lung cancer (NSCLC). Lung cancer has the highest mortality of all cancer types and survival rate for this cancer type therefore poor: 85% of the lung cancer patients die within five years after diagnosis[10]. This type of cancer spiked our interest since it is a very aggressive cancer, yet interestingly, these cancer patients have very low numbers of CTC detected with CellSearch. Therefore, we hypothesized, there must be many EpCAM^{low} CTC present in these patients that would likely be found in the EpCAM depleted fraction discarded by CellSearch. Our results however showed that the number of EpCAM^{low} CTC were in the same order of magnitude as EpCAM^{high} CTC. Moreover, their presence was not associated with poor clinical outcome (**Chapter 4 and 6**). So, the question whether CTC in this aggressive disease are simply present at a much lower level or whether they have a completely different phenotype that is missed by our current approach, remains unanswered. The lower frequency of CTC in colorectal, gastric and pancreas cancer, as compared to prostate and breast cancer, can plausibly be explained by the fact that the blood of the veins draining the tumor first have to pass the liver, where part of the CTC will be destroyed. For lung cancer however, this is not the case. In fact, the tumor is even closer to the vascular system. So, in an effort to answer this question, we traveled closer to the origin of CTC: the tumor! We obtained blood samples during lung cancer surgery from the pulmonary vein that drains the lung lobe that contains the tumor, as well as blood from the peripheral artery in the arm. To our surprise, a large number of cells were detected in the pulmonary vein using our EpCAM^{high} and EpCAM^{low} CTC definition, but no CTC were detected in the radial artery[11]. With only the heart between the pulmonary vein and the radial artery, these cells must be destroyed by mechanical forces or enter the vein intermittently, and we just missed the right time point in the blood sample taken from the artery. Therefore, our question still remains unanswered. Research is still ongoing to determine whether or not the detected EpCAM^{high} and EpCAM^{low} cells are indeed tumor cells by performing copy number variation analysis on

single sorted EpCAM^{high} cells and a FISH test for chromosome aneuploidy on the microsieves, respectively.

CTC can be identified, isolated and characterized with many different methods. The CellSearch technology still is the only FDA-cleared system for clinical practice. While many technologies claim to find more CTC than CellSearch does, the clinical relevance of these cells remains underexposed. Therefore, the most important and puzzling finding in this research was the detection of EpCAM^{low} CTC and their relation to patient survival: they show no correlation with overall survival in metastatic NSCLC and prostate cancer patients. This raises a tremendous amount of questions and opens many new avenues of research to pursue. Are they indeed all tumor cells? Why are these cells different from EpCAM^{high} CTC? Are there more differences we do not see yet, on proteomic or genetic level? While they do not contribute to a shorter survival in patients, what is their function and what is their metastatic potential? Are there subpopulations of EpCAM^{low} CTC that have a different prognostic value than these cells? How many more subpopulations of CTC can we identify and what is their relation to the survival of the patient? We have shown their presence in NSCLC and prostate cancer, but are they also present in other cancer types, like metastatic breast or colon cancer? This, and many other questions will have to be answered with an in-depth characterization of EpCAM^{low} and EpCAM^{high} CTC.

In the future

In this research we were able to identify EpCAM^{low} CTC by depleting the blood sample of EpCAM^{high} CTC with CellSearch. Of course this selects for all leukocytes as well, since they are EpCAM negative as well. Therefore, it would be beneficial to positively select for the EpCAM^{low} CTC, preferably with a surface marker to enable the possibility to refrain from permeabilization and keep the cells viable. This will allow extensive characterization and identify the extent of heterogeneous phenotypes present in CTC between patients and within patients. Perhaps, to find a general surface marker that is the counterpart of EpCAM, we need to fall back on known and new methods to investigate possible candidates in a mass or multiplexed fashion[12,13].

One thing all techniques for CTC detection have in common is the fact they all need an operator to determine which cells are CTC and which cells are not. CellSearch presents thumbnails of CTC candidates, based on DAPI and CK positivity, to a trained operator, who will decide if the cells qualify

for all other pre-set criteria. How the operators score these cells is heavily subjective and influenced by the presentation of the images[14]. Identification of CTC with new technologies requires pre-agreed definitions to adhere by. However, even using clearly defined criteria for operators to follow in scoring CTC, as with CellSearch, the discrepancy between operators can be high and this argues for an automated approach to analyse images for cells of interest[15]. Algorithms for processing images and classifying detected cells are currently under development and will reduce the subjective influence of operators in the future.

The need for effective liquid biopsies is growing in order to keep up with the fast expanding field of targeted therapies. Since CTC are rare events in small volumes of blood, the expected frequency will increase when larger volumes of blood are analyzed. To this end, the Diagnostic LeukApheresis (DLA) was developed and is currently in use to analyze large volumes of blood from metastatic prostate, breast and NSCLC patients for detection and analysis of CTC[16]. With this technique large amounts of mononuclear cells are collected, selected based on their density. Techniques are under development to handle such enormous high concentrations of leukocytes, by means of leukocyte depletion or filtration. Now that we have shown more CTC are captured from DLA compared to whole blood[17], the question remains if we can extract more information from these CTC that will aid the decisions in the clinic.

One of the benefits of liquid biopsies is the low-invasiveness for the patient and thereby the ease of material acquisition for analysis. To use liquid biopsies in treatment decisions will prove the validity in acting fast on actual responses from the patient. We analyzed four biomarkers in a single tube and demonstrated that, with exception of $EpCAM^{low}$ CTC, the presence of $EpCAM^{high}$ CTC, $EpCAM^{high}$ tumor derived extracellular vesicles (tdEV) or circulating tumor DNA (ctDNA) is associated with poor overall survival. These tree biomarkers were also analyzed in patients receiving targeted immunotherapy at two time points in their treatment. We aim to determine if changes in CTC, tdEV or ctDNA can predict tumor response and can be used as an early marker of treatment efficacy[18]. Additionally, the challenge for the researcher is to extract as much useful information as possible from a single blood sample and therefore we are investigating the presence of known mutations in $EpCAM^{high}$ CTC and tdEV (from a cartridge) and $EpCAM^{low}$ CTC (from a microsieve) with the sensitive digital droplet PCR procedure, whereas the presence of mutations in ctDNA from plasma can be detected with sequencing.

This thesis shows the current movement in the field of liquid biopsies, where the clinical utility of two subpopulations of CTC, tumor derived extracellular

vesicles and circulating tumor DNA for precision medicine are investigated. It will be most crucial to use the right biomarker at the right time for the right goal, to ensure a fast and effective treatment and a prolonged survival of the patient.

References

1. ISET - Isolation by Size of Tumor Cells. (2017). Available at: http://www.rarecells.com/accueil.html.
2. Parsortix Technology - ANGLE plc. (2017). Available at: https://angleplc.com/pasortix-technology/how-it-works/.
3. ClearCell FX1 System - Clearbridge BioMedics. (2017). Available at: http://www.clearbridgebiomedics.com/products/clearcell-fx1-system/.
4. Coumans, F. A. W., Doggen, C. J. M., Attard, G., de Bono, J. S. & Terstappen, L. W. M. M. All circulating EpCAM+CK+CD45- objects predict overall survival in castration-resistant prostate cancer. Ann. Oncol. 21, 1851–7 (2010).
5. Epic Sciences. (2017). Available at: http://www.epicsciences.com/.
6. Deelstra, F. Identification of circulating tumour cell subpopulations - University of Twente Student Theses. (2017). Available at: http://essay.utwente.nl/74315/.
7. Hudepol, C. Novel markers for detection of CTCs without EpCAM expression - University of Twente Student Theses. (2017). Available at: http://essay.utwente.nl/74362/.
8. VyCAP. (2017). Available at: https://www.vycap.com/literature/protocols/.
9. Swennenhuis JF, de Wit S, Terstappen LWMM. Digital droplet PCR test for detection of low abundant CTC captured on microsieves. In: International Symposium on Minimal Residual Cancer. ; 2018.
10. Volksgezondheid en Zorg Nederland. (2018). Available at: https://www.volksgezondheidenzorg.info/onderwerp/kanker.
11. Tamminga, M. & de Wit, S. Circulating tumor cells measured in the pulmonary vein and radial artery druing surgery of non-small cell lung cancer. in American Association for Cancer Research (2018).
12. de Kruif, J., Terstappen, L., Boel, E. & Logtenberg, T. Rapid selection of cell subpopulation-specific human monoclonal antibodies from a synthetic phage antibody library. Proc. Natl. Acad. Sci. U. S. A. 92, 3938–42 (1995).
13. Yao, Y. et al. CyTOF supports efficient detection of immune cell subsets from small samples. J. Immunol. Methods 415, 1–5 (2014).
14. Zeune, L. L. et al. Quantifying HER-2 expression on circulating tumor cells by ACCEPT. PLoS One 12, e0186562 (2017).
15. Zeune, L. L., de Wit, S. & Berghuis, A. M. S. Evaluating the consensus in circulating tumor cell scoring. in Advances in Circulating Tumour Cells (2017).
16. Andree, K.C., et al. Circulating tumor cells in the peripheral blood and leukapheresis product of non-small cell lung cancer patients. in American Association for Cancer Research (2018).
17. Andree, K.C., et al. Significant increase in CTC in metastatic breast and prostate cancer through Diagnostic LeukApheresis. Prep. Submiss. (2018).
18. Tamminga, M. & de Wit, S. Circulating tumor cells and tumor derived extracellular vesicles as a possible marker for tumor response and survival in patients with non-small cell lung cancer treated with immunotherapy. in American Association for Cancer Research (2018).

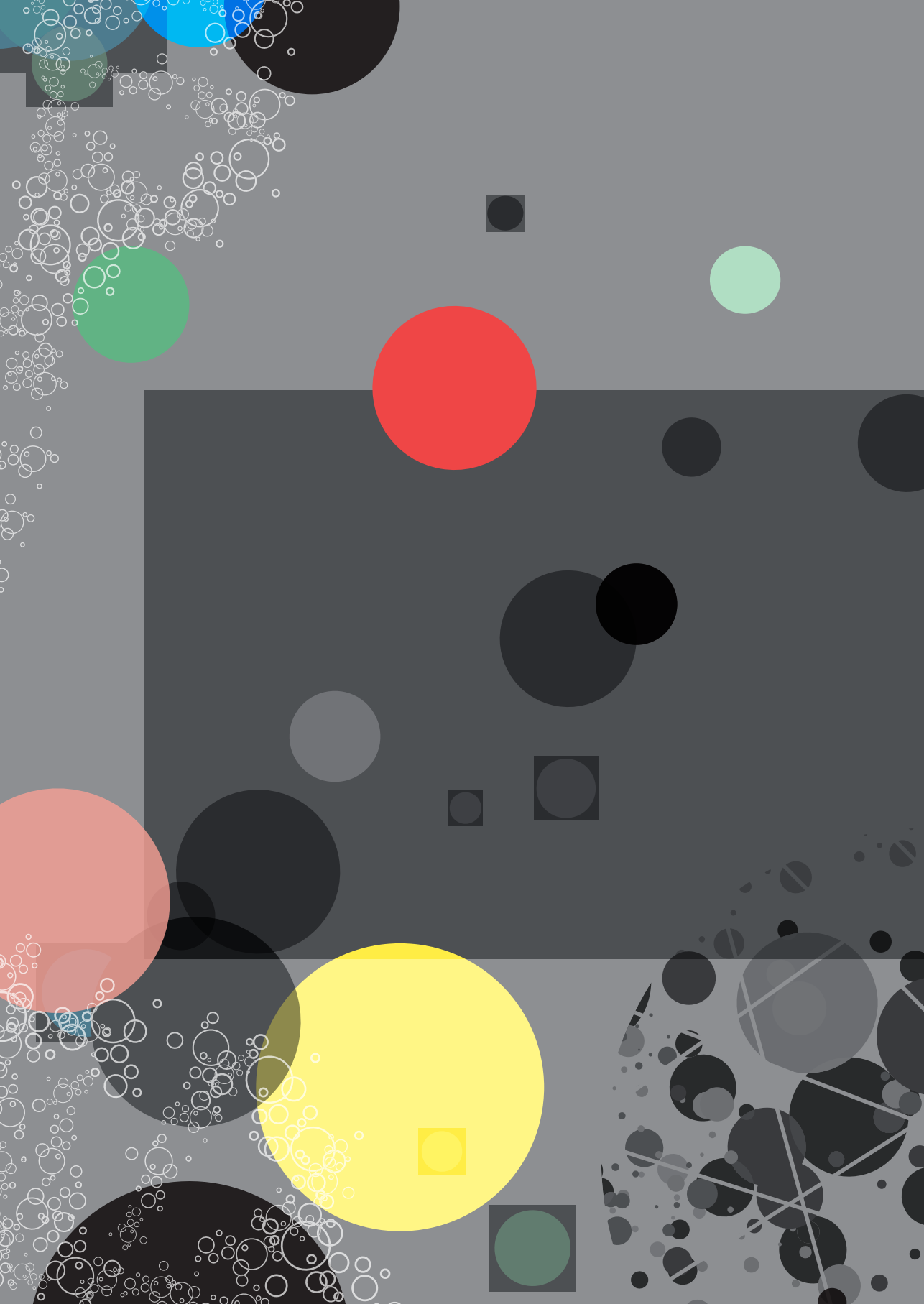

Supplemental

Summary

As cancer progresses, tumor cells can travel through the blood circulation to form tumors at distant sites in the body. These circulating tumor cells (CTC) can be isolated from blood and used as a liquid biopsy for the real-time information they carry about the tumor. Their presence can be used to evaluate and monitor the treatment effect on the patient and is related to a poor overall survival of the patient. CellSearch® is the only CTC isolation system cleared for clinical applications and targets the epithelial cell adhesion molecule (EpCAM) for enumeration of CTC. However, CTC with low EpCAM expression might be missed, and their information subsequently be lost. In the EU-FP7 CTC-Trap project, tools were developed to capture and analyze $EpCAM^{high}$ and $EpCAM^{low}$ CTC in patients. In this thesis we investigated the presence of $EpCAM^{high}$ and $EpCAM^{low}$ CTC with multiple patient studies and explored the potential of multiple cancer biomarkers from a single blood tube as a liquid biopsy.

We looked into the relation of $EpCAM^{high}$ and $EpCAM^{low}$ CTC with survival in metastatic non-small cell lung cancer (NSCLC) patients and metastatic castrate-resistant prostate cancer patients. From one tube of blood $EpCAM^{high}$ CTC were enumerated with CellSearch, followed by $EpCAM^{low}$ CTC capturing and immunostaining on a microsieve. We showed that the presence of $EpCAM^{high}$ CTC correlate with poor overall survival of the patients, whereas $EpCAM^{low}$ CTC were not related. This raises the question whether these identified $EpCAM^{low}$ CTC are of cancerous origin or of epithelial origin. Therefore, the genetic origin of these $EpCAM^{low}$ and cytokeratin expressing cells on a microsieve was investigated by developing a fluorescent in situ hybridization protocol that is performed on the microsieve itself. In one NSCLC patient, we showed the presence of genetic aberrancies in $EpCAM^{low}$ cells, identical to the mutations present in the metastatic tumor of the patient. In addition, cells that were previously not identified with the immunostaining also showed genetic aberrancies. These findings suggest that the captured $EpCAM^{low}$/Cytokeratin+ cells are indeed of cancerous origin and that some CTC might be missed with the current immunostaining.

We analyzed multiple cancer biomarkers in a single tube of blood from 97 metastatic NSCLC patients and explored their potential as a liquid biopsy. The presence of $EpCAM^{high}$ CTC, $EpCAM^{high}$ tumor derived extracellular vesicles (tdEV) and circulating tumor DNA (ctDNA) were associated with poor

overall survival, yet EpCAM^{low} CTC showed no association. The presence of two or more biomarkers discriminated an unfavorable subgroup of NSCLC patients, but the added predictive value of the combined markers was low. We explored the presence of specific DNA mutations in these biomarkers, which might be of indispensable value to the clinical application of these biomarkers. Elevated levels of these biomarkers restrict its potential use to approximately 20% of these patients. Yet, mutations present in the primary tumor could be detected in ctDNA from patients with EpCAM^{high} CTC, with EpCAM^{low} CTC and without any CTC.

To improve detection of CTC, we classified all cell populations present after CellSearch EpCAM-enrichment with advanced image analysis, using the open source imaging program ACCEPT and Deep Learning segmentation. We detected large numbers of nucleated events present in 300 NSCLC patient samples and 127 control samples. Anti-CD16 was added to the CellSearch immunostaining for improved leukocyte detection and showed that a major population of nucleated cells is indeed CD16 positive, which remain unidentified with the standard CellSearch immunostaining. An alternative light source for improved detection of fluorophores showed increased detection of CD45 expressing leukocytes. Unstained nuclei were investigated for the presence of a cell membrane with wheat germ agglutinin staining, which indicated that some cells are without a cell membrane and will remain unidentified with immunostaining approaches. A small cell population with cellular membranes remains unidentified and will need to be investigated further to unveil the presence of any EpCAM^{high} CTC without cytokeratin expression.

To conclude, we investigated the presence of two CTC populations in metastatic cancer patients. The results presented in this thesis warrant an in-depth characterization of EpCAM^{low} and EpCAM^{high} CTC to determine their value as a liquid biopsy and potential use in the clinic, to aid the patient with a fast and effective treatment for prolonged survival.

Samenvatting

Naarmate tumor groeit, kunnen kankercellen door de bloedcirculatie reizen om tumoren te vormen op andere plekken in het lichaam. Deze circulerende tumorcellen (CTC) kunnen uit bloed geïsoleerd en gebruikt worden als een zogenoemde "vloeibare biopsie", omdat deze cellen zeer actuele informatie van de tumor bij zich dragen. De aanwezigheid van CTC kan worden gebruikt om het behandelingseffect op de patiënt te volgen en evalueren en is gerelateerd aan slechte overlevingkansen van de patiënt. CellSearch® is het enige CTC-isolatiesysteem dat goedgekeurd is voor klinische toepassingen en is gericht op het epitheliale celadhesiemolecuul (EpCAM) voor de verrijking van CTC. CTC met een lage EpCAM-expressie kunnen echter gemist worden tijdens deze verrijking en de inforamtie die deze CTC bij zich dragen gaat vervolgens verloren. In het Europese Unie FP7 project "CTC-Trap" zijn hulpmiddelen ontwikkeld om CTC met $EpCAM^{hoge}$ en $EpCAM^{lage}$ expressie van patiënten te vangen en analyseren. In dit proefschrift hebben we de aanwezigheid van $EpCAM^{hoge}$ en $EpCAM^{lage}$ CTC aan de hand van meerdere patiëntenstudies onderzocht, evenals hun potentie als een vloeibare biopsie, met meerdere kankerbiomarkers uit een enkele bloedbuis.

We hebben gekeken naar de relatie van $EpCAM^{hoge}$ en $EpCAM^{lage}$ CTC met overleving van patiënten bij uitgezaaide niet-kleincellig longkankerpatiënten (NSCLC) en bij patiënten met uitgezaaide castraatresistente prostaatkanker. Uit één buis bloed werden $EpCAM^{hoge}$ CTC verrijkt met CellSearch, gevolgd door het vangen van $EpCAM^{lage}$ CTC op een microzeefje en deze vervolgens te kleuren met fluorescerence antilichamen. We hebben aangetoond dat de aanwezigheid van $EpCAM^{hoge}$ CTC correleert met een slechte overleving van de patiënten, terwijl de aanwezigheid van $EpCAM^{lage}$ CTC hier niet mee gecorreleerd was. Dit werpt de vraag op of deze $EpCAM^{lage}$ CTC wel van de tumor afkomstig zijn of dat deze cellen een andere epitheliale oorsprong hebben. Daarom werd de genetische oorsprong van deze $EpCAM^{lage}$ cellen onderzocht. Dit hebben we gedaan door het ontwikkelen van een fluorescent in situ hybridisatieprotocol dat kan worden uitgevoerd op het microzeefje zelf. Bij één NSCLC-patiënt toonden we de aanwezigheid van genetische afwijkingen in de $EpCAM^{lage}$-cellen aan. Deze afwijkingen waren identiek aan de mutaties die aanwezig waren in de uitgezaaide tumor van de patiënt. Bovendien vertoonden andere cellen ook genetische afwijkingen,

terwijl die eerder niet waren geïdentificeerd als EpCAM^{lage} CTC met de immunokleuring op het microzeefje. Deze bevindingen suggereren dat de gevangen EpCAM^{lage}-cellen inderdaad van de tumor afkomstig zijn en dat sommige CTC kunnen worden gemist met de huidige immunokleuring.

We analyseerden meerdere kankerbiomarkers in een enkele buis met bloed van 97 uitgezaaide NSCLC patiënten en verkenden hun potentie als een vloeibare biopsie. De aanwezigheid van EpCAM^{hoge} CTC, EpCAM^{hoge} tumor-afgeleide celblaasjes (tdEV) en circulerend tumor-DNA (ctDNA) waren geassocieerd met een slechte overleving van de patients, maar EpCAM^{lage} CTC vertoonde geen associatie met overleving. De aanwezigheid van twee of meer biomarkers onderscheidde een ongunstige subgroep van NSCLC-patiënten, maar de toegevoegde voorspellende waarde van de gecombineerde biomarkers was laag. We onderzochten de aanwezigheid van specifieke DNA-mutaties in deze biomarkers, die van onschatbare waarde kunnen zijn voor de klinische toepassing van deze biomarkers. Verhoogde niveaus van deze biomarkers beperken het potentiële gebruik ervan echter tot ongeveer 20% van deze patiënten. Toch konden mutaties die aanwezig waren in de primaire tumor worden gedetecteerd in het ctDNA van patiënten met EpCAM^{hoge} CTC, met EpCAM^{lage} CTC en zonder enige CTC.

Om detectie van CTC te verbeteren, hebben we alle celpopulaties die aanwezig zijn na de CellSearch EpCAM^{hoge} CTC-verrijking geclassificeerd met geavanceerde beeldanalyse. Hiervoor hebben we het open source programma ACCEPT en Deep Learning-segmentatie gebruikt. We ontdekten dat hoge aantallen celkernen aanwezig waren in het bloed van 300 NSCLC patiënten en 127 gezonde donoren. Immunokleuring voor CD16 werd toegevoegd aan de CellSearch kleuring voor een verbeterde detectie van leukocyten. Dit toonde aan dat een belangrijke populatie van celkernen inderdaad CD16-positief is, die dus niet geïdentificeerd worden met de standaard CellSearch immunokleuring. Een alternatieve lichtbron voor een verbeterde detectie van de fluoroforen die gebruikt worden tijdens de kleuring, vertoonde een verhoogde detectie van leukocyten die CD45 tot expressie brengen. Ongekleurde kernen werden onderzocht op de aanwezigheid van een celmembraan met een agglutinine-kleuring, wat aantoonde dat sommige cellen geen membraan hebben en daardoor niet geïdentificeerd kunnen worden met immunokleuringen. Een kleine populatie van cellen met celmembranen blijft tot op heden onbekend van oorsprong en moet verder worden onderzocht om de aanwezigheid van EpCAM^{hoge} CTC zonder cytokeratine-expressie te onthullen.

Als conclusie: we hebben de aanwezigheid van twee CTC-populaties bij patiënten met uitgezaaide kanker onderzocht. De resultaten gepresenteerd in

dit proefschrift rechtvaardigen een grondige karakterisering van EpCAM^{lage} en EpCAM^{hoge} CTC om hun waarde te bepalen als een vloeibare biopsie en hun potentiële gebruik in de kliniek. Het doel hiervan is om de patiënt te helpen door een snelle en effectieve behandeling aan te bieden met de kans op een langdurige overleving.

Publications

Journals

Detection of circulating tumor cells
S. de Wit, G. van Dalum, L.W.M.M. Terstappen
Scientifica (Cairo). 2014:819362; doi:10.1155/2014/819362

The detection of EpCAM(+) and EpCAM(-) circulating tumour cells
S. de Wit*, G. van Dalum*, A.T.M. Lenferink, A.G.J. Tibbe, T.J.N. Hiltermann, H.J.M. Groen, C.J.M. van Rijn, L.W.M.M. Terstappen
Scientific Reports 5, 12270 (2015); doi:10.1038/srep12270

$EpCAM^{high}$ and $EpCAM^{low}$ circulating tumour cells in metastatic prostate and breast cancer patients
S. de Wit, M. Manicone, E. Rossi, R. Lampignano, L. Yang, B. Zill, A. Rengel-Puertas, M. Ouhlen, M. Crespo, A.M.S. Berghuis, K.C. Andree, R. Vidotto, E.K. Trapp, M. Tzschaschel, E. Colomba, G. Fowler, P. Flohr, P. Rescigno, M. Sousa Fontes, R. Zamarchi, T. Fehm, H. Neubauer, B. Rack, M. Alunni-Fabbroni, F. Farace, J.S. De Bono, M.J. IJzerman, L.W.M.M. Terstappen
Submitted for publication

Genetic confirmation of cancerous origin in EpCAM negative circulating tumor cells in a non-small cell lung cancer patient
S. de Wit, H.W. Mulder, J.F. Swennenhuis, T.J.N. Hiltermann, H.J.M. Groen, L.W.M.M. Terstappen
Submitted for publication

Single tube liquid biopsy for advanced non-small cell lung cancer
S. de Wit, E. Rossi, S. Weber, M. Tamminga, M. Manicone, J.F. Swennenhuis, K.G.M. Groothuis, R. Vidotto, A. Facchinetti, L.L. Zeune, E. Schuuring, R. Zamarchi, T.J.N. Hiltermann, M.R. Speicher, E. Heitzer, L.W.M.M. Terstappen, H.J.M. Groen
Submitted for publication

Classification of cell populations in CTC enriched samples by advanced image analysis
S. de Wit*, L.L. Zeune*, C. Brune, G. van Dalum, T.J.N. Hiltermann, H.J.M. Groen, L.W.M.M. Terstappen
In preparation for publication

How to agree on a CTC: Evaluating the consensus in circulating tumor cell scoring
L.L. Zeune*, S. de Wit*, A.M.S. Berghuis, G. van Dalum, F. Tanney, M. Repollet, J.F. Swennenhuis, M.J. IJzerman, C. Brune, L.W.M.M Terstappen
In preparation for publication

Conference contributions

Poster presentations

CTC-Trap: the European route to a liquid biopsy for all cancer patients
A.M.C. Barradas, S. de Wit, J.F. Swennenhuis, L.W.M.M. Terstappen
XXII Porto Cancer Meeting; Porto, Portugal; 11-12 April 2013

Circulating tumor cells in metastatic lung cancer enriched by EpCAM expression and physical characteristics
S. de Wit, G. van Dalum, J. van Dalum, A.T.M. Lenferink, A.G.J. Tibbe, C.J.M. van Rijn, T.J.N. Hiltermann, H.J.M. Groen, L.W.M.M. Terstappen
American Association for Cancer Research; San Diego CA, USA; 5-9 April 2014; #4826

EpCAM negative circulating tumor cells in metastatic lung cancer enriched by filtration
S. de Wit, G. van Dalum, A.T.M. Lenferink, A.G.J. Tibbe, C.J.M. van Rijn, T.J.N. Hiltermann, H.J.M. Groen, L.W.M.M. Terstappen
Advances in Circulating Tumor Cells; Crete, Greece; 8-11 October 2014

EpCAM negative circulating tumor cells in metastatic lung cancer enriched by filtration
S. de Wit, G. van Dalum, A.T.M. Lenferink, A.G.J. Tibbe, C.J.M. van Rijn, T.J.N. Hiltermann, H.J.M. Groen, L.W.M.M. Terstappen
MIRA-dag; Enschede, The Netherlands; 27 November 2014

EpCAM+ and EpCAM– Circulating Tumor Cells in Metastatic Lung Cancer
S. de Wit, G. van Dalum, A.T.M. Lenferink, A.G.J. Tibbe, C.J.M. van Rijn, T.J.N. Hiltermann, H.J.M. Groen, L.W.M.M. Terstappen
American Association for Cancer Research, Philadelphia PA, USA; 18-22 April 2015; #377

What is and what is not a Circulating Tumor Cell?
K.C. Andree, A. Mentink, S. de Wit, C. Brune, G. van Dalum, L.L. Zeune, A. Nanou, J.F. Swennenhuis, L.W.M.M. Terstappen
[Oral presentation] 10th ISMRC International Symposium on Minimal Residual Cancer: Liquid Biopsy in Cancer Diagnostics and Treatment; Hamburg, Germany; 19-21 March 2016

Liquid biopsy in advanced NSCLC: EpCAM+ and EpCAM– circulating tumor cells, tumor derived extracellular vesicles and cell-free circulating tumor DNA
S. de Wit, M. Tamminga, E. Heitzer, J.F Swennenhuis, E. Schuuring, L.L. Zeune, M.R. Speicher, T.J.N Hiltermann, L.W.M.M. Terstappen, H.J.M. Groen
American Association for Cancer Research; Washington DC, USA; April 1-5 2017; #LB-250

EpCAM+ and EpCAM– circulating tumor cells in metastatic cancer patients: a multicenter study
S. de Wit, M. Manicone, E. Rossi, E.K. Trapp, R. Lampignano, M. Ouhlen, M. Crespo, L.L Zeune, K.C. Andree, J.F. Swennenhuis, R. Vidotto, R. Zamarchi, M. Alunni-Fabbroni, M. Tzschaschel, B. Rack, H. Neubauer, T. Fehm, E. Colomba, F. Farace, P. Flohr, J. De Bono, L.W.M.M. Terstappen
American Association for Cancer Research; Washington DC, USA; 1-5 April 2017; #3787

Circulating tumor cells measured in the pulmonary vein and the radial artery during surgery of non-small cell lung cancer
M. Tamminga, S. de Wit, J.F. Swennenhuis, C. van de Wauwer, T.J. Klinkenberg, T.J.N. Hiltermann, H.J.M. Groen, L.W.M.M. Terstappen
American Association for Cancer Research; Washington DC, USA; 1-5 April 2017; #3783

Single tube liquid biopsy for NSCLC
S. de Wit, E. Rossi, E. Heitzer, M. Tamminga, M. Manicone, J.F. Swennenhuis, R. Vidotto, A. Facchinetti, L.L. Zeune, E. Schuuring, R. Zamarchi, T.J.N. Hiltermann, M. Speicher, L.W.M.M. Terstappen, H.J.M. Groen
3rd ACTC Advances in Circulating Tumour Cells; Rhodes, Greece; 4-7 October 2017

Improving identification of cells enriched by CellSearch
S. de Wit, L.L. Zeune, L.W.M.M. Terstappen
3rd ACTC Advances in Circulating Tumour Cells; Rhodes, Greece; 4-7 October 2017

Evaluating the consensus in circulating tumor cell scoring
L.L. Zeune, S. de Wit, A.M.S. Berghuis, G. van Dalum, F. Tanney, M. Repollet, M.J. IJzerman, C. Brune, L.W.M.M. Terstappen
3rd ACTC Advances in Circulating Tumour Cells; Rhodes, Greece; 4-7 October 2017

Circulating tumor cells measured in the pulmonary vein and radial artery during surgery of early non-small cell lung cancer
M. Tamminga, S. de Wit, J.F. Swennenhuis, C. van de Wauwer, T.J. Klinkenberg, D. Spierings, T. J.N. Hiltermann, H.J.M. Groen, L.W.M.M. Terstappen
3rd ACTC Advances in Circulating Tumour Cells; Rhodes, Greece; 4-7 October 2017

Circulating tumor cells in the peripheral blood and leukapheresis product of NSCLC patients
M. Tamminga, K.C. Andree, S. de Wit, J.F. Swennenhuis, T.J.N. Hiltermann, D. Spierings, H.J.M. Groen, L.W.M.M. Terstappen
3rd ACTC Advances in Circulating Tumour Cells; Rhodes, Greece; 4-7 October 2017

Classification of cell populations in CTC enriched samples by advanced image analysis
S. de Wit, L.L. Zeune, C.Brune, G. van Dalum, T.J.N. Hiltermann, H.J.M. Groen, L.W.M.M. Terstappen
American Association for Cancer Research; Chicago IL, USA; 14-18 April 2018; #3246

Circulating tumor cells measured in the pulmonary vein and the radial artery during surgery of non-small cell lung cancer
M. Tamminga, S. de Wit, J.F. Swennenhuis, C. van de Wauwer, T.J. Klinkenberg, E.M.D. Schuuring, D. Spierings, H. van den Bos, T.J.N. Hiltermann, H.J.M. Groen, L.W.M.M. Terstappen
American Association for Cancer Research; Chicago IL, USA; 14-18 April 2018; #5594

Circulating tumor cells and tumor derived extracellular vesicles as a possible marker for tumor response and survival in patients with non-small cell lung cancer treated with immunotherapy
M. Tamminga, S. de Wit, J.F. Swennenhuis, E. Heitzer, M. Speicher, T.J.N. Hiltermann, E.M.D. Schuuring, L.W.M.M. Terstappen, H.J.M. Groen
American Association for Cancer Research; Chicago IL, USA; 14-18 April 2018; #3606

Digital droplet PCR test for detection of low abundant CTC captured on microsieves
J.F. Swennenhuis, S. de Wit, L.W.M.M. Terstappen
11th International Symposium on Minimal Residual Cancer; Montpellier, France; 3-5 May 2018

Circulating tumor cells correlate to response of immune modulating therapy in non-small cell lung cancer patients
M. Tamminga, S. de Wit, T.J.N. Hiltermann, E. Schuuring, L.W.M.M. Terstappen, H.J.M. Groen
11th International Symposium on Minimal Residual Cancer; Montpellier, France; 3-5 May 2018

Deep Learning to identify circulating tumor cells by ACCEPT
L.L. Zeune, S. de Wit, G. van Dalum, A. Nanou, K.C. Andree, J.F. Swennenhuis, L.W.M.M. Terstappen, C. Brune
11th International Symposium on Minimal Residual Cancer; Montpellier, France; 3-5 May 2018

Oral presentations

Assay for CTC Filtration and Staining
S. de Wit
CTC-Trap conference meeting; Enschede, The Netherlands; 23-25 September 2013

Clinical samples: Antibodies, Staining and Scanning
S. de Wit
CTC-Trap conference meeting; Talinn, Estonia; 8-9 September 2015

CellSearch waste filtration: validation study
S. de Wit
CTC-Trap conference meeting; London, United Kingdom; 25-26 August 2016

One tube liquid biopsy for NSCLC
S. de Wit, E. Rossi, E. Heitzer, M. Tamminga, M. Manicone, R. Vidotto, A. Facchinett, J.F. Swennenhuis, L.L. Zeune, E. Schuuring, R. Zamarchi, T.J.N. Hiltermann, M. Speicher, L.W.M.M. Terstappen, H.J.M. Groen
CANCER-ID conference meeting; Rhodes, Greece; 3 October 2017

One tube liquid biopsy for NSCLC
S. de Wit, E. Rossi, E. Heitzer, M. Tamminga, M. Manicone, R. Vidotto, A. Facchinett, J.F. Swennenhuis, L.L. Zeune, E. Schuuring, R. Zamarchi, T.J.N. Hiltermann, M. Speicher, L.W.M.M. Terstappen, H.J.M. Groen
DCC-NET Retreat; Schloss Krickenbeck Nettetal, Germany; 3 November 2017


S

Acknowledgements

Mijn lieve familie

Mama
Papa & Annelies
Tico & Luc
"Iets met kankercellen" – dat is de perfecte samenvatting!

Mijn thuis

Thijs – *zonder jou was dit echt nooit gelukt!*
Sofia – *mijn liefste meisje. Ik hou van jullie.*

Mijn promotor

Leon – *dank je wel voor je begeleiding, enthousiaste ideeën, eindeloos geduld en vele contractverlengingen die nodig waren om dit verhaal te schrijven. Bij menig ander begeleider zou het niet mogelijk geweest zijn en dat maakt dit extra bijzonder. Je druk of gepaste afstand op de juiste momenten zorgde ervoor dat ik zelf weer zin kreeg om verder te gaan, wat ons uiteindelijk tot dit boekwerk brengt!*

Thanks to all the **students** *who contributed to one of my many projects*

Maria Coelho
Linda Holland
Anika Schumacher
Esther Smeets
David den Houting
Daniëlle Koerhuis
Chaja Hudepol
Froukje Deelstra
en voor
Heleen Mulder *een speciaal dank-je-wel voor je fantastische bijdrage aan hoofdstuk 5!*

Vanuit het **UMCG** *kwam een eindeloze levering van patiëntenmateriaal en overlevingsdata die dit proefschrift mogelijk maakten*

Harry Groen
Menno Tamminga
Jeroen Hiltermann
Alle patiënten
Dank jullie wel!

Mijn paranimfen — *wat fijn dat jullie deze dag bij mij staan!*

Charlotte — *je bent mijn lieve vriendinnetje met eindeloos support tijdens de afgelopen jaren, waarin we vrijwel alles met elkaar deelden. Ik hoop je nog lang aan mijn zijde te hebben!*

Kiki — *mijn Roomie, projectmaatje en klankbord met wie ik zowat heel Europa doorkruist heb. Altijd supergezellig met jou!*

My Roomies

Kiki
Agustin
Yoon
Guus
Barbara
Bridgette

It has been a blast sharing room 4.435 with you!!!

Special collaborations

Joost S — *met veel enthousiasme op allerlei projecten samengewerkt, studenten en labbench gedeeld en leuke tripjes gemaakt. Dank je wel voor ALLES!*

Leonie — *thank you for letting me be your ACCEPT guinea pig :) I hope you're also proud of what we managed to create in chapter 7 and I really appreciate your hard work in the last weeks before the deadline. I hope I can do the same for you in a few weeks!*

MCBP *would not be MCBP without it's amazing members*

Afroditi*
Anouk*
Arjan
Aufried
Cees
Christian
Dodo*
Fikri
Frank
Hoon
Ingrid*
Ivan
Joost vD
Joris
Joska
Lisa
Markus
Michiel
Niels
Pepijn
Richard
Xichen

* *special hug for you!*

About the Author

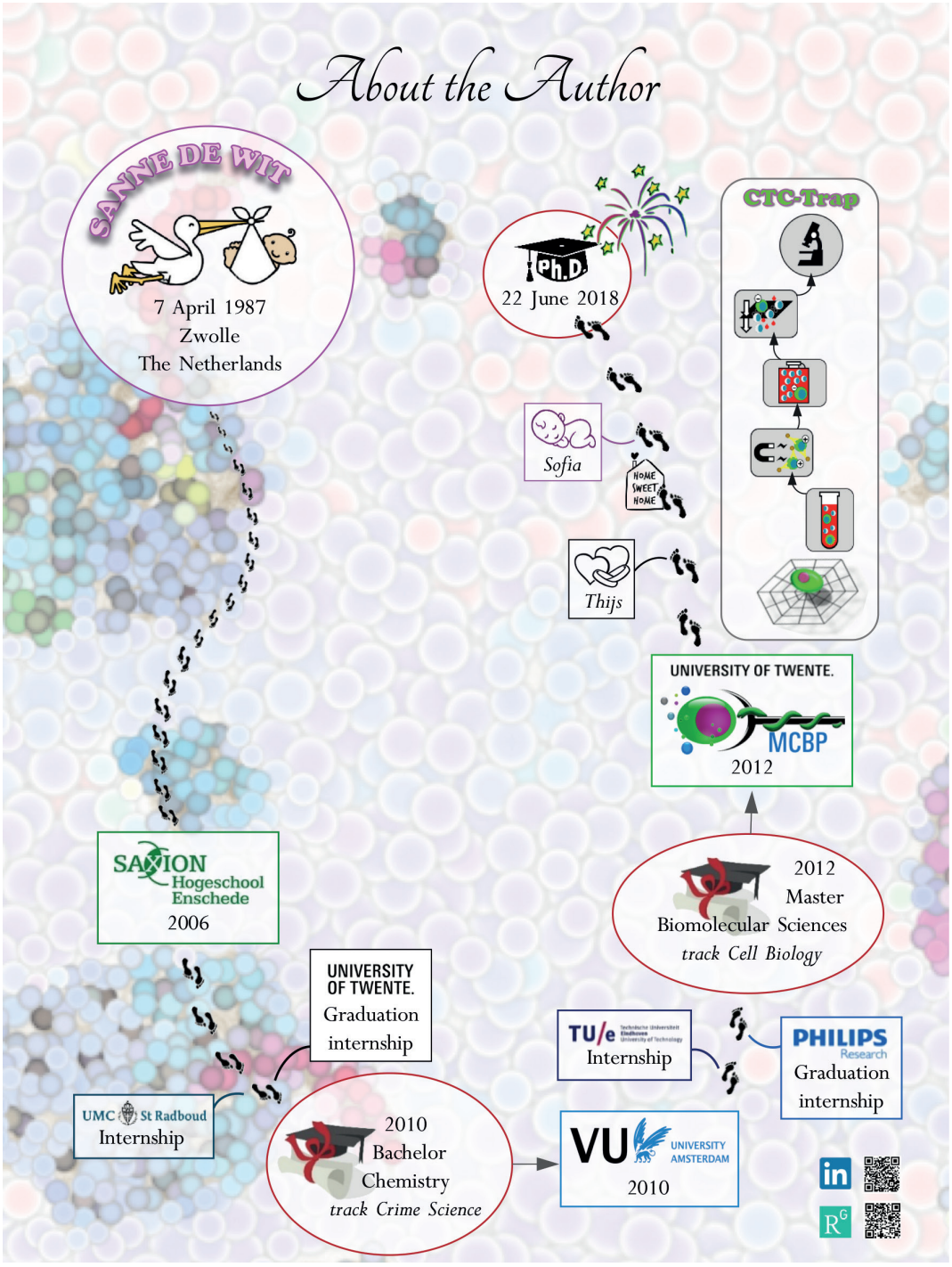

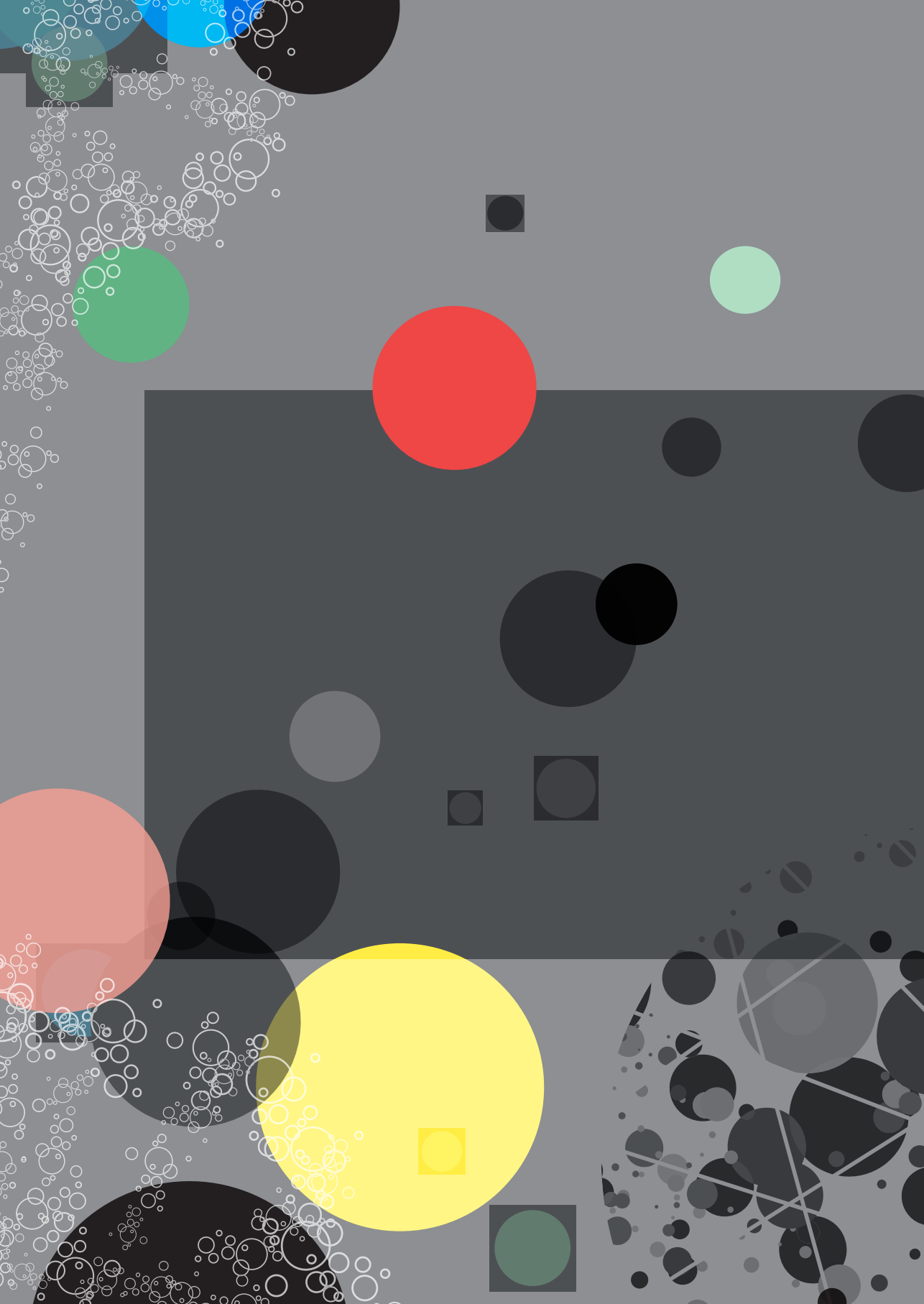

Appendix

Standard Operating Procedures

In the CTC-Trap program several Standard Operating Procedures (SOPs) were designed for all the procedures that were involved in the program (see schematic below). By following these SOPs, equal handling and processing of samples is ensured, thereby obtaining comparative results that can be used for joined papers from the consortium. All SOPs can be found on *https://www.utwente.nl/en/tnw/mcbp/protocolsandtools/*.

This thesis describes the development in collecting EpCAM^{low} cells after CellSearch (SOP.3.: see Protocol I) and the filtration and immunofluorescent labelling of these cells (SOP.6.: see Protocol II). How to proceed with scoring of CTC on a microsieve is described as well (see Protocol III). During the CTC-Trap program, plasma was stored from all patient samples as well for future analysis (see Protocol IV).

For molecular analysis of the cells captured on the microsieve, two protocols were developed. For analysis of the cells on the microsieve, a FISH protocol can be used (see Protocol V). For mutation detection, DNA can be isolated from the microsieves (see Protocol VI).

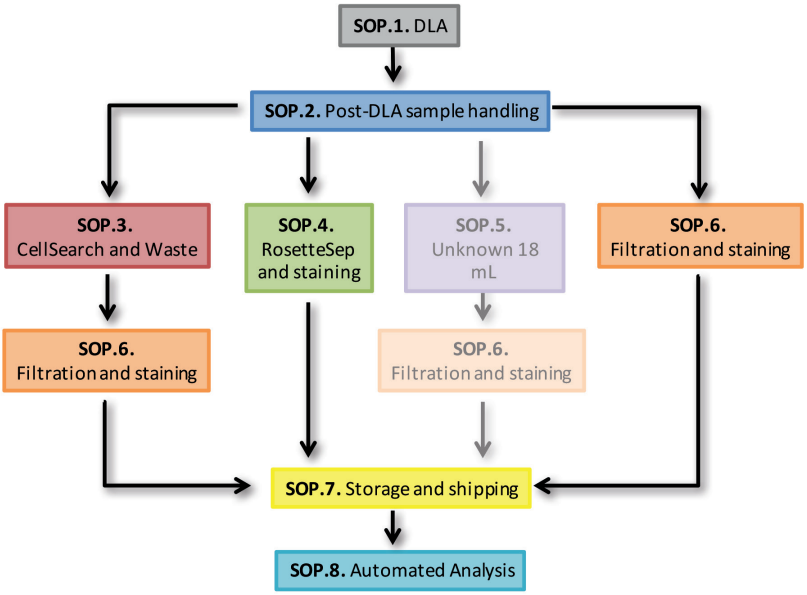

Protocol I Collection of EpCAM^{low} blood samples after CellSearch®

This protocol was first described in Chapter 4 of this thesis, and was used thoughout the CTC-Trap program. The Automated Sample Collection Device (ASCD) can be attached to the outlet tube from the CellSearch® Autoprep. The deviced uses a laptop to control the ASCD program.

Collection of blood samples

ASCD procedure

1. To start the ASCD, start the program on the laptop. Follow the instructions on the screen.
   - Always place a whole blood sample at the first sample station in the Autoprep. The ASCD uses the red colour of the first blood sample to start collection. Based on this, it will determine the schedule of collection of all other samples, not using the red blood cells for detection anymore.
   - If you run the CellSearch Control Cells as well, load these at the last position of the Autoprep to prevent cross contamination with the other collected samples.

2. Add 1 mL 0.2M EDTA (pH 7.6) to the 50 mL Greiner tubes that will collect samples to prevent coagulation.

3. Start the Autoprep first, and start the ASCD collection within 3 minutes after this.
   - It is normal that the total volume of the samples differ from each other. This is dependent on the amount of samples loaded into the Autoprep.
   - The waste tubes can contain some red colour; these are highly diluted red blood cells and is normal.

Manual procedure

The discarded EpCAM^{low} blood samples can be collected manually as well, without the use of the ASCD.

1. Add 1 mL 0.2M EDTA (pH 7.6) to the 50 mL Greiner tubes that will collect samples to prevent coagulation.

2. Unscrew the top of the waste container (see Figure 1, left). When you see the blood coming out of the Autoprep into the tubing, place a 50 mL Greiner tube under the outlet (see Figure 2, right).
   - The waste can exit the tube at a high flow rate and therefore it is advised to start with a larger container to get some feeling for the blood flow.
   - Take proper protection precautions.

3. Stop collecting the sample when you see red blood cells are gone from the waste tubing and Instrument Buffer is discarded.
   - Usually, the amount of volume collected is between 25 mL and 40 mL.
   - Sometimes very diluted blood comes through, be careful not to start collecting the next sample in the previous sample tube.

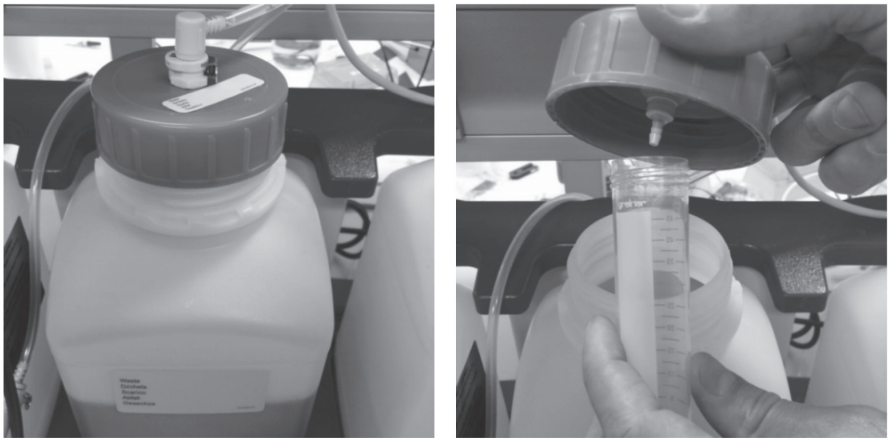

Figure 1. Manual waste collection from the CellSearch Autoprep by unscrewing the top from the waste container (left) and collecting the sample in a 50 mL Greiner tube.

Time line for sample collection

This table lists the approximate time in minutes of CellSearch Autoprep Waste sample exiting the waste tube and arriving at the ASCD.

Total samples in run	Sample number							
	1	2	3	4	5	6	7	8
1	60.7							
2	63.6	73.9						
3	66.1	76.4	88.7					
4	68.6	78.7	91.1	102.8				
5	71.0	81.2	93.5	105.2	118.2			
6	73.4	83.7	96.1	107.8	120.8	133.7		
7	76.0	86.3	98.7	110.4	123.4	136.3	149.3	
8	78.6	88.9	101.3	113.0	126.1	139.0	151.9	164.9

Cartridges

Scan and score the cartridge according to CellSearch protocol. Directly after scanning the cartridge in the CellTracks, remove the cartridge from the Magnest and store this in the refrigerator (4°C) for a maximum of 4 weeks. Use careful labelling to be able to locate samples after a long period, also at different sites in the consortium. Note the CTC count and lot number of the used CTC kit on the label as well.

Checklist

Sample name 1 2 3 4		5 6 7 8	
Operator name			
Draw date	Clinical site		
Prep date	Clinical site		
Cartridge scan date	Clinical site		
Was plasma collected?	☐Yes	☐No	
Did the CellSearch run without errors?	☐Yes	☐No	
Kit and lot number			
Was Waste collected without errors?	☐Yes	☐No	
Was EDTA added to all collection containers?	☐Yes	☐No	
Volume sample in collection tubes 1 2 3 4		5 6 7 8	
Were the cartridges scanned and scored?	☐Yes	☐No	
Cartridge ID 1 5 2 6 3 7 4 8		CTC count 1 5 2 6 3 7 4 8	
Were cartridges stored at 4°C for max 4 weeks?	☐Yes	☐No	
Notes			

Protocol II Filtration and immunofluorescent staining of cells on microsieves

This protocol describes the processing of the EpCAM^{low} blood samples collected after CellSearch®, used in Chapter 3 of this thesis and – with slightly different immunostaining cocktails – in Chapter 4 and 6.

Buffers

- All buffers should be filtered before use. Keep them as much closed as possible to prevent any contamination by dirt or dust particles.
- PBS/BSA 1% for washing
- PBS/BSA 1%/saponin 0.15% for permeabilization (make fresh once per week)
- PBS/BSA 1%/saponin 0.05% for staining (make fresh once per week)
- Formaldehyde 1% in PBS for fixing

Immunostaining solution

- Anti-CD45-PerCP (Life Technologies, MHCD4531, clone HI30): 2 µL from stock solution (when stock solution is 100 µg/mL)
- Anti-CKpan-NanoParticles 575 (AcZon, clone C11 and AE1/AE3): 1 µl from stock solution (is 3.5 µg/mL)
- Add to 50 µL total volume with PBS/BSA 1%/saponin 0.05% (47 µL).
- Mounting medium (20 µL per microsieve): ProLong® Diamond Antifade Mountant with DAPI (Life Technologies, P36971).
- Coverslip: 2x 0.85 by 0.85 cm custom cut coverslips, thickness #1 (0.13-0.16mm) (Menzel-Gläser, Saarbrückener, Germany).

Filtration station

Check before filtering if the pressure is correct. The microsieve has to be in the filter holder and the lid of the tube has to be closed. When the pressure is in the correct range, a green light will show (see Figure 1A).

Filtration

1. Note the total volume of the sample. The eluate tube can contain up to 45 mL during filtration.
2. Pressure is OFF: apply the sample (see Figure 2B).
3. Put the pressure ON, and keep on to filter the complete sample, but do not let the microsieve run dry (see Figure 1C). Filter for a maximum time of 10 minutes.
4. Shut the pressure OFF before the microsieve runs dry.
5. Remove the microsieve carefully from the filtration station.

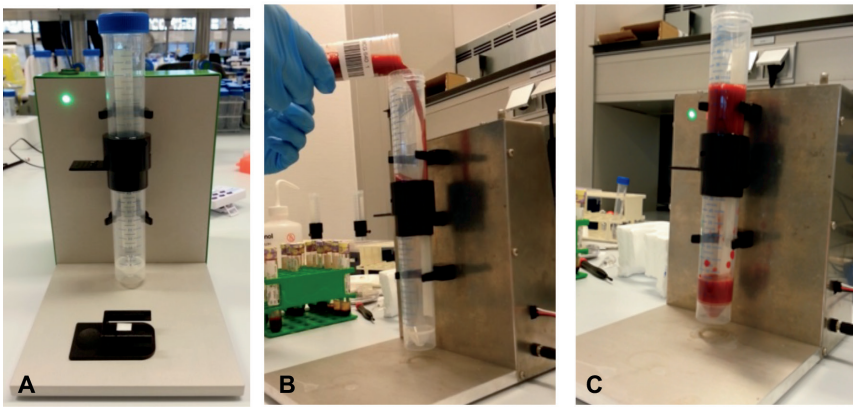

Figure 1. Complete filter tube and microsieve in the filtration station. Correct filtration pressure shows a green light in the corner (A). Filtering a sample in the filtration station. A sample is applied directly on the microsieve in the filter tube (B). Filtration of the sample with the correct pressure can take up to 10 minutes, depending on the amount of white blood cells present in the sample (C).

Clogging during filtration

When a sample contains a lot of white blood cells, it can happen that all the pores of the microsieve are filled before the complete sample is processed. This sample clogs and the volume is passed very slowly without actual filtering. In case of clogging during filtration, proceed as follows:

1. Filter for a maximum time of 10 minutes, after which the pressure can be switched OFF.
2. Transfer the remaining, unfiltered sample to a tube with volume markings (this can be the original tube).
3. Note the volumes which was not filtered and subsequently filtered; these can be used to calculate how much whole blood volume was used for filtration.

4. Discard the remaining, unfiltered sample.
5. Remove the sieve carefully from the filtration station.

Immunofluorescent staining

See Figure 2 for reference.

6. Place the microsieve in a sieve standard and remove any remaining sample on top of the microsieve by gently pressing down the sieve down on the sponge (*).
7. Wash the microsieve once with 50 µL PBS/BSA 1%/saponin 0.15%.
8. Apply 50 µL PBS/BSA 1%/saponin 0.15% and incubate 15 min at RT for permeabilization.
9. Remove the solution by gently pushing the microsieve down.
10. Apply 50 µL of staining solution and incubate 15 min at 37°C in a humidified environment (like a cell culture incubator or hotplate).
11. Remove the solution by gently pushing the sieve down.
12. Wash the microsieve once with 50 µL PBS/BSA 1%.
13. Apply 50 µL PBS/BSA 1% and incubate 5 minutes at RT to remove unbound antibodies.
14. Remove the solution by gently pushing the microsieve down.
15. Fix the cells with 50 µL 1% formaldehyde/PBS for 10 min at RT.
16. Remove the solution by gently pushing the microsieve down (**).
17. Wash the microsieve two times with 50 µL PBS/BSA 1%.
18. Turn the microsieve upside down in the staining holder. Pipet 20 µL ProLong® mounting medium. By moving your pipet on the edge of every lane, the lanes will fill with mounting medium (this requires in total approximately 10 µL medium). This filling of the lanes is visible by eye, but takes a little patience and some practice. Apply the coverslip on the backside of the microsieve.
19. Turn the microsieve back in the upright position. Apply the remaining mounting medium gently on the microsieve. Apply the coverslip and prevent any air bubbles.
20. Scan the samples with the fluorescence microscope. Store the samples at –20°C for storage, distribution or future molecular analysis.

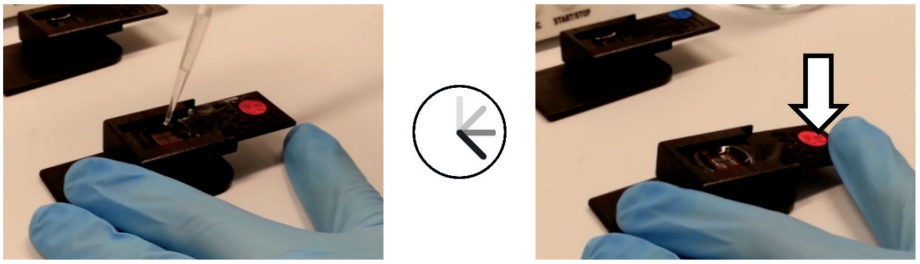

Figure 2. Washing, permeabilization, staining and fixation of the cells are all performed on the sieve in the sieve standard. Solutions can be applied directly on the sieve (left). The solution will stay on the sieve during incubation. By gently pushing down the end of the slide, the sieve will come in contact with the sponge underneath and this will absorb the solution (right).

General notes

- During incubation, make sure the microsieve does not touch the sponge or any other surface to prevent drying of the microsieve.
- (*) At this point the protocol can be stopped and the microsieve can be placed at 4°C with some PBS/BSA1% solution on top. Make sure the microsieve does not touch any surface or that the microsieve dries.
- (**) At this point the protocol can be stopped and the microsieve can be placed in the fridge with some PBS/BSA1% solution on top. However, it is best if the mounting medium and cover slip are immediately placed and the sample is stored at –20°C.
- It is advised to use clean cover slips for optimal analysis.

Scanning

Use the filter cubes described in Table 1 for automatic scanning of the microsieves on a mercury arc fluorescence microscope. Use a 20X objective, with minimal 0.45NA.

Table 1. Characteristics of the filter cubes used in the CTC-Trap project.

Filter cube	Excitation (nm)	Dichroic (nm)	Emission (nm)
DAPI	377/50	409 LP	409 LP
PE	543/22	562 LP	593/40
PerCP	435/40	510 LP	676/29

Define the optimal exposure time for the scanning of the microsieves. Use this exposure time for every sample. Make sure the lamp is not too old and beware of bleaching the sample.

Label the slide with patient number, site of processing, date and other useful information.
Store the microsieve at –20°C after scanning.

Checklist

Sample name			
Operator name			
Draw date	Clinical site		
Prep date	Clinical site		
Microsieve scan date	Clinical site		
Total sample volume			
Was filtration performed at -100mbar (shows green light)?	☐Yes	☐No	☐ I don't know
Total filtration time	_____ min _____ sec		
Volume not filtered after 10 minutes (clogging of microsieve)			
Volume filtered after 10 minutes			
Was permeabilization performed for 15 min with 0.15% saponin?	☐Yes	☐No	
Was staining performed for 15 min at 37°C?	☐Yes	☐No	
Was the staining mix as described in this procedure used?	☐Yes	☐No	
Was the washing step of 5 min performed?	☐Yes	☐No	
Was the sample fixed with 1% formaldehyde for 10 min?	☐Yes	☐No	
Was the coverslip mounted on both sides of the microsieves?	☐Yes	☐No	
What are the excitation/emission values from the cubes used for scanning? DAPI PE PerCP			
Objective	Magnification/NA		
Was the microsieve stored at (at least) –20°C?	☐Yes	☐No	
Notes			

Protocol III Scoring CTC on microsieves

This protocol shows the decision tree that is used for scoring CTC in CellSearch® cartridges, but now adapted for CTC on the microsieves.

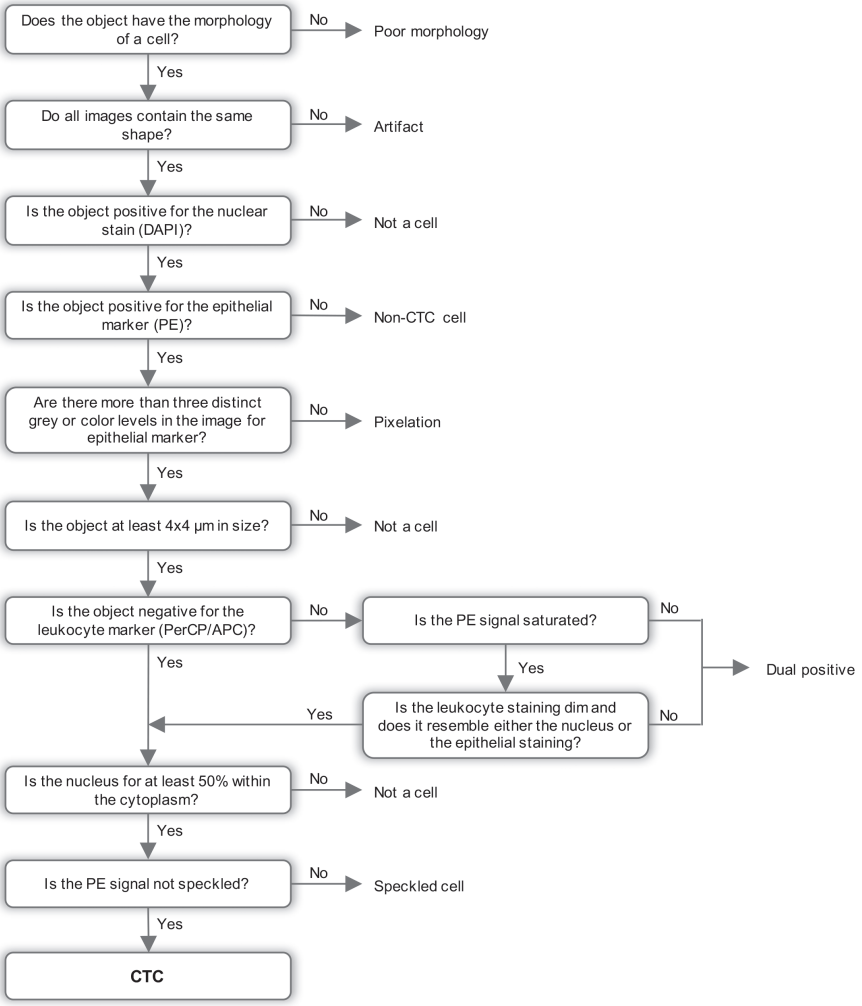

Protocol IV Plasma collection from CellSave blood samples

Throughout the CTC-Trap and CANCER-ID program, plasma is collected from whole blood patients samples in CellSave tubes.

1. Gently invert the blood sample stored into CellSave tubes at room temperature.
2. Transfer 7.5 mL blood sample from the CellSave tube to a CellSearch conical tube.
3. Spin down at 800g for 10 minutes without using the brake.
4. Carefully collect 1-2 mL plasma without disturbing the buffy coat in a sterile 2 mL eppendorf tube. Collect the plasma up to 1 cm above the layer of red blood cells; you will leave behind approximately 1 mL plasma above the buffy coat (see Figure).
5. Label the eppendorf tube acoordingly and store at –80°C.
6. Add the same volume as the collected plasma of CellSearch Dilution Buffer to the patient sample.
7. Continue the regular protocol of preparing the sample by adding 6.5 mL CellSearch Dilution Buffer and spinning down at 800g for 10 minutes without using the brake.

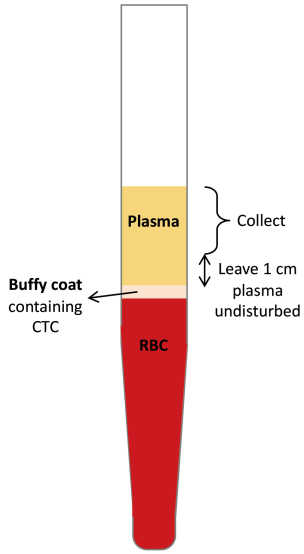

Protocol V FISH on a microsieve

Developed by Heleen W. Mulder.

For analysis of CTC detected on the microsieves with immunofluorescent labelling, this FISH procedure can be applied. This protocol is described in Chapter 5 of this thesis. It was optimized for the ALK 2p23 Break (Leica Biosystems, reference pKBI-10747) and the 4-colour centromeric aneuploidy FISH test (Kreatech Diagnostics, cat# IMM-001).

Removing coverslips

1. Soak the microsieve upside down in 2xSSC/0.1% Tween (Sigma-Aldrich, St. Louis MO, USA and Fisher Scientific Netherlands, Landsmeer, The Netherlands) until the coverslip falls of by itself. This can take up to 30 minutes; if it takes longer, remove coverslip gently using tweezers.

Pretreatment

2. For morphology preservement, apply 50 µL 4% formaldehyde (Sigma-Aldrich) in PBS to the microsieve and incubate for 10 minutes at room temperature. After 10 minutes of incubation, remove the formaldehyde by rinsing with 70% ethanol.

Probe preparation

3. Dehydrate the microsieve in 70%, 85% and 100% ethanol for 1 minute each.
4. Dry the microsieve by air.
5. Dilute 2 µL probe in 18µl hybridization buffer. Apply 10 µL of this mixture to the top of the microsieve and cover with a custom cut 0.85 by 0.85 cm glass coverslip (Menzel-Gläser, Saarbrükener, Germany).
6. Apply also 10 µL of this mixture to the bottom of the microsieve and cover with a coverslip.
7. Apply a generous amount of fixogum (Leica Biosystems) to the coverslip on the bottom of the microsieve to seal the edges. Let the glue dry for around 30 minutes until it is not sticky anymore.
8. Apply a generous amount of fixogum at the front side of the microsieve and let this dry for a while.

Hybridization

9. Put the microsieve onto the humidified Thermobright StatSpin (Leica Biosystems) hot plate.
10. Denature for 10 minutes at 85°C
11. Hybridize for 24 hours at 37°C.

Post-hybridization wash

12. Prewarm wash buffer I (0.4xSSC/0.3% Igepal) (Sifma-Aldich) to 72°C ±1. Note: this temperature is very important; when it is too high, all probe will be washed away; when it is too low, a-specific bound probe will bind the DNA.
13. Carefully remove the fixogum and coverslips using tweezers. Immediately proceed to the washing steps.
14. Wash for 2 minutes in Wash Buffer I at 72°C.
15. Wash for 1 minute in Wash Buffer II (2xSSC/0.1% Igepal) at room temperature.
16. Dehydrate microsieve in 70%, 85% and 100% ethanol for 1 minute each.
17. Air dry microsieve at room temperature.
18. Apply 5 µL counterstain with DAPI (Leica Biosystems) to both sides of the microsieve and cover with a coverslip. Let the counterstain incubate for a ±30 minutes in the dark at room temperature. Proceed with microscopy.

Protocol VI DNA isolation from cells on microsieves

Developed by Joost F. Swennenhuis.

To determine the presence of mutations in the CTC captured on the microsieves this protocol using was developed. It uses a custom made sonication probe that is 1 cm in diameter en therby covers the complete microsieve. For DNA isolation, components from the DNeasy® Blood & Tissue Kit from Qiagen (cat.no: 69504) are used. The isolated DNA can be used for digital droplet PCR approached, of which the sensitivity is high enough to locate low abundance mutations in the background of leukocytes present on the microsieves.

1. Break the microsieve from the plastic holder by dipping it in liquid nitrogen for maximal 3 seconds (repeat if necessary) and use gentle force with a pincer to push it in a well of a 24-wells plate.
2. Remove the glass coverslips from the microsieve, but keep them in the well.
3. Add the mixed Proteinase K solution (200 µL PBS + 200 µL AL Buffer + 20 µL ProtK). Make sure the microsieve and glass coverslips are completely covered.
4. Incubate at 37°C overnight.
5. Add 200 µL Ethanol to the sample and mix well.
6. Sonicate the sample for 1 minute at 0.5 circle/40 amplitude. Keep the wells plate cold in a water/ice bath during sonication.
7. Transfer the solution to a column and centrifuge the column for 1 minute at 6,000g. Discard the flow through.
8. Add 600 µL PBS/AL/EtOH buffer to the well with the microsieve and sonicate again for 1 minute.
9. Transfer the second sonication solution to the same column and centrifuge for 1 minute at 6,000g. Discard the flow through.
10. Clean the sonication probe with MQ and proceed to any additional samples for sonication (start again at step 5) before continuation of the protocol for DNA isolation (step 11-15).
11. Add 500 µL Buffer AW1 and centrifuge for 1 minute at 6,000g. Discard the flow through.

12. Add 500 µL Buffer AW2 and centrifuge for 3 minutes at 20,000g. Discard the flow through.
13. Transfer the spin column to a new 1.5 mL microcentrifuge tube.
14. Add 100 µL MQ to the center of the column and incubate at room temperature for 1 minute. Centrifuge for 1 minute at 6,000g and discard the column.
15. Store the isolated DNA at –30°C.